UNIVERSITY OF SOUTHAMPTON

THE INFLUENCE OF HYGROTHERMAL AGEING ON POLYMERIC COMPOSITE SANDWICH MATERIALS AND STRUCTURES

by

Jacqueline Sonia Earl

of the

SCHOOL OF ENGINEERING SCIENCES
FACULTY OF ENGINEERING AND APPLIED SCIENCE
UNIVERSITY OF SOUTHAMPTON
England

Thesis submitted for the degree of
Doctor of Philosophy

March 2001

UNIVERSITY OF SOUTHAMPTON

ABSTRACT

FACULTY OF ENGINEERING AND APPLIED SCIENCE

SCHOOL OF ENGINEERING SCIENCES

Doctor of Philosophy

THE INFLUENCE OF HYGROTHERMAL AGEING ON POLYMERIC COMPOSITE SANDWICH MATERIALS AND STRUCTURES

by Jacqueline Sonia Earl

The moisture absorption characteristics of closed cell PVC foam core materials and hybrid fibre reinforced epoxy skins have been monitored over a 2½ year duration. The laminates exhibited pseudo-Fickian characteristics, while the foams showed evidence of a multi-stage uptake mechanism. The long-term foam absorption data could not be modelled adequately by existing analytical models and a hypothesis is given. The effects of hygrothermal ageing on material properties has been analysed using DMTA. Room temperature modulus degradation and improved glass transition temperatures were observed. A hypothesis is proposed to explain the seemingly contradictory results, based on plasticisation, postcure and property recovery upon drying. The results from the foam material are believed to be the most comprehensive to date.

To evaluate these effects in a structural context, sandwich construction tee joints were analysed, which represent the bulkhead to hull connections in marine craft and typically suffer from slamming loads in service. The stress distribution was analysed in six joint geometries under compression loading using thermoelastic stress analysis (TSA) and finite element analysis (FEA). The results highlighted areas for siginificant improvement in the design. An important contribution of this work is the application of TSA to determining the effects of hygrothermal ageing on the stress distribution in the tee joints. This shows excellent potential and the data obtained would be impossible to collect by any other means. The information obtained about the ageing of the individual sandwich materials used in conjunction with FEA has also shown significant promise in the prediction of mechanical behaviour in the structural context. The quantitative development of this combined approach will be invaluable in the future analysis of the hygrothermal ageing of foam cored composite sandwich construction.

CONTENTS

ACKNOWLEDGEMENTS

The author gratefully acknowledges the help of the following people, without whom this work could not have been achieved.

Professor Ajit Shenoi, to whom I am indebted for his supervision, guidance and support beyond the call of duty.

Dr. Alan. Chambers, whose plentiful supply of advice and patience as my second supervisor was invaluable.

Dr. Ken Trethewey, for his input into the initial stages of the project before his departure to pastures new.

All the inmates, past and present, in the Department Formerly Known As Ship Science, who made my seven year stay there so memorable. In particular Janice Barton, whose unrelenting enthusiasm for thermoelasticity couldn't help but rub off. Long may the good work continue.

The School of Engineering Sciences' talented team of technicians, particularly Dave Goldsworthy, Jim Baker, Dave Beckett and the lovely Eric, who always managed to get things done for me by yesterday.

Mick Martin at DERA Farnborough, whose CD collection and in-depth knowledge of DMTA made collecting and interpreting the results all the more painless.

My closest friends, who unwittingly provided the greatest inspiration-boosters and therapy sessions in the form of countless coffee breaks, mid-afternoon Bailey's Lattes and 'on-line' help. Shame the bank raid never came off.

My wonderful family and Chris, without whose moral support, endless encouragement and unconditional love I couldn't have made it through. You will always mean everything to me and it is to you this work is dedicated.

PART A

BACKGROUND

1. INTRODUCTION

It is straightforward to determine the mechanical properties of a composite specimen from experimentation after its manufacture. However it is much more difficult to predict the mechanical behaviour of a composite structure after it has been in service for a significant length of time, and as a result, conservative safety factors are applied to the design. Ships in particular tend to have reasonably long life-spans, typically around 25 years and often longer, and many glass reinforced plastic (GRP) hulls of naval mine countermeasure vessels, lifeboats and so on, are now of this age or older and have experienced arduous operating regimes during service. There is therefore a need to be able to assess whether the life of such vessels can be extended, and to be able to give the designer more information about the way in which any composite structure will perform over its service life.

Ageing can be defined in this context as the time-dependent effects of service on the properties of the materials in the structure. During service, large structures such as ships and aircraft experience complex combinations of loads due to their operating environment. Taking ships as a specific example, deterioration of the structural performance is not only due to externally applied mechanical loads from waves and wind or due to the motions of the hull itself, but also directly from environmental factors. Environmental factors which are generally considered to have a degrading effect on polymer composite material structures include solar radiation, micro-organisms, humidity, immersion, ozone/oxygen-rich atmospheres, heat, refrigeration, pollution and industrial chemicals.

The focus of this work is on the effects of exposure to moisture. Deterioration has widely been linked to moisture absorption caused by climatic exposure in marine and aerospace applications (Chapter 2). The effects of the presence of moisture are exacerbated by elevated temperature and for this reason, have been found to cause significant problems in tropical regions. It is reported that unprotected composite materials used in minehunters of the Royal Australian Navy have reached temperatures up to 90°C under normal Australian conditions [1.1]. It has even been shown by temperature mapping of aircraft surfaces that on a sunny summer's afternoon in still air in North Yorkshire, black upper wing tips were also approaching a temperature of 90°C [1.2]. Such temperatures alone would be regarded in these applications as detrimental, being too close to the composite glass transition temperature for comfort; but when combined with high humidity, can have even more significant long-term effects. The effects of combined exposure to moisture and elevated temperature is known as *hygrothermal ageing*. It is this effect with which this work is primarily concerned.

In the last 30 to 35 years, much experimental research has been undertaken into the effects of exposure of polymer matrix composites to environmental conditions, particularly hygrothermal ageing. In some cases the effects of this on mechanical properties have been examined experimentally, and in others, theoretical models have been developed to predict such effects. Most work has been carried out on small, specially made coupons of material, usually from aerospace applications, which does not give the naval architect sufficient information about the deterioration of marine composite structures due to hygrothermal exposure. This is particularly true of foam sandwich materials, which are becoming more widely utilised in the construction of smaller craft requiring high specific strength and stiffness. An additional variable is mechanical loading, which is infrequently considered in conjunction with hygrothermal effects.

Literature reviews have highlighted the areas in which there is a current lack of adequate information. The scope of this work encompasses these in the context of composite foam sandwich constructions and contributes significantly to the current knowledge-base by

- Determining the effects of hygrothermal ageing on 'real' materials, which have not been characterised before;
- Applying existing experimental techniques to measure the effects of hygrothermal ageing in sandwich materials and structures for the first time;
- Using experimental and numerical modelling to make a unique link between material effects and structural performance.

1.1 References

[1.1] **Challis, K.E., Hall, D.J., Hilton, P.R., Paul, D.B.**; *Thermal Stability of Structural PVC Foams; Cellular Polymers*, Vol. 5 (1986), pp103-121.

[1.2] **Foster, N.G.**; *In-service Performance of Composite Materials*; Int. Conf. On Designing Cost-effective Composites, 15-16 Sept. 1998, London, UK, IMechE Conf. Trans. 1998-8, pp109-119.

PART B

CRITICAL REVIEW

2. REVIEW OF THE LITERATURE ON HYGROTHERMAL AGEING OF POLYMER COMPOSITE MATERIALS

This chapter gives an overview of the literature concerning hygrothermal ageing in polymer composite materials, including the pure resin, fibre reinforced polymers and sandwich materials. Much of the early research from the 1970s was concerned mainly with the nature and extent of water uptake by FRP laminates and was soon after extended to include the effects this has on the material and its mechanical properties. At that time concerns had been expressed regarding the durability of the higher performance composites used in aircraft construction, such as epoxy/graphite systems. While not exclusively researched by the aircraft industry, the majority of the materials tested have been epoxy-based laminates and pure epoxy resin, extended later to include polyester/E-glass composites, other polymeric matrices and fibre reinforcements, and more latterly to sandwich construction.

The first half of this review is split into three sections that concern the mechanisms by which moisture is absorbed into polymeric materials, FRP materials and cellular sandwich core materials respectively. A fourth section then covers the ways in which these hygrothermal ageing processes affect the performance of the materials, an area of particular concern in this research. The final two sections consider the analytical models available for moisture absorption and the experimental techniques adopted to achieve hygrothermal ageing in the laboratory.

2.1 Mechanisms of Hygrothermal Ageing in Polymeric Materials

2.1.1 The Moisture Absorption Mechanism

Firstly consider a homogeneous polymeric material typical of the thermoset matrices used in structural FRP materials. It is universally accepted that the primary mechanism by which moisture is absorbed into the material is diffusion controlled [2.1 - 2.13]. Hygrothermal exposure causes the liquid or vapour molecules to diffuse into the polymer and occupy positions among the polymer molecules [2.14]. Generally the specific sites to which water molecules become attached are the polar groups of the polymer molecule.

Penetrant molecules can also move through the polymer either along the axis of a 'tube' formed by 4 adjacent parallel polymer chains or perpendicular to the axis when two

polymer chains separate sufficiently to allow passage of the molecule. The former is assumed to require no activation energy and therefore occurs much more rapidly than the latter. The diffusion rate is therefore increased when defects, vacancies or interstitial gaps are present within the molecular structure.

The process of diffusion of the penetrant (in this case water) into the polymer typically continues until a level of saturation is reached. This level depends primarily on the concentration of the penetrant (i.e. the relative humidity of the exposure environment in the case of hygrothermal ageing) and can also be a function of exposure temperature. The saturation moisture content with an increase in exposure temperature has been reported for epoxies in the literature and has been attributed to the exothermic nature of water absorption in these polymers [2.13].

One of the important parameters for characterising the diffusion process is therefore the maximum moisture content or saturation level, M_∞. The moisture content is usually expressed as a percentage mass increase compared to the original dry mass of the material, i.e.

$$M_t = \frac{m_t - m_0}{m_0} \times 100 \qquad (2.1)$$

where M_t = the specimen percentage moisture content at time t during exposure
m_t = the specimen mass at time t during exposure
m_0 = the dry specimen mass i.e. at exposure time $t = 0$.

Therefore the saturation moisture content is given by:

$$M_\infty = \frac{m_\infty - m_0}{m_0} \times 100 \qquad (2.2)$$

where M_∞ = the specimen percentage moisture content at time t_∞. This defines the level of moisture absorption reached in the specimen corresponding to a length of exposure time sufficiently long that the rate of change of weight increase of the specimen becomes negligible.

Browning *et al* [2.2] estimate that the maximum weight gain obtained by full plasticisation of epoxy resin is approximately 6%, whereas Chamis *et al* [2.15] observe a value of 7.8% and Aronhime *et al* [2.16] report only 2.7%. In fact even for a single resin type, the values obtained can be significantly different depending on the resin/hardener system and the cure regime. Akay *et al* [2.17] state that water absorption may differ by a factor of 10 between different epoxy resins and to a factor of up to 3 for the same resin with a different curing agent. The extent of cure can also have a significant effect [2.13]. As the cure increases, the T_g and room temperature modulus increase but the room temperature density decreases. The decrease in density relates to an increase in free volume, which controls the level of moisture absorption.

The lowest moisture saturation tends to be exhibited by polyester resins (as low as 1.5% [2.9]), followed by vinyl esters, epoxies and phenolics [2.10].

The second important characteristic of the diffusion process is the rate at which diffusion occurs, quantified by a parameter known as the Diffusivity, D. The theory of diffusion (Section 2.5) is based on the hypothesis that the rate of transfer of a diffusing substance through a unit area of a section is proportional to the concentration gradient measured normal to the section. The constant of proportionality is known as the diffusion coefficient or the diffusivity. The mathematics is explored in more detail in Section 2.5 and by Crank [2.18], who also considers more practical aspects. In the physical sense, quantitative measurements of the rate at which a diffusion process occurs are usually expressed in terms of a diffusion coefficient.

The rate of the diffusion process is primarily a function of the exposure temperature, for example the moisture uptake of a polymeric component in service at room temperature can be accelerated by increasing the temperature above ambient. The increase of the diffusivity as a function of temperature can be described by Arrhenius' Law (Section 2.5). The rate of diffusion can also be a function of the concentration of the penetrant.

From the assumption that free volume is one of the controlling factors in diffusivity, it follows that the temperature dependence of diffusivity is determined by the increase in free volume with temperature. At temperatures well below the glass transition temperature T_g, the absorbed molecules will have difficulty moving from one site to another due to the immobility of the surrounding polymer structure. Any factor that tends to render polymer chain segments less mobile or causes them to pack more closely will decrease the diffusion rate. With increasing temperatures, the thermal expansion allows penetrant

molecules to move around more easily. However, Aronhime *et al* [2.13] report that the diffusivity appears to also be controlled by the extent of cure. An increase in cross-linking density with an increase in cure decreases the rate of moisture absorption.

The diffusivity is also a function of the matrix material. Barrie [2.19] states that the rate at which water is transported within a polymer depends on the affinity that a particular polymer may have for water, which varies with the number of reactive groups it contains. Water absorption rates in different resins have been stated to follow the following order (lowest to highest) [2.9]:

- phenolic
- epoxy-based
- vinyl ester
- orthophthalic unsaturated polyester
- isophthalic unsaturated polyester

In many cases the process of diffusion in homogeneous polymers has been shown to conform to Fick's law, which is the basis of the classical diffusion model. The characteristic Fickian diffusion curve is shown in Figure 2.1. D can be determined from the gradient of the initial linear portion of the curve (Section 2.5).

Diffusion can be described as Fickian, provided the following characteristics are exhibited [2.3]:

- Both absorption and desorption are linear in the initial state, such that a plot of *moisture content* M vs. *square root of time* $t^{1/2}$ must be linear up to about 60% of the maximum moisture content M_∞.
- Beyond the linear region, both absorption and desorption curves are concave to the abscissa until M_∞ is reached, i.e. the rate of diffusion slows until the moisture content reaches an equilibrium or saturation plateau.
- When the initial concentration and the final concentration of the diffusing molecules are fixed, a series of sorption curves for specimens of different thicknesses are superimposable to a single curve if each curve is plotted in the form of a reduced sorption curve (M vs. $t^{½}/l$, where l is the specimen thickness).

Diffusion behaviour of many polymers cannot be adequately described by a concentration dependent form of Fick's law with constant boundary conditions (Section 2.5), especially

when the penetrant causes extensive swelling of the material. This is often the case with glassy polymers such as those used in FRP. Not all polymeric materials conform to this model exactly, but the characteristics are usually essentially the same or 'pseudo-Fickian'. In some cases however it has been found that saturation is not reached but the moisture content appears to go on increasing [e.g. 2.13], or the initial part of the curve shown in Figure 2.1 is non-linear. In other cases a saturation value appears to have been reached before further moisture uptake occurs, leaving a point of inflection. These cases are referred to as anomalous because they do not conform to the Fickian model. In fact they may be characteristic of a particular polymer or a function of the moisture measurement process and other active ageing mechanisms.

The deviation from Fickian behaviour is generally considered to be associated with the finite rates at which the polymer structure changes in response to the absorption of penetrant molecules [2.18]. Springer in [2.5] states that the 'anomalies' arise when relaxation processes and changes in the polymer structure occur at a similar rate to the diffusion process. Generally the occurrence of such characteristics can be attributed to three factors [2.20], as follows.

- Diffusivity is a function of both concentration and time.

When the diffusion coefficient decreases with time, it is suggested that a 'clustering' of moisture occurs in microvoids or cracks, or moisture becomes trapped by hydrogen bonds, leading to a higher percentage of water becoming immobile. Marsh *et al* [2.21] hypothesise that an increase in diffusion coefficient may be due to plasticisation causing an increase in free volume and thus an increased mobility of absorbed moisture.

- Boundary conditions for diffusion depend on variables such as time and applied stress.

When a penetrant diffuses into a polymer, internal stresses are set up because the moisture gradient causes non-uniform swelling. This stress distribution changes with time as diffusion proceeds, therefore affecting the value of the diffusion coefficient.

- Multiple transport mechanisms are active.

These could be more than one concurrently activated diffusion/absorption mechanism, which results in more than one phase of absorbed moisture.

Figure 2.2 illustrates the typical characteristics of different types of non-Fickian absorption behaviour [2.20].

- *Pseudo*-Fickian behaviour has a similar shape of the Fickian curve, but the duration of the linear part is much shorter, or may be non-linear.
- Sigmoid can exhibit a single point of inflection, often at around 50% of the equilibrium moisture content.
- The two-stage process is slightly more complex. The first stage is diffusion controlled and is characterised by an increase in moisture content at a near-constant rate (A), followed by a reduction in the rate to a quasi-equilibrium at (B). The second stage (B-C-D) is similar to the first stage, but begins from the quasi-equilibrium moisture content. The driving force for the first stage is in the form of a concentration gradient. The second stage is controlled jointly by diffusion and polymer relaxation, both stages involving swelling of the medium. By the time the quasi-equilibrium has been reached the elastic swelling of the polymer network has increased to such an extent that no further sorption can occur. In time, the elastic forces slowly relax and more penetrant is absorbed (C) to establish equilibrium again (D) [2.18]. This can be described by the Langmuir equation (Section 7.3).

2.1.2 The Hygrothermal Ageing Mechanism

This section discusses how the process of ageing is caused by the absorption of moisture into a polymeric material under the influence of hygrothermal exposure, and how it is manifested in the material. Hygrothermal ageing can take two forms; chemical ageing and physical ageing. Chemical ageing is a non-reversible process that alters the molecular arrangement of the polymer. Processes which can lead to irreversible chemical changes in epoxy resins exposed to moisture, elevated temperature and stress include continued polymerisation or cross-linking of the polymer network, hydrolysis of the resin by the water [2.22] or internal stresses induced by swelling causing bond rupture [2.23]. Physical ageing, however is reversible, whereby the original thermodynamic equilibrium of the material can be restored by heating the material above its glass transition temperature, T_g, removing water molecules present in the polymer.

The diffusion of water molecules into the polymer structure forces the macromolecules apart such that the specimen expands or swells. This increase in chain separation results in a reduction of the secondary intermolecular bonding forces (interchain hydrogen bonding) and as a consequence the material becomes softer and more ductile [2.23]. This process is known as plasticisation and is recognised as the primary effect of hygrothermal ageing [e.g. 2.2, 2.14, 2.24 – 2.26]. It is the cause of much of the observed degradation in properties of polymeric materials. It has the effect of reducing the material stiffness and T_g [2.17], which shifts the elastomeric range to lower temperatures and decreases the strength of the polymer. The temperature range over which matrix-dominated properties in laminates remain stable and the minimum temperature for polymer degradation are reduced. For epoxy resins a drop in T_g of 15-20°C per 1% moisture content has been reported [2.17].

In fundamental terms, the glass transition temperature of a polymer is simply defined as the temperature above which the polymer is soft and below which it is hard. Thus for thermoset resins such as the majority of those discussed in this report, it is the temperature at which the polymer changes from being a strong, glassy solid to a weak, rubbery solid, i.e. it is a point at which there is a rapid change in the physical properties. In practical terms, this is more often a range than a specific temperature.

The reduction in T_g can be explained with reference to the concept of 'free volume', which is essentially the space between molecules. It is an accepted theory [2.2] that at or below the T_g of a thermoset resin, 1/40 of the total volume of the material is free volume. If this is true, then it would be possible to alter the T_g by altering the free volume of the material at a given temperature. If a polymer were mixed with a miscible liquid, such as water, that contains more free volume than the pure polymer, then the T_g will be lowered. Hence the now plasticised polymer must be cooled to a lower temperature in order to reduce its free volume to 1/40 of the total volume of the mixture. This shift in T_g can be predicted by the Bueche-Kelly theory [2.2, 2.22, 2.27],

$$T_g = \frac{\alpha_p V_p T_{g_p} + \alpha_d (1 - V_p) T_{g_d}}{\alpha_p V_p + \alpha_d (1 - V_p)} \qquad (2.3)$$

where α is the coefficient of linear thermal expansion, V is the volume fraction and the subscripts p and d relate to the polymer and diluent respectively and

$$V_p = \frac{1}{1 + \frac{\rho_p}{\rho_d}[0.01M]} \tag{2.4}$$

where ρ is the density and M is the percentage mass gain in the polymer. A simpler approach is the Fox rule of Mixtures [2.22, 2.28]

$$\frac{1}{T_g} = \frac{W_p}{T_{g_p}} + \frac{W_d}{T_{g_d}} \tag{2.5}$$

where W is the weight fraction.

Reductions in T_g of up to 30°C for epoxy have been reported in the literature [2.22, 2.29] and it has been demonstrated that T_g is reduced by 20°C for each 1% moisture absorbed [2.30]. Comyn [2.22] however reports cases where, after an initial reduction, the T_g was observed to rise again with further moisture absorption, in some cases above the original dry T_g of the material. This was attributed to increased cross-linking. It can be concluded therefore that the change in T_g with ageing is dependent on the material and its cure history.

As mentioned in Section 2.1.1, a symptom of moisture absorption is swelling of the polymeric material. Numerous authors have observed swelling in the pure polymer as well as in FRP materials, for example [2.1, 2.2, 2.15, 2.31]. Shirrell and Halpin [2.1] explain how environmentally induced swelling causes internal stresses in the material. On exposure to moisture, the specimen edges absorb rapidly until they reach equilibrium. A diffusion gradient is therefore created in the material. Swelling is resisted by the unswollen, unsaturated central region, inducing compressive stress at the outer edge, which is reacted by an induced tensile stress further into the specimen.

Cracking or microcracking in exposed resins and resin matrices has also been widely observed [2.2, 2.6, 2.22, 2.26] and is attributed to the swelling and associated stresses by some authors [2.2, 2.26]. This irreversible damage is a significant contributor to the reduction in material performance [2.2]. It is also considered to be the cause of several observations of anomalous absorption behaviour [2.3, 2.7, 2.27]. Moist, high temperature environments were considered by Loos *et al* [2.7] to cause microcracks and hence allow rapid entry of moisture and a high rate of weight gain. Several sources also attribute the

loss of resin material from the specimens to a cracking mechanism [2.7, 2.26]. Zhou and Lucas [2.32] specify that the cracking is promoted near the material surface when it is in contact with the water and that internal cracking is significantly less.

2.2 Mechanisms of Hygrothermal Ageing in FRP Materials

In addition to the mechanisms active in the polymeric matrix material (Section 2.1), there are other hygrothermal ageing mechanisms occurring in fibre reinforced materials due solely to the presence of the fibres. This section discusses the effects of hygrothermal exposure on the fibre reinforcements themselves, how the presence of the fibres in the matrix changes the diffusion mechanism compared to the unreinforced polymer, how the fibre-matrix interface can influence the moisture uptake behaviour and how these effects lead to degradation in performance of the composite.

2.2.1 The Effects of Hygrothermal Exposure on the Fibre Phase

The three main types of reinforcement used in FRP composites are glass fibres (most often E-glass), carbon fibres and aramid (aromatic polyamide) fibres such as Kevlar 49© by Dupont de Nemours. Glass and carbon fibres are considered to be resistant to the effects of hygrothermal exposure and do not absorb moisture. Moisture absorption by organic fibres such as the aramids is well known.

However, glass fibres can be prone to a special case of chemical corrosion due to hydrogen ions in locations where they are highly loaded [2.9, 2.10, 2.33]. The phenomenon is known as stress corrosion and results in the propagation of microscopic cracks in individual fibres, which can lead to rapid failure of the laminate at loads less than 1/5 of the initial dry UTS. The fracture surface itself has a brittle appearance. In ships and boat structures, peak stresses experienced by the hull due to slamming and wave loads are usually sporadic and are rarely prolonged, so stress corrosion is unlikely to be a significant problem. Structures within the vessel subjected to dead loads however, such as bottom shell supporting machinery or bulkheads in tanks, could potentially suffer from the problem.

Aramid fibres, which are pertinent to this research, are known to absorb moisture because of their organic composition. The literature available on the subject is not as extensive as

that for glass or carbon/graphite fibre reinforced composites, but covers the subject comprehensively. Moisture absorption by the fibres themselves [2.34 – 2.36] and as part of an epoxy matrix laminates [2.11, 2.16, 2.17, 2.37, 2.38] or hybrid laminates [2.38, 2.39] are covered.

'Aramid' is a shortened name for aromatic polyamide. It is the inherent polarity of the amide group of the molecule *p*-phenylene terephthalamide, from which Kevlar fibres are made, that favours moisture uptake by the material [2.36]. X-ray diffraction has shown [2.34] that the amide-water molecular interactions are likely to be confined to the polymer chains on the surface. In addition, moisture absorption is enhanced by the presence of microvoids on the fibre surface and by the presence of hydrophilic sodium salts (Na_2SO_4) [2.35]. However it has also been reported that Kevlar fibres contain an extensive internal defect structure of microvoids and cracks [2.40], which is penetrated by the moisture, weakening the interfibrillar hydrogen bonding causing extensive internal splitting.

The equilibrium moisture contents reported vary between 1.6 and 3.5% at 50% RH and 23°C [2.35]. The equilibrium moisture contents obtained by immersion are significantly higher, for example 4.9% [2.16], 5.0% [2.38], 6% [2.17]. The maximum moisture content of Kevlar fabric and Kevlar composites has been shown to be a linear function of the relative humidity [2.11].

The moisture uptake mechanism by the fibres was shown by Fukuda and Kawai [2.36] to be generally Fickian in nature, but not tending towards a saturation value with the moisture content tending to increase in the latter stages of absorption. In some cases this was observed to be sigmoidal in form. Gopalan *et al* [2.38] show that for simple and hybrid Kevlar composites, the Fickian diffusion model correlates well with the experimental data. They also show that the equilibrium moisture content and diffusivity are 5 and 10 times higher respectively than equivalent glass or carbon laminates and the hybridisation of impermeable fibres with Kevlar had little effect on these results. Aronhime *et al* [2.16] however observed non-linearity of moisture content with $(\text{time})^{1/2}$, suggesting that this was a sign of multi-dimensional diffusion.

Another interesting finding from literature [2.11, 2.38] is that the diffusivity is dependent on the fibre orientation in the laminate. This implies that untreated fibre ends on the cut edges of a laminate could enhance moisture uptake significantly. Aronhime *et al* also observed anisotropy in the diffusion process of unidirectional Kevlar epoxy composites, in which D_{11} was much greater than D_{22} and the ratio between the two increased further as

the fibre volume fraction increased. Aronhime *et al* attribute these findings to the axial diffusivity of the fibres being much greater than the radial diffusivity, suggesting that there is a link between this phenomenon and that observed by Gopalan *et al* [2.38]. This also suggests that aramid fibres in a laminate provide an easy route for moisture absorption and in turn facilitate a greater degree of plasticisation of the resin at the fibre matrix interface [2.17].

Impermeable fibres also affect the absorption mechanism in composites compared to the unreinforced resin (Section 2.2.2).

2.2.2 The Influence of the Fibre Phase on Diffusion Characteristics

Diffusion of moisture into a polymer matrix composite occurs by essentially the same mechanisms as described in Section 2.1, but the presence of the fibres influences the process and can lead to non-Fickian behaviour [e.g. 2.3]. This influence is due to inhomogeneity and anisotropy in the material. The two diffusion parameters discussed in Section 2.1.1, M_∞ and D, are both affected by the presence of fibres.

In an undamaged laminate, the saturation moisture content (measured by mass as described in Section 2.1.1) is much smaller than that of the pure resin if the fibre phase is impermeable. The measured value is therefore not only dependent on the resin system and cure regime, but also on the matrix volume fraction.

If the equilibrium moisture contents of all the separate components of a laminate can be determined, then the equilibrium moisture content of the whole laminate can be found using expressions suggested by Shirrell [2.3] or Loos and Springer [2.6].

Shirrell suggested use of following equation for situations in which resin, fillers and voids are present:

$$M_\infty = \lambda_r M_\infty(r) + \lambda_f M_\infty(f) + \lambda_v M_\infty(v) \qquad (2.6)$$

where λ is the volume fraction, r, f and v refer to the resin matrix, filler and voids respectively.

It has been shown that $M_\infty(f)$ is zero for graphite fibres, and on this assumption Loos and Springer present a similar expression whereby the maximum moisture content of the composite may be estimated from the maximum moisture content of the neat resin $(M_\infty)_r$:

$$M_\infty = (M_\infty)_r (W_r) \qquad (2.7)$$

where W_r is the weight fraction of the resin in the composite. This gives excellent agreement between the measured and calculated values for the resin compared in the paper [2.6].

These expressions provide methods for determining the saturation of laminates if only the value of the pure resin is known. However, a large volume of data exists which has been determined experimentally. The problem of comparing data between sources in the literature arises because the fibre or matrix volume fractions are rarely quoted. Chamis *et al* [2.15] are an exception, quoting a saturation value of 3% and a resin volume fraction in the laminate of 40%. If we assume zero void fraction and impermeable fibres (graphite), then the saturation value for the pure resin (using Equation 2.6) is calculated as 7.5%. This is very close to the measured value of 7.8% (Section 2.1.1).

Choqueuse *et al* [2.41] however found that it is impossible to extrapolate absorption behaviour of the composite from the behaviour of the neat resin, even if the composite appears to follow Fickian diffusion. The composite was found to absorb in excess of three times the predicted amount, suggesting that the fibre-matrix interface is the preferential path for water migration through the material (Section 2.2.3).

Table 2.1 presents some of the results from the literature for the maximum moisture content in polymeric composites, from materials that have exhibited Fickian or pseudo-Fickian behaviour. From these results it is possible to see how the saturation moisture content is affected by the relative humidity of the environment (i.e. the concentration of the penetrant). It is a fundamental assumption of Fick's law that M_∞ is a function of relative humidity alone. However it is widely accepted that this is not always a valid assumption (Section 2.1.1) and a dependency on time, temperature and degree of cure has been observed [2.3, 2.6, 2.7]. More significantly, the effect of the fibre phase on the results is apparent, particularly in laminates containing Kevlar. A dependency on fibre volume fraction is also exhibited by the materials aged in fresh water (FW) at 23°C. These all had

a nominal fibre weight fraction of 70%, which would have resulted in different fibre volume fractions due to the differences in fibre density.

The effect of the fibre phase on the diffusivity has also received much attention in the literature. Since the diffusivity relates to the rate at which moisture is absorbed into the material, it follows that the fibres and their orientation could also have an effect by acting as an obstruction or by promoting capillary action (Section 2.2.3). Springer and co-workers [2.4 – 2.7, 2.42] show that the diffusivity of a unidirectional composite can be estimated from the diffusivity of the pure resin and the fibre volume fraction of the composite, provided the resin and composite were cured in an identical manner. It is shown that the diffusivity parallel to the fibres is greater than the diffusivity perpendicular to them.

Shirrell [2.3] found greater diffusivities in specimens with increased thickness, suggesting that diffusivity was greater through the cut edges and hence leading to the inference that diffusion could be enhanced by axial moisture transport along the fibre/interface (Section 2.2.3). However, Shen and Springer [2.42] assume only the influence of fibre obstruction upon diffusion.

Some values of diffusivity from the literature are given in Table 2.2.

2.2.3 Moisture Ingress by Mechanisms other than Diffusion

Mechanisms by which moisture can enter a composite material, other than by diffusion, have been alluded to in the previous section. Under certain conditions, moisture has been found to be drawn into the material by capillary action along the matrix-fibre interface or along fibre bundles [2.12, 2.16, 2.43]. Moisture has also been found to collect in cracks and voids on the surface of the material and within it, contributing significantly to the moisture content and causing non-Fickian absorption behaviour [2.17, 2.44].

Shirrell's work [2.3] was some of the earliest to indicate that fibres could assist moisture uptake along their axes. By testing specimens of varying thickness (Section 2.2.2), greater diffusivities were observed as a greater surface area of laminate edges were exposed. This suggests that cut fibre ends at the edges provide pathways for rapid moisture ingress.

In the case of glass and carbon reinforced laminates, it is not the fibres which absorb the moisture however. It has been observed in several cases that it is the interface between the fibres and matrix which degrades and allows moisture to wick along it [2.44]. Fibres are usually sized to promote adhesion to the matrix and it is known that some of these coupling agents (e.g. amino silane, which is used with epoxies) at the interface can be highly hydrophilic, exacerbating the problem further.

2.2.4 Resultant Ageing Effects

Debonding between the fibres and the matrix not only promotes moisture ingress but causes the breakdown of the load transfer mechanism between fibres and matrix, can promote delamination or fibre buckling and hence cause premature failure [2.26, 2.45]. The breakdown in the integrity of the fibre-matrix bond has been attributed by some sources directly to plasticisation of the resin and has been found to increase with greater moisture content. The most dramatic effect was observed by Birger *et al* [2.24] who found that exposure of graphite-epoxy specimens to boiling water caused extensive destruction to the fibre-matrix interface and massive voids in the matrix as large as 20μm. No effect was observed in water or humidity at up to 50°C.

In addition to plasticisation of the matrix material (Section 2.1.2) and possible breakdown of the fibre-matrix interface (Section 2.2.3), other ageing effects which have been observed in laminate materials exposed to hygrothermal environments are predominantly swelling and cracking. These effects have also been observed in the pure resin (Section 2.1.2) but in the case of FRP, the presence of the fibres has been shown to influence the problem by a restraining effect [2.1].

Loos and Springer [2.6], observed cracking only at high temperatures (above 117°C), but the phenomenon has also been found to occur at room temperature [2.2]. Buck *et al* [2.26] observed that the extent of microcracking in the resin is increased during conditioning especially when a mechanical load is applied. This leads to an increase in the water absorption, particularly along the fibre-resin interface, leading in turn to greater material degradation and debonding and thus a greater reduction in strength, even in some cases to premature failure.

The above cases have been attributed to swelling from moisture absorption and to internal stresses as a result of the restraining effect of the fibres. Hygrothermal ageing however often involves high temperature exposure, leading to potential problems caused by the different thermal expansion coefficients of the matrix and reinforcement. Birger *et al* [2.24] thermally aged graphite-epoxy specimens at 170°C without moisture and found that the build-up of thermal stresses was relieved by crack formation in the matrix and in extreme cases by fibre failure.

Resin cracking has also been attributed to a build-up of osmotic pressure in voids which retain water [2.43, 2.46].

The cracking phenomenon and any associated material loss has been attributed as the cause of observed non-Fickian moisture uptake behaviour in several cases [2.3, 2.7, 2.8, 2.26].

2.3 Mechanisms of Hygrothermal Ageing in Cellular Sandwich Core Materials

Little work exists in the literature on the mechanisms of moisture absorption in cellular sandwich core materials, compared to the wealth of research which has been carried out on laminates and matrix resins. This chapter reviews some of the limited literature available. While the core materials most pertinent to this work are closed cell polymeric foams (specifically PVC), it is considered valuable to review the literature on moisture uptake into honeycomb cored sandwich materials since they are also cellular in nature and there may therefore be similar moisture absorption mechanisms active.

2.3.1 Foams and Foam Cored Sandwich Materials

Globally, structural foams are homogeneous, near-isotropic materials and it has been suggested in the literature [2.47] that classical single phase diffusion theory can be applied. This assumption was based only on short-term observations however. At a more detailed level there is great inhomogeneity in closed cell foams due to the cell structure. For this reason, Fick's laws are unlikely to apply for long-term absorption and the non-Fickian models discussed in Section 2.1.2 may be more applicable. However, modelling of the moisture uptake behaviour in these materials is barely touched upon in the literature. This section gives a detailed overview of the findings of the key papers in this area.

The earliest work is by Lee [2.48], who models moisture uptake in closed cell foams as a diffusion process by defining a 'foam diffusivity', distinguished from the diffusivity of water in the base polymer. This work is the only reference alluding to a moisture uptake mechanism, which assumes that the path of diffusing water remains within the cellular structure of the material and any condensation or water entrapment inside the foam is disregarded for the sake of simplicity in the derived model. Although experimental work is carried out and the results compared to the analytical model, no further attempt is made to establish whether the proposed moisture transport mechanism is valid.

Cervenka *et al* [2.49] also suggest that water vapour transport in closed cell foams is diffusion controlled and is described by a permeation constant P and a diffusion coefficient D, which is constant at temperatures above 20°C.

In closed cell foams such as the PVC commonly employed in marine sandwich structures, a significant weight increase is usually observed after only a short time of exposure, particularly during immersion. This is attributable to moisture collecting in the open cells of the cut surfaces of the untreated material, proven using Pyknometric measurements [2.49]. Clark *et al* [2.50], for example quote an instantaneous uptake of around 4% in closed cell PVC cuboid specimens; Cervenka *et al* [2.49] quote up to 27% in polyurethane. The large difference can be attributed to different cell sizes in the two foams and different test specimen surface area to volume ratios.

Granville [2.51] tested polymethacrylimide (PMI) foam alone and in sandwich specimens, finding that the thicker foam specimens tend to absorb more moisture and retain a proportion of it, even after redrying. It was also found that there is greater moisture retention in a sandwich with unsealed edges than in a pure foam specimen. The amount of water taken up has also shown a dependence on the direction in which the sample had been cut (with respect to the direction of foam rise) [2.49].

A mechanism for moisture ingress into partially cross-linked polyurethane foam (PUF) has been proposed [2.49]. It is assumed that when the absorbed moisture plasticises the polymer, disrupting intermolecular hydrogen bonding (as described in Section 2.1), the polymer chains are able to alter their positions relative to each other under an applied external pressure (e.g. hydrostatic). It is suggested that this leads to the rupture of cell membranes, allowing further ingress of moisture into the material as new pathways are

created. It was found that new pathways for moisture ingress are also created by cracks during fatigue cycling [2.50].

Moisture absorption data has also been reported for syntactic foams [2.52, 2.53]. Syntactic foams are not blown from a polymer but generally contain about 50% by volume of glass, phenolic or carbon microspheres in a polymer matrix. Lyle and Collins [2.53] show that the values of diffusion coefficient and solubility (moisture content) for the syntactic are significantly different from the values for the same solid polymer, being dependent on the type of sphere used in the syntactic. The high diffusivity and level of moisture uptake has been attributed to diffusion of water into the glass microballoons through their thin walls [2.52].

Ishai *et al* [2.52] have attempted to correlate moisture uptake results in order to find out the extent of moisture transport through sandwich skins into the syntactic core in encapsulated sandwich panels. This investigation indicated that at 25°C and 50°C, the moisture content in the foam by weight was 0.02% and 0.59% respectively after approximately 300 days of exposure. This suggests that in an intact, undamaged sandwich structure in a ship for example, the skin laminate on the side of exposure can effectively protect the core and delay the effects of moisture ingress. It is suggested that the integrity of a damaged sandwich structure may not be affected. Tests performed by Cise and Lakes [2.54] showed that relatively small, acute punctures or voids do not compromise a large area of the panel as far as moisture ingress is concerned in sandwich structures of high density cellular core materials. However, in a lower density honeycomb, moisture ingress was shown to be significant.

2.3.2 Honeycombs and Honeycomb-cored Sandwich Materials

With regard to moisture ingress mechanisms in polymer-containing or porous honeycomb materials (as opposed to metallic honeycombs), Cise and Lakes [2.54] note that high temperature fabrication processes of honeycomb core sandwich panels can result in a negative gauge pressure within the core. This has the potential to draw moisture through cell walls, sandwich skins and interface adhesive layers.

Moisture uptake rates are reported to be higher in the 'ribbon direction' of a honeycomb core due to a lower cell density with respect to distance and hence fewer cell walls to permeate [2.54]. This may correlate with closed cell foams, where there can be cell

distortion during expansion, resulting in an elliptical shape aligned with the direction of foam rise.

2.4 The Effects of Hygrothermal Ageing on the Performance of Composite Materials

In this work, performance is defined as the ability of the material to retain its structural properties. Much work is reported in the literature on materials that have been aged and then mechanically tested. Most structural properties, such as stiffness, tensile strength, flexural, compressive and fatigue properties have been evaluated for laminated materials, though little exists for sandwich materials, particularly polymeric foams.

Water absorption primarily causes two macroscopic effects that lead to deterioration in the performance of a composite. These are a general reduction in mechanical properties as a result of the effects described in the preceding sections and a weight increase of the structure [2.9]. The changes in mechanical properties as a result of ageing are generally minimal in a laminate for fibre dominated properties (e.g. elastic modulus), but highly significant for the matrix dominated properties (e.g. interlaminar shear strength and flexural properties) and the effects are well documented [2.2, 2.4, 2.24, 2.26, 2.50, 2.55 – 2.65]. There also exists a brief literature review by Hancox [2.66]. The following sections give an overview of the findings in the literature for thermoset matrices and glass, carbon or aramid reinforcement.

2.4.1 Tensile Modulus

In general there is little effect of hygrothermal ageing on the laminate elastic modulus obtained by loading in the 0° fibre direction until after the 0° ply failure, as this is a fibre dominated response [2.17, 2.39]. In 90° laminates however, a serious degradation in modulus has been observed [2.2, 2.4, 2.16, 2.55] as this is a matrix-dominated response, influenced by plasticisation of the resin. The effect is exacerbated by elevated temperature due to the reduction in T_g with moisture content. Relatively few quantitative references are made in the literature to the effects on elastic modulus.

2.4.2 *Tensile Strength*

At low moisture contents (<1%), absorbed moisture has little effect on the tensile strength of 0° and 45° glass and carbon laminates, however with increasing moisture content the strength has been shown to decrease [2.4, 2.56] by up to 20% of the UTS. This is exacerbated by increasing temperature and the application of a static load [2.26]. The longitudinal tensile strength of Kevlar/epoxy composites however has been shown to degrade little [2.16]. The transverse (90°) strength can be seriously degraded in glass and carbon reinforced laminates and strengths of 50-90% UTS have been reported, depending on temperature and moisture content [2.2, 2.4, 2.17, 2.39, 2.56, 2.67, 2.68].

The exposure environment has also been shown to have a significant effect, particularly if boiling water is used [2.40, 2.24], where static strengths can be reduced to only 22% of UTS [2.24].

2.4.3 *Compressive Strength*

For carbon/epoxy laminates there is a consistent reduction in compressive strength with increasing moisture and/or temperature [2.45]. Curtis and Moore [2.68] report a 19% reduction for quasi-isotropic laminates after ageing at 70°C and 95% RH and testing at 100°C, but little effect when tested at room temperature. For Kevlar/epoxy laminates a 5% reduction in strength per 1% absorbed moisture up to 2.5% has also been reported [2.17]. The observed reductions in strength are attributed to premature fibre failure caused by micro- and macro-buckling [2.45], which are sensitive to the lateral support of the matrix. Compressive strength is also sensitive to any degradation in the fibre-matrix interface.

2.4.4 *Flexural Properties and Interlaminar Shear*

Interlaminar shear strength (ILSS) and flexural properties are generally more sensitive to moisture than tensile properties [2.40, 2.55] and a reduction with increased hygrothermal ageing is usually reported [2.16, 2.37, 2.44, 2.69, 2.70]. Strength degradation can be significant, e.g. for a Kevlar/epoxy laminate, reductions of 2% in flexural strength and 4% in ILSS were quoted per 1% absorbed moisture up to 2.5% [2.17]. In some cases however, little change is reported for low temperature (<50°C) [2.24, 2.55, 2.59]. A summary of the findings for laminates is presented in Table 2.3.

With regard to syntactic foam, Ishai *et al* [2.52] observed an abrupt flexural strength drop at the initial stage of moisture absorption and a much slower strength degradation thereafter.

2.4.5 Fatigue

The effect of hygrothermal ageing on the tensile fatigue performance of FRP laminates has been shown to be minimal in general [2.40, 2.60, 2.71, 2.72]. In some cases, particularly with unidirectional or cross-ply reinforcement (glass or carbon), an improvement has been reported [2.71, 2.72], which is attributed to stress relaxation and plasticisation at the crack tip arresting the crack growth. Crack growth rates reduced by five times when immersed in sea water have been reported [2.63]. Improvements in flexural fatigue performance in foam sandwich beams have also been reported [2.50], attributed to the same phenomena.

In some cases, degradation in tensile and flexural fatigue properties has been observed. These are usually in 90° laminates and where glass reinforcement has been affected by stress corrosion, leading to premature fibre breakage [2.55, 2.62, 2.71]. An increase in fibre/matrix interface debonding has also been exhibited with progressive tensile fatigue damage [2.61]. Increased moisture ingress by capillary action along the interface is also reported for cyclic loading combined with immersion [2.60].

2.4.6 Core Shear

It is known that core shear failure is a prime cause of composite sandwich failure, and it is also known that reductions in composite structural strength have been experienced in tropical conditions. The work of Challis *et al* [2.73, 2.74] is concerned with the effect of elevated temperature on the shear properties of structural foams, with specific reference to the RAN minehunters. Temperatures up to 90°C were found to significantly reduce compressive and shear properties. Foams from the same supplier exhibited comparable performance, but there were variations between materials from different suppliers. The foams were generically the same so the differences were attributed to variations in production techniques and additives.

Clark *et al* [2.50] have tested sandwich beams both with open edges and sealed edges under flexural fatigue loading while immersed in saline. The skin materials used were GRP/epoxy and GRP/Kevlar/epoxy laminates. Larger deflections were observed in the immersed case than the dry beam case due to the softening of the skins by the moisture. The softening of the skins also allowed the supports to compress the core material in localised areas, initiating core shear failure. Compared to the results of Challis *et al*, it is apparent that the shear properties are affected much more greatly by moisture than by elevated temperature. Unfortunately, because the combined hygrothermal effects have not been explored by either paper, it is not known whether the effect of moisture is exacerbated by elevated temperature as the laminate results seem to indicate.

Open edged syntactic cored sandwich beams previously exposed to long-term hygrothermal conditions were found to fail prematurely by core shear failure [2.52]. The residual strength values of these specimens were also found to be lower than for identical dry beams. This is a very similar trend to that observed by Clark *et al* in the PVC foam. The residual strength values obtained for encapsulated panels however were found to be superior or equal to those found for identical dry specimens [2.52]. This supports the suggestion that the skin material gives the core significant protection from moisture.

2.5 Analytical Models for Moisture Uptake in Composite Materials

2.5.1 The Kinetics of Moisture Absorption

The mathematics of diffusion, which is primarily based upon Fick's first and second laws, is cited frequently in the literature [2.1 – 2.4, 2.22, 2.27, 2.33, 2.75, 2.76]. The subject has been covered in great detail by Crank [2.18]. The mathematical equation for heat conduction derived by Fourier was adopted by Fick to describe the mechanism of diffusion on a quantitative basis. The Fourier and Fick equations are given as follows:

$$\rho Q \frac{\partial T}{\partial t} = \frac{\partial}{\partial x} K \frac{\partial T}{\partial x} \tag{2.8}$$

$$\frac{\partial C}{\partial t} = \frac{\partial}{\partial x}\left(D \frac{\partial C}{\partial x} \right) \tag{2.9}$$

where ρ = density

Q = specific heat

K = thermal conductivity

t = time

x = space co-ordinate in the direction of sheet thickness

C = concentration of diffusant

D = mutual diffusion coefficient of the system, or diffusivity

An illustration of the problem is given in Figure 2.3, which shows a laminated plate of thickness l and of infinite length and breadth such that the condition for one-dimensional diffusion can be assumed. A moist environment of temperature T and concentration C bounds the plate on both sides and diffusion occurs through the two parallel faces of the plate.

For multi-layered plates, the boundary conditions at the interface of each layer are specified as follows.

- For isotropic substances, the mathematical theory of diffusion is based on the hypothesis that the rate of transfer of the diffusing substance through a unit area of a section is proportional to the concentration gradient measured normal to the section. The interface boundary condition requires the masses of moisture crossing the surfaces of two adjacent layers per unit area and unit time are equal, i.e. the rate of transfer of the diffusant per unit area must be equal in adjacent layers:

$$\left[D\frac{\partial C}{\partial x}\right]_{\text{left layer}} = \left[D\frac{\partial C}{\partial x}\right]_{\text{right layer}} \tag{2.10}$$

- The moisture concentrations at the surfaces of two adjacent layers correspond to the same relative humidity.

In order to solve the above relationships it is necessary to make the following simplifying assumptions:

1. The ambient temperature and ambient moisture content are constant and are the same on both sides of the plate.

2. The temperature inside the material approaches equilibrium much faster than the moisture concentration and hence the temperature inside the material can be taken to be the same as the ambient temperature.
3. Initially the temperature and moisture distributions are uniform inside the material.
4. The thermal conductivity and mass diffusivity depend only on temperature and are independent of moisture concentration or of the stress level inside the material.
5. The plate is made of a single layer only and the material is quasi-homogeneous, so that variations of ρ, C, K and D with position inside the material may be neglected.

For the above assumptions, the temperature inside the material is uniform and constant.

$$T_0 = T_\infty = T \qquad 0 \le x \le l \qquad t \ge 0$$

and the concentration is described by the one-dimensional case of Fick's second law, as shown in Equation 2.9.

This describes a non-steady state before equilibrium is reached, i.e.

$$\frac{\partial C}{\partial x} = f(x) \tag{2.11}$$

where x describes the direction of movement of the diffusion penetrant, i.e. the moisture.

Hence the analysis is based on two basic assumptions - that the diffusion process can be described by a concentration dependent form of Fick's Law and that the diffusivity is a function of temperature only.

For a solid sheet with surface area A much greater than the thickness, where the initial concentrations of moisture are uniform throughout the sheet, and where the sheet is suspended in an atmosphere containing a different concentration of moisture than the one in which it was initially conditioned, the boundary conditions are:

$C = C_0$ @ $t = 0$ and all x

$C = C_\infty$ @ $x = 0$ and $x = l$ at $t > 0$

$C = C_\infty$ @ $t = \infty$ and all x

where C_0 and C_∞ correspond to the initial concentration and the concentration after infinite time respectively, and l is the thickness of the sheet. Equation 2.9 then gives

$$\frac{C_t - C_0}{C_\infty - C_0} = 1 - \frac{4}{\pi}\sum_{n=0}^{\infty}(2n+1)^{-1} \sin\left[\frac{(2n+1)\pi x}{l}\right] exp\left[\frac{-D(2n+1)^2\pi^2 t}{l^2}\right] \tag{2.12}$$

where C_t corresponds to the concentration after time t, n is an integer.

The method of solution of (2.9) to give (2.12) is described by Crank [2.18].

The total amount of moisture absorbed is obtained by integrating Equation 2.12 through the thickness.

$$M = \int_0^l C(x,t)dx \tag{2.13}$$

Substitution of Equation 2.13 into Equation 2.12 gives

$$F \equiv \frac{M_t - M_0}{M_\infty - M_0} = 1 - \frac{8}{\pi^2}\sum_{n=0}^{\infty}(2n+1)^{-2} \exp\left[\frac{-D(2n+1)^2\pi^2 t}{l^2}\right] \tag{2.14}$$

for moderate to long lengths of time, where M_t, M_0 and M_∞ are the moisture content at times 0, t and infinity respectively. This equation provides a solution to Equation 2.9 and is used widely in the literature to predict how the weight change of the material changes over time, knowing the equilibrium moisture content and the diffusivity [2.7].

The value of the diffusivity D is determined by Shirrell [2.3] and others from the initial gradient of the graph $F = f(t^{1/2}/l)$, i.e.

$$D = \left(\frac{\pi}{16}\right)\left(\frac{F}{t^{\frac{1}{2}}/l}\right)^2 \tag{2.15}$$

This is a frequently used method for obtaining D if a moisture sorption plot is available from experimental results. A plot of F vs. $(t^{1/2}/l)$ is known as the reduced sorption plot, as

discussed in Section 2.1.1 and is linear up to $F = 0.6$. The shape of the curve is illustrated in Figure 2.1. In the majority of cases in the literature, the Fickian theory has been shown to hold for reasonably low temperatures and has been used in theoretical calculations with good success. Applications of the theory include the prediction of the maximum moisture or the moisture content after a given time, knowing the diffusivity. Amendments to this theory have been made to give more accurate predictions, as well as other models. These are considered in Section 2.5.2 to 2.5.4.

2.5.2 Determination of the Moisture Content

If the absorption process can be described by the Fickian model, the moisture content in an initially dry material after a time t can be determined by rearranging Equation 2.14 for the M_0=0 case, giving

$$M_t = M_\infty \left\{ 1 - \frac{8}{\pi^2} \sum_{n=0}^{\infty} (2n+1)^{-2} \exp\left[\frac{-D(2n+1)^2 \pi^2 t}{l^2} \right] \right\} \tag{2.16}$$

If the moisture uptake process is non-Fickian then other models can be applied, as indicated in Section 2.1.1. The most commonly used alternative is the two-phase or Langmuir diffusion model [2.59, 2.77]. The Langmuir equation takes the form:

$$\frac{M_t}{M_\infty} = \frac{\beta}{\gamma+\beta} \exp(-\gamma t) \left[1 - \frac{8}{\pi^2} \sum_{n=1}^{\infty odd} \frac{\exp(-kn^2 t)}{n^2} \right] + \frac{\beta}{\gamma+\beta} [\exp(-\gamma t)] + [1 - \exp(-\beta t)] \tag{2.17}$$

where M_t = total weight percent moisture uptake in slab after time t (%)

M_∞ = true moisture uptake at saturation (%)

t = time (s)

$k = \pi^2 D / l^2$ = characteristic diffusion constant (/s)

D = diffusion coefficient for mobile molecule of water (mm^2/s)

β = probability per unit time that a bound molecule of water becomes mobile (/s)

γ = probability per unit time that a mobile molecule of water becomes bound (/s)

In order to determine the moisture content at a time t, in both of the above models it is necessary to have a knowledge of the equilibrium or saturation moisture content M_∞. If this cannot be determined experimentally for either the laminate or the pure resin material, then it is necessary to estimate it theoretically.

It has been noted in previous sections that the equilibrium moisture content can be described as a function of the moisture concentration or the relative humidity (RH). The relationship used by a number of authors [e.g. 2.3 – 2.6, 2.78] is described by the following equation:

$$M_\infty = a(RH)^b \qquad (2.18)$$

where empirical values of the constants a and b are given in several papers. The linear relationship between M_∞ and RH (i.e. b=1.0) is in agreement with Henry's law, although most polymer-penetrant pairs do not obey Henry's Law. Typical values from the papers included in this report and those from other papers evaluated by Loos and Springer [2.6] are as follows:

For graphite-epoxy composites,

$0.014 < a < 0.019 \qquad 1.0 < b < 1.9$

For neat epoxy resin,

$0.049 < a < 0.066 \qquad 1.0 < b < 1.8$

Loos and Springer [2.6] note that the above expression for M_∞ does not account for temperature. Although M_∞ can show some temperature dependence, it is usually within the spread of the data. Note that no data has been found for resins other than epoxy.

It is also necessary to have a knowledge of the diffusivity. The most commonly adopted technique in the literature is to calculate it from the gradient of the initial part of the reduced sorption plot, as explained in the previous section. However, this can yield misleading results if the absorption is not Fickian, or the specimens to not conform to the assumptions of the Fickian model. The most common problem is that of the finite sized specimen, where moisture absorption through the specimen edges is significant and the one-dimensional assumption is invalidated. Some corrections for edge effects exist and these are described in Section 2.5.3. If the experimental results still fail to conform to the

model with edge corrections applied then it may be necessary to adopt the three-dimensional diffusion approach (Section 2.5.4).

If it is not possible to determine the diffusivity experimentally, either from the laminate or from the pure resin, it is possible to determine it theoretically. The transverse diffusivity D through a polymer composite is generally a function of temperature and can be determined from Arrhenius' law [2.1, 2.6, 2.61]:

$$D = \left(\lambda^2 / 2\tau_0\right)\exp\left(-E/RT\right) = D_0 \exp\left(-E/RT\right) \tag{2.19}$$

or simply,

$$D = D_0 \exp\left(-C/T\right) \tag{2.20}$$

where D_0 = frequency factor, constant (function of the material and the ageing environment)

E = apparent activation energy for diffusion (J/mol)

T = absolute temperature (K)

R = perfect gas constant (J/mol.K)

$\therefore$ C = constant

and the units of D are mm^2/unit time.

Data on an Arrhenius plot of log$D$ vs. $1/T$ should therefore be a straight line from which D_0 and C can be evaluated.

Shirrell and Halpin [2.1] also present a method for obtaining the diffusivity from the Halpin-Tsai equations, taking into account the effects of fibre orientation. This approach is not widely adopted however.

2.5.3 Corrections for Edge Effects

The first simple approach to account for the effects of finite specimen size in the diffusivity result was adopted by Springer and co-workers [2.5, 2.7, 2.42]. The apparent diffusivity was calculated from

$$D = \pi\left(\frac{l}{4M_\infty}\right)^2\left(\frac{M_2 - M_1}{\sqrt{t_2} - \sqrt{t_1}}\right)^2\left(1 + \frac{l}{h} + \frac{l}{b}\right)^{-2} \tag{2.21}$$

where l, h and b are the thickness, length and width of the specimens respectively. M_1 and M_2 are the moisture contents at times t_1 and t_2, these times being sufficiently low that the weight change can still be taken to vary linearly with $\sqrt{t}$. The correction factor is in the third set of brackets whilst the rest of the expression is taken from the gradient of the reduced sorption plot. This correction was shown to be adequate for homogeneous materials, however the effects of fibre orientation invalidated this model for use in laminate materials [2.42].

Shen and Springer [2.42] present a theory that culminates in a complex expression for the diffusivity of a laminated composite, taking into account fibre volume fraction and orientation, individual lamina thicknesses and the diffusivity of the resin. The correction factor is given as follows:

$$D = D_r\left(1 - 2\sqrt{V_f/\pi}\right)\times$$
$$\left[1 + \frac{l}{h}\sqrt{\frac{\left(1-V_f\right)\sum_{j=1}^{N} l_j \cos^2\beta_j}{\left(1-2\sqrt{V_f/\pi}\right)\sum_{j=1}^{N} l_j} + \frac{\sum_{j=1}^{N} l_j \sin^2\beta_j}{\sum_{j=1}^{N} l_j}} + \frac{l}{b}\sqrt{\frac{\left(1-V_f\right)\sum_{j=1}^{N} l_j \sin^2\beta_j}{\left(1-2\sqrt{V_f/\pi}\right)\sum_{j=1}^{N} l_j} + \frac{\sum_{j=1}^{N} l_j \cos^2\beta_j}{\sum_{j=1}^{N} l_j}}\right]^2$$

(2.22)

for a laminated composite of N layers. The thickness of the jth layer is l_j. In the jth layer the fibre orientation with respect to the y axis is β_j. The laminate length and breadth are h and b respectively.

2.5.4 Three Dimensional Diffusion Model

The edge correction factors are generally only applicable for the determination of D in the 3D case. If a full absorption model is required for a finite sized specimen then the three-dimensional Fickian model must be used [2.79]:

$$m_t = m_m - (m_m - m_i)\left[\frac{8}{\pi^2}\right]^3 \sum_{K=1}^{\infty}\sum_{L=1}^{\infty}\sum_{M=1}^{\infty}\left[(2K-1)^2(2L-1)^2(2M-1)^2\right]^{-2}$$
$$.\exp\left[-\left[(2K-1)^2\left(\frac{\pi}{2l}\right)^2 + (2L-1)^2\left(\frac{\pi}{2h}\right)^2 + (2M-1)^2\left(\frac{\pi}{2b}\right)^2\right]Dt\right] \quad (2.23)$$

where K, L and M are positive integers.

2.6 Experimental Techniques for Achieving and Quantifying Ageing

The variety of tests reported in the literature illustrates the lack of test standards available and the lack of flexibility in the existing standards for conducting a thorough investigation into the effects of hygrothermal ageing on composite materials. A short review of the available test standards is given in Appendix A. Exposure conditions and techniques have therefore been tailored by researchers to meet the requirements of their individual test programmes.

Moisture absorption is generally achieved by immersion in fresh water [e.g. 2.3, 2.6 – 2.8, 2.16, 2.24 – 2.26, 2.32, 2.33, 2.46, 2.56, 2.61, 2.62, 2.80, 2.81], sea water [e.g. 2.6, 2.7, 2.55, 2.60, 2.63] or by exposure to a prescribed level of humidity [e.g. 2.2, 2.3, 2.6 – 2.8, 2.24, 2.56 – 2.59, 2.71, 2.75, 2.78, 2.82, 2.83]. Elevated temperature is usually employed to either accelerate the absorption process or to simply to investigate the effects of increasingly high temperatures. The degree to which the temperature can be raised to accelerate the process and still maintain ageing mechanisms representative of the service temperature depends on the resin system, its T_g and cure history.

The effects of high humidity at high temperature seem to be less harsh than immersion at high temperature. There are several reports in the literature of accelerated ageing using boiling water [e.g. 2.69, 2.84, 2.85], but in only one case [2.84] has it been claimed that this ageing condition gives the same effects as natural weathering. In most cases it has been found that boiling induces excessive damage in the form of bared fibres and voids. Immersion temperatures more commonly range from room temperature to 90°C and virtual equivalence between immersion and 100% RH has been found [2.7].

Where relative humidity exposure is used rather than immersion, specimens are usually exposed to a prescribed constant level of humidity at a prescribed constant temperature, both being raised as far as possible if accelerating the ageing process is the aim of the test. This single stage conditioning technique is most commonly applied, but two-stage and three-stage methods have also been developed [e.g. 2.78, 2.82, 2.83, 2.86], which achieve the required moisture content in the minimum length of time and have the ability to produce moisture gradients within the materials similar to those achieved from long-term natural exposure in one twentieth of the time. The concept involves driving moisture rapidly into the centre of the laminate using a high initial humidity level, until the central plies have reached the required moisture content. A second, low humidity drying step can then be introduced to reduce the excess moisture content in the outer plies, before adjusting the through thickness moisture distribution by completing the conditioning at the humidity level corresponding to the required final moisture content. The total conditioning time can be reduced further if a moisture content 95% of saturation is acceptable [2.82, 2.83]. This has been shown to result in less than 1% difference in the final aged structural properties. Figure 2.4 illustrates the single stage, two-stage and three-stage accelerated ageing methods. Although the multi-stage concept is simple, few examples exist of its application in the literature because a high level of mathematical modelling capability is required to define each stage of conditioning.

Moisture uptake is most commonly determined by a gravimetric technique, whereby percentage mass gain with respect to the dry specimen mass is assumed to be the mass of moisture absorbed. Specimens are usually dried before exposure either by air-circulating oven or in a dessicator, with occasional reference to the appropriate preconditioning standard [e.g. ASTM D570. Appendix A].

In order to quantify the effects of ageing on mechanical properties, mechanical testing is usually carried out on specimens removed from their ageing environment as this is the simplest approach, requiring no modification to any existing dry specimen test set-up. This is an ideal approach if comparative results of residual properties after ageing are all that are required and any effects of desorption during mechanical testing can be ignored. There are several reports in the literature [e.g. 2.59, 2.75, 2.78] of mechanical tests carried out at elevated temperature after hygrothermal ageing. This is also acceptable if the effects of elevated temperature are being investigated, but cannot be treated as the best alternative to testing within the hygrothermal environment as desorption during testing (and hence recovery of properties) is likely to occur.

There are several examples in the literature of mechanical loading being applied during hygrothermal exposure [e.g. 2.26, 2.46, 2.50, 2.55, 2.57, 2.60, 2.61, 2.63, 2.64]. The majority of these cases of combined loading/conditioning are achieved through immersion in water or sea water, rather than in a high relative humidity environment. This is because it is more feasible to mount a specimen inside a water filled container or bag before inserting it into the test machine rather than using a purpose-built environmental test chamber. In some cases, load frames have been constructed incorporating tanks. Static and fatigue loading in tension, compression and flexure have all been achieved in this way.

2.7 Summary

The literature which has been reviewed in this chapter is by no means exhaustive. However, the papers included here give a good indication of the extent of work that has been undertaken.

On the experimental side, little work has been reported on combined loading and conditioning in an elevated temperature and relative humidity environment, particularly using multi-stage accelerated ageing techniques. Choqueuse *et al* [2.41] also note that long-term immersion data are lacking and that the acceleration procedures necessary to obtain such data are not well established. The literature reports a variety of non-generalised approaches and it is evident that there must be perseverance in the search for a universal model. Little work has been published on ageing of sandwich materials and even less on structural components rather than small test coupons. One reference [2.87] examines 'structural elements' but these are monolithic laminate specimens of 32mm thickness. Much emphasis has been placed on the determination of moisture ingress and ageing mechanisms in fibre reinforced polymers, but similar work on sandwich core materials, particularly foams, is very limited.

This evidence suggests that there is scope for much further experimental work on sandwich structural components, such as tee-joints, beams or large structural panels in addition to detailed work on foam core materials. A necessary step in such a programme of work would be to link the observed ageing mechanisms in small material coupons to the overall ageing process of a larger structure. The use of materials data in the structural context is an approach has not been explored in detail to the author's knowledge.

Finite element analysis approaches and theoretical models linking environmental conditions to mechanical property degradation appear to be few and limited. None of those sourced in literature searches appeared to be directly relevant to this area of work. The use of numerical modelling in structural analysis of unaged composites is well documented and widely employed. To use experimentally derived aged material properties with numerical modelling and to combine this with experimental analysis of aged sandwich structural elements would therefore be a unique approach and would contribute significantly to the limited knowledge in this area.

A significant knowledge base on composite tee joints has been built up at the University of Southampton and for this reason it was decided that a programme of work on hygrothermal ageing of sandwich tee joints and sandwich materials would be appropriate. A short review of the literature on tee joints therefore follows (Chapter 3).

2.8 References

[2.1] **Shirrell, D., Halpin, J.**; *Moisture Absorption and Desorption in Epoxy Composite Laminates*; Composite Materials: Testing and Design (4th Conference), ASTM STP 617, ASTM 1977

[2.2] **Browning, C.E., Husman, G.E., Whitney, J.M.**; *Moisture Effects in Epoxy Matrix Composites*; Composite Materials: Testing and Design (4th Conference), ASTM STP 617, ASTM 1977

[2.3] **Shirrell, D.**; *Diffusion of Water Vapour in Graphite/Epoxy Composites*; Advanced Composite Materials - Environmental Effects, ASTM STP 658 (J.R. Vinson, Ed.), ASTM 1978

[2.4] **Springer, G.S.**; *Environmental Effects on Epoxy Matrix Composites*; Composite Materials: Testing and Design (5th Conference), ASTM STP 674 (S.W. Tsai, Ed.), ASTM 1979 pp291-312

[2.5] **Springer, G.S. (Ed.)**; *Environmental Effects on Composite Materials*; Volume 1; Technomic Publishing Co. Inc., 1981

[2.6] **Loos, A.C., Springer G.S.**; *Moisture Absorption of Graphite-Epoxy Composites Immersed in Liquids and in Humid Air*; Journal of Composite Materials, Vol. 13 (April 1979), p131

[2.7] **Loos, A.C., Springer, G.S., Sanders, B.A., Tung, R.W**; *Moisture Absorption of Polyester E-Glass Composites*; Journal of Composite Materials, Vol. 14 (April

1980), pp142-154

[2.8] **Whitney, J.M., Browning, C.E.**; *Some Anomalies Associated with Moisture Diffusion in Epoxy Matrix Composite Materials*; Advanced Composite Materials - Environmental Effects, ASTM STP 658 (J.R. Vinson, Ed.), ASTM 1978, pp43-60

[2.9] **Shenoi, R.A., Wellicome, J.F. (Eds.)**; *Composite Materials in Maritime Structures, Volume 1*; Cambridge Ocean Technology Series 4, Cambridge University Press 1993

[2.10] **Smith, C.S.**; *Design of Marine Structures in Composite Materials*; Elsevier Science Publishers Ltd. 1990

[2.11] **Allred, R.E., Lindrose, A.M.**; *The Roomer Temperature Moisture Kinetics of Kevlar 49 Fabric/Epoxy Laminates*; Composite Materials: Testing and Design (5th Conf.), ASTM STP 674, S.W. Tsai (Ed.), American Society for Testing and Materials, 1979, pp313-323

[2.12] **Riccieri, J.E., Hecker, L., De Carvalho, Vasquez, A.**; *Interfacial Properties and Initial Step of the Water Sorption in Unidirectional Unsaturated Polyester/Vegetable Fibre Composites*; Polymer Composites, Feb 1999, V20, 1, pp29-37

[2.13] **Aronhime, M.T., Peng, X., Gillham, J.K., Small, R.D.**; *Effect of Time-Temperature Path of Cure on the Water Absorption of High Tg Epoxy Resins*; J. Appl. Polym. Sci., Vol. 32 (1986), pp3589-3626

[2.14] **Callister, W.D., Jr.**; *Materials Science and Engineering – An Introduction* (2nd Edition); John Wiley and Sons Inc., 1985, 1991

[2.15] **Chamis, C.C., Lark, R.F., Sinclair, J.H.**; *Integrated Theory for Predicting the Hygrothermomechanical Response of Advanced Composite Structural Components*; Advanced Composite Materials - Environmental Effects, ASTM STP 658, ASTM 1978, pp160-192

[2.16] **Aronhime, M.T., Neumann, S., Marom, G.**; *The Anisotropic Diffusion of Water in Kevlar Epoxy Composites*; J. Mat. Sci., Vol. 22 (1987), pp2435-2446

[2.17] **Akay, M., Kongahmun, S., Stanley, A.**; *Influence of Moisture on the Thermal and Mechanical Properties of Autoclaved and Oven-Cured Kevlar 49/Epoxy Laminates*; Composites Sci. and Technology, Vol. 57 (1997), pp565-571

[2.18] **Crank, J.**; *The Mathematics of Diffusion (1st Ed.)*; Oxford University Press, 1956

[2.19] **Barrie, J.A.**; *Diffusion in Polymers*; Trans. IMarE (c), International Conference on Polymers in Marine Environments, Vol. 97, Conf. 2, Paper 12

[2.20] **Boinard, E.**; *Influence of Water on Polymeric Materials used in Marine Applications*; Ph.D. Thesis, Department of Shipp and Marine Technology,

University of Strathclyde, 1998

[2.21] **Marsh, L.L., Lasky, R., Seraphim, D.P., Springer, G.S.**; *Moisture Solubility and Diffusion in Epoxy and Epoxy-Glass Composites*; Environmental Effects on Composite Materials, Vol. 3, Technomic Publishing Co. Inc.

[2.22] **Comyn, J.**; *Interaction of Water with Epoxy Resins*; Polymers in a Marine Environment, 2nd Conf. (IMarE), 1989

[2.23] **Levy, R.L., Fanter, D.L., Summers, C.J.**; *Spectroscopic Evidence for Mechanochemical Effects of Moisture in Epoxy Resins*; J. Appl. Polym Sci., Vol. 24 (1979), pp1643-1664

[2.24] **Birger, S., Moshonov, A., Kenig, S.**; *The Effects of Thermal and Hygrothermal Ageing on the Failure Mechanisms of Graphite-Fabric Epoxy Composites Subjected to Flexural Loading*; Composites, Vol. 20, No. 4, July 1989, pp341-348

[2.25] **Mikols, W.J., Seferis, J.C., Apicella, A., Nicolais, L.**; *Evaluation of Structural Changes in Epoxy Systems by Moisture Sorption-Desorption and Dynamic Mechanical Studies*; Polymer Composites, Vol. 3, No. 3, July 1982, pp118-124

[2.26] **Buck, S.E., Lischer, D.W., Nemat-Nasser, S.**; *The Combined Effects of Load, Temperature and Moisture on the Durability of E-Glass/Vinyl Ester Composite Materials*; 42nd International SAMPE Symposium and Exhibition Proceedings, 1997, Vol. 42, No. 1, pp444-454

[2.27] **Lee, M.C., Peppas, N.A.**; *Water Transport in Epoxy Resins*; Prog. Polym. Sci., Vol. 18 (1993), pp947-961

[2.27] **Guedes, R.M., Morais, J.J.L., Marques, A.T., Cardon, A.H.**; *Prediction of Long Term Behaviour of Composite Materials; Mechanics of Composite Materials and Structures*, NATO Advanced Study Institute, Troia, Portugal, July 12-24, 1998

[2.28] **Huston, R.J.**; *The Effect of Glass Transition Temperature an Interlaminar Shear Strength of Glass Reinforced Epoxy Composites*; Proc. ICCST/3, Int. Conf. On Composites Science and Technology, 11-13 Jan 2000, Durban, S.A.

[2.30] **Jones, F.R.**; *Designing Composites for Durability in Aqueous and Corrosive Environments*; Int. Conf. On Designing Cost-Effective Composites, 15-16 Sept 1998, IMechE Headquarters, London

[2.31] **Tompkins, S.S., Tenney, D.R., Unnam, J.**; *Prediction of Moisture and Temperature Changes in Composites During Atmospheric Exposure*; Composite Materials: Testing and Design (5th Conference), ASTM STP 674, ASTM 1979, pp368-380

[2.32] **Zhou, J., Lucas, J.P.**; *The Effects of a Water Environment on Anomalous*

Absorption Behaviour in Graphite/Epoxy Composites; Composites Sci. and Tech., Vol 53 (1995), pp57-64

[2.33] **Chateauminois, A., Vincent, L., Chabert, B., Soulier, J.P.**; *Study of the Interfacial Degradation of a Glass-Epoxy Composite During Hygrothermal Ageing Using Water Diffusion Measurements and Dynamic Mechanical Thermal Analysis*; Polymer, Vol. 35 (1994), No. 22, pp4766-4774

[2.34] **Shubha, M., Parimala, H.V., Vijayan, K.**; *Moisture Uptake by Kevlar Fibres*; J. Mat. Sci. Letters, Vol. 12 (1993), pp60-62

[2.35] **Penn, L., Larsen, F.**; *Physiochemical Properties of Kevlar 49 Fiber*; J. Appl. Polym. Sci., Vol 23 (1979), pp59-73

[2.36] **Fukuda, M., Kawai, H.**; *Moisture Sorption Mechanism of Aromatic Polyamide Fibers: Diffusion of Moisture in Poly(p-phenylene terepkhthalamide) Fibers*; Textile Research Journal, Vol. 63, No. 4 (1993), pp185-193

[2.37] **Allred. R.E.**; *The Effect of Temperature and Moisture Content on the Flexural Response of Kevlar/Epoxy Laminates*; J. Comp. Mats., Vol. 15 (1981), pp100-116 (Part 1), pp117-132 (Part 2)

[2.38] **Gopalan, R., Rao, R.M.V.G.K., Murthy, M.V.V., Dattaguru, B.**; *Diffusion Studies on Advanced Fibre Hybrid Composites*; J. Reinforced Plastics and Composites, Vol. 5 (1986), pp51-61

[2.39] **Haque, A., Mahmood, S., Walker, L., Jeelani, S.**; *Moisture and Temperature Induced Degradation in Tensile Properties of Kevlar-Graphite/Epoxy Hybrid Composites*; J. Reinforced Plastics and Composites, Vol. 10 (1991), pp132-145

[2.40] **Jones, C.J., Dickson, R.F., Adam, T., Reiter, H., Harris, B.**; *The Environmental Fatigue Behaviour of Reinforced Plastics*; Proc. Royal Society of London, A396 (1984), p315-338

[2.41] **Choqueuse, D., Davies, P., Mazeas, F., Baizeau, R.**; *Ageing of Composites in Water: Comparison of Five Materials in Terms of Absorption Kinetics and Evolution of Mechanical Properties*; High Temperature and Environmental Effects on Polymeric Composites:2nd Volume, ASTM STP 1302, American Society for Testing and Materials, 1997, pp73-96

[2.42] **Shen, C.H., Springer, G.S.**; *Moisture Absorption and Desorption in Composite Materials*; J. Comp. Mats., Vol 10 (1976), pp2-20

[2.43] **Gautier, L., Mortaigne, B., Bellenger, V.**; *Interface Damage Stdy of Hydrothermally Aged Glass-Fibre-Reinforced Polyester Composites*; Composites Science and Technology, Vol. 59 (1999), pp2329-2337

[2.44] **Gellert. E.P., Turley, D.M.**; *Seawater Immersion Ageing of Glass-Fibre*

Reinforced Polymer Laminates for Marine Applications; Composites Part A (Vol. 30 (1999), pp1259-1265

[2.45] **Kellas, S., Morton, J. , Curtis, P.T.**; *The Effect of Hygrothermal Environments Upon the Tensile and Compressive Strengths of Notched CFRP Laminates – Part 1: Static Loading*; Composites, Vol. 21, No. 1 (1990), pp41-51

[2.46] **Karama, M., Touratier, M., Pegoraro, P.**; *Tests of Accelerated Ageing of Composite Materials in Shipbuilding*; Proc. 9th International Conference on Composite Materials, pp532-539

[2.47] **Lyle, A.R., Collins, M.H.**; *Predicting Water Uptake in Polymeric Materials*; Polymer Communications, Vol. 29 (1988), pp307-309

[2.48] **Lee, W.M.**; *Water Vapour Permeation in Closed Cell Foams*; J. Cellular Plastics, Vol. 9 (1973), pp125-129

[2.49] **Cervenka A., Batt A.M., Grieveson B.M.**; *Interaction of Polyurethane Foams with Water and its Effect on Material Properties*; Trans. IMarE (c), International Conference on Polymers in Marine Environments, Vol. 97, Conf. 2, Paper 15, 1989

[2.50] **Clark S.D., Shenoi R.A., Allen H.G.**; *Effect of Moisture on the Fatigue Performance of FRP Sandwich Beams*; FRC 98, 15-17 April 1998, Newcastle, England

[2.51] **Granville D.M.**; *Moisture Effects of Polymethacrylimide Foam and Honeycomb Core in Sandwich/Skin Structures*; Proc. 43rd Annual National Forum and Technology Display of the American Helicopter Society, St. Louis, Mo, May 1987, pp907-914

[2.52] **Ishai O., Hiel C., Luft M.**; *Long-term Hygrothermal Effects on Damage Tolerance of Hybrid Composite Sandwich Panels*; Composites, Vol. 26, No. 1, 1995, pp47-55

[2.53] **Lyle A.R., Collins M.H.**; *Syntactic Foam as a Structural Material in a Marine Environment*; Trans. IMarE (c), International Conference on Polymers in Marine Environments, Vol. 97, Conf. 2, Paper 15, 1989

[2.54] **Cise D.M., Lakes R.S.**; *Moisture Ingression in Honeycomb Core Sandwich Panels: Directional Aspects*; Journal of Composite Materials, Vol. 31, No. 22, 1997

[2.55] **Macander, A., Silvergleit, M., Edelstein, H.P.**; *Marine Durability of a Graphite/Epoxy Composite Subjected to Static and Fatigue Loading*; 3rd International Conference on Mechanical Behaviour of Materials (ICM 3), Vol. 2, pp333-343, Cambridge, England, August 1979

[2.56] **Shen, C.H., Springer, G.S.**; *Effects of Moisture and Temperature on the Tensile Strength of Composite Materials*; Journal of Composite Materials, Vol. 11, January 1977, p2.

[2.57] **Ho, Renton, Schapey**; *The Environmental Effects on the Fatigue Behaviour of AS/3501-6 Material*; Advanced Composites, Special Topic, Paper Presented at Conference, El Segundo, California, 1980, pp142-160

[2.58] **Garrett, R.A., Bohlmann, R.E., Derby, E.A.**; *Analysis and Test of Graphite/Epoxy Sandwich Panels Subjected to Internal Pressures Resulting from Absorbed Moisture*; Advanced Composite Materials, Environmental Effects, ASTM STP 658, ASTM 1978, pp234, 253

[2.59] **Cinquin, J., Abjean, P.**; *Correlation Between Wet Ageing, Humidity Absorption and Properties on Composite Materials Based on Different Resins Family*; 38th International SAMPE Symposium, May 10-13, 1993, pp1539-1551

[2.60] **Smith, L.V., Weitsman, Y.J.**; *The Immersed Fatigue Response of Polymer Composites*; International Journal of Fracture, Vol. 82, pp31-42, 1996

[2.61] **Watanabe, M.**; *Effect of Water Environment on Fatigue Behaviour of Fibreglass Reinforced Plastics*; Composite Materials: Testing and Design (5th Conference), ASTM STP 674, pp345-367

[2.62] **Vauthier, E., Chateauminois, A., Bailliez, T.**; *Hygrothermal Ageing and Durability of Unidirectional Glass/Epoxy Composites*; Proc. 10th International Conference on Composite Materials, Vol. 6, pp185-192

[2.63] **Sloan, F.E., Seymore, R.J.**; *The Effect of Seawater Exposure on Mode I Interlaminar Fracture and Crack Growth in Graphite/Epoxy*; Journal of Composite Materials, Vol. 26, No. 18, 1992

[2.64] **Rehfield, L.W., Briley, R.P., Putter, S.**; *Dynamic Tests of Graphite/Epoxy Composites in Hygrothermal Environments*; Composites for Extreme Environments, ASTM STP 768, ASTM 1982, pp148-160

[2.65] **Farley, G.L., Herakovich, C.T.**; *Influence of Two-Dimensional Hygrothermal Gradients on Interlaminar Stresses Near Free Edges*; Advanced Composite Materials - Environmental Effects, ASTM STP 658 (J.R. Vinson, Ed.), ASTM 1978, pp143-159

[2.66] **Hancox, N.L.**; *A Review of the Effects of Temperature and Environment on the Performance of Polymer Matrix Composite Properties*; AEA Technology (Report Produced for DTI), January 1997

[2.67] **Speake, S.D., Gibson, A.G., Hale, J.M.**; *Failure of GRP in High Temperature Marine Environments*; FRC '98 – Consolidating New Applications, 7th Int. Conf.

On Fibre Reinforced Composites, 15-17 April 1998, Newcastle

[2.68] **Curtis, P.T., Moore, B.B.**; *The Effects of Environmental Exposure on the Fatigue Behaviour of CFRP Laminates*; Composites, Vol. 14, No. 3 (1983), pp294-300

[2.69] **Zhang, Y., Liao, Z., Liu, P.**; *Study on the Behaviour of Accelerated Ageing Fabric Reinforced Epoxy Composites*; 29th International SAMPE Technical Conference, Oct 28-Nov 1, 1997, Vol. 29, pp197-206

[2.70] **Collings, T.A., Stone, D.E.W.**; *Hygrothermal Effects in CFC Laminates: Damaging Effects of Temperature, Moisture and Thermal Spiking*; Composite Structures, Vol. 3 (1985), pp341-378

[2.71] **Hofer, K.E., Stander, M., Bennett, L.C.**; *Degradation and Enhancement of the Fatigue Behaviour of Glass/Graphite/Epoxy Hybrid Composites after Accelerated Ageing*; 32nd Annual Technical Conference, 1977, Reinforced Plastics/Composites Institute, The Society of the Plastics Industry, Inc., Section 11-F, pp1-8

[2.72] **Zaffaroni. G., Cappalletti, C., Mariani, U., Rigamonti, M.**; *Hot, Wet Ageing of a Glass Reinforced Epoxy Resin*; ECCM8, Science, Technologies and Applications, 3-6 June 1998, Naples, Italy, Vol. 3

[2.73] **Challis K.E., Hall D.J., Paul D.B.**; *A Novel Method for Determining the Temperature Dependence of Shear Properties of Structural Foams*; Cellular Polymers 5, 1986, 91-101

[2.74] **Challis, K.E., Hall, D.J., Hilton, P.R., Paul, D.B.**; *Thermal Stability of Structural PVC Foams*; Cellular Polymers, Vol. 5 (1986), pp103-121

[2.75] **Valentin, D, Paray, F, Guetta, B.**; *The Hygrothermal Behaviour of Glass Fibre Reinforced PA66 Composites: A Study of the Effect of Water Absorption on their Mechanical Properties*; Journal of Materials Science, Vol. 22 (1987), pp46-56

[2.76] **Shanker Singh, K., Singh, P.N., Rao, R.M.V.G.**; *Hygrothermal Effects on Chopped Fibre/Woven Fabric Reinforced Epoxy Composites. Part A: Moisture Absorption Characteristics*; J. Reinforced Plastics and Composites, Vol. 10 (1991), pp446-456

[2.77] **Carter, H.G., Kibler, K.G.**; *Langmuir-Type Model for Anomalous Moisture Diffusion in Composite Resins*; J. Comp. Mats., Vol. 12 (1978), pp118-131

[2.78] **Ciriscioli, P.R., Lee, W.I., Peterson, D.G., Springer, G.S.**; *Accelerated Environmental Testing of Composites*; Journal of Composite Materials, Vol. 21, March 1987, pp225-242

[2.79] **Fellows, L.M.P.**; *Moisture Absorption in Low-level Porosity Thermoplastic Toughened Epoxy Composites*; Ph.D. Thesis, Department of Engineering Materials, University of Southampton, 1999

[2.80] **Bouadi, H., Sun, C.T.**; *Hygrothermal Effects on Structural Stiffness and Structural Damping of Laminated Composites*; J. Mat. Sci., Vol. 25 (1990), pp499-505

[2.81] **Juska, T**; *Effect of Water Absorption of Fiber/Matrix Adhesion*; Proc. American Society for Composites, 7th Technical Conference, Oct 13-15 1992, Pennsylvania, pp238-246

[2.82] **Collings, T.A.**; *Moisture Management and Artificial Ageing of Fibre Reinforced Epoxy Resins*; Royal Aerospace Establishment Report (unknown reference)

[2.83] **Unknown Authors**; *Environmental Effects in the Testing of Composite Structures for Aircraft*; Royal Aerospace Establishment Report to the Composites Research Advisory Group (CRAG), 1987

[2.84] **Eurin, P., Marechal, J.C., Cope, R.**; *Barriers to the Prediction of Service Life of Polymeric Materials*; Problems in Service Life Prediction of Building and Construction Materials, NATO ASI Series E: Applied Sciences No. 95, 1985, pp21-40

[2.85] **Tsotsis, T.K., Lee, S.M.**; *Long-term Durability of Carbon and Glass Epoxy Composite Materials in Wet Environments*; J. Reinforced Plastics and Composites, Vol. 16 (1997), pp1609-1621

[2.86] **Collings, T.A., Copley, S.M.**; *On the Accelerated Ageing of CFRP*; Composites, Vol. 14 (1983), p180-188

[2.87] **Cappalletti, C., Rivolta, A., Zaffaroni, G.**; *Environmental Effects on Mechanical Properties of Thick Composite Structural Elements*; J. Composites Technology and Resaerch, Vol. 17 (1995), pp107-114

3. REVIEW OF THE LITERATURE ON THE MECHANICS OF SANDWICH CONSTRUCTION TEE JOINTS

Joints are necessary in composite structures due to design requirements and for practicality in production. A composite construction of any kind must be designed such that loads imposed during service are efficiently transferred around the structure. In marine craft for example, hydrostatic and dynamic pressure loads on the hull must be transmitted in an out of plane direction through the stiffeners and bulkheads, preventing excessive bending of the hull. The joint between two orthogonal structural members, such as between a bulkhead and the hull, is known as a *tee joint* or T-joint, because of its geometry. Large, complex composite structures cannot be formed in a single production process, requiring orthogonal structural members to be added in a second production step. In a marine craft, the hull shell would be formed in the initial production process and the bulkheads would then be lowered into position and bonded or laminated into place.

The tee joint is formed using secondary bonds and therefore has inherent weaknesses associated with it, both due to the stress concentrations which are created by the joint geometry and due to the lack of fibre reinforcement across the bond lines. A lack of bond ductility and the crack-arresting action of fibres can result in rapid propagation of small areas of debonding, resulting in catastrophic failure [3.1]. It is therefore necessary to be able to understand its load transfer mechanisms and how these are affected by variation of the geometrical parameters and hygrothermal exposure, so that an efficient, durable design is the result.

An array of literature exists on the subject of the design and analysis of tee connections in composite structures and a review paper of the earlier work (pre-1995) has been published by Junhou and Shenoi [3.2]. Single skin structures have been studied in detail using a variety of experimental and numerical techniques, but there is scope for developing a greater understanding of the performance of sandwich construction tee joints. The following sections outline the major findings from the literature on composite construction tee joints.

3.1 Single Skin Laminated Tee Joints

The typical geometry of a single skin tee joint is shown in Figure 3.1. The flange represents the laminate of the hull in a marine craft and the web represents a bulkhead.

The joint between the two is formed using a thixotropic structural resin, possibly with a filler additive such as colloidal silica, which makes a fillet between the two orthogonal members on each side of the joint. This is usually laminated over on each side using a FRP tape (the overlaminate).

The literature virtually exclusively focuses on the analysis of the performance of joints of varying geometry under different modes of loading, in order to establish the best configuration with respect to structural performance and ease of production. The web and flange constructions are specified to meet structural design requirements, so the performance of the joint can only be assessed on the basis of the following parameters:

- Overlaminate material and thickness;
- Length of overlaminate overlap;
- Fillet radius;
- Fillet and/or filler material;
- Size of gap between base of web and flange;
- Shape of the base of the web (e.g. to reduce stress raisers).

The impact of these parameters on joint structural performance was first investigated by Shenoi, Hawkins and co-workers [3.1, 3.3, 3.4], prompted by the lack of a rigorous design procedure. The standard plate members, around which the joints were formed, were 15 plies of glass woven roving, wet laminated with polyester resin.

The load configuration was a pull-off at 45° to the flange, to simulate the combined bending and vertical tension applied to a joint within a tank structure subject to hydrostatic pressure. In the experiments, the flange was clamped while the 45° tensile load was applied to the free end of the web. Static tests were performed in displacement control up to failure.

The indications were that

- Increasing the gap between the base of the web and the flange allowed greater deflections for a given load and hence a greater energy absorption prior failure;
- Bevelling the end of the web reduced joint stiffness and increased the failure load;
- The presence of an overlaminate increased stiffness and failure load;

- Increasing the overlaminate overlap slightly increased the stiffness and strength, but reduced the deflection to failure, reducing the energy absorbed at failure by the joint;
- Increasing the overlaminate thickness above three plies had no effect on strength but increased stiffness and hence reduced energy absorption;
- Increasing the fillet radius had little effect on stiffness but significantly increased failure load.

A numerical analysis was carried out [3.1, 3.4] using three dimensional finite element modelling in ANSYS. The laminae were modelled using eight-noded layered solid elements and the fillet material was represented using an isoparametric three-dimensional solid element with large deflection and plasticity capabilities. The models were run using combinations of linear and non-linear material properties and small and large deflection analyses, and for certain joint geometries the divergence of the non-linear/large deflection results from the linear/small deflection results was significant. The analysis of the stress patterns within the joint allowed a qualitative assessment of the failure paths to be made but was of limited value because of the inadequate and incomplete nature of basic material data.

An assessment of joint 'efficiency' was made on the basis of the experimental and numerical results, which suggested that there was an optimum case for which the peak stress in the fillet and the through thickness stress in the overlaminate both reach their respective limits at the same load. Efficiency was therefore defined as the ability of the joint to remain integral and intact at as high a load and for as a high a deflection as possible, i.e. peak stresses must be as low as possible for a given load and deflection. This condition was fulfilled by the configuration having a large fillet radius, a flexible fillet material and a very thin overlaminate, suggesting that the traditional criterion for design of a thick overlaminate, could be detrimental to the joint efficiency, and that the fillet radius, given little consideration in design codes, could be critical to the performance of the joint. As a consequence of the findings, a significant reduction in structure weight and production cost would also occur.

Further work has focused on fatigue performance. Service experience on FRP ships indicates that fatigue damage (e.g resin cracking and fibre debonding initiating at stress raisers such as holes and hatch corners) usually remains localised and has a negligible

effect on the overall structural performance. However, at structural connections, particularly out-of-plane joints, fatigue is likely to present serious problems [3.2].

Junhou and Shenoi [3.2] report early (1972) work by Dixon *et al* [3.5] who investigated the static and fatigue response of top-hat (trapezoidal section), tee- and angle joints. The findings from the fatigue work were that crazing and delamination occurred at low numbers of cycles and fatigue caused progressive loss of stiffness but had no significant effect on residual static strength. Interestingly, the work by Dixon *et al* also presents an investigation into the effects of water immersion and elevated temperature on the fatigue performance of top-hat stiffener joints. Tests were stopped after a relatively short time due to extensive delamination damage and it is stated [3.2] that the results support the need for further study. To the author's knowledge, no further work of this type has been published.

Following the dry fatigue work of Dixon *et al*, Junhou and Shenoi report other results from the tee-joint literature, which indicate that

- The fatigue strength of the joint is dependent on the strength of the resin;
- Delamination and crack initiation occur at low tensile loads and low numbers of cycles;
- Cracks tend to develop between layers of reinforcement and particularly in the bond lines of the joints;
- Fatigue does not affect the static tensile strength.

Further work by Shenoi, Hawkins and Read focused on the identification of fatigue failure mechanisms in single skin tee joints [3.6, 3.7]. Using the same joint configuration as in the previous static work, fatigue loads were applied in the form of a sinusoidal cycle between zero and a constant maximum 45° pull-off load of 90%, 70%, 50% or 30% of the ultimate joint strength. The fatigue curves exhibited the characteristic inverse S-shape of FRP materials. The overall findings from the work were:

- The crack propagation path and failure mode are the same under cyclic and static loading and were consistent with internal stress patterns obtained from FEA modelling;
- Damage accumulation during fatigue causes degradation in stiffness;
- There may be a threshold value of the applied load, above which the fatigue process is geometry dependent and below which it is material dependent.

Scatter in the results was greater in joint configurations that were more production sensitive and prone to defects from which fatigue cracks could propagate (e.g. thick overlaminate). In general, failure was found to occur through a delamination in the overlaminate on the tension side followed by disbond of the fillet from the overlaminate, leading to static failure of the fillet resin.

In order to further characterise the performance of single skin tee joints under a 45° pull-off load case, Shenoi, Read and co-workers applied full-field experimental stress analysis techniques to obtain more detailed information about the stress/strain distribution and load path in the joints [3.7 - 3.9]. Two techniques were used with success.

The first, thermoelastic stress analysis, involved the use of an infra-red detector (the SPATE 9000 system – Chapter 6) to measure the temperature change induced in the specimens when subjected to an elastic cyclic stress. A scanned 'thermal' image of the stressed joint surface could then be calibrated to obtain real stress values and directly compared with the results of the FEA. This technique is described in detail in Chapter 6 and the work described here was its first qualitative application to composite constructions.

The second technique employed was photoelastic stress analysis. A thin birefringent coating was bonded to the surface of the joint. This had a thickness of 0.5mm and was bonded to the tee joints using a reflective epoxy adhesive. When the joint was loaded the strains in the joint were fully transferred to the coating. The analysis was performed using a reflection polariscope.

For the thermoelastic work, the joints were loaded to 1.7±0.7 kN at 8Hz in a 45° pull-off mode. For the photoelastic work, the joints were statically loaded to 1.4 kN, i.e. the load range of the thermoelastic work. The resulting stress contours confirmed that the load transfer was primarily through the in-plane stress path in the overlaminate. A second significant finding was that the through thickness strain in the overlaminate was very high. This is consistent with the previous experimental programmes, which showed that failure occurred through delaminations/disbonding of the overlaminate.

Further numerical modelling was carried out, this time using a two-dimensional plane elasticity approach and non-linear geometric and material characteristics in the fillet. This was compared with the thermoelastic results and showed good agreement. In general the

finite element model gave higher values than the thermoelastic results and this was attributed to inadequate manufacturer's material property values used in the FEA. There was almost exact agreement in the distribution of the stresses. The full field data from the thermoelastic work was able to show the transition between the different layers in the overlaminate material and the relative load carrying capacity of each part of the tee joint construction.

An example of the analysis of aerospace tee joints is given by Rispler *et al* [3.10], typical of wing/inlet connections, composite spars and hinge/spar connections. The investigation concerned test specimens made from unidirectional carbon/epoxy pre-preg, having web thicknesses of between 2 and 10mm. The construction of the joints was different to the marine applications, whereby the material was laid up around two angle bars to form two uncured parts of right angle section. These were then placed on a flat plate and contacted face to face such that the double thickness of material between the angle bars formed the web. At this point the flange was half the thickness of the web, but eventually had an additional four plies bonded to its flat underside. This construction results in a triangular resin rich region at the centre of the joint, where the two halves of the web part and form the flange. The purpose of the investigation was to determine the effect of small, cylindrical inserts in this resin-rich region, which were considered to improve the out-of-plane load transfer capacity of the joints.

An experimental analysis was conducted, supported by a 2-D plane strain linear finite element analysis. The mode of loading was 'tension', i.e. clamping the flange while a load was applied to the free end of the web, vertically upwards in the plane of the web. The initiation of failure was found to be dominated by the resin properties and the radius between the web and the flange. Failure initiated just above the resin rich area in the centreline of the web. The inserts were found to be detrimental in the thinnest specimens but were of benefit in the thickest, redistributing the stresses such that delamination in the web was delayed.

3.2 Sandwich Construction Tee Joints

The sandwich tee joint is generically the same as the single skin joint, except that the web and flange are of sandwich construction, as shown in Figure 3.2. The connection is formed in essentially the same way, with a filled gap at the base of the web and a resin fillet either side of the web, which is overlaminated with the required number of plies of fibre

reinforced resin. It should be noted that the wood insert shown in the figure is often used in test pieces to prevent local failure of the core when loaded by the test machine, but is not present in the vessel construction.

Continuing the programme of work on single skin tee joints, some of the significant contributions to sandwich tee joint work originate from the University of Southampton. The other two main sources are collaborative work between the National Technical University of Athens and the Norwegian Institute of Technology, and collaborative work between KTH Stockholm and Aalborg University, Denmark. It should be noted that in all cases, the core material is structural closed cell PVC foam, primarily in marine applications.

Little other work in this area has been published, though some early findings are summarised by Junhou and Shenoi [3.2]. General findings were that for compressive and tensile loading (in the plane of the web) designs with fillets showed higher static strength and stiffness compared to designs with no fillets; and failure was mainly dominated by the core in compression and bending.

Similar results were observed by Shenoi and Violette [3.11], who examined the effects of joint geometry on performance. In this case the imposed loads of interest were hull pressure loads and slamming pressure loads, approximated by loading the joints in compression with the flange simply supported and a load applied to the top of the web in the plane of the web. The geometries considered had a thin overlaminate and included joints with a filler fillet radius of either 10, 25 or 40mm, triangular foam 'fillets' or with a trapezoidal foam pad between the web and flange. The skin laminates in this work were E-glass woven rovings in epoxy resin.

In the experimental work, the highest failure load was exhibited by the joint with the foam pad, followed closely by the 10mm fillet. The lowest failure load was exhibited by the joint with the triangular foam fillet. Shenoi and Violette presented performance indices with respect to weight efficiency (weight/strength and weight/deflection ratios), production efficiency and material cost efficiency. These were used to determine the best overall joint configuration that, for compressive loading, was found to be the 10mm fillet configuration, followed by the foam pad configuration. The triangular foam insert and filler fillet of large radius were found to be the least efficient.

Shenoi and Violette also presented analytical approaches, which combined a sandwich beam theory model with laminated plate theory and buckling characteristics, to predict failure loads and joint behaviour. Comparison between the analytical model and finite element results suggested that the analytical approach was sufficiently accurate for preliminary design purposes.

A further static test programme was reported for similar joints by Hicks *et al* [3.12], which focused on mechanical behaviour of a single geometry joint (30mm fillet radius, 4mm overlaminate thickness) in both compression (clamped and simply supported) and 45° pull-off. Additional joint geometries and the effects of varying geometric parameters were investigated by Shenoi *et al* [3.13]. In the 45° pull-off mode, failure occurred catastrophically through cracking of the fillet and web core, with some delamination and disbonding of the overlaminate on the tension side. In compression (simply supported), the joint failed by a progressive accumulation of damage, with strength degradation occurring after failure of the fillet resin, followed by cracking through the thickness of the overlaminate at the top of the fillet, buckling of the flange inner skin at the point of contact between the web skins and the flange, and bulging of the foam core adjacent to these areas. Under clamped compression, the failure was catastrophic, with global buckling of the web. The failure loads in compression were significantly greater than in bending/tension.

Three dimensional finite element work by Hicks *et al* and Shenoi *et al* allowed the stress distribution to be analysed and the progression of failure to be identified by examination of the relative stress magnitudes within the joint. Layered solid elements were used for the laminae while a three dimensional solid was used for the isotropic materials (foam and fillet). The 45° pull-off was run using a large deflection analysis while the compression loadings were run using a small deflection analysis.

In compression, the maximum stresses in the core materials were found to be adjacent to the top of the fillet in the web and adjacent to the points of contact of the web skins in the flange, concurring with the observation of compression failure in these locations. High stresses in the fillet near the interface with the web skins and overlaminate suggested that cracking would initiate from this region. High interlaminar tensile stresses in the overlaminate near the top of the fillet (adjacent to the web) suggested that delamination would initiate at this point and would result in buckling when combined with high in-plane stresses.

In 45° pull-off, the highest relative stresses were located at the bottom corner of the web core on the tension side, suggesting that failure initiated from this point in the form of core shear, followed by cracking at 45° through the fillet from the corner of the web to mid-radius on the tension side and delamination of the overlaminate, where high interlaminar stresses were found to exist. The dominance of the web in all the failures was thought to be because of its proximity to the flange (i.e. no filled gap as in Figure 3.2).

A finite element parametric study was carried out by Shenoi *et al*, to investigate variation in fillet radius from 5 to 40mm and variation in overlaminate thickness from 0 to 6mm, for compression (in the plane of the web), 45° pull-off (tension/bending), 90° pull-off (bending) and tension (in the plane of the web). Increasing the fillet radius and overlaminate thickness both had the effect of stiffening the joint and reducing the stresses in all joint components for the bending modes. In tension, there was an interdependency between the overlaminate thickness and fillet radius, requiring further clarification.

The 45° pull-off mode was further analysed using thermoelastic stress analysis by Dulieu-Smith *et al* [3.14], which was the first application of the technique to sandwich structures. Further details of this technique are given in Chapter 6 and are described briefly in Section 3.1 above. The experimental work was supported by two-dimensional finite element analysis with non-linear geometric properties (large deflection) using ANSYS. Good qualitative correlation between the static tests, FEA and thermoelastic work was found, though the FEA under predicted stresses compared to the thermoelasticity by up to 60%. This could have been attributed to deficiencies in the material properties used for the FEA, however there is clearly scope for further work on the application of the thermoelastic technique to foam sandwich structures.

Comparisons between non-linear FEA and experimental results have also been made by Theotokoglou and Moan [3.15, 3.16], who considered foam sandwich tee joints under tensile loading in the plane of the web. The joints were of PVC foam core construction with E-glass polyester skins and a single ply in the overlaminate, with no fillet. The FEA accounted for non-linear material behaviour in the core and large deflection analysis.

Similar to the findings of Shenoi *et al*, the region of peak stresses occurred at the bottom corner of the web adjacent to the fillet. There was also evidence of high stresses indicating load transfer between the fillet and the overlaminate. The failure was found to initiate at the corner of the web, followed by crack propagation into the web core and through the fillet towards the overlaminate, resulting in delamination. Other failure mechanisms

involved pure shear failure of the core and debonding of the overlaminate from the flange/fillet. These modes of failure agree in general with the work of Shenoi *et al*, highlighting the areas of stress concentration and the path of load transfer. Further experiments with thicker overlaminates suggested that the thickness of the overlaminate has little effect, in agreement with Dodkins *et al* [3.4].

The finite element work was extended to incorporate different overlaminate configurations (two and three layers) for the tensile load condition [3.17]. From this analysis it was found that increasing the thickness of the overlaminate only slightly affected the principal stresses in the bond between the web and flange but significantly reduced the in-plane and interlaminar stresses in the overlaminate. The web and flange core stresses (principal and shear) were not affected by the thicker overlaminate but the FEA predicted a weak decrease in global joint strength, not detected in the experimental work.

This work has been extended further to incorporate a numerical crack design procedure based on fracture mechanics considerations [3.18]. The fracture mechanics study was performed using linear FEA to investigate the cracking at the tee joint connections when subject to tensile loading. A path independent J-integral was used to develop a computational technique for evaluating the critical fracture energy at crack initiation. The localised area of study was at the interface between the overlaminate and the flange, where it was thought that interlaminar cracks could have resulted during manufacture. For linear elastic material behaviour, the J-integral is identical to the energy release rate, which was found to be constant for a range of fillet radii.

Bech and Moan [3.19] considered the performance of sandwich tee joints on a ferry car deck application, where there were concerns about the strength of the joints when subject to localised wheel loads from cars. Static analyses (including a dynamic magnification) were performed for localised loads acting either in the plane of the web (centric) or just off the axis of the web (eccentric). The loads were applied over a small area on the flange outer skin, with supports on the flange inner skin. The centric load case was therefore similar to the tensile load case described in other work but with the load applied towards the joint from under the flange rather than away from the joint at the top of the web. Two specimen geometries were investigated, with either a small filler fillet or a triangular foam 'fillet'. A comparison of all the tests showed that the eccentric load case was more critical than the centric case. There was a moderate strength increase in the joints when the filler fillet was replaced with the triangular foam fillet inserts but the latter would be more expensive to produce. This performance conclusion is contrary to that of Shenoi and

Violette [3.11], who found that the configuration with triangular foam fillets performed worse than any other configuration in compression. This illustrates that it is important to evaluate a range of possible in-service loading modes for each joint geometry under consideration.

Rosander and Burchardt [3.20, 3.21] have conducted an extensive experimental and numerical investigation on the performance of sandwich tee joints loaded in tension symmetrically (by the application of a load in the plane of the web attached to its free end) and anti-symmetrically, in compression and in fatigue. The antisymmetric tensile case involved a similar test set up to symmetric tension, but with a steel bar attached to the top of the web (parallel to the flange), in the style of a cantilever. A rope was attached between the free end of this bar and the test machine crosshead. This is similar to the combined tension/bending mode investigated by Shenoi *et al* and was considered because a 3D numerical analysis of a complete hull structure indicated that there was a bending moment between the hull and bulkhead.

The joints tested were of foam sandwich construction as in previously described investigations. In this case the fillet material was pre-formed from the core material (PVC foam), though this configuration was compared to the more general resin fillet. The foam fillet approach is common practice in Scandinavia in order to simplify the manufacture of the joint [3.22].

For the joints with the foam fillets, the tensile tests were difficult to evaluate because of a rapid catastrophic failure. In compression, core shear was the dominant failure mode, as in three point bending. In fatigue (±25% of ultimate failure load), the tips of the fillet were found to initiate failure. A numerical optimisation was therefore carried out to improve the geometry of the fillet (Figure 3.3), which was intended to introduce a 'spring' into the joint to alleviate stress concentrations at the tips of the fillet. The crack initiation occurred after more cycles than in the original geometry, crack propagation was slower and there was a change in failure mode, but it was concluded that the tests carried out were not sufficient to unconditionally determine that the new fillet geometry was better than the original. The new geometry would evidently be more difficult to manufacture.

An experimental investigation into the influence of various material and geometrical properties on the ultimate strength of the tee joints was also carried out for the symmetrical and anti-symmetrical tensile loading, with supporting linear, non-linear and

fracture mechanics FE analyses. The geometrical and material parameters varied were as follows:

- Fillet radius – constant at 40mm
- Fillet material – different density foam materials or replacement with Crestomer structural adhesive.
- Overlaminate thickness – 'thick' or 'thin'
- Web bonding laminate – with or without addition of 1 layer of CFRP.

In the symmetric load case, use of a thick overlaminate did not significantly increase the strength. By increasing the density of the fillet material, the strength increased. The case with the Crestomer fillet performed well and was easy to manufacture, however it was heavy and had a less satisfactory fatigue strength.

For the antisymmetric load case, failure initiated in thin overlaminate configuration from the end of the web skin, just above the flange (forming a stress concentration), and propagated into the web core, avoiding the fillet. With the thick overlaminate, the failure initiated when the maximum stress was exceeded at a point on the interface between the fillet and overlaminate on the tension side. Increasing the thickness of the overlaminate was found to increase the strength and rotational stiffness.

Results indicated that the overlaminate is integral to the load carrying capability of the tee joint in anti-symmetric loading. In the symmetric load case, the fillet was found to be the primary load carrier and the overlaminate was of less importance. A significant conclusion was that the additional stiffness of the flange skin from the web bonding laminate was integral to the load bearing capability of the joint.

The computational fracture mechanics indicated that the most critical crack location was not the fillet tip adjacent to the flange, as suggested by the FEA, but a location just above this in the lower half of the fillet curve. The main conclusion from the non-linear FEA was that the large extra computational effort gave little reward. The stress distribution did not significantly differ from the linear case, but did provide lower stresses in the core fillet due to the linear limit of the foam being exceeded.

In production, the stress concentration caused by the web skin going all the way down to the flange between the web core and the fillet was usually overcome by 'trapping',

whereby just above the fillet over a length of 200mm, the web skin laminate was tapered down to zero, while over the same region the overlaminate was tapered up from zero to its full thickness. In the fillet region therefore, the fillet foam is bonded directly to the web core and not to the web skin. Changes in vessel production techniques (e.g. resin infusion) have prevented trapping from being employed and an alternative method of alleviating the stress concentration was required.

Having identified the possible stress concentrators at the 'sharp' bulkhead laminate ends, i.e. the corners of the web skins adjacent to the fillet, the strength of the singularities induced by the material corners was calculated using analytical and numerical methods. It was shown that changing the material and geometrical parameters does not significantly change the stress distribution in the tee joint or the strength of the singularity. The analytical results suggested that the introduction of a stiffer filler material would not alleviate the problem and that reducing the elastic modulus of the web core material would increase the stress concentration further, therefore the stiffer and heavier the better. The FEA results indicated that increasing the filler stiffness would increase the stress concentration. Increasing the overlaminate stiffness alleviated the stresses in the foam core fillet but the stress concentration was unaltered. To avoid initiation of failure from the stress concentration a more radical re-design of the joint geometry was recommended.

An alternative tee joint design, containing prefabricated foam beams with dry fibre reinforcement, was therefore proposed, alleviating the stress concentration by continuing the stiff load path from the web skins (Figure 3.4).

3.3 Summary

Extensive investigations have been carried out under a variety of loading modes for single skin tee joints and their response is generally well understood. Sandwich construction presents a much more complex problem and it is evident that there is significant scope for further work on improving the joint geometry.

It is apparent from the literature on sandwich construction tee joints that the stress distribution and resultant failure mode is dependent not only on the material and geometric variables of the joint but also on mode of loading. Contradictions have arisen regarding the best joint geometry in investigations using different loading modes. A significant volume of work exists on the performance of the joints under asymmetric (tension/bending) and

tensile loading but further investigation of the compression mode is required, particularly as this is a dominant mode in slamming. The application of thermoelastic stress analysis has shown potential and warrants further investigation. The effect of hygrothermal ageing on tee joints has not been given further attention since the aborted attempt in the early 70's by Dixon *et al*, and clearly warrants extensive examination.

3.4 References

[3.1] **Shenoi, R.A., Hawkins, G.L.**; *Influence of Material and Geometry Variations on the Behaviour of Bonded Tee Connections in FRP Ships*; Composites, Vol. 23, No.5 (1992), pp335-345

[3.2] **Junhou, P., Shenoi, R.A.**; *Examination of Key Aspects Defining the Performance Characteristics of Out-of-Plane Joints in FRP Marine Structures*; Composites: Part A, Vol. 27 (1996), pp89-103

[3.3] **Hawkins, G.L., Holness, J.W., Dodkins, A.R., Shenoi, R.A.**; *The Strength of Bonded Tee Joints in FRP Ships*; Plastics, Rubber and Composites Processing and Applications, Vol. 19 (1993), pp279-284

[3.4] **Dodkins, A.R., Shenoi, R.A., Hawkins, G.L.**; *Design of Joints and Attachments in FRP Ships' Structures*; Marine Structures, Vol. 7 (1994), pp365-398

[3.5] **Dixon, R.H., Ramsey, B.W., Usher, P.J.**; Proc. Symp. GRP Ship Construction, RINA, London, Oct 1972, p1

[3.6] **Shenoi, R.A., Read, P.J.C.L., Hawkins, G.L.**; *Fatigue Failure Mechanisms in Fibre-Reinforced Plastic Laminated Tee Joints*; Int. J. Fatigue, Vol. 17 (1995), pp415-426

[3.7] **Read, P.J.C.L.**; *Fatigue Characterisation of FRP Structural Tee Joints*; Department of Ship Science, University of Southampton, PhD Thesis, 1997

[3.8] **Read, P.J.C.L., Dulieu-Smith, J.M. and Shenoi, R.A.**; *Thermoelastic and Photoelastic Analyses to Characterise Stresses in FRP Connections*; Proc. Int. Conf. on Composite Science and Technology, 1996, Durban, pp 415-420

[3.9] **Dulieu-Smith, J.M., Quinn, S., Shenoi, R.A., Read, P.J.C.L., Moy, S.S.J.**; *Thermoelastic Stress Analysis of a GRP Tee Joint*; Applied Composite Materials, Vol. 4 (1997), pp283-303

[3.10] **Rispler, A.R., Steven, G.P., Tong, L.**; *Failure Analysis of Composite T-Joints Including Inserts*; J. Reinforced Plastics and Composites, Vol. 16 (1997),

pp1642-1658

[3.11] **Shenoi, R.A., Violette, F.L.M.**; *A Study of Structural Composite Tee Joints in Small Boats*; J. Comp. Mats., Vol. 24 (1990), pp644-666

[3.12] **Hicks, I.A., Read, P.J.C.L., Shenoi, R.A.**; *Tensile, Compressive and Flexural Characteristics of Tee Joints in Foam Cored Sandwich Structures*; Proc. Sandwich Construction 3, 3rd Int. Conf. On Sandwich Construction, Sept1995, Southampton, Vol. 2, pp579-591

[3.13] **Shenoi, R.A., Read, P.J.C.L., Jackson, C.L.**; *Influence of Joint Geometry and Load Regimes on Sandwich Tee Joint Behaviour*; J. Reinforced Plastics and Composites, Vol. 17 (1998), pp725-740

[3.14] **Dulieu-Smith, J.M., Read, P.J.C.L., Shenoi, R.A.**; *Thermoelastic Analysis of Foam Cored Sandwich Construction Tee Joints*; Proc. 11th Int. Conf. on Composite Materials, Gold Coast, Australia, 14-18th July 1997, pp699-708

[3.15] **Theotokoglou, E.E., Moan, T.**; *Non-Linear Behaviour of Sandwich T-Joints*; Proc. Sandwich Construction 3, 3rd Int. Conf. On Sandwich Construction, Sept1995, Southampton, Vol. 2, pp591-601

[3.16] **Theotokoglou, E.E., Moan, T.**; *Experimental and Numerical Study of Composite T-Joints*; J. Comp. Mats., Vol. 30 (1996), pp190-209

[3.17] **Theotokoglou, E.E.**; *Strength of Composite T-Joints under Pull-Out Loads*; J. Reinforced Plastics and Composites, Vol. 16 (1997), pp503-518

[3.18] **Theotokoglou, E.E.**; Study of the Numerical Fracture Mechanics Analysis of Composite T-Joints; J. Reinforced Plastics and Composites, Vol. 18 (1999), pp215-223

[3.19] **Bech, S.M., Moan, T.**; *Behaviour of Sandwich T-Joints under Concentrated Loads*; Proc. Sandwich Construction 3, 3rd Int. Conf. On Sandwich Construction, Sept1995, Southampton, Vol. 2, pp601-612

[3.20] **Rosander, M.**; *T-Joints in Sandwich Structures*; Report No. 97-29, Kungliga Tekniska Hogskolan (KTH), Stockholm, Sweden, 1997

[3.21] **Burchardt, C.**; *Bonded Sandwich T-Joints for Maritime Applications*; PhD Dissertation, Institute of Mechanical Engineering, Aalborg University, Denmark, Special Report No. 32, 1996

[3.22] **Zenkert, D.**; *An Introduction to Sandwich Construction*; Engineering Materials Advisory Services Ltd. (EMAS), 1995, ISBN 0947817778

PART C

SCOPE

4. RESEARCH APPROACH

Based on the findings of Chapters 2 and 3 (see Sections 2.7 and 3.3), this programme of work is based on furthering the knowledge in the area of hygrothermal ageing of foam sandwich materials and structures. Unique aspects of this work are the focus on

- Characterisation of the long-term performance of sandwich materials in a hygrothermal environment, concentrating particularly on closed cell structural foams and 'real' laminates of a typical marine quality;
- The use of existing experimental and numerical techniques for new applications, namely the analysis of hygrothermally aged sandwich structures;
- The link between material and structural behaviour under hygrothermal conditions.

PVC foam cored polymer composite sandwich construction, typical of that employed in small, fast marine craft such as the RNLI Trent Class lifeboat, is the focus of this study. The particular structural detail under consideration is the sandwich tee joint, which characterises the out-of-plane connection between two orthogonal sandwich plates. In marine craft this is typically between a bulkhead and the hull. This element has been chosen as it not only provides a variety of materials to be studied, but an interesting and complex stress regime under load. This work will therefore contribute to the hygrothermal ageing knowledge base (Chapter 2) by introducing the effects of ageing on structures and materials not previously characterised, and also contributes to the tee joint knowledge base (Chapter 3) by introducing the effects of ageing and new applications for experimental techniques that have not been used in this area previously.

The overall aims of the work are therefore to

- Determine the long-term hygrothermal ageing mechanisms in foam cored polymeric composite sandwich materials;
- Perform a detailed analysis of the load transfer mechanisms in foam cored sandwich construction tee joints under a specific load regime;
- Ascertain how the durability of such joints may be affected by exposure to hygrothermal environments, through the analysis of structural elements and knowledge of the constituent material effects.

This chapter gives an overview of the structure of the work carried out and the way in which it fits together. Full details of the materials and structural elements are given in Chapter 5.

4.1 Experimental Programme on the Sandwich Constituent Materials

The aim of this programme is to determine the effects of hygrothermal exposure on the constituent materials that make up the sandwich structure. In this case they are closed-cell PVC foam core materials and fibre reinforced epoxy laminate skins (described in Chapter 5). The moisture uptake characteristics of these materials are monitored in fresh water environments by immersion and exposure to high relative humidity at a temperature of 40°C. The effects of immersion may not only be indicative of composite durability in water contact applications but also of worst-case atmospheric ageing for composites in humid environments [4.1]. Constant temperature exposure is used rather than varying temperature cycles and the temperature is chosen to be well below the glass transition region of the materials. This approach is considered to be the most appropriate as it accelerates the hygrothermal ageing process without changing the mechanisms that would be active at ambient.

The trends in moisture uptake are evaluated in terms of the shape of their curve of mass increase over time. The active mechanisms are hypothesised upon, with supporting evidence from existing models and microscopic examination.

In addition to the moisture uptake monitoring, the changes in material properties due to the ageing process are also determined from a mechanical test programme for materials immersed at 40°C and 60°C. The DMTA (Dynamic Mechanical Thermal Analysis) technique is used to monitor the evolution of the materials' viscoelastic properties during ageing. This yields interesting trends in the evolution of the room temperature stiffness and changes in the glass transition temperature.

4.2 Experimental Programme on Sandwich Construction Tee Joints

Full field stress information is obtained from tee joints loaded in compression using Thermoelastic Stress Analysis (TSA). This work enables the determination of the load

transfer mechanisms within the joints and how these are affected by variations in the joint geometry. Testing of hygrothermally-aged joints is also undertaken. These joints are exposed to high relative humidity at 50°C under a variety if loading conditions, including static, cyclic and unloaded. Thermoelastic results are obtained from these joints at intervals throughout testing, enabling any change in the thermoelastic signal and hence stress state, to be determined. Combined with the results from the hygrothermal ageing of the constituent materials, it is possible to make links between the material effects and global joint behaviour.

The ageing of the joints is carried out in a unique facility in the form of a modular environmental chamber, dedicated air conditioning unit and hydraulic ram arrangement for the mechanical loading of large structural specimens concurrently with hygrothermal exposure.

4.3 Numerical Modelling of Sandwich Construction Tee Joints

Extensive finite element modelling of unaged joints of varying geometries is carried out using ANSYS 5.4 and 5.5. The purpose of this work is primarily to validate the experimental technique, as the use of TSA for the analysis of foam cored sandwich structures has not previously been proven quantitatively. The finite element work also allows more extensive investigation into the effects of slight changes in joint geometry than is possible in the experimental programme.

Further modelling is also undertaken to investigate changes in the response of joints after hygrothermal exposure. In this case, values obtained from the DMTA programme are used to modify material properties in the models. The changes in the joint structural behaviour are compared to those obtained from the experimental programme.

4.4 References

[4.1] **Gellert, E.P., Turley, D.M.**; *Seawater Immersion Ageing of Glass Fibre Reinforced Polymer Laminates for Marine Applications*; Composites: Part A, Vol. 30 (1999), pp1259-1265

5. MATERIALS AND STRUCTURAL DETAILS

This chapter provides information about the construction of the tee joint test specimens and their constituent materials used in the moisture uptake and DMTA experimental programmes. The materials characterisation combines information supplied by the manufacturer with extensive microscopy and image analysis carried out by the author.

5.1 Sandwich Tee Joint Construction

A schematic of a generic sandwich tee joint is shown in Figure 3.2. This is typical of the test specimens used in this work and is characteristic of any out-of-plane joint in sandwich composite marine vehicle structures. The dimensions of the test pieces used in this work are shown in Figure 5.1. The joints in this work are representative of the bulkhead (web) to hull (flange) connections in the RNLI Trent Class lifeboat and were supplied by Green Marine Ltd. of Lymington, a company contracted by the RNLI for production of the Trent Class lifeboats. Full details of all the constituent materials are given in Section 5.2.

During manufacture of a vessel of this type, the outer skin of the hull would be laid up inside the mould first and vacuum consolidated. In this case the material is a GRP/Kevlar hybrid pre-preg (to provide better robustness than GRP alone), which requires an elevated temperature cure. The cross-linked PVC foam core of the hull (flange) is then bonded to the outer skin and the inner skin is then laminated by hand lay-up on top of the core. The inner skin undergoes a lower temperature cure (with vacuum assisted consolidation) because the foam core material cannot withstand the elevated temperature cure.

The bulkhead sandwich (web) is then bonded at right angles to the flange. The web consists of a foam core of the same generic type as the flange, but of a lower density, faced with GRP skins of the same material as the flange inner skin. If, during placement of the web, a gap occurs at its base where it is supposed to touch the flange (due to inconsistencies in curvature between the bulkhead and hull for example), it is usually filled with resin. This detail has important implications as discussed in Chapters 9 and 10.

A fillet is then formed at the joint using a thixotropic resin with a filler additive, and this is overlaminated with layers of GRP tape. A web bonding laminate is used between the web and flange. This consists of a layer of the GRP tape laid up onto the flange inner skin at the position where the web is bonded, to provide extra stiffness in this area.

5.2 Sandwich Materials

This section provides full details of the constituent materials of the sandwich construction that are studied in this work. All material property values given are those quoted by the manufacturers. In some cases, information on the exact composition was not forthcoming, so typical constituents have been assumed. Image analysis work by the author has provided more detailed materials characterisation.

5.2.1 Laminate Materials (Sandwich Skins)

All of the laminate materials used in the tee joint construction (flange inner and outer skin, web skins, overlaminate and web bonding laminate) are supplied by SP Systems, Newport, Isle of Wight. Their designations are given in Table 5.1 and their manufacturer's quoted properties in Table 5.2. The details of the cure cycles are given in Table 5.3.

SP Systems are suppliers of the raw materials – stitched fibre reinforcements, formulated resin products and pre-pregs. The finished laminates used in the testing came from two sources. The materials used in the moisture uptake experiments (Batch 1) were supplied by Green Marine Ltd. and the materials used in the DMTA programme (Batch 2) were laid up by SP Systems. Both sources employed the same cure regimes, which are specific to the production of the RNLI vessels.

5.2.1.1 Quality Comparison Between Laminate Materials

Although Batch 1 and Batch 2 use the same materials and cure regimes, there are likely to be inconsistencies between the two in terms of volume fractions and laminate quality, simply because they originate from two different sources. It is therefore important to examine the microstructure of these materials so that any trends exhibited by the experimental results, which could be linked to material quality, can be accounted for. Metallographic techniques (resin mounting followed by grinding and polishing to 1 micron diamond finish) were used to prepare the specimens for examination under the microscope. This was followed by void fraction determination using a Zeiss Image Analysis system.

The first point to note is that while the quality of the two batches was found to be quite different, there is good consistency between specimens within each batch. Beginning with the unaged QEA1200 laminates from Batch 1 (moisture uptake); Figure 5.2 shows a representative cross-section of the material where the quadriaxial fibre orientations within each ply can be clearly seen. It is obvious from this image however, that the percentage volume of voids is significant. It is also possible to see from this image that there tends to be areas between the laminae that are resin rich. In some localised areas on the polished surfaces of the specimen there was evidence of poor wet-out with large voids between plies. This is illustrated by Figure 5.3.

The quality of the QEA1200 material from Batch 2 (DMTA) is of similar quality to Batch 1. Noting that the Batch 1 specimens are 5 plies thick while the Batch 2 specimens are only 2 plies thick it would be expected that better consolidation be found in the Batch 2 specimens. There appear to be fewer resin-rich areas between plies in the Batch 2 laminate (Figure 5.4) compared to Batch 1, but the thinner laminate is prone to more resin rich areas and defects at the surface (Figure 5.5).

Similar characteristics are observed in the two batches of the QE1200 material. Figure 5.6 shows a representative cross-section of Batch 1 material which has large void areas between laminae but reasonably good consolidation elsewhere and no evidence of large resin-rich areas between plies or at the laminate surface. Figure 5.7 shows material from Batch 2, which clearly shows poorer consolidation than Batch 1.

5.2.1.2 Laminate Void Fraction Determination

In view of the observed laminate quality and in order to characterise the materials as fully as possible, a process of volume fraction determination was carried out. An Image analysis technique was used to obtain constituent volume fractions from a large number of micrographs (like those in Figures 5.2 to 5.7). For each image this required grey-scale boundaries to be set which encompassed the 'colour' range of each of the constituent materials in the image. For example, fibres were clearly near white, voids were near black and the matrix lay somewhere in between. In reality however, the boundaries were very indistinct and the results highly subjective, relying heavily on the quality of the image contrast. It was only possible to obtain plausible values for void content, as shown in

Table 5.4. Ranges are given, as the results were highly dependent on the specific location being examined.

These void volume fractions appear rather large, particularly for the pre-preg QEA1200. SP Systems quote values for typical 'wet' laminates of 5-8%, whereas comparable pre-pregs usually contain 0-2%. It is possible that the image analysis technique is erroneous and may include areas in its analysis that are not voids. However, visual inspection of Figures 5.2 to 5.7 indicates void fractions certainly much larger than 2% and nearer 10%, in some cases possibly higher. The values in Table 5.4 must therefore be considered representative of these materials but approximate.

5.2.2 Foam Core Materials

The materials used in the flange and web cores are closed cell cross-linked PVC foams supplied by Divinycell and Airex. The two manufacturers produce virtually identical materials and either (sometimes both together) are used in the joint and vessel construction. Little information on the exact chemical formulation and manufacture of these foams was forthcoming from the manufacturers, however it is known that their composition is 30-75% PVC and 20-50% aromatic polyurea/polyamide [5.1]. It is therefore evident that large variations are possible. The foams are expanded from the bulk polymer using an inert gas, the identity of which was withheld by the manufacturer but is typically known to be Freon. The expanding process makes the cells slightly elongated in the direction of foam rise, which causes a small degree of anisotropy in the material. The cell structure is illustrated in Figure 5.8, while Table 5.5 gives the full range of nominal properties supplied by the manufacturer for the two densities of foam material used in the joints, i.e. 80 kg/m^3 in the web core and 130 kg/m^3 in the flange core.

The relative density is a useful parameter, which is not supplied by the manufacturers. Gibson and Ashby [5.2] however give a formulation from which it may be calculated depending on the geometry of the cells. These cells are typically tetrakaidecahedra, i.e. edge connectivity = 4, face connectivity = 3, average number of edges per face = 5.14 and average number of faces per cell = 14. For this geometry, Gibson and Ashby give the relative density as

$$\frac{\rho^*}{\rho_s} = 1.18\frac{t}{l} \qquad (5.1)$$

where ρ^* = density of foam

ρ_s = density of solid from which foam is made

t = cell wall thickness

l = cell edge length i.e. side length of face

The manufacturer quotes a nominal cell size (see Table 5.5) but does not provide any information on cell wall thickness. The image analysis technique has therefore been used to obtain representative measurements. A range of micrographs (such as that shown in Figure 5.9) has been obtained and measurements of cell wall thickness and cell edge length have been taken from them. Cell length and width have also been recorded for comparison with the manufacturer's quoted value of cell size.

For example, for the foam of density 130 kg/m^3 (H130/C70.130), the mean cell wall thickness was found to be 10 μm and the mean length of the cell sides was 189 μm. The mean cell size was found to be 343 μm, which is in excellent agreement with the manufacturer's quoted value of 0.35 mm.

Equation 5.1 was used with the measured values to determine the relative densities of the foam materials, which are given in Table 5.6.

5.3 Miscellaneous Materials

The tee joint specimens also contain other materials. These are

- A thixotropic epoxy resin (SP120) with a colloidal silica additive for the fillet;
- A wood insert at the top of the web, which prevents local core failure when loaded by the test machine (but which is not present in the vessel sandwich construction).

The fillet resin has a Young's modulus typically 3300 MPa and a shear modulus of 3500 MPa.

The wood is treated as isotropic and has a Young's modulus typically 1120 MPa and a shear modulus of 120 MPa.

5.4 References

[5.1] *Divinycell Technical Manual, H Grade*; Divinycell International Ltd., 1, Eastville Close, Gloucester, GL4 7SJ

[5.2] **Gibson, L.J. and Ashby, M.F.**; *Cellular Solids: Structure and Properties*; Pergamon, 1988

6. EXPERIMENTAL TECHNIQUES

6.1 Moisture Uptake Measurement

The aim of the moisture uptake experimental programme is to obtain an overall understanding of the moisture absorption behaviour in the materials of interest when exposed to a specific hygrothermal environment over a prolonged period. The choice of exposure environment and the choice of technique to determine the moisture content were two important aspects which were considered when designing these experiments. The lack of test standards suitable for application to long-term exposure experiments has meant that there is often little consistency between the techniques reported in the literature. It has therefore been necessary to develop an approach that is specifically suitable for this experimental programme, based on information given in the standards, literature and available resources. Sections 6.1.1 and 6.1.2 below give details of the exposure environments which have been used in this experimental programme and the gravimetric technique which has been used to determine the moisture content of samples.

6.1.1 Exposure Environments

In this experimental programme, the following hygrothermal exposure environments have been used:

- Immersion in fresh water at 40°C
- Exposure to 95% relative humidity at 40°C

Many authors have conducted tests at temperatures far in excess of 40°C [6.1 – 6.10], in some cases in boiling water [6.11]. In these cases in the literature however, the materials tested are often of aerospace origin and have significantly higher glass transition temperatures (T_g) than the typical marine materials tested here. Evidence exists [6.12] to suggest that at exposure temperatures in the region of T_g and above, highly anomalous behaviour can be exhibited whereas at lower temperatures it has often proven to be Fickian in nature. Collings and Stone [6.13] note that many commonly used resins exhibit non-Fickian behaviour above only 60°C. A temperature of 40°C was therefore chosen in this case as it was considered to be a suitable temperature at which the materials detailed in Chapter 5 could be aged without the risk of anomalous behaviour occurring. This

temperature is considered to be sufficiently lower than the lowest material T_g, such that it will not be approached by the material T_g values if they are caused to decrease by the ageing process. It is also a reasonable temperature for handling the specimens without special thermal protection, which was an important consideration when designing experiments requiring frequent human intervention (see Section 6.1.2). It will also serve to accelerate the moisture uptake process above the rate that would occur at ambient. With regard to applicability to the natural ageing process, in equatorial areas, deck temperatures on composite ships can occur well above 40°C. An immersion temperature of 30°C is representative of maximum summer service temperatures in Australian tropical waters [6.14]. In these geographical locations high humidity environments are also present.

Immersion in fresh water is the easiest approach to maintain over prolonged periods and has been found to offer the greatest degree of accuracy in results. The experiments have been carried out in a thermostatically controlled heated bath manufactured by Grant Instruments, which is capable of maintaining the set temperature to ±1°.

Material specimens have also been aged in an environmental chamber manufactured by Cee-Tel, which has the ability to maintain a temperature set point to ±1°C and relative humidity to within ±3%. The working volume of this chamber is approximately $1m^3$ and small access ports enable specimens to be removed without disrupting the contained environment. The relative humidity set point was taken as 95% as good control above this value was very difficult to obtain with this particular piece of equipment. Some authors, e.g. Loos *et al* [6.12], have cited comparable results between high (90-100%) relative humidity exposure and immersion. A temperature of 40°C was chosen for this test to enable direct comparison between results from the environmental chamber and results from the water bath.

All bath and chamber internal surfaces are of sheet stainless steel. Specimens were therefore placed in each environment on specially made stainless steel mesh and studding racks, which allow the moisture to have unimpeded access to all surfaces of the specimens. The PVC foam materials being tested caused the rack arrangements to become buoyant so these were therefore weighed down with machined stainless steel blocks (Figure 6.1).

6.1.2 *Gravimetric Measurement*

The gravimetric technique for monitoring moisture uptake in material specimens involves the weighing of specimens periodically during the ageing process. Therefore, if a specimen has been dried before immersion or exposure to a relative humidity environment it is assumed that any subsequent mass increase during ageing is attributed to moisture held in the material. That is, the percentage moisture content of a specimen by mass is given by

$$M = \frac{M_t - M_0}{M_0} \times 100 \qquad (6.1)$$

where M_t = the specimen mass at time t during exposure

M_0 = the dry specimen mass i.e. at exposure time $t = 0$.

The procedure used for obtaining the mass measurements must ensure that the readings are as accurate as possible. When specimens are removed from the ageing environment they must be weighed and replaced as quickly as possible so that desorption of moisture is kept to a minimum. It is also necessary to remove surface moisture from specimens so that the readings taken measure only the moisture held by the material itself. Several techniques have been reported in the literature such as wiping, blotting, air drying and oven drying. Fellows [6.15] performed a comparison of three different techniques including towel blotting, warm airflow drying and oven drying. The oven drying technique was found to eliminate fluctuations in the moisture uptake data by evaporating all surface moisture and beginning a temporary desorption process. The results of moisture content by mass using this method were however significantly lower than the other two methods due to the specimens being removed from the exposure environment to a dry, hot environment for 1 hour before being weighed each time. Although Fellows considered this to be the preferred method for her epoxy samples, in this case (particularly for the very low density foam materials) it was considered likely that this technique would provide unrepresentative results. The towel blotting technique was therefore adopted.

The weighing process involved removing a small number of specimens from the exposure environment, blotting each one systematically on paper towel directly before weighing, then returning the specimens to their environment. The maximum length of time during which any specimen was out of its environment was 5 minutes. Specimens were always

removed and weighed in the same order and blotted in the same way, to eliminate as far as possible any variations in the results obtained. Mass readings were taken using a Mettler analytical balance to an accuracy of 0.0001g.

As discussed in Chapter 2, Fickian modelling of moisture uptake behaviour requires moisture uptake data to be plotted on a base of the square root of time. For this reason it was necessary to weigh samples frequently during the first stages of exposure and less frequently as the test progressed. A compromise was reached between obtaining as much data as possible and not disrupting the absorption process. Specimens were weighed no more frequently than twice in 24 hours during the first 48 hours and then no more frequently than once every 24 hours subsequently. The moisture uptake data obtained is reported in detail in Chapter 7.

6.2 Dynamic Mechanical Thermal Analysis (DMTA)

The DMTA programme has focused on examining the dynamic mechanical properties of the materials described in Chapter 5 and how these change during the hygrothermal ageing process. Of particular interest are the changes in stiffness or modulus and glass transition temperature. This section describes the background to the experimental technique, the associated theory and the tests carried out to obtain the required data.

6.2.1 Background

The DMTA technique involves the determination of dynamic mechanical properties of polymers. As a result of the analysis, the relationship between the dynamic properties, the structural parameters (e.g. crystallinity, cross-linking, plasticisation) and the environmental or external variables (e.g. temperature, time, frequency, type of deformation) can be determined. The technique measures the deformational response of the material to vibrational forces. Measurements can be obtained as a function of frequency (at constant temperature), as a function of temperature (at a fixed frequency) or a combination of both. The most useful parameters that are obtained are:

- *dynamic modulus*; a measure of the stiffness of the material
- *loss modulus*; a measure of the viscous behaviour of the material

- *mechanical damping*; a measure of the energy dissipated as heat during the deformation of the sample

The physical phenomenon underlying the technique is viscoelasticity. Most materials, particularly polymers, do not exhibit purely elastic (ideal solid) or purely viscous (ideal liquid) behaviour, but a combination of both; i.e. they are viscoelastic. All the energy supplied to a purely elastic material is stored by the material during deformation, such that there is no time dependence in the behaviour of the material and it is described by Hooke's Law. In contrast an ideal fluid stores no deformational energy and its behaviour, referred to as viscous flow, is described by Newton's law, which linearly relates the applied stress to the rate of shear.

When a stress is applied to a viscoelastic material, it will show some time-dependent deformation, i.e. any viscoelastic material, given time, will flow under an applied stress. Thus when the stress is removed, the material will not completely recover, i.e. when the material is deformed, part of the energy is stored as potential energy and part is dissipated as heat. The proportion of strain recovered on release of the stress relates to the energy stored during the material's response to deformation. The unrecovered proportion relates to the energy dissipated as heat, i.e. the viscous portion of the material's response. This manifests itself as mechanical damping or internal friction.

If the applied stress varies sinusoidally at a prescribed frequency then the strain is also sinusoidal, having an amplitude proportional to the amplitude of the stress at a given temperature and frequency. In this case the behaviour is described as linear and can be characterised by DMTA.

6.2.2 DMTA Theory

During dynamic testing, an oscillatory (sinusoidal) strain (or stress) is applied to a small sample of material and the resulting stress (or strain) developed in the material is measured. For a purely elastic material, the induced stress is proportional to the applied strain and the phase angle between the stress and strain is 0°. For an ideal fluid, the stress is proportional to the strain *rate* and the stress signal leads the strain signal by 90°. For a viscoelastic material, the stress lags behind the strain by some angle δ. This phase lag

results from the time required for molecular rearrangements within the material and is associated with relaxation phenomena. It is described as follows:

$$\text{Strain} \quad \varepsilon = \varepsilon_0 \sin \omega t \tag{6.2}$$

$$\text{Stress} \quad \begin{aligned} \sigma &= \sigma_0 \sin(\omega t + \delta) \\ \sigma &= \sigma_0 \sin \omega t \cos \delta + \sigma_0 \cos \omega t \sin \delta \end{aligned} \tag{6.3}$$

The stress therefore has two component parts:

- an elastic stress (denoted by σ' or τ') which is in phase with the strain, having an amplitude of $\sigma_0 \cos \delta$
- a viscous stress (denoted by σ'' or τ'') which is 90° out of phase with the strain, having an amplitude of $\sigma_0 \sin \delta$

The elastic modulus, or storage modulus (E' or G') and the viscous modulus, or loss modulus (E'' or G''), can then be calculated directly from the elastic and viscous stress,

$$\sigma = \varepsilon_0 E' \sin \omega t + \varepsilon_0 E'' \cos \omega t \tag{6.4}$$

where

$$\begin{aligned} E' &= \left(\frac{\sigma_0}{\varepsilon_0} \right) \cos \delta \\ E'' &= \left(\frac{\sigma_0}{\varepsilon_0} \right) \sin \delta \end{aligned} \tag{6.5}$$

E' is the real part of the modulus and the E'' is the imaginary part, i.e.

$$E^* = E' + iE'' \tag{6.6}$$

where E^* is the complex modulus. The damping in the system is given by

$$\tan\delta = \frac{E''}{E'} \quad or \quad \tan\delta = \frac{G''}{G'} \text{ in shear notation}^{1} \tag{6.7}$$

since
$$E' = E^{*}\cos\delta$$
$$E'' = E^{*}\sin\delta \tag{6.8}$$

The real parts of the elastic and shear moduli are known as *storage* moduli because they correspond to the storage and release of potential energy during periodic deformation. The imaginary parts of the moduli are known as *loss* moduli because they are associated with the energy dissipated as heat during deformation.

The interpretation of the characteristic curves of these parameters and the significance of the loss ($tan\delta$) peaks are discussed with reference to the experimental results in Section 8.1.

6.2.3 DMTA Experimental Programme

The DMTA programme has been carried out with the assistance and equipment of the Vibroacoustics Group in the Mechanical Sciences Sector at DERA Farnborough. The aims of the tests are primarily to determine the effect of moisture ageing on the mechanical properties of the materials, particularly stiffness, which cannot be obtained by other test methods; and also to track the change in glass transition temperature as a function of moisture content or ageing time of the material. The DMTA technique has been used successfully for hygrothermally aged laminate specimens by Boinard [6.16], however to the author's knowledge it has not been used before to assess hygrothermally induced changes in PVC foam material.

Some commercially available DMTA equipment has the facility to immerse specimens in a bath during testing, but data generation as a function of temperature is then restricted by the boiling point of the liquid. With the apparatus used for the testing described in this section, moisture could not be introduced into the test system. However, specimens that were aged for a pre-determined length of time could be directly transferred from their ageing environment to the DMTA apparatus

[1] In all of the above analysis it should be noted that in order to determine the shear properties the notation can simply be changed from the direct stress and strain and elastic modulus σ, ε and E to the shear stress, strain and modulus τ, γ and G.

The apparatus used was a TA Instruments DMA 2980 Dynamic Mechanical Analyser, in conjunction with the Windows NT based *Thermal Solutions* data acquisition software and the *Universal Analysis* analysis software.

When performing a DMTA test, a variety of specimen clamping configurations may be used to impose the required mode of deformation on material specimens of the appropriate geometry. This programme of testing employed the use of the single cantilever type clamp, whereby a thin specimen of rectangular cross-section is clamped at both ends – one end in a fixed clamp and the other in a clamp free to move in the vertical plane. The moveable clamp applies the oscillatory force in a cantilever mode at a prescribed amplitude. This arrangement is shown schematically in Figure 6.2 and the specimen details are given in Section 8.1. It was necessary to ensure that the clamps were tightened by exactly the same amount in each test. Variation in clamp tightness between tests can cause a variation in results, particularly if the specimens are weak and easily crushed, for example the PVC foam material. An Allen key with a torque meter attached was therefore used for tightening the clamps.

The following gives an outline of the stiffness calculations used by the *Thermal Solutions* Instrument Control Software [6.17]. Also described are the relationships for deriving stress and strain from the force and amplitude of deformation. These assume linear viscoelastic behaviour, as described in Section 6.2.1.

The fundamental measurement of the DMTA test equipment is the sample stiffness, K, [6.17, 6.18] given by

$$K = \frac{F}{u} \tag{6.9}$$

where F is the applied drive force and u is the measured displacement or amplitude. The measured stiffness is dependent on the sample geometry, but the elastic modulus, being a material property, is not.

In dynamic experiments, the equipment measures the raw signals of force, amplitude of deformation and phase angle. Force and amplitude are used with the phase angle and instrument calibration factors to calculate the storage and loss stiffness (K' and K''). Tan δ is the ratio of K'' to K'. Storage and loss moduli are calculated by multiplying the raw

stiffness measurements by the appropriate geometry factors. Further details on these calculations are given in the Thermal Solutions Manual [6.17].

The tests were carried out on specimens at different degrees of ageing, as detailed in Section 8.1. Un-aged material was also tested for reference, as the DMTA results can differ significantly from the manufacturer's quoted values. The experimental parameters were set such that specimens were tested at a constant frequency of 10 Hz and prescribed amplitude of 50 μm. The temperature was ramped during each test from ambient to 180°C at a rate of 2°C per minute. This range was chosen to encompass room temperature as well as the possible range of glass transition temperatures of the materials of interest (approximately 80 to 150°C, based on manufacturers' data). In practice, the tests were terminated after approximately 120°C, once the required data in the T_g region had been obtained. The duration of each test was approximately 1 hour.

Results were automatically obtained for all parameters, including storage modulus, loss modulus, tan δ, time, temperature, amplitude, mean position, frequency, stress and strain. Amplitude, for example, is a useful parameter to record if unexpected results are observed. These can sometimes be due to material shrinkage during heating, causing the specimen to become loose in the clamps. The amplitude can then suddenly become large and noisy because the drive force is affected. Recording the amplitude during the test can therefore help diagnose anomalous data. The data acquisition and analysis software allows real-time monitoring of the results in graphical form so the progress of the test can be monitored.

The most important of the recorded results are the storage modulus, loss modulus, tan δ and temperature. Curves of the moduli and tan δ plotted as a function of temperature supply all the information required about the behaviour of the specimen. Of particular interest in this study are the value of the storage modulus at ambient temperature and the shape of the glass transition region in all three parameters. In particular, tan δ exhibits a peak in the transition region and the temperature at which the peak occurs is commonly quoted as the glass transition temperature[2]. The curves' characteristics are discussed with reference to the experimental results in Section 8.1.

[2] The glass transition phenomenon occurs over a range of temperature and not at a discrete temperature value.

6.3 Thermoelastic Stress Analysis (TSA)

6.3.1 Thermoelastic Theory

Thermoelastic Stress Analysis (TSA) is a well-established non-contact NDE technique, whose engineering applications are wide ranging [6.19, 6.20]. It has proven to be an excellent tool for successfully obtaining full-field stress information from the sandwich tee joints.

The thermoelastic technique is based on the measurement of the small temperature change that occurs in solids when they are subject to an elastic cyclic stress. In isotropic materials, this temperature change, ΔT, is directly proportional to the change in the sum of the principal stresses in the material, $\Delta(\sigma_1 + \sigma_2)$, as follows,

$$\Delta T = KT\Delta(\sigma_1 + \sigma_2) \tag{6.10}$$

where T is the absolute temperature of the material and K is the thermoelastic constant,

$$K = \frac{\alpha}{\rho C_p} \tag{6.11}$$

where α is the coefficient of linear thermal expansion, ρ is the density and C_p is the specific heat of the material at constant pressure. This simple relationship is known as the thermoelastic effect and was first formulated by Kelvin in 1853 [6.21].

In orthotropic materials however it can be shown [6.19] that ΔT is not directly proportional to the stresses but to a combination of the stresses and linear thermal expansion coefficients of the material,

$$\Delta T = \frac{T}{\rho C_p}\left(\alpha_{11}^P \Delta\sigma_{11} + \alpha_{22}^P \Delta\sigma_{22}\right) \tag{6.12}$$

where α_{11}^P and α_{22}^P are the coefficients of linear thermal expansion in the principal material directions 11 and 22, and similarly $\Delta\sigma_{11}$ and $\Delta\sigma_{22}$ are the changes in the direct stresses in the principal material directions. In the case of orthotropic materials such as the FRP components of the tee joints, the principal material directions denote the directions

parallel to the 0° ply and through the thickness of the laminate, since the edges of the laminates are the surfaces of interest when examining a cross-section of the joint (as described in Chapter 9).

Two types of equipment have been used in this work that measure the temperature change, ΔT. These are described in more detail in Section 6.5.2. In both cases, the systems contain highly sensitive detectors that convert the photon emission from the specimen, due to the small temperature change, into a voltage signal. It is a straightforward matter to relate this output voltage signal from the detector to the stresses being experienced in the specimen. For isotropic materials, the relationship is given by,

$$\Delta(\sigma_1 + \sigma_2) = AS \tag{6.13}$$

where S is the detector output, known as the thermoelastic signal and A is a calibration constant.

The calibration constant A is dependent on the material properties of the specimen and the properties of the detector. For the SPATE equipment (Section 6.5.2), A is expressed as [6.19]:

$$A = \frac{DGR}{Te2048K} \tag{6.14}$$

where D is the detector responsivity,
G is an amplification factor,
R is a temperature correction factor for readings taken at other than 20°C,
T is the absolute temperature of the surface of the test specimen,
e is the surface emissivity,
and 2048 is included as a consequence of the 12 bit analogue to digital converter.

For orthotropic materials the relationship between the stresses and the thermoelastic signal is as follows:

$$\alpha_{11}^{P}\Delta\sigma_{11} + \alpha_{22}^{P}\Delta\sigma_{22} = A^{*}S \tag{6.15}$$

where A^* is a further calibration constant identical in form to A except that K is replaced by $1/\rho C_p$.

Quantitative stress values can be obtained directly from Equation 6.13 if A is known. It is clear from Equation 6.15 that stress values for an orthotropic material cannot be obtained directly from the thermoelastic signal. Nevertheless, for these materials, the quantity ΔT is an important stress metric and can be used as a basis for validation. As both isotropic and orthotropic materials are used to construct the sandwich tee joints, both A and A^* must be determined for all constituent materials. A generic approach to the calibration is given in Section 6.5.3. The specimen details, load levels and results are given in Chapter 9.

6.3.2 TSA Equipment

The two types of equipment used in the thermoelastic work are the SPATE 9000 (Stress Pattern Analysis by Thermal Emissions) system and the DeltaTherm 1000 system [6.19]. The SPATE system (shown in Figure 6.3) contains a single infra-red (cadmium-mercury-telluride) detector, which operates in a raster scanning mode with the aid of two mirror drive systems, over a selected area of the specimen to provide a contour map of the detected thermoelastic signal. Resolution can be as fine as 0.5 mm, which allows more detailed measurement than that given from strain gauges, however the length of time taken to scan the selected area can be hours, depending on the resolution required. The relatively new DeltaTherm system (shown in Figure 6.4) incorporates a 128 × 128 indium antimonide (InSb) detector array, which obviates the need for scanning by effectively taking a snapshot of the specimen area, building it up over seconds rather than minutes or hours. The resolution can be changed using a selection of lenses that focus the detector array onto the required area of the specimen. A zoom lens attachment provides the ability to focus all 16384 detectors on an area 3 × 3 mm, allowing much more detailed work than was previously possible.

The technique offers many advantages when studying elements of sandwich structures. It is non-contact and therefore does not use attachments that may stiffen the joints. A full field representation of the stresses is obtained which permits an immediate visualisation of the stress distribution through the joint and hence the importance of each of the joint constituents in the load transfer process.

The test machines used to load the specimens were FORTReSS (Section 6.6), a large, purpose-built load rig with various hydraulic ram attachments, and an Instron 8501 servo-hydraulic test machine.

6.3.3 Material Calibration Technique

Since the joints are made up from a variety of materials, each having a different thermoelastic response and hence thermoelastic constant, K, it is necessary to derive a means of calibrating each material so that the thermoelastic signal can be related to the stresses in each part of the joint. This can be achieved theoretically using Equation 6.14 but this approach may produce unreliable results because of inherent variations in the material. A description and critical appraisal of thermoelastic calibration techniques is given in [6.19]. One possible approach would be to bond strain gauges to the material, measure the strain at that point and compare this to the thermoelastic signal. However, this is impractical, particularly for the sandwich core material, as the gauges cause local reinforcement. The most appropriate technique is to use a method of direct calibration whereby the material is loaded in such a way that the stress distribution is known.

The technique can be very simply applied to isotropic materials by using the relationship in Equation 6.13. By loading a specimen cyclically in tension, one of the principal stresses is eliminated from the equation and the other is equal to the applied stress. The applied stress range, $\Delta\sigma_{app}$, is therefore related to the measured signal by

$$A = \frac{\Delta\sigma_{app}}{S} \tag{6.16}$$

For orthotropic materials, it is necessary to use Equation 6.15 as a basis for calibration. In order to obtain a simple expression for calibration purposes, Equation 6.15 is rearranged in the following form,

$$\Delta\sigma_{11} + \alpha^{*}\Delta\sigma_{22} = A^{**}S \tag{6.17}$$

where $\alpha^{*} = \alpha_{22}^{P} / \alpha_{11}^{P}$

and $A^{**} = A^{*} / \alpha_{11}^{P}$

A^{**} is required to calibrate the thermoelastic data and α^{*} is required for comparing the thermoelastic data with the FE analysis. The latter is described in more detail in Chapter 10.

The calibration of the orthotropic materials is achieved in a similar manner to the isotropic materials by cyclically loading specimens in tension, such that the direction of the applied stress is parallel to the principal material direction. That is, $\Delta\sigma_{11} = \Delta\sigma_{app}$ and $\Delta\sigma_{22} = 0$. Equation 6.17 can therefore be rearranged such that

$$A^{**} = \frac{\Delta\sigma_{app}}{S} \tag{6.18}$$

To determine α^{*}, $\Delta\sigma_{11}$ must be eliminated from Equation 6.17. To achieve this with the tee joint laminate materials, slices of the laminate were bonded together in a 'tower-block' type configuration and loaded in compression, such that the direction of load was perpendicular to the plane of the laminates. Details of the specimen and loading configuration are given in Chapter 9. This arrangement was such that $\Delta\sigma_{22} = \Delta\sigma_{app}$ and $\Delta\sigma_{11} = 0$, allowing Equation 6.17 to be rewritten as

$$\alpha^{*} = \frac{A^{**}S}{\Delta\sigma_{app}} \tag{6.19}$$

In all cases, to obtain the calibration constants, a representative area of material is scanned and a mean value of the thermoelastic signal taken. The applied stress range can be obtained from the specimen geometry and applied load range. In order to achieve a uniform surface emissivity from the specimens, they are coated with two passes of RS matt black paint.

This section has provided a generic overview of the material calibration procedures. Specimen details and specific experimental arrangements and parameters are discussed in Chapter 9.

Once all the different materials have been calibrated and the scans of the joints taken, the contour plots of the thermoelastic signal are simply multiplied by the relevant calibration constants to obtain a contour plot of the change in the sum of the principal stresses. The process is simplified such that numerical signal data is output in a spreadsheet format

whereby each pixel on the scan plot corresponds to a spreadsheet cell. It is therefore relatively easy to identify the data corresponding to the constituent materials.

6.4 Hygrothermal Ageing of Large Structural Specimens using FEARLESS

While small material specimens can be aged easily in heated water baths (Section 6.1), structural specimens such as the tee joints require a much larger facility for their hygrothermal ageing. It was apparent from the literature that facilities for the hygrothermal testing of large structural elements are rare; and rarer still are large facilities which have the ability to combine an accelerated hygrothermal environment with mechanical loading of the test specimen.

The University of Southampton School of Engineering Sciences undertook a project in 1996 to design, build and commission a large, flexible environmental test facility, incorporating mechanical loading. The equipment was designed by a M.Eng. project group in 1997 [6.22] and commissioned by a second project group in 2000 [6.23]. During the intervening time, the construction of the facility was undertaken and the author was involved in this phase to a large degree. The facility, known as FEARLESS (Fortress Environmental Ageing Rig for Large Elements of Ship Structures), has been used in this work for the hygrothermal ageing of tee joints. The results of this programme are reported in Chapter 11. The present section describes the facility and its use.

6.4.1 The Environmental Chamber

The hygrothermal environment is contained within a chamber that has an internal working volume of 5.5 m^3 and allows simultaneous hygrothermal ageing and mechanical (static or cyclic) loading of the test specimens.

The chamber is designed to be of lightweight modular construction. The internal faces, which contain the environment, are of sheet aluminium. These are attached to cavity walls constructed from treated marine plywood and the cavities are filled with 'Rockwool' mineral wool slab insulation, which is resistant to moisture. The total wall thickness is 10 cm.

The mechanical loading of the test specimens contained within the chamber (Section 6.4.3) is applied by FORTReSS (Flexible Orthogonal Rig for Testing Real Ship Structures) [6.24]. FORTReSS is a heavy structures test rig which consists of a large orthogonal framework to which hydraulic rams can be attached. The FEARLESS chamber is constructed within the Fortress framework in a modular form so it can be dismantled when not in use. The details of the construction are given in the 1997 M.Eng. project report [6.22].

6.4.2 The Air Conditioning Unit

The hygrothermal environment is created and supplied to the chamber by a specially designed air conditioning unit, known as the RAT (Remote Air-handling Trolley). The RAT is connected to the chamber by ducting, such that a continuous circuit is formed between the two. Air from the chamber is drawn into the RAT by a fan, it is passed over a heater and then injected with moisture from a steam humidifier before being returned to the chamber. A Euortherm control system is used in conjunction with a PT100 thermal probe and Viasala combined temperature and humidity sensor, to continuously monitor and adjust the hygrothermal environment supplied to the chamber. A master-slave controller arrangement prevents temperature overshoot and allows the temperature to be maintained to ±0.1°C within the range ambient to 120°C. The relative humidity can be maintained to within ±1% below 90% and ±2% above. Complete details can be found in [6.22 and 6.23].

6.4.3 Load Application

As mentioned previously, the mechanical load is supplied to the test specimens by FORTReSS. The chamber is constructed within the FORTReSS framework and rams, displacement transducers etc. are attached to FORTReSS in the usual way. The actuators have extensions that pass through gaiters in the chamber wall and are attached to the specimen within the chamber. The specimen itself is rigidly mounted to a structure that passes through the opposite wall of the chamber and is attached to the FORTReSS structure. All loads are therefore reacted by FORTReSS and are not transmitted into the chamber structure. The versatility of FORTReSS means that under normal circumstances loading can be applied in any plane. However, with the chamber in position, loads may

currently only be applied and reacted in the horizontal plane. It is possible to test at loads up to 50 tonnes in this orientation. Static or cyclic regimes may be applied and are controlled using PC based Instron software. Full details of FORTReSS operation alone and in conjunction with the chamber are given in [6.24] and [6.23] respectively.

6.4.4 Experimental Programme

Three nominally identical joint specimens have been aged using the FEARLESS facility, one of which was unloaded, one statically loaded in compression and one under cyclic loading in compression. The cyclic load was prescribed and controlled using the FORTReSS software and the load applied as described above using a hydraulic ram attached to the FORTReSS framework.

The static load on the second joint was applied using a specially designed stainless steel stand-alone rig [6.23], which contains the joint specimen and is placed inside the environmental chamber. The technique used for applying the static load was to position the rig and joint arrangement within an Instron test machine, apply the required static load to the rig and screw it down on to the specimen, then remove the assembly from the test machine into the chamber. This means however that the initial static load applied to the specimen does not remain constant throughout environmental exposure due to material stress relaxation effects. The extent of this can be quantified upon removal from the chamber by inserting the load rig and specimen into the Instron machine and measuring the residual load.

The cyclic load regime was chosen carefully such that long-term environmental ageing could be carried out without the risk of the cyclically loaded joint failing prematurely. The choice was based on knowledge of the ultimate properties of the joint and past experience [6.23]. The load level was selected in conjunction with the environmental condition, which was chosen to maximise the extent of hygrothermal ageing within the time allowed, but which would not create ageing mechanisms within the materials that are different from the ageing process at ambient. In addition, the DMTA results (Chapter 8) demonstrated that a significant reduction in material stiffness begins to occur at temperatures well below the quoted (peak tan δ) glass transition temperature. The onset of the glass transition region has been shown to occur below 60°C. It was decided that the ageing temperature should be constant and should not be within the glass transition region of any constituent material, as this would increase the likelihood of premature failure of the cyclically loaded joint. The

relative humidity level was set to 90% as this was approaching the highest level that could be maintained without fluctuation.

The chosen environmental conditions and load levels may appear conservative, but this approach was required to ensure long-term results could be obtained successfully, since little experience had been gained in the long-term exposure of loaded specimens using this equipment. Once the technique has been proven using low load and exposure levels, then future test programmes can extend the boundaries further.

In order to determine any changes in the mechanical behaviour of the joints during exposure, two approaches were adopted. The first was to record the maximum and minimum positions of the actuator every thousand load cycles for the cyclically loaded joint. Any changes in specimen compliance were therefore detected as changes in mean position and displacement amplitude. The second was to terminate the test at intervals of approximately two months, remove the three specimens from the chamber, load them in turn using a servo-hydraulic Instron test machine and obtain full field stress data using TSA (DeltaTherm 1000). This data was then compared with baseline scans taken from an unaged joint of the same geometry. The results of this programme are discussed in Chapter 11.

6.5 References

[6.1] **Browning, C.E., Husman, G.E., Whitney, J.M.**; *Moisture Effects in Epoxy Matrix Composites*; Composite Materials: Testing and Design (4th Conference), ASTM STP 617, ASTM 1977

[6.2] **Shirrell, D.**; *Diffusion of Water Vapour in Graphite/Epoxy Composites*; Advanced Composite Materials - Environmental Effects, ASTM STP 658 (J.R. Vinson, Ed.), ASTM 1978

[6.3] **Mikols, W.J., Seferis, J.C., Apicella, A., Nicolais, L.**; *Evaluation of Structural Changes in Epoxy Systems by Moisture Sorption-Desorption and Dynamic Mechanical Studies*; Polymer Composites, Vol. 3, No. 3, July 1982, pp118-124

[6.4] **Karama, M., Touratier, M., Pegoraro, P.**; *Tests of Accelerated Ageing of Composite Materials in Shipbuilding*; Proc. 9th International Conference on Composite Materials, pp532-539

[6.5] **Shen, C.H., Springer, G.S.**; *Effects of Moisture and Temperature on the Tensile*

Strength of Composite Materials; Journal of Composite Materials, Vol. 11, January 1977, p2.

[6.6] **Cinquin, J., Abjean, P.**; *Correlation Between Wet Ageing, Humidity Absorption and Properties on Composite Materials Based on Different Resins Family*; 38th International SAMPE Symposium, May 10-13, 1993, pp1539-1551

[6.7] **Vauthier, E., Chateauminois, A., Bailliez, T.**; *Hygrothermal Ageing and Durability of Unidirectional Glass/Epoxy Composites*; Proc. 10th International Conference on Composite Materials, Vol. 6, pp185-192

[6.8] **Rehfield, L.W., Briley, R.P., Putter, S.**; *Dynamic Tests of Graphite/Epoxy Composites in Hygrothermal Environments*; Composites for Extreme Environments, ASTM STP 768, ASTM 1982, pp148-160

[6.9] **Valentin, D, Paray, F, Guetta, B.**; *The Hygrothermal Behaviour of Glass Fibre Reinforced PA66 Composites: A Study of the Effect of Water Absorption on their Mechanical Properties*; Journal of Materials Science, Vol. 22 (1987), pp46-56

[6.10] **Ciriscioli, P.R., Lee, W.I., Peterson, D.G., Springer, G.S.**; *Accelerated Environmental Testing of Composites*; Journal of Composite Materials, Vol. 21, March 1987, pp225-242

[6.11] **Birger, S., Moshonov, A., Kenig, S.**; *The Effects of Thermal and Hygrothermal Ageing on the Failure Mechanisms of Graphite-Fabric Epoxy Composites Subjected to Flexural Loading*; Composites, Vol. 20, No. 4, July 1989, pp341-348

[6.12] **Loos, A.C., Springer, G.S., Sanders, B.A., Tung, R.W**; *Moisture Absorption of Polyester E-Glass Composites*; Journal of Composite Materials, Vol. 14 (April 1980), pp142-154

[6.13] **Collings, T.A., Stone, D.E.W.**; *Hygrothermal Effects in CFC Laminates: Damaging Effects of Temperature, Moisture and Thermal Spiking*; Composite Structures, Vol. 3 (1985), pp341-378

[6.14] **Gellert. E.P., Turley, D.M.**; *Seawater Immersion Ageing of Glass-Fibre Reinforced Polymer Laminates for Marine Applications*; Composites Part A (Vol. 30 (1999), pp1259-1265

[6.15] **Fellows, L.M.P.**; *Moisture Absorption in Low-level Porosity Thermoplastic Toughened Epoxy Composites*; Ph.D. Thesis, Department of Engineering Materials, University of Southampton, 1999

[6.16] **Boinard, E.**; *Influence of Water on Polymeric Materials used in Marine Applications*; Ph.D. Thesis, Department of Shipp and Marine Technology, University of Strathclyde, 1998

[6.17] TA Instruments DMA 2980 Technical Reference Manual, 1997

[6.18] **Cardon, A.H., Hiel, C.C.**; Unknown reference

[6.19] **Dulieu-Barton, J.M. and Stanley, P.**; *Development and Applications of Thermoelastic Stress Analysis*; J. Strain Analysis 33 (1998), pp 93-104

[6.20] Strain; the Journal of the British Society for Strain Measurement, 35, No. 2 (May 1999)

[6.21] **Thompson, W. (Lord Kelvin)**; *On the Dynamical Theory of Heat*; Trans. R. Soc. 20 (1853), pp 261-283

[6.22] **Arriaga, A., Cooper, I., Meunier, M. and Potter, S.**; *Environmentally Aged Materials Test Facility*; Master of Engineering Group Design Project, University of Southampton, 1997

[6.23] **Hoddinott, J. and Radue, P.A.**; *Design of a Test Procedure to Investigate the Effects of Environmental Ageing on Composite Structures Under Load*; Master of Engineering Group Design Project, University of Southampton, 2000

[6.24] **Read, P.J.C.L., Thelu, S.C.M. and Walters, C.L.**; *Design, Fabrication and Commissioning of a Flexible Rig for Testing Large Marine Composite Structures*; Master of Engineering Group Design Project, University of Southampton, 1992

PART D

CHARACTERISATION OF MATERIAL AGEING PROCESS

7. DETERMINATION OF THE HYGROTHERMAL AGEING MECHANISM IN SANDWICH MATERIALS

The purpose of this chapter is to determine the way in which moisture enters and travels through the individual constituent materials of the sandwich, i.e. the mechanism by which the hygrothermal ageing takes place. The effects that this has on the material properties are discussed in Chapter 8.

7.1 Experimental Programme

In order to determine the characteristics of the hygrothermal ageing mechanism it is necessary to examine the moisture uptake trends exhibited by the materials of interest when exposed to a hygrothermal environment. The experimental technique and gravimetric measurement approach used to obtain information about the materials' moisture uptake behavior have been described in detail in Section 6.1. Coupon specimens of the constituent sandwich materials detailed in Chapter 5 have been tested. The following section gives details of the specimens and tests carried out in the two hygrothermal environments outlined in Section 6.1.

7.1.1 Immersion in Fresh Water at 40 ℃ and Exposure to 95% Relative Humidity at 40 ℃

The specimen geometries for these tests are given in Table 7.1. They consisted of small coupon specimens of each of the laminate materials (QE1200 and QEA1200 – Batch 1; see Section 6.1) and small rectangular blocks of the 130 kg/m^3 PVC foam material (C70.130). The lower density (80 kg/m^3) PVC foam material was not tested under these conditions because it was found that the large cell size contributed to significant errors in the moisture uptake results. Since the material morphology and macrostructure was identical to the higher density foam, the mechanisms of ageing were assumed to follow the same trends.

The small test coupons of each material were cut from the same larger panel. All specimens of the same material were therefore manufactured at the same time and under the same conditions and have experienced the same ambient environmental conditions from the time of manufacture. The foam specimens were cut from a large sheet supplied by the manufacturer using a fine band saw and the cut surfaces were neatened using 200

grit wet/dry and any loose particles removed. The laminate specimens were cut from the cured panels using a high quality water jet technique to ensure there were no edge defects or protruding fibre bundle ends.

The specimens were placed in a dessicator at room temperature for 10 days prior to exposure to the hygrothermal environment. This ensured that any moisture from the ambient environment or cutting process absorbed since manufacture was removed and that the specimens had reached a constant initial mass. They were then immersed/exposed as described in Section 6.1.

One of the aims of the moisture uptake test programme was to determine whether existing absorption models such as Fick's law could fit the experimental results. Fick's law in its classical form is applicable only to a one-dimensional diffusion case whereby specimens must approximate an infinite plate or be thin enough that the effects of ingress through the edges can be considered negligible (Chapter 2). The specimens used in this test programme were cut from material as it would be used in marine structures (as detailed in Chapter 5) and were therefore too thick to approximate the one-dimensional case. Although edge correction formulae exist it was thought to be of value to attempt to approximate the one-dimensional case experimentally. Of the foam specimens immersed in fresh water at 40°C, two each of the thick and thin specimens were sealed around the four narrow edges (noted by Shen and Springer [7.1]) using a high temperature silicon based sealant from *Loctite*. The purpose was therefore that moisture ingress should only be allowed into the foam through the two opposite faces of the specimens. In order to determine the effectiveness of the sealant, two each of the thick and thin foam specimens were completely covered in the sealant.

The specimens immersed in fresh water at 40°C were exposed to their environment for almost two and a half years. Consistent data was obtained from the specimens exposed to 95% RH in the environmental chamber up to 560 hours only. After this time the experiment was terminated due to the failure of the environmental chamber control system. The initial uptake data is compared to the data obtained from the immersion tests but long-term trends under high RH exposure cannot be deduced. The moisture uptake results from these tests are presented in Section 7.2.

7.2 Determination of the Mechanisms of Moisture Absorption

This section presents the results obtained from the experimental programme described in Sections 6.1 and 7.1. The gravimetric data is presented graphically for each material and the trends discussed qualitatively. The applicability of existing moisture uptake models to this data is discussed in Section 7.3.

7.2.1 QEA1200 Laminate Material

This section describes the moisture uptake results from the two ageing environments for the QEA1200 glass/Kevlar hybrid laminate material. The results are presented graphically and discussed qualitatively and reasons for the observed characteristics are considered throughout.

7.2.1.1 Immersion in Fresh Water at 40°C

The results from the immersion in fresh water at 40°C are the most extensive and show the characteristic long-term moisture uptake trends exhibited by this material at temperatures below the glass transition region. The moisture uptake percentage by mass (Section 6.1) plotted to a base of square root of time for the four specimens is shown in Figure 7.1.

The first point to consider is why the four specimens, which are nominally identical, exhibit different moisture uptake behaviour. The shape of all four curves is similar but specimen LAU2 exhibits a greater diffusivity than the other three and appears to be a approaching a saturation value 1.5% by mass higher than LAU1. LAU3 and LAU4 show almost identical behaviour. After testing, microscopic examination of the polished edges showed some resin rich areas and large voids near the surface of LAU2, which were not present to the same extent in LAU1. This is a plausible reason for the observed trends.

The solid line through the data represents the mean of the results from the four specimens and is not a trend line. This shows that the global moisture uptake of these specimens exhibits pseudo-Fickian characteristics, indicating a diffusion-dominated process. Pure Fickian behaviour is not expected since the material is not homogeneous. This is discussed in Section 7.3.

The initial part of the curve shows a very steep gradient up to approximately 100 hours exposure (10 hours^{½}). A high rate of moisture uptake can be expected initially and is likely to occur almost instantaneously upon initial immersion. This mass increase between the time of immersion and the first mass reading was considered to be associated with free water finding its way into open pathways into the material such as at fibre bundle ends at the cut edges or into small surface voids, equivalent to that experienced by the foam material where moisture enters open cells on the cut surfaces (Section 7.2.3). Microscopic examination of the cut edges showed that fibre ends, resin voids and small areas of damage due to the cutting process were indeed present. It has been shown in the literature [7.2, 7.3] that moisture uptake into aramid fibre bundles from the cut edges can be rapid and significant. In addition, Shubha *et al* [7.2] have shown that the moisture uptake curve for the fibres themselves exhibit a steep initial gradient, attributed to the rapid filling of sites that permit entry of moisture into the material, e.g. surface microvoids.

To assess whether voids filling with moisture (specifically on the cut edges) was a contributing factor in this case, a specimen of the material, prepared in exactly the same way as all the others, was coated around the edges with a thin layer of epoxy resin to seal any exposed fibre ends. The initial moisture uptake of this specimen (LA8) is shown in Figure 7.2. The overall rate of uptake (gradient) is lower and the percentage mass increase is less than the other specimens.

The rate of moisture uptake progressively reduces from this high initial value before subsequently exhibiting globally linear behaviour up to 58 hours^{½}. This indicates that during the initial period the ingress of free water slows down before the diffusion process becomes dominant between 10 hours^{½} and 58 hours^{½}.

Beyond 58 hours^{½}, the curve gradually becomes concave to the abscissa and tends towards a saturation value, though after almost 900 days exposure, saturation was not yet reached and the moisture content by mass was approximately 8%. This value is significantly higher than would be expected from an epoxy pre-preg laminate such as this. Values quoted in the literature do not exceed 3-4% and are usually lower, though these are often quoted for carbon reinforced aerospace quality materials [7.4]. Browning *et al* [7.5] estimate that that the maximum mass gain obtained by full plasticisation of unreinforced epoxy resin is approximately 6%. If the initial rapid ingress of 1.6% is taken away from the 8% then the 6.4% mass increase remaining is still higher than the 3-4% quoted in the literature. This suggests that the moisture held in the QEA1200 laminate material is not

only that which has diffused into the resin matrix or has collected in surface voids or cut edges. Possible explanations for this include moisture absorption by the aramid fibres, the filling of voids with absorbed moisture or degradation mechanisms such as fibre/matrix debonding causing further ingress of moisture. It is also perhaps significant that saturation has not been reached. This may be attributable to the presence of aramid. Fukuda and Kawai [7.6], show that the sorption curve for Kevlar deviates from the simple Fickian curve in the latter stages and shows an upward trend characteristic of the sigmoidal form (Chapter 2).

The maximum possible moisture uptake for this material has therefore been theoretically determined and compared to the level observed experimentally. A nominal fibre volume fraction, V_f, of 0.6 was assumed (based on typical SP Systems data). By weight, the ratio of glass content to Kevlar content was 4.95:1, which was calculated to be equivalent to 2.892:2 by volume. The matrix volume fraction, V_m, was assumed to be

$$V_m = 1 - V_f - V_v \tag{7.1}$$

where V_v is the volume fraction of voids. From the image analysis discussed in Chapter 5, void fractions of 13.8 and 9.6% were assumed.

For the calculations it was also assumed that

- Glass fibres do not absorb moisture,
- Aramid fibres saturate at approximately 5% by mass [7.3, 7.7],
- Epoxy resin saturates at 6% by mass.

Three conditions of moisture uptake were calculated:

a) Voids completely fill with water
b) Surface voids only fill with water[1]
c) Voids do not fill with water at all

The values of percentage moisture content by mass are given in Table 7.2 for the three conditions and two extremes of void fraction. It can be concluded from these results that a significant proportion of the voids present must fill with water. The experimental result is in excess of the theoretically derived value for surface voids being filled, so it follows that

[1] To determine an approximation of the proportion of the voids at the specimen surface, the surface area to volume ratio of the specimens was used.

water must also collect in voids within the laminate. This observation has also been made in the literature [7.8]. It is also possible that there are inaccuracies in the assumptions made. For example the fibre volume fraction may be lower than the assumed 0.6. However, with the theoretical values being comparable to the experimental values, it is unlikely that any further ageing mechanisms are active such as fibre/matrix interface degradation, leaching or microcracking. This was substantiated by microscopic examination of polished edges of aged specimens, which showed no apparent changes compared to the unaged case. It can therefore be assumed that no microscopic damage mechanisms have occurred, or that they are sub-microscopic. Similar observations have been made in the literature [7.9, 7.10].

7.2.1.2 Exposure to 95% Relative Humidity at 40°C

Some authors, for examples Loos *et al* [7.11], have found that exposure to 100% relative humidity yields equivalent results to those from immersion. To examine this here, specimens were exposed to 95% RH at 40°C. This was the highest level of humidity attainable with accurate control in the particular environmental chamber being used (see Section 6.1). The comparison of results from identical specimens exposed to high humidity and immersed in fresh water is particularly pertinent as results from aged sandwich tee joints have been obtained from an environmental chamber (Chapter 11) and a link to the long-term material behaviour was required.

Figure 7.3 shows the short term (560 hours) results obtained for the QEA1200 specimens exposed to 95% RH at 40°C. The experimental approach is described in Section 6.1. The results clearly show linear behaviour when plotted against the square root of time, indicating the initial stages of a diffusion mechanism. The first point to note is the magnitude of percentage mass increase, which is very small compared to that obtained from immersion. This illustrates how liquid water finds its way into voids and openings, whereas water vapour does not show a tendency to collect as a liquid in these locations. Blotting of excess surface moisture prior to weighing was not required for these specimens as their surfaces were dry to the touch. After 560 hours exposed to 95% RH, the percentage mass increase due to moisture uptake in the QEA1200 material had reached 0.75%. After the equivalent length of time immersed in fresh water at the same temperature, the mass increase had reached 2.5%. However, Section 7.2.1.1 describes the initial rapid uptake upon immersion up to 100 hours exposure, which is due to ingress of

water into surface voids and cut edges. This amounts to a 1.6% mass increase. Taking the 1.6% from the 2.5% gives a 0.9% mass increase due only to diffusion of moisture into the material after immersion up to 560 hours. This value is similar to the value of 0.75% recorded for 95% relative humidity exposure.

If complete equivalence between 100% RH and immersion can be assumed, it may be expected that a slightly lower value is obtained from exposure to 95% RH than from immersion. It is also possible that the drying effects of the ambient atmosphere during weighing had a greater effect, because of the lack of moisture trapped in surface voids compared to immersion.

7.2.2 QE1200 Laminate Material

This section describes the moisture uptake results from the two ageing environments for the QE1200 hand lay-up glass/epoxy laminate material. The results are presented graphically and discussed qualitatively and reasons for the observed characteristics are considered throughout.

7.2.2.1 Immersion in Fresh Water at 40°C

Figure 7.4 presents the results from the samples immersed in fresh water at 40°C with the solid line showing the mean of the results. The trends exhibited here are qualitatively similar to those shown by the QEA1200 material in the same conditions, apart from a pronounced oscillatory effect between 10 hours^{½} and 50 hours^{½}. In the QE1200 case there is more scatter in the results but a smaller variation between specimens. The scatter can be attributed to the quality of the specimens and sensitivity to the drying technique. The gravimetric approach relies on a consistent drying and weighing technique. While every effort has been made to maintain consistency, the surface quality of the QE1200 specimens (as with the QEA1200 specimens) is such that small water droplets can become trapped and may be dried by the blotting process on some occasions more efficiently than on others. Any trapped moisture will have a greater contribution to the mass of these specimens than their QEA1200 counterparts, as they are much lower in mass.

The oscillatory nature of the mean moisture uptake curve between 10 hours$^{1/2}$ and 50 hours$^{1/2}$ can be partially attributed to the above, and also to changes in the ambient atmosphere of the laboratory during weighing. During these early stages of moisture uptake, while the majority of absorbed moisture is close to the specimen surface, evaporation from the surfaces while the specimen is removed from its ageing environment can have a significant effect. While consistency in the weighing process was maintained, the ambient laboratory temperature and relative humidity was found to vary. The ambient temperature varied between 25 and 29°C. The atmosphere varied between being dry (37% RH) to moderate (48% RH). This is likely to have lead to surface evaporation being greater on some occasions than on others. This hypothesis is substantiated by the fact that the effect reduces as ageing time progresses; the specimens gain in mass and more moisture is held within the material rather than close to the surface.

The QE1200 moisture uptake curve exhibits a steep initial gradient of the same form as in the QEA1200, but is relatively more pronounced. The initial part of the curve is concave to the abscissa up to10 hours$^{1/2}$, the same duration is in the QEA1200 material. This substantiates the hypothesis of rapid ingress into voids and surface defects. The percentage mass increase at 10 hours$^{1/2}$ is greater in the QE1200 material (2.1%) than in the QEA1200 material (1.7%). This can be attributed to a larger surface area to volume ratio in the thinner QE1200 specimens.

Disregarding the oscillatory nature of part of the curve, approximately linear uptake behaviour is exhibited between 10 hours$^{1/2}$ and 82 hours$^{1/2}$, indicating a diffusion dominated process. This linear portion has a longer duration than in the QEA1200 specimens. The QE1200 specimens are less than twice the thickness of the QEA1200 and more closely approximate a one-dimensional case, thus suffering less from 'impeding diffusing fronts', described by Fellows [7.12] as a factor which can cause the shape of a 3D experimental diffusion curve to differ from a typical 1D case. This is particularly true at the 'shoulder' i.e. the transition between the linear part of the curve and the asymptote to the equilibrium value.

Saturation appears to be approached in the QE1200 material at a moisture content level of approximately 5.5%, which is higher than expected for a laminate material. If however the initial uptake of up to 2% by mass can be attributed solely to water trapped in surface voids, then the total moisture uptake attributable to diffusion into the resin is of the order of 3.5%. This value is in agreement with similar hand lay-up laminate results from the literature (Chapter 2).

In the same way as for the QEA1200 material (Section 7.2.1.1), a theoretical analysis was carried out to determine the theoretical maximum moisture uptake in this material and compare this to the apparent saturation observed in the experimental results. A representative nominal fibre volume fraction, V_f, of 0.5 was therefore assumed. The matrix volume fraction, V_m, was calculated from Equation 7.1. From the image analysis discussed in Chapter 5, void fractions of 15.3 and 8.8% were assumed.

For the calculations it was also assumed that

- Glass fibres do not absorb moisture,
- Epoxy resin saturates at 6% by mass.

Three conditions (a, b and c) of moisture uptake were calculated as described in Section 7.2.1.1.

The values of percentage moisture content by mass are given in Table 7.3 for the three conditions and two extremes of void fraction. It can be concluded from these results that surface voids fill with water and that it is unlikely that any further ageing mechanisms are active such as fibre/matrix interface degradation, leaching or microcracking. This is substantiated by microscopic examination of polished edges of aged specimens which showed no apparent changes compared to the unaged case. It can therefore be assumed that no microscopic damage mechanisms (such as those mentioned above) have occurred, or that they are sub-microscopic.

Two plateaus are discernible in the data prior to final saturation. These are at 40 hours^{½} and 85 hours^{½}. These are more evident in individual sample data (LBU2 and LBU4 for example) than in the mean result. The possibility was considered that these showed evidence of a two-stage process, indicating the presence of moisture in two phases, i.e. in 'liquid' and 'diffusing vapour' states. It was concluded however that these effects are not pronounced enough to show anything conclusive and are within the scatter of the data.

7.2.2.2 Exposure to 95% Relative Humidity at 40°C

Figure 7.5 gives the moisture uptake results up to 560 hours exposure to 95% relative humidity at 40°C. As with the QEA1200 material, these results exhibit broadly linear

behaviour vs. hours$^{1/2}$, but with much lower mass increases than obtained from immersion. Making the same assumptions as discussed in Section 7.2.1, the difference between the initial uptake on immersion at 40°C (2.1%) and the percentage mass increase after 560 hours immersion (2.7%) amounts to 0.6%. This increase can be attributed to the diffused moisture after 560 hours immersion. After 560 hours exposure to 95% relative humidity, the mass increase recorded was 0.44%. This is slightly lower than the immersion value as expected and the discrepancy has been attributed to the lower level of humidity and evaporation during weighing, as described in section 7.2.1.

7.2.3 130 kg/m^3 PVC Foam Specimens

7.2.3.1 General Observations

Figures 7.6 and 7.7 show the moisture uptake results of the thick and thin foam samples respectively on a base of time, during immersion in fresh water at 40°C. The results for the unsealed specimens, the specimens with their edges sealed and the completely sealed specimens are shown. The results for FTS and FNS 1 and 2 are very consistent and describe the moisture uptake behaviour of the sealant on the specimen surfaces. There is very little scatter in these results due to the homogeneous nature of the sealant material. The results from FTU and FNU 1 and 2 exhibit unusual trends, which will be discussed in detail. The results for FTE and FNE 1 and 2 exhibit a combination of trends from the unsealed and sealed specimens but do not show the approximation of a one-dimensional case because of the significant moisture uptake by the sealant itself. A method of separating the results of the sealant and foam materials has been devised and is discussed in Section 7.3, in addition to a discussion on the applicability of existing models to these results. The present section deals qualitatively with the trends that have been observed.

The overall trends exhibited by the thin and thick specimens are the same (Figures 7.6 and 7.7). The differences in magnitude of the results are a function of the surface area to volume ratios. The thin specimens are of much lower mass and have a larger surface area to volume ratio than the thick specimens. Initial moisture uptake into the open cells on the cut surfaces of the specimens therefore contributes more significantly in the thin specimens than the thick, hence the much larger moisture uptake results in the thin specimens. A method of analytically separating the moisture taken into the open cells from the moisture absorbed into the bulk material is described in Section 7.3.

Figure 7.8 shows the results from the thick foam specimens plotted against hours$^{1/2}$. It can be seen that while the sealed specimens exhibit pseudo-Fickian behaviour due to the sealant, the unsealed foam specimens do not. The specimens with their edges sealed exhibit the same trends as the unsealed specimens but to a lesser extent.

The initial rapid ingress of water into the open cells on the cut surfaces of the specimens is evident and most pronounced in the unsealed specimens. There is little evidence of this effect in the sealed specimens, further supporting the proposed reason for this phenomenon.

7.2.3.2 Uptake Characteristics of the Sealed Specimens

The Fickian characteristics of the uptake in the sealed specimens is to be expected since the diffusing fronts are passing through a homogeneous polymeric material, albeit a thin layer on the surface of the foam. Figure 7.8 shows how these specimens have linear uptake behaviour (vs. hours$^{1/2}$) up to 95 hours$^{1/2}$, after which time the rate of diffusion slows down. Saturation does not appear to be approached however and the rate of uptake (gradient) becomes similar to that of the foam after the same length of exposure time. This is to be expected as one would assume that once the moisture had diffused through the thin layer of sealant, it would continue to diffuse into the foam material and might begin to show some of the characteristics exhibited by specimens FTU1 and FTU2.

Visual examination of the sealed specimens has shown that a wet layer had formed at the interface between the sealant and the foam material, in some areas causing moisture filled blisters. Prior to saturation of the sealant, it is suggested that the diffusion through the sealant material continues to occur as it has through the initial stages but the rate of subsequent diffusion into the foam material is much slower, forcing diffused moisture to collect at the interface between the sealant and the foam. This 'bottleneck' experienced by the diffusing fronts could explain the decrease in the rate of moisture uptake observed from 95 hours$^{1/2}$ onwards. It does not suggest that a saturation value is being approached: By the end of the test duration, the sealant material is likely to be saturated, fully plasticised and possibly degrading (thus allowing the collection of moisture to more easily degrade the interface), however a gradient or driving force for the diffusion process still exists in the foam material.

7.2.3.3 Uptake Characteristics of the Unsealed Specimens

While Section 7.2.3.2 has provided a possible argument for the observed results from the sealed specimens, the results from the unsealed specimens require a more detailed examination and experimental verification. The results from FTU1 and FTU2 are consistent with each other and show evidence of a multi-stage moisture uptake process, with plateaus at 50 hours^{½} and 90 hours^{½}. Similar trends are exhibited by FTE1 and FTE2, but are less pronounced.

Chapter 2 describes the characteristics of the classic non-Fickian absorption curves and those of the foam are similar to the two-stage model. However, the characteristics of the model are explained by polymer relaxation phenomena during absorption for a homogeneous material. Although there may indeed be a contribution of the relaxation effect on the observed results in the foam, it is unlikely that this is the sole mechanism, bearing in mind its highly inhomogeneous nature. None of the available literature discussed in Chapter 2 has presented data of a similar duration that exhibits trends like those observed here and none have alluded to a proven mechanism of moisture uptake in foams. However, several cases for laminates have been reported where increased moisture uptake is observed after saturation should have been reached, which has been attributed to water in voids within the laminate or at the fibre/matrix interface [e.g. 7.8, 7.10]. It is therefore suggested that the observed multi-stage process in the foam materials is a result of moisture movement through the cell walls and into the cell cavities. A hypothesis has therefore been developed to explain these characteristics.

Stage 1

Up to the first plateau at 50 hours^{½}, the curve's characteristics may be considered pseudo-Fickian. The curve is not perfectly linear in the initial stages, but for a 3D diffusion case, perfectly linear behaviour would not be expected. The applicability of models to this data is discussed in Section 7.3. This indicates that up to 50 hours^{½}, a diffusion process is taking place that reaches saturation relatively quickly. This could be attributed to diffusion of moisture into the cell walls of the first 'layer' of open cells at the surface, i.e. diffusion into polymeric material that is directly exposed to the hygrothermal environment. The cell walls are thin (of the order 10 μm as determined by image analysis in Section 5.2.2), which would explain the rapid attainment of an initial saturation at 50 hours^{½}.

Stage 2

Beyond this plateau at 50 hours$^{1/2}$, a second linear uptake trend is observed before a second, less distinct plateau at 90 hours$^{1/2}$. Once moisture has saturated the first 'layer' of cell walls, it is hypothesised that further uptake occurs not only by further diffusion through the cell wall network, but also by movement of moisture into the first layer of closed cells. It appears that this occurs at a similar or slightly slower rate to the diffusion process observed in the first part of the curve. The linear nature of this part of the curve suggests that it is a diffusion controlled process, indicating that moisture travels into the cells at the rate at which it diffuses through the cell walls. The duration of this process is approximately twice the length of time taken to reach the first plateau. For these reasons it is believed that no cell wall rupture is caused by the hygrothermal ageing process, otherwise a much more rapid uptake would be expected. It is further hypothesised that once moisture is travelling into these cells then diffusion can occur into the second 'layer' of cell walls more easily as well as continuing to travel through the cell wall network from the surface. A second saturation plateau is exhibited at 90 hours$^{1/2}$, when it is hypothesised that this second 'layer' has saturated. It is thought that this plateau is less distinct than the first due to the variation in cell sizes and cell wall thickness. The process of diffusion and filling of cells is then thought to continue in the same manner throughout the material.

This hypothesis depends on the assumption that moisture can diffuse from the cell wall into the cell cavities. A co-researcher (Lembessi [7.4]) suggested that the moisture diffuses around the cells within the polymer but is prevented from leaving the cell walls because of a high internal cell pressure, left from the expansion process at manufacture. It is also suggested by Lembessi that if adjacent cells are of different sizes then their internal pressures will also be different. If this were the case, an expected observation after prolonged ageing and plasticisation would be rupture of the cell walls due to differential pressures. This, however, is not the case. Microscopic examination has shown that there is no cell wall distortion or rupture and it must be assumed that for equilibrium, gas pressures (especially in cells near the surface) must have equalised with ambient. Despite the suggested moisture transport mechanism, the presence of moisture within cell cavities was actually observed under the microscope by Lembessi.

In support of the author's hypothesis, a two-stage model may be expected due to the presence of water in two phases –in the bulk PVC material and in the cells. The trends exhibited are characteristic of this mode of ingress. However, in light of the levels of moisture ingress observed in the laminate results for example, it is difficult to believe that after two years exposure the moisture ingress in the foam has only reached the third 'layer'

of cells. This equates to an ingress depth of only 1-2 mm. A specimen was therefore removed from immersion, sliced through its centre and immediately examined visually and under optical microscope. It was impossible to determine the presence of moisture within cells from microscopic examination, as the process of cutting the specimen had badly damaged the material surface. However, visual examination and a blotted imprint of the cut surface on a paper towel suggested that significant moisture ingress had only occurred to a maximum depth of around 2mm. The central part of the specimen was completely dry. However, it is unclear whether this method of evaluation was able to discern the presence of diffused moisture within the polymeric cell walls further into the specimen, or whether such material would have appeared dry while containing bound moisture. The only possible way of determining whether this was the case would be to employ a more complex experimental analysis, such as the use of nuclear magnetic resonance imaging (NMRI), which has been used previously to measure moisture gradients in polymeric specimens [7.13, 7.14]. This is recommended as an area for further work, but from the present basic techniques it can be concluded that the above philosophical argument has significant value, particularly as it is based on the longest duration of moisture uptake data known to the author to date.

7.2.3.4 Exposure to 95% Relative Humidity at 40°C

Figure 7.9 gives the short term results (560 hours) of the thick foam specimens exposed to 95% relative humidity at 40°C. These appear to exhibit a large mass increase between initial exposure and the first mass reading, before subsequently showing diffusion type behaviour. However, after 560 hours exposure the mass increase only reached 0.91%. This differs greatly from the results obtained from immersion at 40°C, which reached a mass increase of 16% after the same time. If the same assumption is made as for the laminates whereby initial ingress is assumed to last up to 100 hours before the diffusion process dominates, then a mass increase of 10.6% can be taken away from the value of 16%. This still amounts to a 5.4% increase due to diffusion, far greater than the 0.91% increase observed from the 95% relative humidity results. At present this discrepancy has proved to be inexplicable, though a similar trend has been noted for foam cores in the literature [7.15], from which it is concluded that the core must be directly exposed to water for significant absorption to occur and that it will not accumulate greatly from only a humid environment.

7.3 The Applicability of Existing Diffusion Models to the Experimental Results

The aim of this section is to determine whether the classical diffusion models cited in the literature are able to model the experimental results successfully. That is, it is considered of value to assess whether these models are applicable for the analysis of moisture uptake in laminate materials of a quality representative of the real structure and in closed cell foam materials.

Section 7.2 has highlighted some areas that will be examined analytically. There is scope here for extensive theoretical analysis of the experimental results, however detailed modelling is not required in order to fulfill the aim above.

7.3.1 QEA1200 Laminate Material

The discussion in Section 7.2.1 describes the moisture uptake characteristics of the QEA1200 material immersed in fresh water at 40°C and these are illustrated in Figure 7.1. Beyond an initial rapid ingress, the absorption curve has been shown to be approximately linear for a significant proportion of its duration. The approach, which has initially been assessed with regard to its applicability to these results, was therefore the classical Fickian model. The specimen geometry cannot strictly be approximated to a one-dimensional case, however initially it is the one-dimensional form of Fick's law which has been used.

If it is assumed that the moisture content prior to immersion (M_0) is zero, then the model used (as described in Chapter 2) is given by

$$M_t = M_\infty \left\{ 1 - \frac{8}{\pi^2} \sum_{n=0}^{\infty} (2n+1)^{-2} \exp\left[\frac{-D(2n+1)^2 \pi^2 t}{l^2} \right] \right\} \tag{7.2}$$

where $$D = \pi \left[\frac{l}{4M_\infty} \right]^2 \left[\frac{M_2 - M_1}{\sqrt{t_2} - \sqrt{t_1}} \right]^2 \tag{7.3}$$

and the second term in brackets in Equation 7.2 is the gradient of the linear part of the absorption curve.

The shape of the absorption curve is not linear from the time of immersion due to the rapid initial ingress, so the fit of the Fickian model has been assessed using two different gradients:

a) The gradient of the linear portion of the curve beyond time 10 hours$^{1/2}$,
b) The gradient of the tangent to the curve at time zero.

It was also necessary to assume an approximate value of saturation (M_∞) by extrapolating the existing experimental results.

The experimental results and the two Fickian curves are shown in Figure 7.10. It is clear that a much better fit is obtained from the model using the linear gradient beyond the initial ingress. The Fickian curve lies below the experimental results because it does not account for this initial ingress and hence if the initial uptake value were taken away from the experimental results, the fit of the Fickian model would be much improved. It would however then either over-estimate the moisture content at saturation or depart from the experimental curve at the 'shoulder' in a similar way to case (b). Greater conformity could be gained at the shoulder by using the three-dimensional form of Fick's law (as described in Chapter 2), however the relatively protracted programming required was not warranted for this exercise.

7.3.2 QE1200 Laminate Material

The same approach was taken for this material as described in Section 7.3.1 for the QEA1200 material. The results for the QE1200 immersed in fresh water at 40°C are given in Figure 7.11. The one-dimensional form of Fick's law for case (a) would provide the most reasonable fit if the initial rapid ingress was removed from the experimental results. However, the model would then over-estimate the moisture content at saturation or depart from the experimental results in the region of the 'shoulder' of the curve. Overall, the fit of the models is worse in this material than in the QEA1200 material, which is unexpected considering that the QEA1200 is thicker (more 3D) than the QE1200. The greatest influence on the success of the theoretical models fitting to the experimental data is the quality of the specimens. It is evidently the rapid initial uptake and subsequent high value of saturation, which cause the shape of the experimental curve to depart from the classical model.

Aronhime *et al* [7.16] report NMR evidence that indicated that, at low moisture contents (<1% in an epoxy), the water was strongly bound to polar sites. At higher moisture contents however, there was evidence of the presence of mobile or free water in the material. Given the moisture uptake trends for the QE1200 material, this is likely to be the case here. A more appropriate diffusion model should therefore account for water existing in both bound and mobile forms, for example a two-phase model. This is discussed in connection with the foam materials (Section 7.3.3).

7.3.3 Closed Cell PVC Foam Material

As discussed in Sections 7.1 and 7.2, moisture uptake in the foam materials has been examined in specimens completely unsealed, with edges sealed to approximate a one-dimensional diffusion case, completely sealed to assess the effectiveness of the sealant and of two different thicknesses. The characteristics of the long-term moisture uptake curves (Figures 7.6 – 7.8) are governed by absorption into the bulk material, ingress into open cells on the cut surfaces and absorption by the sealant. The analysis of these results is therefore more detailed.

Three aspects have been examined:

- Separation of moisture absorption into the sealant from moisture absorption into the foam
- Separation of moisture ingress into open cells on the cut surfaces from absorption by the bulk material
- The fit of diffusion models to the experimental results

7.3.3.1 Separation of Moisture Absorption into the Sealant from Moisture Absorption into the Foam

In order to assess the fit of a one-dimensional diffusion model to the one-dimensional absorption data, it is necessary to theoretically remove the moisture absorbed by the sealant in the specimens with their edges sealed. In order to achieve this, the moisture uptake by the sealant was determined.

Four specimens (FTS1, FTS2, FNS1, FNS2) were completely sealed and their moisture uptake monitored. It was assumed that the absolute mass gain per unit area of these

specimens should be the same up to the point where uptake begins by the foam. These results are given in Figure 7.12, which shows that the curves of the four specimens are virtually superimposed on one-another up to 106 hours$^{1/2}$, where there is a departure marked by the appearance of bubbles at the interface between the sealant and the foam. For the purposes of this analysis, this was assumed to be the point of 'saturation' of the sealant where absorption by the foam begins. This data, from time zero to 106 hours$^{1/2}$, with an assumed constant value of saturation beyond 106 hours$^{1/2}$, was then multiplied by the surface area of sealant in specimens FTE1, FTE2, FNE1 and FNE2. This was assumed to equate to the moisture content of the sealant round the edges of these specimens and was therefore taken away from the original measured mass gain results. The known dry mass of the sealant was also taken away from these results, finally giving the results for moisture uptake by the material from the two opposite faces, i.e. the true one-dimensional moisture absorption case. The moisture uptake % by mass is shown in Figure 7.13. However, it should be noted that these results still include the mass contribution of the ingress of water into open cells on the two cut faces. The next stage of the analysis was to remove this mass contribution from the data.

7.3.3.2 Separation of Moisture Ingress into Open Cells from Absorption by the Bulk Material

The ingress of water into the open cells on the cut surfaces of the specimens was assumed to occur virtually instantaneously, compared to the overall length of exposure time. The cell size may have prevented water entering all open cells upon initial immersion due to surface tension effects or trapping of air bubbles, but it was assumed that after 24 hours and two weighing/blotting procedures, the contribution of water in open cells to the overall mass would have stabilised. It was also assumed that up to this time the contribution from moisture diffused into the bulk polymer would be negligible.

The mass gain per unit surface area was therefore determined for the four unsealed specimens (FTU1, FTU2, FNU1, FNU2) after 24 hours immersion. This was found to be consistent between specimens with a coefficient of variation of only 0.85%. The absolute mass gain from ingress into open cells for all specimens was therefore determined and taken away from the original experimental data for the 3D (unsealed) and 1D specimens. The results are shown in Figure 7.14.

7.3.3.3 The Fit of Diffusion Models to the Foam Experimental Results

The qualitative discussion of Section 7.2 has suggested that the shape of the absorption curve up to the initial plateau is governed by diffusion of moisture into the bulk polymeric material directly in contact with the environment. A valid approach to assessing the applicability of diffusion models to the experimental results is therefore to begin by applying the one-dimensional Fickian model to the initial part of the experimental curve.

The results from Figure 7.14 were shifted along the time$^{1/2}$ axis so that zero mass increase coincided with zero time. The same approach as with the laminates was adopted (Section 7.3.1) whereby the diffusivity was calculated from the initial linear gradient (Equation 7.3) and saturation was assumed at the first plateau in the absorption curve. The one-dimensional Fickian curve was then obtained using Equation 7.2. The result for the unsealed thick foam is given in Figure 7.15 and shows how the one-dimensional model does not conform well to the three-dimensional experimental data in the region of the 'shoulder' i.e. the region of greatest curvature. The three dimensional form of Fick's law may improve the correlation significantly.

Figures 7.16 and 7.17 show the fit of the 1D model to the modified one-dimensional experimental data of the thick and thin specimens respectively. Here it can be seen that the fit of the model is greatly improved, being slightly better for the thick specimens than the thin. This shows that the one-dimensional form of Fick's law models the initial part of the foam absorption curve adequately, provided one-dimensional absorption results can be successfully obtained from the experimental data.

The next stage of the analysis was to find a model that would conform to the full range experimental results, i.e. a model that could accommodate a two or even three stage absorption process. Chapter 2 (Section 2.1 and Figure 2.2) has given a brief overview of such models and the two-stage Langmuir model seemed the most appropriate. The Langmuir model is given by

$$M_t = M_\infty \left\{ \left(\frac{\beta}{\gamma+\beta} \right) e^{-\gamma t} \left[1 - \frac{8}{\pi^2} \sum_{n=1}^{\infty(odd)} \frac{e^{-kn^2 t}}{n^2} \right] + \frac{\beta}{\gamma+\beta} \left[e^{-\beta t} - e^{-\gamma t} \right] + \left[1 - e^{-\beta t} \right] \right\} \quad (7.4)$$

where M_t = total mass % moisture uptake after time t (%)

M_∞ = moisture uptake at saturation %

D = diffusion coefficient for mobile molecule of water (mm^2/s)

t = time (s)

$k = \pi^2 D/l^2$ = characteristic diffusion constant (/s)

l = specimen thickness (mm)

β = probability per unit time that a bound molecule of water becomes mobile (/s)

γ = probability per unit time that a mobile molecule of water becomes bound (/s)

If the exposure time is long enough that kt is large compared to unity, the following approximation holds:

$$M_t \approx M_\infty \left[1 - \frac{\gamma}{\gamma+\beta} e^{-\beta t}\right], \qquad 2\gamma, 2\beta << k, t >> \frac{1}{k} \tag{7.5}$$

Relationships for β and γ can be derived from Equation 7.7, as given by Carter and Kibler [7.17] as follows:

$$\left.\begin{aligned} -\left(\frac{dM_t}{dt}\right)^{-1} \frac{d^2 M_t}{dt^2} &\approx \text{ constant } \equiv \beta \\ e^{-\beta t}\left[\beta\left(\frac{dM_t}{dt}\right)^{-1} M_t + 1\right] &\approx \text{ constant } \equiv 1 + \frac{\beta}{\gamma} \end{aligned}\right\} \begin{aligned} &2\gamma, 2\beta << k \\ &t >> \frac{1}{k} \end{aligned} \tag{7.6}$$

In this work, the equations of trend lines through the moisture uptake data plotted against time were obtained and differentiated as appropriate to obtain the expressions in Equation 7.8. and hence values of β and γ. This is the same method as used by Carter and Kibler, who then used Equation 7.7 to obtain a predicted value of the saturation moisture content M_∞. D could then be obtained from the expression for the characteristic diffusion constant k, as follows,

$$D = \frac{kl^2}{\pi^2} \tag{7.7}$$

where k is obtained by rearranging the following expression [7.18],

$$M_t = \frac{4}{\pi^{3/2}} \left(\frac{\beta}{\gamma+\beta} M_\infty\right) \sqrt{kt} \tag{7.8}$$

D and k are therefore both functions of time and moisture content.

This technique was not able to adequately model the moisture uptake curve for the foam materials, primarily because suitable constant values for β and γ could not be obtained. This may have been due to the inadequacy of the automatically generated trend lines in adhering to the shape of the uptake curve. The solution to this may be to use more accurate and complex curve fitting techniques, or to adopt a more scientific method for determining the various parameters. No such analysis has been presented in the literature reviewed by the author.

7.4 Summary

It is apparent that the levels of moisture uptake in the laminate materials are much higher than usually reported in the literature due to their quality, leading to significant ingress of water into voids. For this reason, the classical diffusion model does not adequately fit the experimental data.

In the foam material there is a complex mechanism of moisture uptake, due to its inhomogeneity. A hypothesis for moisture transport in the material has been proposed, based on absorption data more extensive than any in the open literature to date. It was not possible to find an existing analytical model to adequately fit the data. It can therefore be concluded that the moisture uptake mechanism in the foam material is more complex than current models are able to accommodate and further work is required to analyse the characteristics more fully.

7.5 References

[7.1] **Shen, C.H., Springer, G.S.**; *Moisture Absorption and Desorption in Composite Materials*; J. Comp. Mats., Vol 10 (1976), pp2-20

[7.2] **Shubha, M., Parimala, H.V., Vijayan, K.**; *Moisture Uptake by Kevlar Fibres*; J. Mat. Sci. Letters, Vol. 12 (1993), pp60-62

[7.3] **Gopalan, R., Rao, R.M.V.G.K., Murthy, M.V.V., Dattaguru, B.**; *Diffusion Studies on Advanced Fibre Hybrid Composites*; J. Reinforced Plastics and

Composites, Vol. 5 (1986), pp51-61

[7.4] **Lembessi, E-M.M.**; *Hygrothermal Ageing of Composites*; M.Sc. Thesis, School of Engineering Sciences, University of Southampton, 1999

[7.5] **Browning, C.E., Husman, G.E., Whitney, J.M.**; *Moisture Effects in Epoxy Matrix Composites*; Composite Materials: Testing and Design (4th Conference), ASTM STP 617, ASTM 1977

[7.6] **Fukuda, M., Kawai, H.**; *Moisture Sorption Mechanism of Aromatic Polyamide Fibers: Diffusion of Moisture in Poly(p-phenylene terepkhthalamide) Fibers*; Textile Research Journal, Vol. 63, No. 4 (1993), pp185-193

[7.7] **Aronhime, M.T., Neumann, S., Marom, G.**; *The Anisotropic Diffusion of Water in Kevlar Epoxy Composites*; J. Mat. Sci., Vol. 22 (1987), pp2435-2446

[7.8] **Gellert. E.P., Turley, D.M.**; *Seawater Immersion Ageing of Glass-Fibre Reinforced Polymer Laminates for Marine Applications*; Composites Part A (Vol. 30 (1999), pp1259-1265

[7.9] **Huston, R.J.**; *The Effect of Glass Transition Temperature an Interlaminar Shear Strength of Glass Reinforced Epoxy Composites*; Proc. ICCST/3, Int. Conf. On Composites Science and Technology, 11-13 Jan 2000, Durban, S.A.

[7.10] **Chateauminois, A., Vincent, L., Chabert, B., Soulier, J.P.**; *Study of the Interfacial Degradation of a Glass-Epoxy Composite During Hygrothermal Ageing Using Water Diffusion Measurements and Dynamic Mechanical Thermal Analysis*; Polymer, Vol. 35 (1994), No. 22, pp4766-4774

[7.11] **Loos, A.C., Springer, G.S., Sanders, B.A., Tung, R.W**; *Moisture Absorption of Polyester E-Glass Composites*; Journal of Composite Materials, Vol. 14 (April 1980), pp142-154

[7.12] **Fellows, L.M.P.**; *Moisture Absorption in Low-level Porosity Thermoplastic Toughened Epoxy Composites*; Ph.D. Thesis, Department of Engineering Materials, University of Southampton, 1999

[7.13] **Salisbury, M.K., Clague, A.D.H., Herbert, I.R., Cotgreave, T., Mansfield, P. and Taylor, D.**; *Application of Nuclear Magnetic Resonance Imaging to the Study of Water Ingress into non-Metallic Materials*; Polymers in a Marine Environment, 17, 1989, pp 131-135

[7.14] **Rothwell, W.P., Holecek, D.R. and Kershaw, J.A.**; *NMR Imaging Study of Fluid Absorption by Polymer Composites*; J. Polymer Sci: Polym. Lett. Ed., 22, 1984, pp 241-247

[7.15] **Frye, B.**; *Water Ingression in Composite Sandwich Parts: A Multi-Year, Multi-Organisational Team Investigation*; Proc. 21st Int. SAMPE Europe Conference

of the Society for the Advancement of Material and Process Engineering, Paris, 18-20 April 2000, pp559-569

[7.16] **Aronhime, M.T., Peng, X., Gillham, J.K., Small, R.D.**; *Effect of Time-Temperature Path of Cure on the Water Absorption of High Tg Epoxy Resins*; J. Appl. Polym. Sci., Vol. 32 (1986), pp3589-3626

[7.17] **Carter, H.G., Kibler, K.G.**; *Langmuir-Type Model for Anomalous Moisture Diffusion in Composite Resins*; J. Comp. Mats., Vol. 12 (1978), pp118-131

8. DETERMINATION OF THE EFFECTS OF HYGROTHERMAL AGEING

An overview of the literature concerning the effects of hygrothermal environments on the material and mechanical properties of polymeric composite materials has been given in Chapter 2. These effects are primarily caused by chemical and physical changes in the polymers as a result of diffusing moisture. The aim of this chapter is to investigate how the properties of the laminate and foam materials being considered in this work are affected by prolonged exposure to a hygrothermal environment. The technique used to achieve this is Dynamic Mechanical Thermal Analysis (DMTA). By testing specimens periodically throughout the exposure process, the evolution of their viscoelastic properties can be monitored. Of specific interest in this work is the evolution of the glass transition temperature and modulus, giving a measure of the extent of plasticisation and degradation (or otherwise) of the mechanical performance.

The DMTA technique and an overview of the tests conducted are described in Section 6.2. The present section gives details of the structure of the experimental programme and test specimens and then goes on to explain the overall characteristics of the DMTA results before discussing the trends in the recorded data.

8.1 Programme Structure and Specimen Details

As described in Section 2.2, the primary aim of this programme was to obtain storage modulus, loss modulus and tan δ results for the constituent sandwich materials at intervals throughout the hygrothermal ageing process. A set of test specimens was manufactured from each of the four materials of interest:

- QEA1200 laminate material
- QE1200 laminate material
- Divinycell H130 PVC foam material (130 kg/m^3)
- Divinycell H80 PVC foam material (80 kg/m^3)

Further details of these materials are provided in Chapter 5.

All specimens were of nominal dimensions 30.0 × 12.0 × 2.0 mm and were prepared from the parent panels with high quality cut edges. All specimens were stored in a dessicator

prior to testing or hygrothermal exposure. Three specimens of each material were tested dry to provide a reference base. Nine specimens of each material were kept immersed in fresh water at 40°C and six of each were kept immersed in fresh water at 60°C. It was assumed that the global moisture uptake behaviour of these materials would have the same characteristics at any temperature below the glass transition region and were therefore originally immersed at a single temperature (40°C). However, it was considered that changing the exposure temperature could have an effect on the mechanical properties of the materials. The DMTA programme therefore investigates the results of two ageing temperatures.

Prior to testing, the required specimens were removed from the heated baths, weighed to obtain an approximate moisture content value and then placed in a small container for transport filled with water at the same temperature as their environment. Prior to fixing a specimen in the instrument, a measurement of thickness to 0.001 mm was taken by averaging three micrometer readings over the specimen's length. The width was measured using vernier calipers to an accuracy of 0.01 mm. The test length of the specimen, which was the unsupported length between clamps, was also measured using the calipers. These were the required input parameters in the data acquisition software.

Only a single specimen could be tested at any one time. Specimens were usually tested in groups of three to provide a mean of three sets of results. It was possible to test up to eight specimens in one day but usually two groups of three were tested. Test sessions were conducted on one day at approximately monthly intervals. Results have been obtained for a range of exposure times between 0 and 292 days. A summary of the test programme is given in Table 8.1.

8.2 Characteristics of DMTA Results

Figures 8.1, 8.2, 8.3 and 8.4 show examples of the reference (unaged) results for the QEA1200, QE1200, H130 and H80 materials respectively. These plots illustrate the typical shapes of storage modulus, loss modulus and tan δ as a function of temperature for the four materials. It is apparent from these figures that all of the materials show similar trends although the actual numerical values are quite different. The plots are characteristic of any amorphous polymer and certain features are significant.

8.2.1 Storage Modulus

The characteristic plot of the storage modulus is in three stages. In the 'glassy' region below the polymer T_g, the storage modulus remains approximately constant until the onset of the glass transition region where it falls sharply before settling to a low constant value in the 'rubbery' region. The temperature of the onset of the transition is known as T_{g1} and is useful in design as it describes the absolute temperature limit for structural properties to remain stable. The temperature at mid-transition (i.e. steepest gradient) is known as T_{g2}.

The storage modulus is supposed to be representative of the elastic modulus or Young's modulus. However, for the four materials tested here, the correspondence seems to be markedly worse for the higher moduli. Values at 35°C have been extracted from the DMTA results and mean values taken. These are compared to the manufacturers' quoted values in Table 8.2.

The reason for the discrepancy, particularly with the laminate materials is not absolutely clear. The materials are well within the acceptable modulus range for the equipment [8.1] and it has been shown [8.2] that there is no frequency dependence at ambient temperature or the test frequency of 10 Hz. Three sources have been identified as the likely cause, and the discrepancy may be due to one or a combination of these.

Firstly, it is possible that the discrepancy can partly be attributable to the relatively small sample length to thickness ratio causing a significant shear component in the flexural deformation. If the background theory implicitly assumes that all deformation results from bending, then the shear component is ignored, causing the measured stiffness and hence modulus to be significantly compromised. Zweben *et al* [8.3] refer to the same phenomenon in three point bending tests carried out to ASTM D 790. They note that it is common to find in the open literature, flexural moduli that are significantly lower than extensional moduli, particularly for laminated materials, because there is no consideration of the contribution of shear deflection to total beam deflection. The results of their study suggest that to obtain valid data, flexural modulus values should be determined using at least a 60/1 span-to-depth ratio. This is clearly not possible for the DMTA specimens.

An approach, based on that by Zweben *et al*, is described in Appendix B, which analytically determines the proportion of deformation due to shear, from which the approximate reduction in modulus can be calculated. For the foam materials, on the basis

of this approach, it was found that the proportion of the deflection due to shear was only 3.9%. This leads to a slight improvement in the actual moduli (84.8 MPa for the H130 and 48.4 MPa for the H80) but does not bring them into line with those quoted by the manufacturer.

The effect of shear is more pronounced in the laminated materials due to interlaminar effects, however the theory suggests that for both laminate materials the shear contributes only 6.5% to the overall deformation. This leads to only slightly improved moduli (3350 MPa for the QEA1200 and 3596 MPa for the QE1200). This is clearly not the expected result and it can be assumed that the analytical approach underestimates the real case. Zweben *et al* substantiate this: A plot of apparent modulus vs. span-to-depth ratio for a Kevlar/epoxy laminate is presented which, when extrapolated to small span-to-depth ratios, clearly shows that a reduction in apparent modulus of 80% is possible for span-to-depth ratios twice that of the DMTA specimens. This region is not accurately modelled by the theory.

Secondly, if there is any variation in thickness along the sample length, or any error in the measurement, the accuracy of the stiffness can be compromised. The stiffness relies on an accurate specimen thickness measurement (t) and is a function of t^3.

Finally, a likely significant contributor to the discrepancy is the reduction in perceived properties due to sample geometry. The values that the manufacturer quotes are often based on testing of high quality, thick specimens. Since the DMTA laminate specimens are only two plies in thickness, any resin rich or resin starved areas or regions of defects on the surfaces (such as illustrated in Figure 5.5), can have a greater contributing effect than in the manufacturer-tested specimens. A similar scale effect is present in the foam specimens, which have a very low thickness to cell size ratio and are therefore likely to behave differently compared to the bulk material.

8.2.2 Loss Modulus

The loss modulus characteristics are similar to those of the storage modulus in that values are high and constant below the transition region and low and constant above it. The loss modulus curve also exhibits a hump at the start of the transition region, which corresponds to the maximum heat dissipation per unit deformation.

8.2.3 Tan δ

The tan δ curve is derived from the ratio of the loss modulus to the storage modulus. The most important feature is its peak in the glass transition region, which corresponds to high damping due to the initiation of micro-Brownian motion. The peak is known as the primary α-transition and is associated only with the motion of the main polymer chain. The temperature at which the peak occurs is commonly quoted as the glass transition temperature, in addition to T_{g1} and T_{g2} (Section 8.2.1). Peak tan δ is generally easier to identify as a discrete temperature than T_{g1} or T_{g2}. For the comparative work here, peak tan δ is therefore quoted as the T_g. Table 8.3 summarises the mean results from the tan δ curves, giving the peak magnitude and the temperature at which it occurs.

There is little difference between the magnitudes of the Tan δ peaks in the two foam materials. This is to be expected as they are of the same material, albeit a different density. The slightly higher value exhibited in the lower density foam indicates its higher energy absorption. There is a much larger difference between the laminates however, with a significantly greater viscous damping contribution from the QE1200 than the QEA1200. The main contributing factor to this effect is likely to be the higher matrix volume fraction in the wet lay-up QE1200 material compared to the pre-preg QEA1200 material. The significantly higher T_g in the QEA1200 is to be expected due to the higher temperature cure of the pre-preg compared to the wet lay-up material.

It would be expected that the two foam materials would exhibit the same glass transition temperature as they are made from the same polymer, but there is a difference of 7.64°C between them. This could be partially attributed to slight variations in the composition of the polymer (as outlined in Chapter 5). The most significant contributor is likely to be a temperature lag effect. In the higher density H130, the temperature equilibration in the material is slightly slower than in the lower density H80. This means that the observed trends in the DMTA results appear to occur at a slightly higher temperature in the higher density material than in the lower density material.

Figures 8.3 and 8.4 show a large amount of noise in the results. This is because the instrument drive force was required to be very low for the prescribed amplitude, due to the samples being very weak. The greatest noise is observed in the rubbery region of the H80 material because of its very low stiffness above T_g. It is evident from these tests that useful

data beyond the transition cannot be obtained. A partial solution would be to use a stiffer sample (i.e. thicker) but this may add to the possible errors due to shear, as discussed previously.

8.3 Effects of Ageing in QEA1200 Laminates

Figures 8.5, 8.6 and 8.7, (a) and (b), show the overall storage modulus, loss modulus and tan δ results respectively for the QEA1200 material at the two hygrothermal exposure temperatures. The following section summarises and discusses the results of primary interest, i.e. the room temperature storage modulus changes and the effects of ageing on the tan δ peak.

Table 8.4 summarises the storage modulus results at 35°C. The dominant trend is a decrease in the room temperature storage modulus values with an increase in duration of ageing, at both 40°C and 60°C. There is reasonable consistency within sets of specimens, apart from in the case of those aged at 40°C for 285 days, which are more widely spaced. This scatter may be attributable to variation in specimen quality, though there was little evidence of this on inspection of the polished edges under the microscope. Checks have also been made for other possible errors such as inaccurate thickness measurement, but these were not found to be a problem.

Examination of the gravimetric data from these specimens shows negligible weight increase between consecutive readings after 285 days exposure, indicating that at this time a reasonable approximation to saturation was reached. The storage modulus results in Table 8.4 for 285 days exposure at the two temperatures have only 0.8% between them. This indicates that the reduction in modulus due to ageing in this material is a function of moisture content, but not ageing temperature. That is, there is no evidence of increased modulus degradation from exposure at a higher temperature. These results are qualitatively as expected, considering the evidence for modulus reduction resulting from plasticisation in epoxy composites given in the literature (Chapter 2).

Although there is potentially significant variation between samples, the loss modulus trends between the aged and unaged samples remain consistent, as shown in Figure 8.6. The first point to note is the overall shape of the loss modulus distribution. This is much broader in form for the unaged specimens than for the aged specimens. The 'aged'

distribution is more skewed and the position and magnitude of the loss modulus peaks is also different between the aged and unaged specimens. These results are summarised in Table 8.5.

The reduction in the temperature at which the peak occurs indicates that after exposure to a hygrothermal environment, the onset of rubbery behaviour occurs at a lower temperature, leading to a reduction in the temperature range over which glassy properties are maintained. If the observed storage modulus reduction can be attributed to plasticisation as the literature suggests then it follows that an increase in the viscous behaviour of the material may also be expected. However this is not the case since a reduction in the peak loss modulus values is observed, which may be evidence for a possible embrittlement phenomenon. Evidence of this effect is also present in the tan δ results, which exhibit a reduction in T_g (indicating plasticisation) as well as a reduction in the peak value with increased ageing (reduced damping). The tan δ results are summarised in Table 8.6. This effect may be attributable to the 'antiplasticisation' phenomenon cited by Boinard [8.4] and is discussed in more detail in Section 8.7.

The first point to note from Table 8.6 is the observed reduction in glass transition temperature with ageing. The difference between the three results is considered to be within the scatter of the data and therefore indicates that for long-term exposure to a hygrothermal environment, a 10-12% reduction in T_g can be expected in this material.

With regard to the magnitude of the peak, the slight increase after 82 days is considered to be within the scatter of the data. It is therefore only subsequently that any substantial changes are observed. After 285 days, a significant reduction is observed which is larger after exposure to 60°C than to 40°C. This indicates a reduction in the viscous damping behaviour of the material, which is not consistent with the possible increase in plasticisation indicated by the reduction in T_g. Akay *et al* [8.5] state that a decrease in the peak height is an indication of uneven plasticisation throughout the specimen, which is often accompanied by a broadening of the peak. This could be attributed to a different level of plasticisation of the fibre/matrix interface compared with the bulk of the matrix (Section 2.2.1), or inhomogeneous ingress such that there remain regions within the specimen of little or no moisture absorption. This characteristic is also observed by Zhang *et al* [8.6]. Chateauminois *et al* [8.7] attribute a broadening of the damping peak to the occurrence of specific morphological changes and debonding at the fibre-matrix interface.

8.4 Effects of Ageing in QE1200 Laminates

Figures 8.8, 8.9 and 8.10, (a) and (b), show the storage modulus, loss modulus and tan δ results respectively for the QE1200 material at the two temperatures, and are more consistent than in the QEA1200 material.

Table 8.7 summarises the storage modulus results at 35°C and a reduction is observed with increased duration of hygrothermal exposure, as in the QEA1200 material. The degradation of the modulus appears to get progressively worse with ageing at 60°C, but the behaviour seems to show the reverse trend at 40°C. It is unlikely that the 40°C result shows evidence of the antiplasticisation phenomenon (Section 8.7), as a similar trend would have also been expected in the 60°C results. There is no obvious reason for this that can be related to the ageing process and must therefore be treated as an anomaly, the cause of which is likely to be specimen variation. Visual inspection of the specimens has shown the presence of surface defects, particularly on the mould face. These seem to be greatest in specimen 1A, which could explain its very low modulus reading. Specimen 2B is possibly the best quality, which may be reflected in its high modulus result.
The variability between specimens is also illustrated by the loss modulus results, which are illustrated in Figure 8.9 and summarised in Table 8.8. With ageing at 60°C, there is a large range in peak values. The peaks have been shifted by a significant amount to a higher temperature compared to the unaged case. Outside the peak region there is not a great difference between the unaged and aged results. The peaks are also shifted to a higher temperature with ageing at 40°C, though to a lesser extent than at 60°C. The shape of the curve from specimen 1A is very different from 1B and 1C. The anomalous behaviour shown by 1A concerns the dramatic decrease of low temperature values from an abnormally high room temperature value. The initial part of this curve is also very noisy. The curve then exhibits two peaks, the second of which occurs at the same temperature as the other 'aged' peaks but is at a much lower value. Its first peak is at a lower temperature but a higher value.

The results from all the aged specimens exhibit a 'hump' or 'shoulder', which occurs at a temperature slightly lower than the main peak at around half the peak magnitude. It is suggested that this phenomenon could be attributable to two possible phases in the resin – a plasticised part where the moisture has had an effect and a non-plasticised part where the moisture has not reached. This argument is substantiated by the location of the shoulder

occurring at approximately the same temperature as the peak of the unaged composite. The same conclusion was drawn by Akay *et al* [8.5].

This phenomenon was not observed in the QEA1200 material. However, a significant broadening of the low-temperature side of the peak shown in Figure 6.6 is discernible which was attributed to a lower temperature onset of viscous behaviour. This could be the same effect as observed in the QE1200 material, but to a lesser extent.

There is better consistency between the tan δ results from the 60°C case than the 40°C case. The anomalous behaviour of specimen 1A is again evident in Figure 8.10. The shape of the peak is very similar in the unaged and aged specimens on the lower temperature side, but above T_g, the aged curves broaden out and exhibit a shoulder between 100 and 110°C. This again is more pronounced and consistent in the 60°C case than the 40°C case. This could be attributed to incomplete cure of the resin [8.8]. The results are summarised in Table 8.9.

In all aged specimens, the magnitude of the peak is considerably reduced from the unaged condition, to a greater extent from ageing at 60°C than at 40°C. This indicates a reduction in viscous damping with ageing, as exhibited by the QEA1200 material. The change in T_g is not as pronounced as in the QEA1200 material. Hygrothermal ageing at 60°C appears to induce a 6-7% increase whereas ageing at 40°C has caused very small changes that are within the scatter of the data.

8.5 Effects of Ageing in H130 Foam Material

The storage modulus, loss modulus and tan δ results are shown in Figures 8.11, 8.12 and 8.13 (a) and (b) for the two temperatures respectively. It is difficult to distinguish trends between the aged and unaged specimens as there is a large amount of variation between results, attributable to a variety of sources. As mentioned previously (Section 8.2.1), error in the thickness measurement can lead to large errors in the results. The foam was so weak that measurement of the specimen thickness with a micrometer caused indentations in the specimen surface. Careful use of the micrometer in not damaging the specimens may have caused the micrometer 'tightness' to vary between the three readings taken over the specimen length. Likewise, care was taken in ensuring that the specimens were not damaged by the instrument clamps. As mentioned in Section 6.2, this was achieved by

tightening the clamps to a pre-determined torque using an Allen key with a sensitive torque meter attached. Even this method sometimes caused slight crushing of the foam specimens, which could have had a significant effect on the results. It is possible that the variation can also be attributed to slight variations in the foam density and hence material properties. This effect is very difficult to quantify in samples that weigh only 0.09 g (likewise in the H80 material where the average specimen weight is of the order 0.06 g).

The mean storage modulus results are summarised in Table 8.10. Having described the sources of error, it is apparent from the recorded standard deviations that the scatter tends to be greater between the aged specimens than those that are unaged. The sources of error described above indicate that a random scatter might be expected. The 'selective' scatter observed must be a function of the degree of ageing. The reason for this could be due to specimen shrinkage during the temperature ramp of the test. If swelling has been caused by moisture ingress then it follows that as this moisture is evaporated upon heating, shrinkage may occur. In fact, foam specimens examined after testing have shown a necked region between the clamps, which indicates that shrinkage has occurred in the unclamped region but has been constrained by the clamps nearer the ends. This may not completely explain the scatter in the storage modulus results as these are taken at 35°C by which time little moisture would have evaporated.

The significant reductions in storage modulus observed with increased duration of immersion at 40°C are consistent with a plasticisation process, as observed in the laminate materials (Sections 8.3 and 8.4).

As with the storage modulus, a large amount of scatter was observed in the loss modulus results. The variation is greater between the aged specimens than the unaged. It can be seen from Figure 8.12 that the shape of the aged curves is similar to the shape of the unaged curves in the peak region, but at lower temperatures a slight hump or shoulder is observed in the aged results. This has similar characteristics to those observed in the QEA1200 and QE1200 laminate materials (Sections 8.3 and 8.4). The reduction in the peak temperature with ageing (see Table 8.11) however contradicts the observed increase in peak temperature in the laminates. It is possible that the hygrothermal ageing process alters the foam material chemically or morphologically, thus causing the observed response.

Similar scatter is observed in the tan δ results (Figure 8.13 and Table 8.12). Data beyond the peak cannot be assumed reliable because of the large amount of noise due to the very low drive force when the material becomes rubbery (as discussed in Section 8.2). Trends up to the peak are reasonably well defined. The shape of the curve in the aged specimens is broader than the unaged case and the peak values are much higher, which can indicate a greater degree of viscous behaviour. The changes in Tg can be considered negligible and within the scatter, other than the result for immersion at 60°C for 275 days. In conjunction with the storage modulus results, these results show evidence of an increase in plasticity with ageing.

8.6 Effects of Ageing in H80 Foam Material

The storage modulus, loss modulus and tan δ results are given Figures 8.14, 8.15 and 8.16 (a) and (b) respectively for the two ageing temperatures. There is a considerable amount of noise in these results, though it appears to be less than in the higher density H130 material.

The mean storage modulus results at 35°C are summarised in Table 8.13. The unaged specimen results are very close to one another but the scatter is much greater between the aged specimens. As discussed in Section 8.5, this could be due to shrinkage during the temperature ramp of the test. It is likely that moisture would be evaporated quickly as the specimens are small and light.

The decrease in storage modulus with increased ageing is in agreement with the other materials tested and shows evidence of plasticisation due to exposure to the hygrothermal environment. The reduction of almost 16% is greater than observed in the other materials however. This could be because this particular material is of very low density and the specimens are thin, allowing the moisture to have had a greater degrading effect over the same time scale. The changes in loss modulus are however less pronounced than in other materials. These are summarised in Table 8.14.

The shapes of the loss modulus curves do not vary much between the aged and unaged cases, apart from a slight hump on the low temperature side of the aged results, which is more discernible in the 60°C immersion cases. The peaks occur at similar temperatures to the unaged case and there is little variation between the magnitudes of the peaks. Again the data is very noisy due to the low sample stiffness and hence low drive force. It can be

deduced from these results that the hygrothermal ageing has had little effect on the viscous behaviour of the material. The tan δ results however show very significant changes. These are summarised in Table 8.15.

In conjunction with the modulus values, the substantial increases recorded in the magnitude of the tan δ peak indicate an increase in plasticity. However, the increases in T_g cannot be considered negligible, particularly after a longer duration of hygrothermal exposure, indicating evidence of embrittlement or antiplasticisation (Section 8.7). This is not in complete agreement with the results obtained from the higher density H130 foam, where the change in T_g was much less significant. This could be due to a more rapid evaporation and greater influence of the temperature ramp in the lower density H80 material. This may be evidence to suggest that the antiplasticisation phenomenon cited by Boinard [8.4] is not solely an effect of the hygrothermal ageing, but also an effect induced by the rapid heating during the DMTA test. This is discussed in more detail in Section 8.7 below.

8.7 Hypothesis

The results of all four materials show substantial evidence for a plasticisation or softening process caused by the hygrothermal ageing. This has manifested itself as a reduction in the storage modulus results with increased ageing time, extracted from the DMTA data at 35°C. These results are representative of the room temperature properties as this temperature is close to the start of the test and so little evaporation from heating will have occurred. Although there are large discrepancies between the DMTA results and the manufacturer's quoted values, particularly for the laminate materials, the comparative results can be considered valid.

This plasticisation is further substantiated in the foam materials by a general trend of a lower temperature onset of the loss modulus peak and an increased magnitude of the tanδ peak with ageing. However, the increased tanδ peak temperature in both foam materials indicates an increase in T_g, suggesting the opposite of plasticisation is occurring, i.e. a possible embrittlement process.

In the laminate materials the trends are slightly different, with the loss modulus and tanδ peak magnitudes both reducing with increased ageing, suggesting embrittlement. This

trend is supported in the QE1200 material with an increase in T_g, but contradicted in the QEA1200 with a reduction in T_g.

Boinard [8.4] observed a similar increase in Tg in polyester and vinyl ester laminates and attributed the trend to 'antiplasticisation', where an 'antiplasticiser' is a chemical defined by its ability to increase the modulus of a cured product, in contrast to the effect expected from the addition of a plasticiser [8.9]. The antiplasticisation phenomenon is reportedly due to the leaching of 'free' (non-cross-linked) styrene monomer residues that were acting as a plasticiser in the laminate [8.4]. It is also noted that Unsworth and Ng [8.10] attribute an increase in modulus of bulk PVC immersed at 70°C to the loss of a plasticiser. The leaching out of unreacted monomer or hardener has also been suggested in the literature as a cause for non-Fickian behaviour in resins when material is lost and the gravimetric technique cannot distinguish it from reduced moisture uptake. However, desorption analysis of a full range of specimens has shown that (within a band of scatter of approximately ±5%) the re-dried mass is the same as the original dry mass. In fact, nine out of the eleven specimens re-dried were within ±1.5% of the original dry mass. This shows that, within the accuracy of the technique, there is no evidence for material loss due to leaching.

The author therefore hypothesizes that the antiplasticisation phenomenon observed here is a combination of interrelated effects due both to the hygrothermal ageing process and to the rapid heating action of the DMTA technique. Firstly consider the reduction in modulus exhibited in all of the aged specimens. This shows clear evidence for a plasticisation process caused by moisture diffusion into the polymeric materials. Secondly, consider the increased T_g in all materials apart from the QEA1200. This shows clear evidence of an increase in cross-linking, characteristic of postcure. It is possible that the rate of heating of the DMTA tests (2°C/minute) is slow enough to cause some postcure, but it would have occurred to the same degree in all specimens, whether aged or unaged. This alone is therefore not enough to explain the observed increase in T_g with ageing, nor the fact that the QEA1200 material did not exhibit this increase.

The postcure must therefore be caused by the heating action of the hygrothermal environment. There is very strong evidence to suggest that this is the case, as follows. None of the materials tested were postcured at the time of manufacture. The QE1200 material was cured at a maximum temperature of 45°C and the QEA1200 pre-preg at a maximum temperature of 80°C. The maximum processing temperature of the PVC foam is

quoted as 80°C. In both the foams and the QE1200 material, the increase in T_g is negligible in the specimens aged at 40°C, indicating that only a small amount of further cross-linking is taking place at this temperature, the small increase observed being offset by the action of the plasticisation reducing the T_g. This is not surprising considering the cure temperature at manufacture. In the specimens aged at 60°C however, the increase in T_g is much more significant, indicating a large increase in cross-linking. The QEA1200 exhibits a decrease in T_g because neither ageing temperature is sufficient to increase cross-linking, so the observed effect is due to plasticisation only.

The above argument may appear to contain a contradiction however. Increased cross-linking should also manifest itself as an increase in modulus, but the opposite is observed. A similar effect is also reported by Aronhime *et al* [8.9]. It is believed that the perceived reduction in modulus is due to a combination of two effects; stress relaxation in the material caused by the heating action of the hygrothermal environment [8.11] and the effect of plasticisation partially out-weighing the effect of increased cross-linking. However, it is also noted that Levy *et al* [8.12] observe spectroscopic changes in epoxies exposed to hygrothermal environments, which indicate a *water*-induced postcure reaction. In this case it is inferred that the water acts as a plasticising catalyst for the postcure reaction both at elevated temperature and at room temperature, the postcure being facilitated by relaxation of internal stresses induced by the plasticising effect of water, i.e. the postcure is enhanced by increased molecular mobility.

In addition to the above effects, it is believed that a significant effect occurs due to the rapid heating induced by the DMTA test. This is also noted by Akay *et al* [8.5]. It is known that some effects of hygrothermal ageing in polymers are irreversible chemical changes, however it is also known that some effects are reversible upon evaporation of the absorbed moisture. It is therefore hypothesized that in addition to the cross-linking caused by postcure, there is some recovery in properties of the aged specimens compared to ambient as they are heated during the DMTA test; these combined effects resulting in the observed reduction in modulus at room temperature as well as the apparent increase in T_g.

In order to substantiate the property recovery hypothesis, a short test programme was carried out on samples of the C70.130 foam material, which had been immersed in fresh water at 40°C (FNU1 and FNU2, see Chapter 7). Initially, specimens of as-manufactured material of the same geometry as the above specimens were tested in compression and load deflection traces obtained. Foam material which had been immersed for 2.5 years and

had reached an approximation to saturation, was removed from the water bath and compression tested immediately. Finally, material that had been immersed for 2.5 years and then had been completely re-dried was then also tested.

Compared to the unaged material, the aged, wet foam exhibited a 4.1% reduction in compression modulus, which is of a similar order to those results obtained by the DMTA. The re-dried material however exhibited a 34.9% increase in modulus compared to the unaged case. This proves that there is indeed a reversal of plasticisation upon drying which, in addition to the postcuring effects of the ageing environment and drying process, can lead to a significant increase in properties compared to the unaged case.

A final note is that strong evidence for embrittlement has been exhibited in the results for aged specimens in the form of reduced viscoelastic behaviour. Raman spectroscopy has shown that the rapid heating of specimens (particularly the foams) to above their T_g causes irreversible damage in the materials that have been aged. To support this, inspection of the specimens after the test has shown discolouration and shrinkage and also that they are indeed more brittle than the unaged, untested material. This is likely to be related to the evaporation of the moisture, which is effectively boiling off as the test progresses. This, combined with the tiny applied vibrational force, could be enough to cause significant morphological changes, as well as macroscopic damage such as cell rupture, though it was not possible to find evidence of this during microscopic examination of tested specimens.

8.8 Summary

In summary therefore, the overall trends in the DMTA results have yielded the following hypothesis:

- At room temperature, a reduction in modulus is observed because the stress relaxation and plasticisation effects of hygrothermal exposure out-weigh the effects of any ageing-induced postcure.
- A reduced T_g is observed in high-temperature-cured materials due to the plasticisation effects of ageing.
- An increased T_g is observed in low-temperature-cured materials due to postcure induced by hygrothermal exposure. The increase is greater with increasing ageing temperature.

- The heating action of the DMTA test may cause a further small amount of postcure. The main effect of the heating however is the drying of the test specimens. This may cause a partial recovery in properties due to reversible ageing effects.

The above discussion may question the applicability of the DMTA technique in the determination of hygrothermally aged material properties. However, limited results of mechanical tests from aged specimens of the same materials have proven to be consistent with those obtained by the DMTA [8.13].

8.9 References

[8.1] TA Instruments DMA 2980 Technical Reference Manual, 1997

[8.2] **Meunier, M.**; Ongoing Ph.D. Research Work, School of Engineering Sciences, University of Southampton (Personal Communication, 2000)

[8.3] **Zweben, C., Smith, W.S., Wardle, M.W.**; *Test Methods for Fiber Tensile Strength, Composite Flexural Modulus, and Properties of Fabric Reinforced Laminates*; Composite Materials: Testing and Design (Fifth Conference), ASTM STP 674, S.W. Tsai, Ed., American Society for Testing and Materials, 1979, pp228-262

[8.4] **Boinard, E.**; *Influence of Water on Polymeric Materials used in Marine Applications*; Ph.D. Thesis, Department of Ship and Marine Technology, University of Strathclyde

[8.5] **Akay, M., Kongahmun, S., Stanley, A.**; *Influence of Moisture on the Thermal and Mechanical Properties of Autoclaved and Oven-Cured Kevlar 49/Epoxy Laminates*; Composites Sci. and Technology, Vol. 57 (1997), pp565-571

[8.6] **Zhang, Y., Liao, Z., Liu, P.**; *Study on the Behaviour of Accelerated Ageing Fabric Reinforced Epoxy Composites*; 29th International SAMPE Technical Conference, Oct 28-Nov 1, 1997, Vol. 29, pp197-206

[8.7] **Chateauminois, A., Vincent, L., Chabert, B., Soulier, J.P.**; *Study of the Interfacial Degradation of a Glass-Epoxy Composite During Hygrothermal Ageing Using Water Diffusion Measurements and Dynamic Mechanical Thermal Analysis*; Polymer, Vol. 35 (1994), No. 22, pp4766-4774

[8.8] **Riccieri, J.E., Hecker, L., De Carvalho, Vasquez, A.**; *Interfacial Properties and Initial Step of the Water Sorption in Unidirectional Unsaturated*

Polyester/Vegetable Fibre Composites; Polymer Composites, Feb 1999, V20, 1, pp29-37

[8.9] **Aronhime, M.T., Peng, X., Gillham, J.K., Small, R.D.**; *Effect of Time-Temperature Path of Cure on the Water Absorption of High Tg Epoxy Resins*; J. Appl. Polym. Sci., Vol. 32 (1986), pp3589-3626

[8.10] **Unsworth, J., Ng, Y.S.**; Effects of Immersion in Sea water on the Properties of Polymers used in Special Marine Cable; Trans. IMarE (C), In. Conf. on Polymers in Marine Environments, Vol. 97, Conf. 2, Paper 10

[8.11] **Pethrick, R.A.;** Personal Communication, November 1998

[8.12] **Levy, R.L., Fanter, D.L., Summers, C.J.**; *Spectroscopic Evidence for Mechanochemical Effects of Moisture in Epoxy Resins*; J. Appl. Polym Sci., Vol. 24 (1979), pp1643-1664

[8.13] **Lembessi, E-M.M.**; *Hygrothermal Ageing of Composites*; M.Sc. Thesis, School of Engineering Sciences, University of Southampton, 1999

PART E

CHARACTERISATION OF TEE JOINT MECHANICAL BEHAVIOUR

9. EXPERIMENTAL ANALYSIS OF TEE JOINT LOAD TRANSFER MECHANISMS

This chapter describes the TSA programme of testing which has characterised the load transfer mechanisms within sandwich tee joints of varying geometry. This has been supported by detailed finite element work, which is described in Chapter 10.

The sandwich tee joint construction and constituent materials are detailed in Chapter 5. The joint characterises out-of-plane connections in small, fast marine craft such as between a bulkhead and the hull in Trent Class RNLI Lifeboats. A substantial amount of work has been conducted into the behaviour of single skin tee joints, as outlined in Chapter 3 [e.g. 9.1 – 9.4], however there is scope for further work on sandwich construction joints. This work builds on an initial static test programme carried out on similar joints at the University of Southampton [9.5, 9.6].

9.1 Experimental Programme: Unaged Joints

As described in Chapter 3, out of plane joints are constructed using secondary bonds and therefore have inherent weaknesses associated with them, both due to the stress concentrations they create and due to the lack of fibre reinforcement across the bond lines. It is therefore important to understand the load transfer mechanism within the critical joint area in order to ensure they are designed for adequate mechanical performance. Small, fast craft of sandwich construction tend to be relatively stiff compared to larger single skin craft, such that the influence of hull girder bending is small but slamming can impose significant loads on the structure. One of the primary modes of loading imposed on the tee connections is therefore compression, yet this mode has not been as extensively analysed as tension and bending.

For these reasons, the experimental programme has focused on the analysis of joints loaded in compression. Six different joint geometries were examined, to investigate the effect of three different joint parameters (fillet radius, overlaminate thickness and filled web gap). These are summarised in Figure 9.1 and Table 9.1. These tests were carried out using the SPATE equipment, which is described in Section 6.3 with the thermoelastic theory and background to the technique.

The following sub-sections describe the TSA work carried out on the unaged joints, including the material calibration and the SPATE scans of the joints themselves.

9.1.1 Calibration of the Foam Materials

The experimental approach to the material calibration is described in Section 6.3. This section gives the specimen details, loading and results.

The materials used in the web and flange cores were made from the same foamed polymer (cross-linked PVC) but were of different density (80 kg/m^3 in the web and 130 kg/m^3 in the flange, as detailed in Chapter 5). Their thermoelastic responses were therefore different so a calibration constant was required for each. A block of material 180 mm in length and 26.5 mm × 11.5 mm in cross section was machined from the flange and a block 130 mm in length and 28 × 11.5 mm in cross section was machined from the web of a tee joint. As the foam was globally isotropic, Equation 6.16 was used as a basis for the calibration.

The foam was very weak, so to facilitate the tensile testing, the test specimens were reinforced at each end by bonding 1 mm thick aluminium alloy stiffeners to the material. In order to ensure even loading across the specimens and reduce any stress concentration effects, the load was transferred from the end grips to the foam via the two pins. Anti-bending shackles were also attached at each end of the specimens. In order to improve the emissivity of the foam surfaces for the thermoelastic work, the specimens were coated with two passes of R.S. matt black paint.

An Instron 8501 servo-hydraulic test machine was used to load the specimens. The load control mode of the test machine could not be used due to the flexible nature of the material so cyclic longitudinal strain was applied, of a range 2.38×10^{-3} for the flange and 3.44×10^{-3} for the web. By multiplying these by the tensile modulus values given in Table 5.5, stress ranges of 0.45 MPa for the flange material (H130/C70.130) and 0.28 MPa for the web material (H80) were obtained. The strain frequency was maintained at 8 Hz throughout.

The SPATE detector was set at a working distance of 600 mm giving a scanning spot size of 0.8 mm, which was larger than the deflection range of the specimens therefore negating

the requirement for any motion compensation [9.7]. The average thermoelastic signal recorded for the specimens was 633 U for the flange material and 958 U for the web material, where U is the uncalibrated signal unit.

By substituting the values for σ_{app} into Equation 6.16, the value of A was determined as 7.07×10^{-4} MPaU^{-1} for the flange core and 2.89×10^{-4} MPa U^{-1} for the web core. The variations in the signal were around ±15%, which is large in comparison to that obtained from metallic specimens (usually around 5%). This variation is a direct result of the cellular nature of the material. The cells are 0.35 mm and 0.5 mm in diameter for the flange and web respectively. The scanning spot diameter is greater than the cell size but is of the same order and therefore a slight point-by-point inhomogeneity is to be expected. In metals the morphology of the material is orders of magnitude less than that of the scanning spot size. To achieve this relationship in the foam the detector would have needed to be at least five metres away from the specimen, which would have been impractical.

9.1.2 Calibration of the Laminate Materials

The laminate materials are orthotropic in the through-thickness plane. It is therefore necessary to use Equation 6.18 as a basis for the calibration. A similar experimental set-up to that adopted for the foam materials was used to determine the material constants for the laminate materials. A schematic of the approach is shown in Figure 9.2. The XE900 overlaminate material was used for the calibration and was manufactured into 3 laminated flat strips of 200 mm length, 50 mm width and 10 mm thickness. The strips had steel plates bonded to the ends. Two pins were passed through both the overlaminate material and the steel end plates to ensure uniform loading. As with the foam specimens, the laminates were coated with two passes of R.S. matt black paint. The specimens were loaded in tension as shown in Figure 9.2 to levels of 6 ± 2 and 6 ± 4 kN at a frequency of 8 Hz using an Instron 8501 servo-hydraulic test machine in load control mode.

SPATE scans were taken from the two longitudinal edges of each of the three test specimens for both load ranges. Two load ranges were used and the results compared to ensure that the loading was within the linear regime. From these results values of A^* were calculated by taking an average of the signal over the scan area in each case and calculating the applied stress range from the applied load range and the cross sectional area of the specimen. An average A^* value was calculated as 16.05×10^{-3} MPa U^{-1}. There

was however considerable scatter in the data, the coefficient of variation being around 14%. This has been attributed to the inherent variability in the surface of the material, due to its inhomogeneity and not to any non-linear behaviour.

The quantity α^* was determined on the basis of Equation 6.19, using the technique described in Section 6.3.3. In order to achieve this, two specimens were constructed from nine pieces of 30 mm by 30 mm by 10 mm thick laminate, bonded together in a 'tower block' type configuration as shown in Figure 9.3. Each end had a steel plate bonded to it, which provided a locating point for a ball bearing at its centre. The ball bearings at each end then located in similar fixtures on the test machine, which ensured that there was no asymmetry in the loading. The specimens were coated with two passes of R.S. matt black paint and loaded in compression to a level 8 ± 6.5 kN at 8 Hz. SPATE readings were taken from the four faces of each specimen.

The mean signal was found to be -1421 U with a coefficient of variation of 11%. This value was used in Equation 6.19 along with the A^* value to give an α^* value of 1.61, indicating that α_{22}^P is only slightly larger than α_{11}^P. This value seems low as it may be expected that α_{22}^P would be much greater than α_{11}^P for most composite materials. However, in this through-thickness mode the influence of the fibres is small, as the in-plane lay-up is ±45°. A more isotropic behaviour would therefore be expected, as only an elliptical cross-section of the fibre would be influencing the response in the plane of scanning.

The other laminate materials in the tee joint construction are the QEA1200 and QE1200 materials. The QEA1200 is outside the main area of interest in the joints (see Section 9.1.4) so a calibration constant was not required. As will be seen in Section 9.2, absolute stress values were also not required for the flange inner skin; and the web skins were found not to be significant contributors to the trends in the results so a specific A^* value for the QE1200 was not determined. The resin matrix used in this material is generically the same as that used in the XE900. Although the lay-up of the XE900 is biaxial and the QE1200 is quadriaxial, it has been assumed that the calibration factor derived for the XE900 overlaminate material can also be used in the calibration of the QE1200 material without significant loss of accuracy.

9.1.3 Calibration of the Fillet Material

The properties of the resin that was used for the fillet material are considered to be less variable than those of the overlaminate and the foam. Therefore the fillet material was calibrated theoretically using Equation 6.14, where D for the detector used in the current work is 12.9 KV^{-1}, G was set to 10mV, T was taken to be 293 K, therefore R = 1 and e was 0.92.

The density of the fillet material was calculated as 1161 kgm^{-3}, knowing the proportions of resin and colloidal silica in the mixture. In order to calculate α it was necessary to make some assumptions. Consider a unidirectional FRP laminate where the fibre reinforcement is in the transverse (90°) direction. On the edge it is only the fibre ends that are apparent in the matrix. It is assumed that the colloidal silica filled epoxy shows a similar surface since it is a particulate. Since the thermoelastic technique measures only the response at the surface, it is therefore assumed that the filled epoxy also exhibits similar properties as the 90° laminate. The theoretical expression adopted for the calculation of α in the fillet is therefore [9.2]:

$$\alpha_{22} = \alpha_f(1+\nu_f)V_f + \alpha_m V_m(1+\nu_m) - \nu_{12}\alpha_{11} \tag{9.1}$$

where ν is the Poisson's ratio and V is the volume fraction, the subscripts f and m refer to the 'fibre' and matrix respectively.

It was assumed that the material is completely isotropic, hence $\alpha_{22}^{P} = \alpha_{11}^{P} = \alpha$ and $\nu_{12} = 0.25$. This means that Equation 9.1 becomes

$$\alpha = \frac{\alpha_f(1+\nu_f)V_f + \alpha_m V_m(1+\nu_m)}{1.25} \tag{9.2}$$

where α_f is 5×10^{-6} /°C for silica, ν_f is 0.2, α_m is 5.5×10^{-5} /°C for epoxy, ν_m is 0.37 and V_f and V_m have been calculated as 0.022 and 0.978 respectively. α for the fillet resin was therefore calculated as 5.906×10^{-5} /°C. Equation 6.11 was used to calculate the thermoelastic constant for the fillet material where C_p is quoted by the manufacturer as 3000 J/kgK. Substitution into Equation 6.14 gives the calibration constant for the fillet material as 12.926×10^{-3} MPa U^{-1}.

9.1.4 Tee Joint SPATE Work

A compression mode of loading was designed to simulate the deformation that the joint would experience during a vessel slam. The tee joints were supported by rollers spaced 350 mm apart symmetrically about the centreline of the web on the flange outer skin, as illustrated in Figure 9.1. The FORTReSS rig (Section 6.3) was used for loading the specimens and the nature of the test set up required the plane of the joint to be horizontal rather than in the more usual vertical orientation. Plates were therefore clamped on the flange outer skin in line with the rollers in order to support the weight of the joint and prevent movement. A compressive load of 6.4 ± 3.4 kN was applied directly to the end of the web in the plane of the web using a hydraulic ram, at a frequency of 8 Hz, shown schematically in Figure 9.1. This set-up puts the 'bulkhead' and critical area of the joint into compression while the flange is caused to bend in a similar way to hull panels between bulkheads when subject to an external pressure. The level of load chosen was considered low enough such that non-linear material or global joint behaviour would not arise. The maximum compressive load of 9.8 kN corresponds to approximately 25% of the ultimate joint compressive strength.

The SPATE detector was positioned in the normal vertical working plane. Since the plane of the joint to be scanned was in the horizontal plane, a mirror positioned at 45° below the specimen enabled the signal from the specimen to be reflected into the detector, as shown in Figure 9.4. The approximate SPATE scan area is illustrated in Figure 9.5. The SPATE detector was set at a working distance of 960 mm giving a scanning spot size of 1.23 mm with a spatial resolution of 1.44 mm. Each scan took approximately two hours to complete.

The use of the mirror meant that the signal received by the detector was less than the signal emitted by the specimen during the test, as the mirror was not 100% reflective. The amount of signal attenuation due to the mirror was determined separately by taking SPATE scans from a mild steel specimen loaded in axial tension, with and without the mirror. The scan taken from the specimen without the mirror gave a signal result of 1096 ± 40 U, with a coefficient of variation of 3.6%. The area scan taken from the signal reflected from the mirror gave a result of 1017 ± 87 U, with a coefficient of variation of 8.6%. The mirror therefore reduces the signal by 7.2%. In this work the calibration factor was

determined without the mirror and the signal readings were taken with the mirror. Therefore, once the data for the joints had been obtained it was necessary to multiply it by a factor of 1.077 before calibration.

The raw scan data was exported to a spreadsheet package in an array format where one pixel of the scan corresponded to one cell in the spreadsheet. The different component materials of the joint were identified from the raw data and the areas multiplied by their appropriate calibration factor, A or A^{**}, to give the stress sum values in the joint.

The centreline of the joint (through the centre of the web) was identified and used as a datum (Figure 9.5). By using the spatial resolution of 1.44 mm, horizontal co-ordinates were derived for each column of data across the scan area. This enabled plots of distance vs. stress for horizontal lines of interest through the joint scan area to be obtained easily. Two lines of interest were identified and plots were taken for each joint: One line through the flange core, parallel to and 14 mm away from the inner skin; the other horizontally across the web at the top (root) of the fillet. The positions of the two lines are shown in Figure 9.5. The plots of data along these lines are used to compare the TSA results with FEA results and are shown in Chapter 10. The key results are discussed quantitatively in Section 9.2.

9.2 Results of TSA Work on Unaged Joints

The values and positions of maximum stress sums are presented in Table 9.2, taken along the two lines of interest described in Section 9.1.4 above. The stress sum maxima each side of the centreline (see Figure 9.5) are given with their location (positive or negative). The values each side of the centreline datum are not perfectly symmetrical in any of the joints, neither in magnitude nor position. Asymmetry in the test set up was reduced as far as possible by careful mounting of the specimens, so it is considered to be asymmetry in the test specimens themselves (due to variations in the manufacture) that is the main contributing factor.

9.2.1 Results for Flange Core

The maximum stress sum values in the flange core occur in positions in line with the web skins in Joints 1 and 2, without the fillet (i.e. average positions of ±27.3 and 24.5

respectively). The 30 mm fillet in Joint 3 has the effect of spreading the load so that the maxima occur further away from the centreline beyond the plane of the web. In Joint 4 (30 mm fillet with a thin overlaminate), the maxima occur within the plane of the web. The largest stress values occur in Joint 1 with no fillet and a 4-ply overlaminate. At these loading conditions, the stress magnitude remains below the compressive failure strength of the material of 2.5 MPa. Reducing the thickness of the overlaminate in the configurations without a fillet appears to have a large beneficial effect on the stresses in the flange core. In the configurations with the 30mm fillet however, the opposite effect is observed. This is illustrated by the results of Joints 6, 4 and 3 (of 0, 2 and 4 plies thickness respectively), which show a progressive decrease in flange core stress. It is therefore apparent that the fillet and a thick overlaminate are essential for reducing flange core stresses. The lowest stress values are exhibited by Joint 5, which has a 25mm filled gap at the base of the web. Here the maxima occur further away from the plane of the web than in any other configuration, indicating that the stiff filler material also has the effect of spreading the load.

9.2.2 Results for Web Core

In the web core, the maximum stress sum values occur in each case adjacent to the web skins. As with the flange core, the lowest overall value occurs in the filled gap configuration (Joint 5). Low values also occur in the two configurations without a fillet, with the thinner overlaminate being more beneficial. The highest values are exhibited in the joints with a 30 mm fillet. These show the same trend as for the flange core, whereby increasing the overlaminate thickness reduces the stress sum in the core material. The highest overall stress sum occurs in the configuration with no overlaminate, which exceeds the compressive failure strength of the material of 1.0 MPa. Therefore, for the web it is shown that if a fillet is present, a thick overlaminate is essential but stresses may be reduced further by having no fillet.

9.2.3 Results for Overlaminate and Web Skins

The maximum $\Delta\sigma_{11} + \alpha^{*}\Delta\sigma_{22}$ in the web skin and overlaminate material do not exhibit such clear trends, however it is apparent that where there is a 30 mm fillet the maximum tends to occur in the web skin, whereas in the configurations without the fillet the maximum tends to occur in the overlaminate. The positions reported in Table 9.2 do not

show this clearly since the dimensions of the six joints are slightly different. The lowest stress values are exhibited by the joint with the filled gap and also by the configuration with a thin overlaminate and zero fillet radius. Increasing the overlaminate thickness appears to increase the stress for the zero fillet configuration. In the 30 mm fillet configurations, the thickness of the overlaminate has little effect on the magnitude of the stress in the web laminates, apart from when there is no overlaminate present. In this latter case, the stress in the web skins far exceeds the stress in any other joint. Assuming that the compressive strengths of the laminates are of the order 80% of their tensile strengths quoted in Table 5.2, then it is apparent that none of the laminates are close to failure in these tests.

9.2.4 Results for the Fillet Material

In the fillet area, the maximum stresses tend to occur in two key areas. These are (i) adjacent to the web skin near the top (root) of the fillet and (ii) adjacent to the overlaminate at the centre of the fillet curve or slightly lower. In the two joint configurations with the 30 mm fillet and the overlaminate (Joints 3 and 4), high stresses occur in both these locations. In the case without the overlaminate, the maxima occur adjacent to the web skin only. In the configuration with the filled gap, the maxima occur adjacent to the overlaminate in the lower half of the fillet curve. The lowest maximum values are exhibited by the joint with the thin overlaminate (4). Values twice this occur in the joints with the thick overlaminate and with the filled gap. The highest values occur in the configuration with no overlaminate.

9.3 Discussion of Results from Unaged Joints

The work described in the preceding sections has identified two main areas for discussion. These include (a) the asymmetry and noise in the experimental data and (b) the significance of the trends in the results.

Considerable scatter was observed throughout all of the data. In the material calibration tests the coefficient of variation in the foam materials was found to be approximately 15%, and in the overlaminate material it was around 14%. In the metal specimen used to investigate the mirror attenuation however, the coefficient of variation was found to be only 3.6%. The large variation in the foam and laminate results can therefore be attributed

chiefly to the inhomogeneity of the material surface. In the laminates this is primarily influenced by the fibre tows and plies. In the foams it is the cellular nature of the material which causes the effect. In the calibration tests, the spatial resolution of the SPATE scans were of the order 0.8 mm. The cell size of the flange core material is 0.35 mm while in the web it is 0.5 mm. Coupled with the cyclic deflection during the tests it is apparent how the inhomogeneity could significantly influence the reading in each pixel of the scan.

When examining the results of the metal specimen to determine the attenuation factor of the mirror, it was apparent that the mirror contributes significantly to the noise in the results. The scan taken from the mirror had a coefficient of variation of 8.6%, which was 2.4 times higher than the scan taken directly from the specimen. The increased scatter in the scans of the joints can therefore be attributed in part to the effect of the mirror.

The asymmetry in the joint scans has been attributed to minimal asymmetry in the loading of the specimens during the tests and to asymmetry in the joints themselves. Asymmetry in the test set up was reduced as far as possible so it is considered to be the asymmetry in the specimens, caused by manufacturing variations, which is the main contributing factor. For example, Joint 5 exhibits the greatest asymmetry in the flange core results and on closer inspection it was found that the gap filler was non-uniform through the thickness of the web. In most cases however, there is a reasonable correspondence between the maximum values on either side of the centreline datum.

The results of this work have produced some interesting trends. It is apparent that it is the core materials, particularly in the web, which are the critical components of the joints. In some cases the compressive failure strengths of the materials are approached or actually exceeded, even at the relatively low loads used in the TSA work. The results indicate that the presence of a fillet and a thick overlaminate can reduce flange core stresses. Web core stresses can be reduced most effectively by having no fillet and a thin overlaminate, but if a 30 mm fillet is present then a thick overlaminate must be regarded as essential.

Some previous experimental work has been carried out on these types of joint under static loading [9.5]. Compression failure was observed in the web and flange cores, characterised by a bulging of the foam. In the case of the flange, this was in the area contacted by the web skins, the position shown in the SPATE work to experience the greatest stresses.

Where there is a fillet present, it has been found to carry a substantial proportion of the stress, particularly when there is no overlaminate. Although in these tests the stress sum values are much less than the failure load, it is evident that with increasing loads the fillet would be the second constituent to fail after the cores. In the static study [9.5], as the load was increased the joints exhibited a progressive accumulation of damage, with the majority of the strength degradation occurring after the initial failure of the fillet resin. The finding from the thermoelastic work is therefore supported by the initial static loading study.

After the fillet failure in the static work, cracking occurred through the thickness of the overlaminate accompanied by delamination and fibre buckling. Buckling was also observed in the top skin of the flange adjacent to the areas identified in the SPATE work as having the maximum value. The maximum in-plane stresses in the overlaminate and the skins were not large enough to cause this failure. This is substantiated by the SPATE work, which shows small stress values in these constituents compared to the quoted failure stress values. It is clear that an interlaminar tensile stress large enough to cause delamination must exist. This is not apparent in any of the SPATE plots because the resolution of the equipment is not high enough to detect this very localised effect. New equipment for thermoelastic stress analysis, the DeltaTherm 1000 [9.7], described in Section 6.3, uses an array of detectors. It is possible to obtain resolutions of the order 0.01 mm by using specially designed lenses. Therefore future work could focus on studying the laminates in the level of detail necessary to identify the interlaminar tensile stresses. A further feature which must play a role in the joint failure is the adhesive bond between the skins and the core; the high resolution lens would also permit the study of this.

A final interesting and important point to note is the beneficial effect that a filled gap at the base of the web has on the results. This has the effect of substantially reducing the magnitudes of the stress maxima, particularly in the foam core materials. The inclusion of such a filled gap in the joint design would therefore be beneficial from the point of view of preventing premature core compression failure, but would significantly undermine the weight savings gained by using sandwich construction. It was considered worthwhile to investigate the stress reducing effect of the web filler further, with a view to improving the joint design. This has been achieved numerically, as described in Chapter 10.

9.4 References

[9.1] **Shenoi, R.A., Hawkins, G.L.**; *Influence of Material and Geometry Variations on the Behaviour of Bonded Tee Connections in FRP Ships*; Composites, Vol. 23, No.5 (1992), pp335-345

[9.2] **Dulieu-Smith, J.M., Quinn, S., Shenoi, R.A., Read, P.J.C.L. and Moy, S.S.J.**; *Thermoelastic Stress Analysis of a GRP Tee Joint*; J. Applied Composite Materials, Vol. 4, No. 5, 1997, pp 238-303

[9.3] **Read, P.J.C.L., Dulieu-Smith, J.M. and Shenoi, R.A.**; *Thermoelastic and Photoelastic Analyses to Characterise Stresses in FRP Connections*; Proc. Int. Conf. on Composite Science and Technology, 1996, Durban, pp 415-420

[9.4] **Shenoi, R.A., Read, P.J.C.L. and Hawkins, G.L.**; *Fatigue Failure Mechanisms in Fibre Reinforced Plastic Laminated Tee Joints*; Int. J. Fatigue, Vol. 17, No. 6, 1995, pp 415-426

[9.5] **Hicks, I.A., Read, P.J.C.L., Shenoi, R.A.**; *Tensile, Compressive and Flexural Characteristics of Tee Joints in Foam Cored Sandwich Structures*; Proc. Sandwich Construction 3, 3rd Int. Conf. On Sandwich Construction, Sept1995, Southampton, Vol. 2, pp579-591

[9.6] **Shenoi, R.A., Read, P.J.C.L., Jackson, C.L.**; *Influence of Joint Geometry and Load Regimes on Sandwich Tee Joint Behaviour*; J. Reinforced Plastics and Composites, Vol. 17 (1998), pp725-740

[9.7] **Dulieu-Barton, J.M. and Stanley, P.**; *Development and Applications of Thermoelastic Stress Analysis*; J. Strain Analysis 33 (1998), pp 93-104

10. NUMERICAL VALIDATION OF EXPERIMENTAL RESULTS

Finite element (FE) models of the six joint geometries detailed in Chapter 9 have been produced using ANSYS 5.4. These have enabled the load transfer mechanisms within the joints to be examined numerically and compared with the results of the thermoelastic work described in Chapter 9. Further studies of the joints have also been achieved using the FE approach that could not be carried out experimentally, such as the web gap size and filler type in the Joint 5 configuration (Table 9.1).

10.1 Modelling Approach

10.1.1 Choice of Element, Material Properties, Geometry Definition and Meshing

ANSYS has the capability to model layered structures by the provision of layered shell and brick elements, however since the tee joints being investigated in this programme represent slices of ship structure, a 2-D eight noded (quadratic) structural solid element (PLANE82) was used which allows both plane stress and plane strain analyses. These quadratic elements permit the use of orthotropic material properties, and in the case of plane stress, the thickness (depth) may also be input. They can tolerate irregular shapes with minimal loss of accuracy, have compatible displacement shapes and are well suited to model curved boundaries such as the fillet and overlaminate.

Linear geometric properties have been used since in this mode of loading a large deflection analysis was considered not to be required. In the fully clamped compression case reported by Shenoi *et al* [10.1] for similar joints under the same loading conditions, the non-linear experimental deviation from the FE analysis occurred at a load of around 35 kN, which is far in excess of the maximum load applied in the SPATE test of 9.8 kN.

The foam core materials have been modelled as isotropic. The slight anisotropy in these materials due to the direction of foam rise during manufacture has been acknowledged and the appropriate material properties used to allow for this, as follows. The plane of the sheet material is perpendicular to the direction of foam rise so that the compressive modulus in the plane is less than through the thickness due to the elongation of the cells. The joint web is loaded in compression parallel to the plane of the sheet, but the area of interest in the flange core is loaded in compression perpendicular to the plane. The compression in this region of the flange core is assumed to arise from the compression in the web. The

effect of '3-point' bending in the flange, which would cause the layers of foam nearest to the inner skin to be in compression parallel to the plane, is considered to be small compared to the local effect of the web. The material properties in the plane of the sheet quoted by the manufacturer are used for the web material, and those quoted for the through-thickness direction are used for the flange material. A full description of the material properties is given in Chapter 5.

The laminate materials have been modelled as orthotropic. Since the model is 2-D and represents a slice of ship structure, the properties of interest in the laminates are in the plane and through the thickness, i.e. the properties parallel to the principal material direction and the interlaminar tensile properties. These are also given in Chapter 5.

The models were generated with reference to the global cartesian co-ordinate system in the *x-y* plane. It was only the curves at the fillet that were generated using local (cylindrical) co-ordinate systems. The orthotropic material properties for the laminates are specified with respect to a co-ordinate system that can be either the global Cartesian system or a local Cartesian system. To aid data extraction for direct comparison with the TSA results it was easier to specify all orthotropic material properties with respect to the global Cartesian system (other than the curved part of the overlaminate, which was specified with respect to its local cylindrical system). This required particular care because some laminates were oriented in the horizontal plane and others in the vertical plane. Taking as an example the web skins, oriented vertically, and the flange inner skin, oriented horizontally, both made of the same material (QE1200). In these cases the through-thickness and in-plane properties were defined the opposite way around to each other and the major/minor Poisson's ratios reversed.

The models were created using the solid modelling approach using keypoints, lines and areas to define the geometry. The solid models were map-meshed by manually defining the required mesh density and line bias. This enabled a very regular mesh to be generated with extra refinement in required areas such as in the region of the fillet. For the laminates, the mesh was generated such that there was one element per lamina through the thickness. Quadrilateral elements were used in all cases apart from in irregular areas such as the fillet resin, where triangular elements were used. For these areas where the curve of the fillet meets the vertical and horizontal, slight modification to the geometry was required. This is because the vertical and horizontal corners of the fillet tend towards zero thickness, meaning that any element in these areas would far exceed its limit of accuracy due to its high aspect ratio. These areas were generated using local cylindrical co-ordinate systems,

so simply by moving the centre of the curve outwards and upwards by as little as 0.1 mm, this problem was overcome. The mesh for the complete joint is shown in Figure 10.1. A more detailed view of the area of interest is shown in Figure 10.2.

10.1.2 Load Application and Analysis

The models were restrained by applying constraints to the keypoints at the support locations, which were transferred to the nodes at these points. Two load cases were run: A simply supported case with displacement constraints in the vertical (y) direction only, and a fully clamped case with constrains in x and y translations and rotations. In the experimental work, because the tee joints were oriented in the horizontal plane, the outer skin of the flange was supported on rollers at the prescribed separation but clamping of plates was necessary on the inner skin opposite the rollers to prevent movement of the joints during testing. This condition was not truly clamped with regard to the boundary conditions, as some rotation of the flange in bending was allowed. However, it was not a true simply supported case either. For this reason the two constraint cases were run in the FE work, as a semi-clamped case could not be created to model the experimental set-up with any accuracy. It should be noted however, that the difference between the results for the two cases was small in the area of interest and within the scatter of the experimental results, so only the results for the simply supported (worst) case are reported for comparison with the TSA. The results from the clamped case are used for the model validation (Section 10.1.3).

For the simply supported case, it is necessary to ensure that the model is constrained adequately in all directions to prevent any rigid body motion. The simple supports provide restraint only in the vertical direction. If there is any slight asymmetry in the model due to asymmetry in areas of free mesh each side of the centreline (such as in the fillet areas), a tiny out of balance force could be produced causing translation in the horizontal direction. It would therefore not be possible to solve the model numerically. To prevent this occurring, a single node at the top of the web at the line of symmetry was constrained in the x direction. The addition of this constraint has no effect on the stresses.

As described in Chapter 9, the load applied to the joints was in compression across the top of the web. In the models, the loads were applied to the top of the web in a way that approximated a uniformly distributed load as follows. The analysis was static so the force applied was equal to the load *range* used in the SPATE tests (6.8 kN). This load was

divided by the number of nodes across the top of the web and applied to each node as a point load. The mesh density was fine and regular, such that the series of point loads accurately represented the required UDL.

The options for the analysis using the PLANE82 element are plane stress and plane strain, as outlined in 10.1.1. The tee joint represents a slice through a part of the ship structure, which would be a plane strain case if the structure were continuous either side of the plane of interest. The experimental work however examines the relatively thin structural specimen in isolation, not as an integral part of the structure. Moreover, the TSA scan examines only the joint surface and the stress component perpendicular to this surface must be zero. For these reasons, a plane strain analysis (although used in previous studies [10.1]) would be invalid and therefore a plane stress analysis has been performed. The option of specifying the joint thickness (100 mm) was chosen so that the real loads could be input rather than a load per unit thickness.

It is acknowledged that in reality, when loading the joint in isolation, there will be a non-uniform stress distribution through the thickness of the joint, which is a maximum at the mid-thickness plane and a minimum at the surfaces due to edge effects. The use of the 2D PLANE82 elements in the FEA does not allow the modelling of this through-thickness loading effect. The FEA will therefore produce results that are the average of those obtained from the 3D (experimental) case, since the work done in deforming the joint must be the same in both cases. The SPATE however gives a result for the surface only. It is considered, for the joint thickness and mode of loading, that the non-uniformity of the stress distribution would not be pronounced and would be within the noise of the SPATE results.

10.1.3 Model Validation

An initial validation of the FE model was carried out by comparing deflection results to load-deflection curves from a previous static test programme [10.2]. This gives a measure of how well the model reproduces the global joint behaviour. In these tests the joints were fully clamped, so the results from the clamped FE models were used. The nodal deflection results were taken on the centreline at the top of the web, equivalent to the point of attachment of the displacement transducer in the experiments. A summary of the results is given in Table 10.1.

In each case the deflection value from the static case was no more than 6% higher than that of the FEA for the clamped condition. The reasons for the slight discrepancy include the fact that the clamping applied in the experiment cannot achieve as stringent clamped boundary conditions as applied in the FE model, and also that the FE approach tends to produce a slightly stiffer model than the test specimen. A variation in material properties between those assumed for the model and the actual values in the experimental joint materials could also have an effect. These factors are discussed in Chapter 12. The correlation is good when compared to previous work [10.1] where the difference in deflection between the FE results and the experimental data was approximately 12%, and it demonstrates that the global behaviour of the joint is being adequately modelled.

10.2 Results from Unaged Joint Models Compared to TSA Results

In order to produce results that are comparable with the TSA data, nodal stress values were extracted along the required lines (as shown in Figure 9.5). In the flange and web cores, principal nodal stress values were extracted and added together (Equation 6.13). In the web skins and the overlaminate material, the component (x and y) nodal stress values were taken, the through thickness component multiplied by α^* (derived by calibration in Chapter 9) and then added to the in-plane component (Equation 6.17). For the fillet resin, the nodal principal stress values were extracted over the entire fillet area. In each case, nodal co-ordinates were also extracted enabling the nodal position to be associated with the nodal stress result. This was achieved manually by exporting the stress data to a spreadsheet package.

The maximum stress sum values and positions along the lines of interest in the joints are presented in Table 10.2. To compare the TSA results with these results, average values have been taken from the two sets of data for each joint constituent given in Table 9.2 and these are shown in Table 10.3. Although this has the effect of 'smoothing' the SPATE results for the joints that produced asymmetric results, it is a necessary step in attempting to examine the trends. All results with differences in maxima either side of the datum greater than 15% are indicated with an asterisk (*) in Table 10.3. The level of 15% is representative of the noise noted in the calibration work.

10.2.1 Results for Flange Core

In the flange core, the maxima coincide with positions in line with the web skins in all cases apart from in the configuration with the filled gap (Joint 5), in which the maximum is shifted further outwards 20 mm beyond the edge of the web. The highest values occur in the joint without the overlaminate and in the joints without the fillet. In the joints with the 30 mm fillet, increasing the overlaminate thickness has the effect of reducing the maximum flange core stress sum. The lowest maximum value is exhibited by the configuration with the filled gap. These trends and positions of the maxima correlate very well with those exhibited in the SPATE results. However, the *magnitude* of $\sigma_1 + \sigma_2$ is at least 50% less than that given by SPATE for all joint configurations.

A comparison between the FEA and TSA stress distributions along the line of interest in the flange core, for each of the six joints, is given in Figures 10.3 (a) to (f). Upon initial inspection, the correlation between the experimental and numerical results could be considered poor. On closer inspection however, it is evident that the greatest discrepancies arise in the peak stress regions, while correlation in the lower stress regions can be considered very good in some cases, for example in Joints 2 and 3. Other discrepancies arise because of asymmetry in the experimental results, which have been attributed to non-uniformities in the joint construction, for example in Joints 4 and 5. The overall shapes of the stress distributions produced by the FEA have the same characteristics as the experimental results, apart from the more pronounced peaks in the TSA. This shows that although the FE model has been proven to represent the global behaviour of the joints, a physical phenomenon exists in the contact region between the web and flange, which is not being modelled adequately. This problem is examined in more detail in the discussion (Chapter 12).

10.2.2 Results for Web Core

In the web core, the maxima occur adjacent to the web skin in every case. The lowest value occurs in the joint with the filled gap. Of the other joints, low maximum stresses occur in the joint configurations without a fillet. The highest maxima occur in joints 6, 4 and 3, the stresses decreasing in magnitude as the overlaminate thickness increases. These trends correlate exactly with those from the SPATE work. The positions of the maxima also concur with the SPATE results. In joints 1, 2 and 3 the magnitude of $\sigma_1 + \sigma_2$ is in

good agreement with that of the FE. In joints 4 and 6 the FE results are 50% less than those of the SPATE results and in joint 5 the FE result is very small compared to the thermoelastic results. In all cases the FE results are less than the experiment.

Figures 10.4 (a) to (f) give a graphical comparison of the FEA and TSA stress distributions through the web core along the line of interest. On the whole there is much greater correlation than in the flange core results, particularly in Joints 1, 2 and 3. Again, the FE fails to model areas of high stress adequately, such as the region adjacent to the web skins in Joint 6. The reasons for this are explored in more detail in the discussion (Chapter 12).

10.2.3 Results for Overlaminate and Web Skins

Considering the values of $\Delta\sigma_{11} + \alpha^{*}\Delta\sigma_{22}$ in the web skin and overlaminate material, the maxima occur in the overlaminate in joints 1 to 4, but in the cases with the filled gap and with no overlaminate the maxima occur in the web skin. This trend is generally in line with the SPATE results apart from in joints 3 and 4. In joints 1 and 2 the values obtained from the FE far exceed those given by the thermoelastic work. However in joints 3 to 5 the correlation between the FE and the experimental data is very good. In joint 6 however, the FE gives a maximum that is 53% less than the SPATE maximum.

10.2.4 Results for the Fillet Material

In joints 3 and 4 the maximum stress sum in the fillet occurs adjacent to the overlaminate, in a position slightly lower than the middle of the curve. For the configuration with the filled gap (Joint 5), the location is almost the same, but slightly lower. For the joint without the overlaminate however, the maximum occurs adjacent to the web skin near the top of the fillet. The FE results show that for joints 3 and 4 the increase in the thickness of the overlaminate has virtually no effect on the stresses, but by removing the overlaminate (Joint 6) the stress is effectively doubled. The values for the fillet in Joint 5 show that the only area of the joint that does not benefit from the filled gap is the fillet. These trends correlate well with the SPATE results.

10.3 Parametric Study

It has been shown from the TSA and FEA work that the joint configuration with the 25 mm filled gap at the base of the web (5) experiences the lowest stresses in the flange and web cores due to the local stiffening effect of the resin filler. Although this specimen was designed to represent a manufacturing defect or variation, the surprising result suggested that it could be beneficial to incorporate such a gap into joints in order to improve their mechanical performance in compression. However, the inclusion of a large filled gap would considerably increase the weight of the structure, undermining the main advantage of lightweight sandwich construction. It was therefore considered appropriate to investigate the effect of different gap sizes, both filled with the epoxy filler and left as air gaps. The joint 5 configuration was used and the FE model for the simply supported case modified to model gap thicknesses of 5, 10, 15, 20, and 25 mm.

10.3.1 Stresses Through Web Core

Changing the gap size and the filler can have a significant effect on the magnitude and distribution of stresses within the web core, as illustrated by Figure 10.5. These plots are taken as before along a line through the web core a distance 30mm from the flange at the top of the fillet. The stress values presented are the sum of the principal stresses, directly comparable with the TSA results as before. The distribution of the stress within the core material is as expected with a minimum at the centre, rising to a maximum at the edges adjacent to the web skins. This distribution is most pronounced in the configurations with an air gap and these cases also produce the highest stress magnitudes, as shown in Table 10.4.

The stresses are lower in the configurations with the filled gap, decreasing as the gap size increases. The stress distribution also becomes more constant with increasing gap thickness for the position considered in this comparison. As the gap size increases, the difference between subsequent minimum stress results also decreases, for example the difference between the minimum values of the 5 mm and 10 mm cases is several times the difference between the 20 and 25 mm cases.

10.3.2 Stresses Through Flange Core

As shown in Figure 10.6 and Table 10.5, changing the gap size and filler has a marked effect on the magnitude of the stresses within the flange core and particularly on the distribution. The line plots taken for this comparison are 2.16 mm away from the flange inner skin and are the sum of the principal nodal stresses as before.

As with the web, the most pronounced change in the stress distribution is caused by the presence of an air gap, and in this case, the magnitude of the stresses is not affected greatly by the size of the gap. The air gap almost always produces the lowest minimum stress values (within the plane of the web), in all cases at a position in line with the centreline of the web. The magnitude of the maximum stresses is also greatest where an air gap is present, in a position in line with the web skins.

The presence of the filled gap produces an overall much flatter distribution and the effect of the size of gap is much more obvious in these configurations. In all but the 5 mm filled gap configuration, the maxima are shifted outwards beyond the plane of the web to between 45 and 50 mm away from the centreline. Beyond around 50 mm the stress magnitude drops off rapidly with a discontinuity at around 85 mm corresponding to the end of the overlaminate, tending to zero stress towards the ends of the flange. The flattest distribution is exhibited by the 5mm filled gap case, having the lowest maximum stresses but also the highest of the minimum stresses (within the plane of the web).

10.4 Summary

Since the TSA has not been proven previously as a valid technique for the analysis of foam sandwich structures such as this, is was deemed necessary to validate the experimental approach by comparing the results to detailed numerical modelling. The FE model was shown to be adequate, as the global deflection behaviour correlated particularly well with deflections obtained experimentally. Excellent qualitative correlation was also obtained between the FEA and TSA results. Quantitatively the correlation was good in areas of nominal stress, however this was not the case in areas of peak stress. If, in these areas, non-linear deformation behaviour due to local effects has occurred, then the linear FEA could not model this adequately. However, the TSA also assumes a linear (adiabatic) condition and can therefore not produce representative results in areas of non-linearity.

On the whole it can therefore be concluded that TSA is a suitable technique for the analysis of sandwich construction joints as the response has been found to agree qualitatively with a validated finite element model.

Finally, with regard to improving joint design, the parametric study has shown that any unfilled gap at the base of the web is highly detrimental to the joint performance, whereas even the smallest filled gap can significantly improve it.

10.5 References

[10.1] **Shenoi, R.A., Read, P.J.C.L., Jackson, C.L.**; *Influence of Joint Geometry and Load Regimes on Sandwich Tee Joint Behaviour*; J. Reinforced Plastics and Composites, Vol. 17 (1998), pp725-740

[10.2] **Hicks, I.A., Read, P.J.C.L., Shenoi, R.A.**; *Tensile, Compressive and Flexural Characteristics of Tee Joints in Foam Cored Sandwich Structures*; Proc. Sandwich Construction 3, 3rd Int. Conf. On Sandwich Construction, Sept1995, Southampton, Vol. 2, pp579-591

11. DETERMINATION OF THE EFFECTS OF AGEING ON JOINT PERFORMANCE

The aim of this programme was to determine how hygrothermal ageing affects the stress distribution in the joints as a result of changes in the constituent materials. The experimental and numerical analyses of the joint mechanics described in Chapters 9 and 10 provide a basis from which changes in the stress distribution can be assessed. These are discussed and compared with the constituent material results presented in Chapter 8. The DMTA results are also used in conjunction with the finite element models to numerically investigate the response of a structural element after long-term ageing. This combination of experimental and numerical approaches combined with material and structural information, provides a comprehensive basis from which the possible mechanical response of an aged structure can be assessed. This is an approach that has not been presented before in the open literature.

11.1 Experimental Programme

11.1.1 Test Specimens

The tee joint test specimens used in this programme were all nominally identical so that direct comparisons could be made between them. They were of exactly the same construction as described in Chapter 5 and as used in the thermoelastic work in Chapter 9. The fillet radius was 25 mm and the overlaminate was 4 plies in thickness. The specimens had a small (2 mm) unfilled gap at the base of the web.

In a 'real' environment, the only parts of the joints directly exposed would be the sandwich skins, the cores being protected by the skins themselves [11.1]. In the test specimens however, the sandwich cores are also exposed to the environment, which is not a realistic condition but is unavoidable when considering what is effectively a two dimensional slice of a three dimensional continuous structure. Encapsulating the joints with the laminate skin material would partially overcome this problem, but would artificially stiffen them. Likewise, coating the exposed foam surfaces with epoxy resin would limit moisture contact with the core but would affect the thermoelastic response.

For the thermoelastic work in Chapter 9, the uniformity in the emissivity of the specimens was improved by coating their surfaces with black paint, hence reducing the noise in the

thermoelastic readings. It was not possible to paint the surfaces of the ageing specimens prior to hygrothermal exposure, as this would impair the absorption of moisture. Painting them after ageing and prior to taking thermoelastic readings would not be viable either, as the specimen surfaces would need to be completely dry and the coating would subsequently prevent further moisture uptake upon return to the hygrothermal environment. The effect of the lack of coating on the noise in the results is discussed in Section 11.2.2.

11.1.2 Ageing Environment and Load Regime

The experimental technique is described in detail in Chapter 6. Three tee joints were exposed to a hygrothermal environment within the purpose-built test facility, FEARLESS (Section 6.4). The temperature of the environment was set at 50 ± 0.1°C. This temperature was chosen with regard to the test time available, the previously used ageing temperatures and the findings from the DMTA programme (Chapter 8). Firstly, it was necessary to accelerate the ageing process as far as possible to obtain the greatest degree of ageing within the timescales of the test programme. Secondly, it was decided that a temperature should be chosen which was similar to those used for the moisture uptake and DMTA programmes (i.e. 40 and 60°C) so that any active ageing mechanisms would be consistent with those already discovered. Finally, it was found in the DMTA programme that for the constituent materials of the sandwich, the onset of the glass transition region, and hence the reduction in modulus, occurred at around 60°C. Since specimens were being mechanically loaded whilst being aged it was necessary to maintain room temperature material properties if possible. A temperature of 50°C was therefore considered most appropriate.

The relative humidity of the environment was set at 90% ± 1%. This was the maximum to which it was safe to go without the risk of instability. During commissioning it was found that running at very high humidities caused occasional rapid fluctuations that took some time to stabilise. Since this was the first full experimental programme to be run using the equipment, a conservative approach was taken.

Of the three joints exposed to the hygrothermal environment, one was left unloaded, one was statically loaded and one was cyclically loaded, as described in Section 6.4. The loaded joints were simply supported on the outer skin of the flange, with a support

separation of 350 mm, and were loaded in compression with the load applied to the top of the web. The load arrangement was consistent with all the previous work as shown in Figure 9.1. Figure 11.1 shows a photograph of the three joints within the environmental chamber. The cyclically loaded joint is shown on the right of the picture, loaded in compression horizontally by the hydraulic ram protruding through the chamber wall from FORTReSS on the outside (Figure 11.2). The unloaded joint is shown furthest from the camera in Figure 11.1, resting on two wooden stands. The statically loaded joint is shown within the static load rig closest to the camera.

The statically loaded joint was initially loaded within the load frame (Figure 11.1) to a level of 8 kN and left untouched whilst in the ageing environment, i.e. a constant deformation of the order 1.5 mm was imposed, but the imposed load reduced over time due to stress relaxation effects. A reduction in stiffness during ageing due to stress relaxation could therefore be quantified.

The load cycle imposed on the cyclically loaded joint by FORTReSS was carefully chosen with regard to the ultimate properties of the joint and the length of the test programme, so that the joint would not fail during the test time. The approach was conservative as there was no fatigue data available for these structural specimens. Since the ultimate compressive failure load of these joints was of the order 40 kN, a maximum load level of approximately 10% was chosen. The cyclic frequency was set very low also. The cyclic load regime applied to the joint was therefore -3 ± 1.5 kN at 0.25 Hz. In the dry joint at the start of testing, this corresponded to a range of deflection of 0.814 mm. Every thousand cycles, the maximum load, minimum load, maximum position and minimum position were written to file, so that overall changes in specimen compliance during testing could be determined.

11.1.3 Thermoelastic Test Procedure

The TSA technique was used to obtain full-field stress information from the joints at intervals during ageing. The thermoelastic equipment used in this case was the DeltaTherm 1000, which is described in Section 6.3. This has the advantage over the SPATE that it can produce a full-field image in a few seconds, whereas the SPATE would have taken up to two hours to develop the same image. The rapid accumulation of data was vital, as surface evaporation from the aged joints had a significant impact on the results (as discussed later in this section). A photograph of the test set-up with the

DeltaTherm is shown in Figure 11.3. The tests were conducted in the normal vertical working plane, precluding the requirement for the mirror as in Chapter 9, when FORTReSS was used to load the joints. Note that the Chamber within the FORTReSS structure can be seen in the background of the photograph.

FEARLESS was shut down and scans from the aged joints were taken on two occasions during the test programme. The first shut-down was at 1437.5 hours (60 days) after the start of testing and the second shut-down was 3450.75 hours (144 days) after the start of testing.

The procedure for obtaining the required information from the joints was as follows. Immediately after shut-down, the unloaded joint was removed from the chamber and weighed. It was then positioned in a servo-hydraulic Instron test machine and loaded at 6.4 ± 3.4 kN at 8 Hz, while thermoelastic readings were taken using the DeltaTherm equipment. The statically loaded joint was then removed from its load rig, noting the residual load, and then weighed. Thermoelastic readings were then taken and the procedure repeated with the cyclically loaded joint.

A preliminary investigation into the ability of the DeltaTherm to obtain thermoelastic readings from a wet, warm surface showed that evaporation and convection from the surface have a significant effect on the results. A soaking wet surface, immediately after being removed from immersion, cannot provide useful results because of excessive noise in the data. Figure 11.4 shows a DeltaTherm scan of a wet joint surface after immersion. The noise in the data is clear and the constituent parts cannot easily be distinguished. It is only after the surfaces have begun to dry that realistic readings can be obtained. Figure 11.5 shows a typical scan of a dry, unpainted joint surface. This is much less noisy compared to Figure 11.4. For this reason, scans from each joint undergoing hygrothermal ageing were obtained at regular intervals up to 3.5 hours after removal from the chamber, until the surfaces were essentially dry. It was found to take approximately 2 hours, allowing the joints from the chamber to equilibrate in the laboratory environment, before reasonable results could be obtained. The joints were then weighed again before being returned to FEARLESS.

11.2 Experimental Results

11.2.1 Analysis Procedure for DeltaTherm Results

Results from the DeltaTherm were obtained in the same format as from the SPATE, whereby the uncalibrated signal unit value from each pixel on the scan plot was directly converted to a spreadsheet 128 columns by 128 rows. The raw SPATE data could be converted into stress results by multiplying by the appropriate calibration factors (Chapters 6 and 9). This however was not possible for the DeltaTherm data, as the unaged material calibration constants cannot be used to calibrate aged materials, since the response of the materials may have changed after exposure to a hygrothermal environment. It would be possible to use 'travellers', which are small specimens of the joint materials (e.g. calibration specimens, Section 9.1) that are aged at the same time under the same conditions as the joints. Scans could then be taken from these to derive calibration constants. However the degree of ageing is a function of specimen geometry so the results obtained from the travellers may not be representative of the state of ageing in the joints. For example, consider two specimens, both square in section, but one cuboid and the other very thin. After some time the thin specimen would become saturated, but after the same length of time the cuboid specimen would not be saturated. The mechanical response of the thin specimen would show the characteristics of the saturated material. The cuboid specimen however would show a response partly influenced by the saturated part of the material and partly influenced by the remaining unaged part of the material.

To overcome the difficulty of not being able to obtain absolute stress values from the aged joint data, all the aged results were normalised with respect to data from an unaged joint of identical geometry, which was tested with the aged joints. Line plots were taken through the web and flange cores of the aged joints in the same way as described in Chapter 9 for the SPATE data. These line plots were normalised by dividing the raw data by the equivalent line data from the results of the unaged joint.

The normalised data could then be directly converted to a percentage change from the unaged case. These results were then compared in regions of peak stress and regions of nominal stress, to determine whether the level of local stress had any influence on the results. Regions of peak stress in the web core were defined as a 5 mm thickness of core adjacent to the skins, while nominal stress regions were defined as 10 mm either side of the centreline. In the flange, the peak stress regions were defined as the regions of maximum stress in the core in line with the web skins and fillet region, and were identified

for each joint from a line plot of the results. The nominal stress region in the flange for the area of interest was defined as a small distance either side of the centreline, as in the web. The reason for distinguishing between nominal and peak stress regions is because of the correlation between the FEA and TSA results (Chapter 10), which was good in the regions of nominal stress but poor in regions of peak stress due to possible non-linear effects. In addition, there are suggestions in the literature (Chapter 2), that higher stresses may increase the material ageing process.

11.2.2 Results from DeltaTherm Scans

The full set of raw data in uncalibrated signal units is presented as line plots in Figures 11.6 (a) to (d), 11.7 (a) to (d) and 11.8 (a) to (d) for the unloaded joint, the statically loaded joint and the cyclically loaded joint respectively. In each set of figures, (a) and (c) are for the first set of tests (after 60 days) and (b) and (d) are for the second set of tests (after 144 days). Results for the web are given in (a) and (b) while results for the flange are given in (c) and (d). In each plot the unaged joint reference 'dry' data is also given. The legend identifies each line of data with respect to the time it was obtained, in hours and minutes after the chamber was shut down. It is obvious that there is a large amount of noise in the early results, which decreases as time progresses, converging to a single curve. It is also clear that there is a difference between the aged results and the unaged results, an indication that thermoelastic stress analysis can indeed be used as a technique to determine hygrothermally-induced changes.

The next step was therefore to examine the extent of these changes, determine any trends and interpret their meaning. The data used in the analysis was that obtained after the greatest length of time after the chamber was shut down. In the first set of tests (after 60 days exposure), the greatest 'out-time' was 3.25 to 3.75 hours whereas in the second set of tests (after 144 days exposure), the greatest 'out-time' was only 2.5 to 2.75 hours. An analysis of the noise in the data however showed that 'stability' had been reached after only 2 hours, so it can be assumed that although the readings were taken after different lengths of time, they are equivalent and hence any differences can be attributed to ageing only.

The coefficient of variation in the results was found to vary as a function of the loading (as well as surface dryness), but not as a function of ageing time. In the unaged joints the coefficient of variation was between 18 and 25%. This is slightly higher than the value of

15% obtained during the calibration work of the foam material (Section 9.1.1), but is to be expected due to these joints not being coated with black paint. The unloaded joint data was found to have a coefficient of variation of around 21.7%, similar to the unaged joint, while the value for the statically loaded joint was 29.2% and for the cyclically loaded joint it was 44.3%. It therefore appears that the noise in the data is related to the stress state in the joint at the time of testing. The statically loaded joint would have had a degree of residual stress at the time of testing, after experiencing stress relaxation while being clamped in the static load rig. The cyclically loaded joint would have had the greatest degree of residual stress after being cyclically loaded in a load control mode where creep could have had a significant effect. The reason why the residual stress state affects the noise in the results however is unclear. The possibility that prolonged exposure causes some surface degradation, which causes the thermoelastic signal to become noisier, may be a contributory factor but does not explain the differences between the three joints.

The percentage changes compared to the unaged case for the normalised data are given in Table 11.1 and are illustrated in Figure 11.9. From Table 11.1 it is possible to distinguish some interesting trends. It was concluded from the work in Chapter 9 that the foam cores in the web and the flange are the most 'critical' parts of the tee joint construction, i.e. they are the first components to fail under increasing load. It has been shown that they carry stresses that are a greater proportion of their ultimate strengths than other materials such as the laminates. Further, it can be interpreted from the results in Chapter 9 that the web core is more highly loaded than the flange core, i.e. the web carries stresses which are a larger proportion of its strength than the flange does. By using this information to interpret the results in Table 11.1 it is clear that the most severely loaded locations exhibit a reduction in signal (indicated by ↓ in the table) compared to the unaged case, while all other areas in the cores exhibit an increase (assuming that a cyclic load regime results in a more severe stress state than the initial application of a static load).

Figure 11.8 illustrates this phenomenon even more clearly. In addition to the results in Table 11.1, results for a third web region have been included in an attempt to establish these trends more clearly. This is for a 'moderate' stress region, between the peak stress and the nominal stress regions. The bar chart shows that the overall trend in the web is for the normalised signal to reduce dramatically as the severity of the stress state increases.

Considering all the results in more detail and examining the trends between the results of the tests after 60 days and after 144 days, it can be seen that the predominant trend is for the signal to increase (or become 'less negative' in the case of the negative results) as

ageing progresses. This is illustrated by red arrows pointing upwards to the right. This is true in all joint locations apart from in the nominal stress areas of the flange in the unloaded and statically loaded joints and in the moderate stress region of the web in the unloaded joint. These opposite trends are shown by a blue arrow pointing down and to the right. If the moderate stress region in the web is considered as an inexplicable anomaly, the remainder of the results suggest that the trend highlighted by the blue arrow is present only in the least loaded or least stressed regions of the joints. The very large difference between the two results from the nominal stress region in the flange of the unloaded joint could also be considered anomalous, but it is assumed that the trend can be considered valid.

11.2.3 Implications of the Thermoelastic Results

The next stage in the analysis of the results was to determine the implications of an increase or decrease in the signal compared to the unaged case. Consider two joints, both of the same geometry and both loaded in the same manner, one having been exposed to a hygrothermal environment, the other having been left in ambient conditions. In the webs of these joints for example, the same load is applied in each so for a given cross-section there must be the same average stress. It is known from the DMTA results that the rate of reduction in room temperature properties in the laminate skin materials is greater than the rate in the foam materials (as after the same length of exposure time the degree of 'ageing' in the laminates was greater than in the foams). In the joint specimens, all surfaces are exposed to the environment, including a large area of the web skins over the depth of the joints, which also acts to protect the core. Since saturation of the core materials could not have occurred over these test timescales for moisture entering through the two opposite surfaces only, there must therefore be a large volume of core material within the joint which has not experienced any effects of moisture. As ageing progresses, the skins are able to carry proportionately less and less of the applied load, therefore causing it to be increasingly sustained by the core material. This implies that an increased signal should be observed within the core material as the stress distribution within the joint changes. While an alteration in the stress distribution within the joints is undoubtedly the primary cause of the observed changes in thermoelastic signal, the complexity of the joints means that all of the results cannot be explained so simply. The following discussion examines the possible reasons for the observed trends in more detail.

The thermoelastic signal, S, is a function of the thermoelastic constant, K (Equation 6.11), but is also a function of the Young's modulus, E, and Poisson's ratio, ν, in the strain formulation of Equation 6.10 [11.2], i.e.

$$\Delta T = \frac{KE}{1-\nu} T\Delta(\varepsilon_1 + \varepsilon_2) \tag{11.1}$$

where ε_1 and ε_2 are the principal in-plane surface strains. Thus,

$$S = f(K),\ f\left(\frac{E}{1-\nu}\right) \tag{11.2}$$

The change in the signal with hygrothermal exposure must therefore be due to a change in one or more of these parameters. The thermoelastic constant is a function of the coefficient of linear thermal expansion and the specific heat of the material, neither of which are likely to change significantly. It is also a function of the density of the material, which would be expected to change with moisture absorption. The mass readings taken from the joints however indicate that there was little appreciable mass increase as a result of exposure to a humid environment (<1%), which was within the range of accuracy of the balance. This is not a surprising result and is in agreement with the results in Chapter 7, which showed a very small mass increase after exposure to humidity compared to immersion, particularly for the foam materials.

It is unlikely that the Poisson's ratio of the material would have changed significantly after this duration of exposure; therefore it must be a change in the Young's modulus that is the primary contributing factor to the changes in signal from the aged joints compared to the unaged case.

Since the thermoelastic signal is proportional to the Young's modulus as a consequence of Equations 11.1 and 6.13, i.e.

$$AS = \Delta(\sigma_1 + \sigma_2) \equiv E\Delta(\varepsilon_1 + \varepsilon_2)(1-\nu) \tag{11.3}$$

then the trend of an increase in signal after ageing compared to the unaged case would intuitively suggest an increase in modulus. The tee joints have a relatively thick section such that diffused moisture would not necessarily have a significant impact on the global

performance of the joint after a relatively short period of exposure. Since temperature equilibrates through the specimen virtually instantaneously compared to the moisture, it could be assumed that the effect of postcure was dominating the joint performance, hence the increased signal after hygrothermal exposure and the tendency for the normalised signal to become 'more positive' with increased duration of exposure. This would indeed be the case if the applied strain in the unaged and aged conditions were the same. The thermoelastic signal would therefore be only a function of the Young's modulus and Poisson's ratio and the latter is assumed not to change significantly. However, in the tests performed here, the specimens were loaded in load control rather than position control. This means that the same load (and hence stress) was applied in the unaged and aged cases. From the relationship in Equation 11.3 it is obvious that if the same stress is applied then the same thermoelastic signal is produced, regardless of whether there is a change in stiffness, as this is compensated for by a change in strain. The increase in signal exhibited in these sets of results cannot therefore be attributed to an increase in stiffness, even though postcure has been shown to be a dominant effect of hygrothermal ageing in these materials (Chapter 8).

It should be remembered that the thermoelastic signal is a function of the condition of the joint surface and is therefore not necessarily representative of the global joint performance. While the global joint performance was governed by the bulk of the material (i.e. the unaged, possibly postcuring, material within the specimens dominating the load-deflection response), the surface that was scanned had been directly exposed to the hygrothermal environment and would have been affected by it. A possible scenario is that the surface had been plasticised during ageing and was then re-dried while out of the chamber. With reference to the results of the foam compression tests discussed in Section 8.7, a significant increase in modulus would therefore be expected in this surface material after ageing and subsequent re-drying. The resulting situation would therefore be of a stiffened surface layer on a slightly more compliant substrate. Dulieu-Smith and Stanley [11.2] have studied the effect of surface coatings on the thermoelastic response of materials. The biaxial surface strains of the substrate are 'copied' directly into the coating, i.e. $\varepsilon_s = \varepsilon_c = \varepsilon$, where the subscripts s and c refer to the substrate and coating respectively. The stress in the substrate is therefore $\sigma_s = E_s\varepsilon$ and the stress is the coating is $\sigma_c = E_c\varepsilon$. Since the assumption is that $E_s < E_c$, the *stress* in the coating will therefore be higher than in the substrate and the thermoelastic signal from the aged surface will therefore be higher than from the unaged surface.

In summary therefore, an increase in thermoelastic signal compared to the unaged case could be attributed to

a) A greater rate of degradation in the skins than the core;
b) Recovery or improvement of properties after exposure and re-drying;

In the most severely loaded regions of the joints (i.e. all of the peak and moderate stress regions in the web cores of the three joints and the nominal stress region in the web core of the cyclically loaded joint), the thermoelastic signal was found to reduce compared to the unaged case. There is a possibility that the reverse of (b) is occurring, whereby the surfaces have not experienced a recovery in properties as above but are plasticised and are therefore more compliant than the material underneath. This could be considered equivalent to a compliant surface coating on a substrate of greater stiffness. By the same argument as above, this would result in a reduction in the signal, but this cannot explain why the effect seems to be localised to the most highly loaded areas.

The only remaining explanation is that it is due to structural mechanics. The high peak stresses in the web core observed adjacent to the skins are a result of the required compatibility between the stress in the skins and the stress in the core at the interface between the two. It has been shown in the DMTA (and is mentioned at the start of Section 11.2.3), that the rate of stiffness reduction with ageing is greater in the skin materials than in the core. Therefore at any time during the ageing process, the percentage reduction in modulus of the skin material is greater than the percentage reduction in modulus of the core material. This causes the stress distribution to become flatter, i.e. the peak stresses reduce and the minimum stress at the centreline increases. The reduction or increase in stress relates directly to a reduction or increase in thermoelastic signal. In light of this effect it is understandable why there should be an increased signal exhibited in the nominal stress region (about the centreline) and a reduction in signal in the peak stress region (near the skins).

In summary therefore, a decrease in thermoelastic signal compared to the unaged case could be attributed to

c) Plasticisation of the surface material;
d) Changes in the stress distribution due to different rates of ageing in different materials.

It therefore appears that the dominant effect is the different rates of ageing in the different joint constituents, which results in a change in the load path in the critical region of the joint. This is as a result of a uniform applied strain distribution across the top of the web and strain compatibility between the skins and the core.

11.2.4 Stress Relaxation Analysis of Statically Loaded Joint

As explained in Section 6.4.4, the static load was applied to the joint within its load frame by an Instron Test machine at the start of exposure. When removed from the chamber for testing, the static load frame was removed from the specimen in the same way in which it was applied, such that the residual load could be recorded. By determining the deformation imposed on the joint in its unaged condition and assuming that this remained constant throughout exposure until being removed, the stiffness change due to stress relaxation can be quantified:

$$\Delta k = k_i - k_r = \frac{P_i}{\delta} - \frac{P_r}{\delta} \tag{11.4}$$

where k = stiffness (kN/mm)

P = applied load (kN)

δ = imposed deflection (mm)

and the subscripts i and r refer to the initial and residual conditions respectively.

The results of this calculation are given in Table 11.2.

11.2.5 Compliance Analysis of Cyclically Loaded Joint

Changes in stiffness could manifest themselves in two ways in the cyclically loaded specimen. Figure 11.10 shows schematically how a reduction in stiffness could change both the amplitude of deformation (in load control) and the mean position of the ram at the point of application of the load. It is assumed that deformation is within the linear elastic regime. The schematic P-δ graph in Figure 11.10 shows a load deflection curve taken at time t_1 (e.g. the unaged case) and a second taken at time t_2 (after a duration of hygrothermal exposure), which has a reduced gradient and hence reduced stiffness. The

maximum load, minimum load and mean load are marked on the vertical axis and their corresponding deflections for t_1 and t_2 are marked on the horizontal axis.

The displacement amplitudes a_1 and a_2 are shown. These are the difference between the maximum and minimum displacements in each case and $a_1 < a_2$.

The changes in the maximum deflections and minimum deflections ($\Delta\delta_{max}$ and $\Delta\delta_{min}$) are also shown. $\Delta\delta_{max}$ is greater than $\Delta\delta_{min}$, which means that the mean position of the ram (or point of application of the load) also increases with duration of exposure. The ram is therefore more extended for the application of the same compression load because the specimen has become more compliant.

A change in displacement amplitude and a change in the mean position of the ram were therefore the two characteristics examined in the data recorded by FORTReSS (maximum and minimum position every 1000 cycles).

The results appear to be contradictory. The analysis of the change in amplitude yielded an overall decrease, hence an increase in stiffness, from approximately 5 kN/mm at the start of testing to approximately 12 kN/mm at the end. These results cannot be considered reliable however, due to progressive misalignment in the displacement transducer.

The change in the mean position of the ram however, has yielded creep results that show a reduction in compliance consistent with that determined from the statically loaded joint. These are presented in Table 11.2 and were calculated as follows. The initial displacement of the unaged joint for the mean load of 3 kN was first determined. The change in mean position between the start and the end of the exposure duration was calculated from the data acquisition files. This value was added to the initial displacement to give the final displacement (corresponding to the mean load of 3 kN). The change in stiffness was then determined using Equation 11.4.

11.2.6 Comparison of Stiffness Reduction in Loaded Joints

The results from the analyses outlined in Section 11.2.4 and 11.2.5 above are given in Table 11.2. The results are presented as a reduction in 'stiffness', which is specifically a measure of the time dependent reduction in viscoelastic relaxation modulus and

viscoelastic creep modulus for the statically loaded joint and cyclically loaded joint respectively. The correlation between the results from the two joints is excellent. This illustrates how the exhibited stiffness reduction is a function of time, temperature and the effects of ageing and not a function of the applied load. That is, the reduction in 'stiffness' is not greater in the statically loaded joint although the initially applied load (and hence strain) was greater than in the cyclically loaded joint. The results indicate that after prolonged ageing and stress relaxation/creep, there could be considerable residual stress levels within the joints after they are unloaded. This could result in a change in the stress distribution compared to the unaged case, when re-loaded for taking thermoelastic readings. It is not known whether the effects of residual stress have an appreciable effect on the thermoelastic response in polymeric materials. This is considered in Chapter 12.

11.3 Finite Element Model of an Aged Joint

The aim of this work was to determine the possible response of a joint after long-term exposure to a hygrothermal environment. Assuming a worse case condition of all materials in the joints being saturated, the results from the material test programme could be applied to the finite element models, yielding results that could be compared with the partial ageing results of the experimental programme described in Sections 11.1 and 11.2. In doing so, a link can be made between aged material data and the structural element. This is an approach that, to the author's knowledge, has not been reported in the open literature.

11.3.1 Modelling Approach

The results from the DMTA programme for ultimate reduction in room temperature modulus were applied to the material properties used in the finite element models. The existing models for Joints 3 and 4 were used (30 mm fillet radius, 4 ply and 2 ply overlaminate respectively), as these were closest in geometry to the aged joints (described in Section 11.1.1). The existing models were considered valid since a comparative result was all that was required.

Several assumptions were made:

- Poisson's Ratio is unaffected by ageing
- Longitudinal, transverse and shear moduli are all affected equally

- XE900 laminate material is affected in the same way as the QE1200 laminate material
- Properties of the wood insert are not affected
- Filled resin fillet material is affected to the same extent as the QE1200 laminate material

Findings of many tests in the literature indicate that these assumptions are not strictly valid in every case. However, a lack of consistency in results reported in the literature meant that the extent to which different materials and properties are affected by specific ageing conditions was impossible to quantify. It was therefore necessary to make these generalisations and assume that for the purposes of this exercise, reasonably representative results would be obtained.

On the basis of these assumptions, the material property values given in Table 5.2 for the laminates and Table 5.5 for the foams were modified as shown in Table 11.3, where the percentage reduction is taken from the Results of the DMTA (Chapter 8).

11.3.2 Analysis Approach

In order to obtain results that could be compared to those from the experimental programme described in Sections 11.1 and 11.2, it was necessary to normalise the aged results with respect to the unaged results in the same way as with the DeltaTherm data. Line plots were therefore taken through the flange core and web core and nodal principal stress results extracted (as in Chapter 10). Since the thermoelastic signal is a function of the sum of the principal stresses in the isotropic core materials, the two principal stress results for each node were added together. Then each nodal stress sum from the 'aged' joint was divided by the equivalent nodal stress sum from the unaged joint results. The normalised results for the key areas of the joint (e.g. peak and nominal stress regions in the web and flange cores) could then be compared with those obtained from the DeltaTherm scans, in terms of percentage change in the quantity $\Delta(\sigma_1 + \sigma_2)$. A comparison between global deflections could also be made.

The comparison between the experimental and numerical results can only be qualitative however. The first reason is that the aged condition of the joints at the time of testing was obviously different from the aged condition (saturation) of the DMTA specimens. The

second reason is that the normalised signal is proportional to the normalised stress, but not equal to it as follows.

From Equation 6.13 it is apparent that the thermoelastic signal is proportional to the change in the sum of the principal stresses and the constant of proportionality (a function of the thermoelastic constant) is a function of the thermoelastic response of the material in question. It can be assumed therefore that

$$A_u S_u = \Delta(\sigma_1 + \sigma_2)_u \tag{11.5}$$

and $$A_a S_a = \Delta(\sigma_1 + \sigma_2)_a \tag{11.6}$$

where the subscripts u and a pertain to the unaged and aged case respectively.

Therefore

$$\frac{S_a}{S_u} = \frac{\Delta(\sigma_1 + \sigma_2)_a}{\Delta(\sigma_1 + \sigma_2)_u} \frac{A_u}{A_a} \tag{11.7}$$

Hence the normalised signal is related to the normalised stresses by a factor $\frac{A_u}{A_a}$, which effectively quantifies the extent to which the thermoelastic constant has been affected by hygrothermal exposure. It should be noted that this is valid for isotropic materials and that in laminated materials, α_{11}^P and α_{22}^P would also need to be accounted for. As stated in Section 11.2, it has not been possible in this work to obtain thermoelastic constants for aged materials. This could be an important focus of further work.

11.3.3 Results from the Aged Joint Models

The normalised change in the sum of the principal stresses in the material regions of interest are shown as a percentage in Table 11.4. The trends in the results are as expected, considering the physics of the situation. By using the DMTA results for room temperature modulus it has been assumed that the effect of ageing is to plasticise and hence reduce the modulus of the constituent materials. The modulus was reduced to a greater extent in the

laminate materials than in the foam materials so it is to be expected that a greater stress is carried by the core materials in the aged models compared to the unaged case.

11.3.4 Deflection Comparison between Unaged and Aged Condition

The reduction in modulus of the materials in the aged joint models manifests itself as an increase in global joint deflection as expected. The deflection measured on the centreline at the top of the web (equivalent to the point of attachment of the displacement transducer in the test specimens) was found to be 22% higher in the aged models.

11.4 Comparison Between Experimental and Numerical Results

The first point to note is that the numerical values given in Table 11.4 are significantly smaller than those exhibited by the TSA. It is unlikely that such differences could be due solely to the effects described in Section 11.3.2 (i.e. it is unlikely that the change in thermoelastic constant with ageing is large), but must also include factors such as the FEA producing a conservative result (as seen in Chapter 10) and the thermoelastic signal being enhanced (as discussed in Section 11.2). The observed qualitative trends however, are reasonably consistent between the FEA and TSA. An increase compared to the unaged case is exhibited in all the FEA results, consistent with the TSA results for the nominal flange, peak flange and nominal web regions. There is a discrepancy however in the peak stress region of the web core, which exhibits a decrease compared to the unaged case in the experimental results. Given that the increase in stress is greater in the nominal stress region than in the peak stress region, it can be argued that the trend for a 'flattening' of the stress distribution in the web core (discussed in Section 11.2.3) is evident in the FEA results, though not to the same extent as in the TSA results.

The increased deflection measured in the FEA is a similar order of magnitude to the stiffness reduction measured in the experimental statically and cyclically loaded joint specimens after a period of hygrothermal exposure.

11.5 References

[11.1] **Ishai O., Hiel C., Luft M.**; *Long-term Hygrothermal Effects on Damage Tolerance of Hybrid Composite Sandwich Panels*; Composites, Vol. 26, No. 1, 1995, pp47-55

[11.2] **Dulieu-Smith, J.M., Stanley, P.**; *On the Interpretation and Significance of the Gruneisen Parameter in Thermoelastic Stress Analysis*; J. Materials Processing Technology, Vol. 78 (1998), pp75-83

PART F

CLOSURE

12. DISCUSSION

12.1 Moisture Absorption Behaviour

Some particularly interesting results have been obtained from the laminate and foam materials, which have provided evidence of the active moisture uptake mechanisms. This work is particularly valuable, as little information of this kind exists in the literature for hybrid laminates containing Kevlar of a 'ship-building' quality and even less for closed-cell foam materials. It is thought that this collection of data may be the most extensive in existence for cross-linked PVC foam core materials.

For the laminate materials, moisture uptake results were obtained which are significantly different to those in the literature. Reasons why this may be so are explored and the main conclusion drawn from the work is that laminate quality is poor compared to the predominantly aerospace materials reviewed in the literature. It could be argued that better quality specimens should be used for an experimental programme such as this. However, the author considers that because they are of a quality representative of the real-life application, the results will have an impact on existing marine structures and will be of greater interest to the designers concerned.

A hypothesis has been presented for the moisture uptake mechanism active in the foam materials at 40°C. Little work in the literature has focused on this aspect of the research; the data that does exist is short term and its analysis cursory. Detailed quantitative analytical work is also scarce in the literature, particularly in non-Fickian or 3D diffusion cases, especially in the hybrid materials and is non-existent for PVC foam core materials.

Substantiating the hypotheses for moisture ingress, particularly in the foam material, presented considerable difficulty. An attempt was made experimentally to determine the extent of moisture ingress and the transport pathways by immersing foam and laminate materials in fresh water containing food dye at 50°C for 1 year. While some staining of the surfaces of the materials was apparent, it was not possible to discern any traces of the dye within the specimens when examined under the microscope. However, evidence to support the hypotheses has been discussed in Chapter 7 and while further verification is clearly required, the work presented here does provide a significant knowledge base from which research can progress.

The analytical modelling of the moisture uptake results was limited but of considerable value, since it has highlighted the inadequacy of existing models in describing the long-term moisture uptake behaviour of the foam materials. Further work is required in this area, which may focus on the development of a new model or the modification of an existing theory. This analytical development should be conducted in conjunction with experimental investigative work, leading to a more detailed knowledge of the moisture absorption and transport mechanisms in closed cell foams.

12.2 Effects of Hygrothermal Exposure

Despite significant scatter in the DMTA results, some interesting trends have emerged, as discussed in Chapter 8. It is apparent that the room temperature modulus results have proved that plasticisation processes and stress relaxation are indeed occurring in all the materials as a result of hygrothermal exposure. However it is also apparent that the elevated temperatures of the immersion baths, while accelerating the ageing process, have also caused significant postcure. Further work to quantify this could be carried out using DSC (Differential Scanning Calorimetry), to measure the degree of cure before and after hygrothermal exposure.

While every effort was made to choose hygrothermal ageing temperatures well below the material T_g, so that anomalous behaviour (with respect to ambient ageing) was not observed, this work has proven that accelerated ageing will always give different results to long-term ambient ageing unless the materials being tested have been postcured. This has implications on the method of drying used prior to hygrothermal exposure. Prolonged oven drying at elevated temperature is evidently preferable to desiccant at room temperature.

Although DMTA has been used previously to quantify the effects of aging in composites [12.1], to the author's knowledge, this work is the first example of its application to the analysis of foam materials and to determining the effects of ageing therein. This has presented practical difficulties due to the low strength of the materials and the very small size of the specimens. However, a comparative analysis has been carried out successfully, resulting in quantitative information about the change in material properties with ageing. No such data exists for these materials in the open literature to date.

Despite the difficulties mentioned above with regard to using very small specimens, the main advantage is that the DMTA has been able to provide material property data up to saturation without the effects of moisture gradients significantly affecting the results. Mechanical testing of larger specimens would be influenced not only by ageing of the material in the outer plies but also by the proportion of unaged material at the centre. This would be a particular problem for foams, which would require the use of thick blocks of material. DMTA overcomes this problem.

12.3 Experimental and Numerical Analysis of Unaged Joints

Almost all of the trends exhibited in the TSA results presented in Chapters 9 and 10 have been found to correlate well with the finite element work. The stress sum magnitudes and the shapes of the distributions also correlate very well in the webs of joints 1, 2 and 3, but the correlation can only be described as moderate in the other cases, particularly in the flange cores. This is believed to be due to a number of sources.

A possible contributory factor may be a deficiency in the material properties assumed for the FEA. Manufacturer's quoted values were used but it is known that the variation in density of the foam core materials can be up to ± 20% of the manufacturer's quoted value. From [12.2], the relationship between the foam density and its stiffness is linear. In the elastic region, the relationship between the stress in the material and its stiffness is also linear. The mathematics shows that the variation in the stress due to the variation in the density is therefore also 20%. It has been found that an increase in the stiffness of the foam by 20% in the FE model leads to a 35.5% improvement in the correlation. It is therefore also significant that the manufacturer's quoted modulus values were used in the foam calibration.

A factor that must also be considered concerns the position of the line of interest within the flange core. Initially, a line a distance 2.16 mm away from the inner skin was taken and it was found that the correlation between the results from this line and an equivalent line from the FEA results was very poor. The correlation between the TSA and FEA results was found to improve by 16% when a line deeper into the core was examined. This line was 13.68 mm away and it is these results that have been reported in Chapters 9 and 10. It is thought that the reason for this is that during the manufacturing process of the joints, a combination of the laminate resin and the vacuum pressure could have caused changes in the material properties of the foam very close to the inner skin. Since the flange

core is made up from layers of the foam material, then it can be assumed that different degrees of correlation between the FE and experimental values may be found at different positions within the flange core.

These are plausible reasons, which go some way to explaining the discrepancy between the FEA and TSA results. However, they cannot explain why the difference between the two results is so much greater in the peak stress areas, particularly in the flange. There must therefore be the occurrence of a phenomenon in the peak stress regions, which is not modelled adequately by the linear FEA. The most likely reason for this is that the joint behaviour where the web meets the flange is similar to a classic contact problem. This hypothesis is substantiated by the fact that the effect is most pronounced in the flange core, directly in line with the web skins, where the peak stresses occur. The in-plane load in the web skins is transferred to the flange over these two localised areas, manifesting itself as two regions of high deformation in the flange core. This is typical of a contact problem between two materials of significantly different stiffness. The deformation in the foam material is not necessarily plastic, merely not linear elastic. Since a fundamental assumption of the TSA technique is that materials deform within the linear elastic regime, in this case there must be inaccuracies in the TSA results in the contact regions. The resulting effect is that the observed stresses are larger than expected, and larger than modelled by the linear FEA.

The filled gap at the base of the web in Joint 5 substantially reduces this problem and has a beneficial effect on all joint components apart from the fillet. This is due to its local stiffening effect (i.e. 100 fold increase compared to the stiffness of the web). The effect clearly warranted further investigation. Some important factors have arisen from the parametric study. It has been shown that if any air gap is present at the base of the web, it has a very large detrimental effect on the stresses in both the flange and web cores. The shape of the resultant stress distribution in the flange was found to be similar to some of the distributions exhibited by the TSA results, particularly Joints 1 and 2. Upon inspection of the joint test specimens it was found that small gaps were indeed present and this was initially considered to be the reason for the departure of the TSA results from the FEA. Further FE analysis proved however that although the shape of the stress distribution could be changed markedly by the presence of these gaps and the stress magnitudes were increased, the discrepancies between the two sets of results were not greatly improved. The contact problem discussed above is therefore considered to be the single major contributing factor to the departure.

This work has yielded some interesting results which are highly relevant to joint design and in-service performance. The geometrical configurations (fillet radius and overlaminate thickness) of similar joints have been considered in detail in the literature, but the effect of an air gap has hitherto been overlooked. This work has highlighted the requirement to fill any gaps occurring in production, to prevent premature core compression failure. The interesting result of even a small filled gap actually benefiting joint performance due to its local stiffening effect is highly significant. The greatly improved stress profiles within the joint would lead to improved durability of this critical area. These advantages may be considered to outweigh the penalty of a slight weight and cost increase due to the extra resin required.

Aside from the practical considerations of joint design, the work has also shown the versatility of the thermoelastic technique in the analysis of complex composite structures, and has highlighted forthcomings in the validation of FE models. A lot of scatter has been observed in the results and this has been attributed to the nature of the material. The scanning spot size used in the SPATE work was larger than desired to keep the scan times to a reasonable length. This problem can be overcome with the DeltaTherm 1000 equipment, which allows higher resolution scans to be obtained within minutes.

12.4 Analysis of Aged Joints

This work has presented the first application of TSA to aged materials and the first link between aged material property data and structural performance.

The experimental work detected significant changes in the tee joint behaviour after ageing, which were manifested as changes in the thermoelastic signal compared to the unaged condition. Detailed discussion has been presented on the implications of an increase or decrease in the signal. The most significant outcome of this work was that localised signal changes can be related to global changes in the stress distribution within the joint. These result from different rates of ageing in the constituent materials, and more significantly, from the protection the sandwich core receives from the skins. This has implications for the structure in service, which would not have core material exposed other than in the event of damage.

While providing an interesting focus for analysis and having important implications with regard to sandwich structures, the complexity of the tee joint has not assisted in the

validation of the use of TSA for detecting ageing. It is possible that factors associated with the joint geometry have contributed to the observed effects. For example, it has been shown that for steel, residual stresses can cause perceived changes in material properties as a result of a change in microstructure, which lead to a change in the thermoelastic constant [12.3]. A similar effect may occur in polymeric materials, in which case the effect of creep and stress relaxation due to the static and cyclic loading could have caused changes to the thermoelastic signal in different parts of the joint, depending on the level of localised stress. This requires further clarification on a specimen for which the stress distribution is known and for which a closed form solution exists, such as a sandwich beam in bending.

A simpler specimen would also aid the analysis of the changes in stress distribution with longer-term ageing and the investigation of other possible effects such as changes in Poisson's ratio or the thermoelastic constant. It would also be beneficial to conduct further tests in displacement control so that the TSA can detect the significant effects of postcure that were established from the results of the DMTA. Difficulties associated with strain control have been experienced in the form of significant drift, resulting in sudden high loading and hence a risk of breaking test specimens. This is not ideal when specimens need to be returned to the hygrothermal environment afterwards for continued ageing. Future work would therefore require a large number of specimens to be aged simultaneously and a small number of these to be removed on each occasion for testing, so that returning them to the chamber after testing would not be required. This has the additional advantage that ultimate properties could also be obtained at intervals throughout the ageing process.

Ultimate properties however would be a function of the moisture gradient in the material, not merely the 'moisture content', which is clearly a significant factor for thick sandwich constructions. Further work is recommended on the determination of moisture gradients in sandwich construction, either experimentally using techniques such as NMRI (as discussed in Chapter 7), or analytically, which may require the modification of existing models.

If the moisture distribution in the sandwich is highly non-uniform, it is possible that the effects of temperature are more significant than the effects of moisture, resulting in a possible increase in properties if the effects of postcure are important. However, it was assumed for the FEA that there was a uniform reduction in material moduli, based on the results of the DMTA. The highly significant outcome from this work was that

qualitatively, the trends in the FEA and TSA were the same, suggesting that the hypothesised changes in stress distribution as a result of ageing are true.

This has important implications for future work as it has shown that:

- **thermoelastic readings taken from an aged component can successfully characterise modifications in structural behaviour and**
- **measured material property degradation can be used to successfully predict changes in structural performance as a result of hygrothermal ageing.**

The correlation at present is largely qualitative, though it is clear that with further work, quantitative predictions may be made.

12.5 References

[12.1] **Boinard, E.**; *Influence of Water on Polymeric Materials used in Marine Applications*; Ph.D. Thesis, Department of Ship and Marine Technology, University of Strathclyde, 1998

[12.2] Divinycell Technical Manual, H Grade; Divinycell International Ltd., 1, Eastville Close, Gloucester, GL4 7SJ

[12.3] **Dulieu-Barton, J.M.; Quinn, S.**; *The Effect of Plastic Deformation on the Thermoelastic Response of Steel*; Proc. Int. Conf. on Mechanics in Design, Nottingham, UK, 6-9 July 1998

13. RECOMMENDATIONS AND FURTHER WORK

Several areas for further work have been identified and are discussed in more detail in the relevant sections of the preceding chapters. This chapter provides a summary of these.

13.1 Moisture Uptake

The hypothesised moisture absorption and transport mechanisms require further substantiation, particularly for the closed cell foam materials. This could be achieved experimentally using nuclear magnetic resonance imaging.

The same technique could be used to determine moisture gradients within the foam material and also in the sandwich construction. Such information is required for further numerical modelling of aged structures (Section 13.3).

Further work on the application of analytical models to the moisture absorption data is required. An improved fit to the laminate results may be obtained by using a three-dimensional diffusion model. Further work is required in assessing the suitability of existing models to the foam absorption results, which may lead to the development of a new model.

13.2 Material Effects

In order to fully quantify the effects of ageing due solely to moisture absorption, the postcuring effects of the elevated temperature environment need to be separated if possible from the existing data. The extent of cure of the materials needs to be quantified before and after hygrothermal exposure. This can be achieved using differential scanning calorimetry. Any further work should be conducted on materials that have been fully cured prior to exposure.

13.3 Numerical Modelling

Further work is required to improve the correlation between the FEA and TSA results. This may lead to the use of a three-dimensional model, with non-linear geometric and

material properties, to further analyse the region of contact between the web skins and the flange.

Numerical models of the aged joints require refining through the use of moisture gradient results – either predicted or experimentally determined. The material property degradation determined from the DMTA could then be applied as a function of moisture content through the thickness of the sandwich. This will result in a more accurate prediction of changes in structural performance with ageing.

13.4 TSA as a Tool for Quantifying Ageing

It is necessary to identify the causes contributing to the changes in thermoelastic signal from the unaged to the aged condition. Through the use of a simplified test specimen (e.g. a sandwich beam in flexure), the effects of surface ageing, changes in the stress distribution, residual stress and changes in material parameters such as Poisson's ratio can be more easily determined. Tests to quantify changes in stiffness must be conducted in displacement control.

In order to quantitatively validate the TSA technique for determining the effects of ageing, it is necessary to be able to directly compare the experimental and numerical results. This requires the TSA to be presented in the form of the principal stress sum, rather than the normalised signal, requiring the determination of the calibration constant A. It is necessary to determine the extent to which the thermoelastic constant is affected by ageing and how this can be quantified with respect to global joint behaviour. Attempts should be made to measure this experimentally, but the difficulties associated with it are outlined in Chapter 11. It could be estimated theoretically, using aged material properties obtained from DMTA. It may also be possible to determine a calibration constant using the FEA.

The numerical modelling first needs to be made to correlate with the TSA for the dry condition (Section 13.3). Then for a given moisture gradient or known state of material ageing, the factor $\frac{A_u}{A_a}$ (Equation 11.7) can be estimated by comparison of normalised stresses from the FEA with the normalised signal from the TSA.

The fact that it is not possible to take meaningful scans from a wet joint surface is significant and the implications of allowing the joint to dry before taking readings should be investigated. Attempts to reduce the signal noise by reducing the electronic iris on the detector were unsuccessful and further work is required to determine whether this problem can be overcome.

14. CONCLUSION

The work described in this thesis has provided a comprehensive examination of the behaviour of sandwich materials and structural elements under the exposure of hygrothermal environments.

It has shown that the absorption behaviour for laminates of moderate quality exhibits pseudo-Fickian characteristics, but is influenced by significant ingress into voids, leading to high values of moisture content compared to the literature.

The absorption behaviour of closed cell PVC foams in immersion has been monitored over 2½ years duration, longer than in any other published work. A multi-stage absorption process has been observed and is attributed to the progressive diffusion into the polymeric cell wall structure, as well as into the cell cavities. No detailed uptake mechanism has been reported in the literature, so a hypothesis has been proposed based on available evidence. It has also been shown that current diffusion models are inadequate in describing the foam moisture uptake behaviour over the long-term. This work will serve as a broad basis from which further research can be conducted.

The effects of the hygrothermal environment on material properties have been investigated using DMTA. The application of this technique to aged laminate materials is relatively scarce. It is thought that this work is the only application of DMTA to aged closed cell foam materials. The results yielded clear evidence for the classic effects of hygrothermal ageing, such as a reduced room temperature modulus due to plasticisation and stress relaxation. Evidence of postcure from elevated temperature hygrothermal ageing was also observed in the form of an improved T_g in materials that had undergone low-temperature cure cycles prior to ageing. The heating action of the DMTA test was also thought to contribute to a recovery in properties.

The thermoelastic stress analysis technique has successfully been applied to foam sandwich construction tee joints. Quantitative information has been obtained about the complex load transfer mechanism within the joints under compression loading. The results have been compared to numerical modelling and a departure has been attributed to a contact phenomenon between the web and flange. The work has provided recommendations for improved design, the most significant of which is a small filled gap at the base of the web, which dramatically reduces high local stresses in the core materials that could otherwise result in failure.

TSA has also been applied to hygrothermally aged tee joints, which is the first time this technique has been used to attempt to detect ageing of any kind. Changes in the thermoelastic signal were observed in the aged joints and the significance of these was examined in detail. Comparison to a finite element model using aged material properties derived from the DMTA programme showed that a change in the stress distribution in the joints had occurred as a result of ageing.

These findings are highly important. The application of TSA to aged sandwich structures shows excellent potential and the data obtained would be impossible to collect by any other means. The information obtained about the ageing of the individual sandwich materials used in conjunction with the experimental and numerical analyses has also shown significant promise in the prediction of mechanical behaviour in the structural context. The quantitative development of this combined approach will be invaluable in the future analysis of the hygrothermal ageing of foam cored composite sandwich construction.

APPENDICES

APPENDIX A

SUMMARY OF ASTM STANDARDS PERTINENT TO MOISTURE CONDITIONING OF POLYMERIC MATERIALS

This Appendix lists the standards which are applicable to hygrothermal and moisture ageing of polymeric materials and provides a summary of the methods contained in each which are specifically relevant to this research.

The six standards of relevance are:

ASTM	D 570 - 95	Standard Test Method for Water Absorption of Plastics
ASTM	D 2842 - 94	Standard Test Method for Water Absorption of Rigid Cellular Plastics
ASTM	D 618 - 96	Standard Practice for Conditioning Plastics for Testing
ASTM	D 756 - 93	Standard Practice for Determination of Weight and Shape Changes of Plastics Under Accelerated Service Conditions
ASTM	D 1042 - 93	Standard Test Method for Linear Dimensional Changes of Plastics Under Accelerated Service Conditions
ASTM	D 2126 - 94	Standard Test Method for Response of Rigid Cellular Plastics to Thermal and Humid Aging

A.1 D750 For Water Absorption of Plastics

The method for water absorption of plastics (D 570) covers the determination of the relative rate of absorption of water by plastics when *immersed.* It is intended to apply to the testing of all types of plastics including cast, hot moulded and cold moulded resinous products, both homogeneous and laminated plastics in rod and tube form and in sheets 0.13 mm or greater in thickness. Although fibre reinforced composites are not mentioned specifically, it can be assumed that the last case listed is appropriate.

The test specimen size is recommended to be 76.2mm long by 25.4mm wide by the thickness of the material. Three specimens are then conditioned by drying in an oven and then cooling in a dessicator, the temperature and length of time depending on whether the

water absorption characteristics are affected up to or above 110°C. This presumably refers to the glass transition temperature of the material.

The test procedures presented include

- *Twenty-four hour immersion* at 23±1°C.
- *Two-hour immersion* at 23±1°C for thin materials or those with a fast rate of absorption.
- *Repeated immersion* at 23±1°C - a combination of the first two whereby specimen is weighed after two hours and then again after 24 hours.
- *Long-term immersion* at 23±1°C until specimen is saturated. Weighings at 24 hours, 1 week and every two weeks thereafter.
- *Two-hour boiling water immersion* followed by cooling for 15 minutes in distilled water at room temperature.
- *One half hour boiling water immersion* for thin materials or those with a fast rate of absorption.
- *Immersion at 50±1 ℃* for 48 hours

Interestingly, it is recommended that prior to weighing, specimens are removed from the water one at a time and have all surface water wiped off with a dry cloth. Although this is the generally accepted method in the literature, it was found not to be the most efficient by Fellows [A.1].

A method for reconditioning and re-weighing is also given for cases where it is likely that water soluble matter was lost during the immersion test.

A.2 D2842 For Water Absorption of Rigid Cellular Plastics

The method for water absorption of rigid cellular plastics (D 2842) presents a technique for measuring the change in buoyant force resulting from immersion under a 5.1 cm head of water for the specified immersion period of 96 hours, rather than a gravimetric technique. Two procedures are presented - one for those materials which experience a rapid water absorption or show an increase in volume under immersion, and one for materials which do not exhibit either of these characteristics. The method works on the simple principle that when an object less dense than water is submerged (i.e. held under water so that it is completely immersed), its buoyant force is equal to the weight of water it displaces less the

dry weight of the object. An underwater weighing assembly is used to measure this whereby the specimen floats against a ceiling with its face in the horizontal plane.

For this method, surface cells opened during specimen preparation result in an error when calculating the apparent volume of the test specimen. The degree of this error is a function of cell size. This test method accounts for this error in that all calculations are based on the true specimen volume. The true specimen volume is determined in Procedure A of the method as the measured volume minus the volume of surface cells opened by cutting. The cell size is measured using a thin slice of the material on a slide mounted in a slide projector. A calibrated scale is also mounted on the slide.

The test specimen size in the case of these tests is rather larger than those in the literature, being 15×15×7.5 cm or the thickness of the material, whichever is the thinner. Conditioning of specimens is similar to that for the plastics method - in an oven at 50±3°C for a minimum of 24 hours until a constant weight is obtained.

Although this technique appears to be quite comprehensive and can be very accurate if conducted properly, none of the papers in the literature review have adopted this method for monitoring water uptake of foams.

A.3 D618 For Conditioning Plastics for Testing

The standard practice for conditioning plastics for testing (D 618) defines procedures for conditioning plastics (though not necessarily to equilibrium) prior to testing and the conditions under which they shall be tested. The purposes of conditioning are listed as follows:

- for the purpose of bringing the material into equilibrium with normal or average room conditions,
- to obtain reproducible results, regardless of previous history of exposure,
- or to subject the material to abnormal conditions of temperature and humidity in order to predict its service behaviour.

Six standard procedures for conditioning prior to test are presented. These include various time periods for conditioning at specified temperatures, immersion in water or at high

relative humidity, or simply at standard controlled laboratory conditions. Table A.1 (at the end of this Appendix) summarises the information given in the Standard.

A.4 D576 and D1042 For Weight, Shape and Dimensional Changes

There are two standards concerned with the determination of dimensional and weight changes of plastics under accelerated service conditions (D 576 and D 1042), specifically related to environments in which there are changes in atmospheric temperature and humidity. In D 576, procedures are provided for exposing plastics to combinations of extreme humidity and temperature that will accelerate the effect of the environmental conditions experienced by the plastics concerned. Seven test procedures are provided which prescribe conditions for different types of exposure. Six of the procedures cover exposures at graduated levels of temperature and extremes of humidity; the seventh prescribes conditions involving alternate exposure to high and low temperatures. During these experiments, the weight and dimensions are monitored by simple measurement using a balance and micrometer respectively.

Procedure A develops warping, weight change and exudation in plastic parts. It involves exposure for 24 hours at 60°C and 88% relative humidity, followed by 24 hours at 60°C in an oven. Procedure B reveals poorly cured plastics by developing cracks in them, and simply involves exposure for 72 hours at 60°C in an oven. Procedures C and D are more severe versions of Procedure A. Procedure C involves 24 hours exposure at 70°C and 70-75% RH, followed by exposure for 24 hours at 70°C in an oven. Procedure D may cause chemical decomposition in many plastics and involves exposure for 24 hours at 80°C over water followed by 24 hours at 80°C in an oven. Procedure E is valid for testing the behaviour of plastic parts with metallic inserts and laminates, for cracking on exposure to temperature change. This involves 24 hours at 80°C and 70-75% RH followed by 24 hours at -40°C or -57°C as specified, 24 hours at 80°C in an oven and finally 24 hours at -40°C or -57°C as specified. Procedures F and G are modifications of procedure A, applying to impact-resistant and low heat-distortion temperature types of thermoplastics respectively. Procedure F involves exposure for 24 hours at 38°C and 100% RH, followed by 24 hours at 60°C in an oven. Procedure G requires 24 hours at 49°C and 100% RH, followed by 24 hours at 49°C in an oven.

Standard D 1042 is designed to provide a means for measuring in plastic specimens the dimensional changes resulting from exposure to service conditions. In particular, the test method is suitable for measuring shrinkage or elongation developed in accordance with the procedures described above in Standard D 756. The apparatus required is simply a scriber with the ability to scribe marks 100 mm apart and no thicker than 0.2mm on the specimen surface. In addition, a measuring microscope is required. Specimen dimensions must be 150 by 25 mm by the full thickness of the material.

The purpose of the scribe is to scribe an arc of 100mm radius on the surface of the test specimen. One needle of the scribe is pressed firmly into the specimen to form a centre for the initial and subsequent measurements. The other needle scribes the arc which is used as a reference for all subsequent measurements. At each phase of the test where it is required to measure linear changes, one needle is reinserted into the original centre and another arc drawn with the other. The distance between the original arc and the new arc represents linear strain.

A.5 D2126 For Thermal and Humid Ageing of Rigid Cellular Plastics

Finally, D 2126 covers procedures for the thermal and humid exposure of rigid cellular plastics. There are no specific conditioning tests specified in this standard. Instead the test method recommends a variety of conditions from which one or more of the desired exposure conditions can be selected. The recommended specimen size is 100 by 100 mm by the thickness of the material. Specimens are conditioned to a constant mass at 23±2°C and 50±5% RH before exposure to the ageing environment. Mass and dimensional measurements are taken before exposure. The temperature and relative humidity combinations are given in Table A.2.

Specimens are exposed for two weeks at the selected conditions and measurements taken after 24 hours, one week and at the end of the two weeks. After exposure, specimens should be allowed to come to room temperature for two hours before measuring and testing.

A.6 Reference

[A.1] **Fellows, L.M.P.**; *Moisture Absorption in Low-level Porosity Thermoplastic Toughened Epoxy Composites*; Ph.D. Thesis, Department of Engineering Materials, University of Southampton, 1999

Procedure	Duration (hours)	Temp. (°C)	Rel. Humidity (%)
A (Thickness < 7mm)	40	23	50
A (Thickness > 7mm)	88	23	50
B	48	50	oven
C	96	35	90
D	24	23	water
E	48	50	water
+	1	23	water
F	As specified	23	96

Table A.1: Conditioning Procedures (ASTM D 618)

Temperature (°C)	Relative Humidity (%)
23±2	50±5
38±2	97±3
70±2	97±3
To be selected	95±3
-40±3	ambient
-73±3	ambient
70±2	ambient
100±2	ambient
150±2	ambient
200±2	ambient

Table A.2: Temperature and Relative Humidity Combinations (ASTM D 2126)

APPENDIX B

CALCULATION FOR THE SHEAR CONTRIBUTION IN FLEXURAL BENDING OF A RECTANGULAR BEAM

This appendix considers an analytical method that can be used to calculate the proportion of flexural deformation that is due to shear for a beam of rectangular cross-section. Zweben *et al* [B.1] show that the measured apparent modulus of a beam in flexure can be significantly smaller than the actual extensional modulus because the contribution of shear is ignored. This approach has been adopted in order to determine whether the discrepancy between the measured DMTA storage modulus and the manufacturer's quoted Young's modulus can be attributed to this effect in the four materials studied.

Zweben *et al* present the theory for a beam under three point bending. This is outlined here and the appropriate equivalent expressions for a tip-loaded cantilever are also given.

In three point bending the Bernoulli-Euler expression for deflection arising from flexural stress only given by Zweben *et al* is

$$\Delta_f = \frac{PL^3}{4EbD^3} \tag{B.1}$$

where P = load
L = specimen length
E = extensional modulus
b = width of bean cross-section
D = Depth of beam cross-section (thickness)

The equivalent expression for a tip-loaded cantilever, to model the DMTA condition, is

$$\Delta_f = \frac{PL^3}{3EI} = \frac{4PL^3}{EbD^3} \tag{B.2}$$

where I = inertia of the cross-section, which for a rectangle is

$$I = \frac{bD^3}{12} \tag{B.3}$$

The expression for shear deformation for a beam under three point bending is

$$\Delta_s = \frac{PL}{4GA_s} \tag{B.4}$$

where G is the shear modulus and is the effective cross-sectional area for shear deformation. For a rectangular beam, A_s is given by

$$A_s = \frac{bD}{1.2} \tag{B.5}$$

Substituting Equation B.5 into Equation B.4, the shear deflection of a beam under three point bending becomes

$$\Delta_s = \frac{0.3PL}{GbD} \tag{B.6}$$

The equivalent expression to Equation B.4 for shear deformation in a tip-loaded cantilever is given by

$$\Delta_s = \frac{PD^2}{8GI} \tag{B.7}$$

By substituting Equation B.5 for the effective area into Equation B.3 for the inertia, and substituting the resulting expression for the 'effective inertia' back into Equation B.7, an expression for the shear deflection in a tip-loaded cantilever equivalent to Equation B.6 for three point bending is obtained:

$$\Delta_s = \frac{1.8PL}{GbD} \tag{B.8}$$

Zweben *et al* state that to ensure that the apparent flexural modulus is equal to the true flexural modulus, the shear deflection must be small compared to the flexural deflection. This requires that

$$\frac{\Delta_s}{\Delta_f} = 1.2\left(\frac{E}{G}\right)\left(\frac{D}{L}\right)^2 \quad << 1 \tag{B.9}$$

An equivalent expression for a tip-loaded cantilever is therefore obtained from Equations B.2 and B.8:

$$\frac{\Delta_s}{\Delta_f} = 0.45\left(\frac{E}{G}\right)\left(\frac{D}{L}\right)^2 \tag{B.10}$$

For the DMTA specimens the requirement is to calculate the proportion of the total flexural deformation that is attributable to shear, where the total deformation is given by

$$\Delta_t = \Delta_f + \Delta_s \tag{B.11}$$

By manipulating Equation B.11, the proportion of the total deflection due to shear is obtained:

$$\frac{\Delta_s}{\Delta_t} = \frac{\Delta_s}{\Delta_f + \Delta_s} = \frac{\Delta_s/\Delta_f}{1 + \Delta_s/\Delta_f} \tag{B.12}$$

In order to determine a value of E that takes into account both deflection due to bending and to shear, a simple method has been devised using the above theory. If the DMTA software assumes no shear contribution then Equation B.2 is valid. Δ_f is then equivalent to the prescribed amplitude of 50μm and the modulus value is that derived by the software (Table 8.2). The only unknown for the purposes of this calculation is P, which is equivalent to the drive force and can therefore be calculated from

$$P = \frac{\Delta_f E b D^3}{4L^3} \tag{B.13}$$

Equation B.8 can then be used to obtain a value of the deformation due to shear, which when taken away from the assumed deformation due to bending of 50μm (which actually includes the shear contribution and is therefore equal to the total deformation), then gives the actual deformation due to bending alone, $\Delta_f' < \Delta_f$.

The 'true' modulus can then be recalculated from Equation B.2 by substituting the assumed deformation for the actual deformation due to bending alone:

$$E = \frac{4PL^3}{bD^3\Delta_f'} \tag{B.14}$$

Reference

[B.1] **Zweben, C., Smith, W.S., Wardle, M.W.**; *Test Methods for Fiber Tensile Strength, Composite Flexural Modulus, and Properties of Fabric Reinforced Laminates*; Composite Materials: Testing and Design (Fifth Conference), ASTM STP 674, S.W. Tsai, Ed., American Society for Testing and Materials, 1979, pp228-262

TABLES

Material	**Conditioning Environment**	**M_∞(%)**
UD E-glass/Epoxy	Immersion in FW at 23°C	1.4
UD Graphite/Epoxy	Immersion in FW at 23°C	2.64
Kevlar/Epoxy	Immersion in FW at 23°C	6.8
Biaxial E-glass/Epoxy	Immersion in FW at 23°C	2.6
Biaxial Graphite/Epoxy	Immersion in FW at 23°C	2.8
E-glass/Graphite/Epoxy	Immersion in FW at 23°C	2.78
Graphite/Kevlar/Epoxy	Immersion in FW at 23°C	3.62
Kevlar/E-glass/Epoxy	Immersion in FW at 23°C	3.49
UD Graphite Epoxy	Immersion in Distilled water	1.7
UD Graphite Epoxy	100%RH at 21°C	1.2
UD Graphite Epoxy	74%RH at 63°C	0.9
UD Graphite Epoxy	30%RH at 63°C	0.3
Quasi-isotr. Carbon/Epoxy (60% V_f)	95%RH at 70°C	1.46
WR/CSM E-glass/Polyester (45%W_r)	Immersion in SW at 30°C	0.85
WR/CSM E-glass/Phenolic (33%W_r)	Immersion in SW at 30°C	0.88
WR/CSM E-glass/Vinylester (45%W_r)	Immersion in SW at 30°C	0.44

Table 2.1 Summary of Maximum Moisture Content Values for Composites from Various Sources in the Literature [2.3, 2.6, 2.38, 2.44]

Material	**Conditioning Environment**	**$D \times 10^7$ (mm^2/sec)**
Neat Epoxy	Immersion in FW at 23°C	1.64
Neat Epoxy	Immersion in FW at 70°C	2.93
E-glass/Epoxy	Immersion in FW at 23°C	1.09
E-glass/Epoxy	Immersion in FW at 70°C	6.82
Graphite/Epoxy	Immersion in FW at 23°C	1.05
Graphite/Epoxy	Immersion in FW at 70°C	5.99
Kevlar/Epoxy	Immersion in FW at 23°C	10.55
Kevlar/Epoxy	Immersion in FW at 70°C	29.30
E-glass/Graphite/Epoxy	Immersion in FW at 23°C	1.25
E-glass/Graphite/Epoxy	Immersion in FW at 70°C	5.01
Kevlar/Graphite/Epoxy	Immersion in FW at 23°C	4.39
Kevlar/Graphite/Epoxy	Immersion in FW at 70°C	17.56
Kevlar/Graphite/Epoxy	Immersion in FW at 23°C	5.03
Kevlar/Graphite/Epoxy	Immersion in FW at 70°C	20.01
Quasi-isotr. Carbon/Epoxy (60% V_f)	95%RH at 70°C	4.81
WR/CSM E-glass/Polyester (45%W_r)	Immersion in SW at 30°C	2.5
WR/CSM E-glass/Phenolic (33%W_r)	Immersion in SW at 30°C	2.3
WR/CSM E-glass/Vinylester (45%W_r)	Immersion in SW at 30°C	4.3

Table 2.2 Summary of Diffusivity Values from the Literature [2.3, 2.38, 2.44]

Material	**Conditioning Environment**	**ΔILSS**	**ΔFS**	**ΔFM**
Carbon/Epoxy	100%RH at 70°C	45.6% ↓	36.2% ↓	11.5% ↓
Carbon/Epoxy	Boiling Water	41.0% ↓	31.8% ↓	6.6% ↓
Carbon/Epoxy	Boiling +re-drying	3.3% ↓	2.0% ↑	0%
UD Carbon/Epoxy	96%RH at 60°C	17% ↓	~	~
UD Carbon/Epoxy	96%RH at 60°C with thermal spiking to 135°C	25% ↓	~	~
Kevlar/Epoxy	5% moisture content	50% ↓	35% ↓	~
Kevlar/Epoxy	Immersion in FW at 21°C	~	40% ↓	~
E-glass/Polyester	Immersion in SW at 30°C	12% ↓	17% ↓	6% ↓
E-glass/phenolic	Immersion in SW at 30°C	19% ↓	25% ↓	6% ↓
E-glass/vinylester	Immersion in SW at 30°C	21% ↓	21% ↓	2% ↑

Table 2.3: Summary from Literature of Changes in Interlaminar Shear Strength and Flexural Properties with Hygrothermal Exposure (ΔILSS denotes change in interlaminar shear strength, ΔFS denotes change in flexural strength, ΔFM denotes change in flexural modulus, ↓ denotes decrease and ↑ denotes increase.) [2.37, 2.44, 2.69, 2.70]

Laminate	Material Designation	Reinforcement	Matrix
Flange Outer Skin	QEA1200	Hybrid E-glass and Kevlar 1200 g/m^2 stitched quadriaxial (0/90/±45°) fabric	Ampreg 75 high temperature curing epoxy resin (pre-impregnated)
Flange Inner Skin & Web Skins	QE1200	E-glass 1200 g/m^2 stitched quadriaxial (0/90/±45°) fabric	Ampreg 26 low temperature curing epoxy resin with Ultraslow hardener (hand lay-up)
Overlaminate & Web Bondg. Lam.	XE900	E-glass 900 g/m^2 stitched angle ply (±45°) fabric tape	Ampreg 26 low temperature curing epoxy resin

Table 5.1: Laminate Material Designations (Supplied by SP Systems as per RNLI Specification)

Material	Tensile Modulus (E_x in plane) (MPa)	Tensile Modulus (E_y through thickness) (MPa)	Shear Modulus (MPa)	Tensile Strength (MPa)	Poisson's Ratio
QEA1200	23150	~	8203	347	0.29
QE1200	20707	5800	7450	310	0.28
XE900	14400	5800	4500	216	0.10

Table 5.2: Laminate Material Properties (Supplied by SP Systems)

Prepreg Cure Schedule (Ampreg 75)	Wet Laminated Cure Schedule (Ampreg 26)
Vac. Bag @ 97% vacuum	Vac. Bag @ 78% vacuum
2 hours @ 45°C	24 hours @ RT
2.33 hours ramp to 80°C	2 hours @ 30°C
5 hours @ 80°C	1 hour ramp to 45°C
Cooling @ room temperature (RT) (19°C)	7 hours @ 45°C
	Cooling @ RT

Table 5.3: Laminate Cure Schedules (Supplied by SP Systems)

Material	Volume Fraction of Voids
QEA1200 Batch 1	13.8 - 9.6%
QEA1200 Batch 2	13.4 - 8.8%
QE1200 Batch 1	15.3 - 8.8%
QE1200 Batch 2	16.0 - 12.0%

Table 5.4: Values of Void Fraction in Laminate Materials obtained by Image Analysis

Property	Divinycell H80	Divinycell H130 Airex C70.130
Density (kg/m^3)	80	130
Compressive Strength* (MPa)	1.2	2.5
Compressive Strength** (MPa)	1.0	2.1
Compressive Modulus*$^{\spadesuit}$ (MPa)	40	85
Compressive Modulus*$^{\clubsuit}$ (MPa)	85	175
Compressive Modulus**$^{\spadesuit}$ (MPa)	32	70
Tensile Strength* (MPa)	2.2	4.20
Tensile Strength** (MPa)	1.95	3.00
Ultimate Tensile Strain** (%)	6.5	8
Tensile Modulus* (MPa)	80	140
Tensile Modulus** (MPa)	75	130
Shear Strength (MPa)	1.0	2.0
Shear Strain (%)	22	30
Shear Modulus (MPa)	31	52
Operating Temperature Range (°C)	-200 to +70	-200 to +70
Max. Processing Temperature (°C)	+80	+80
Open Cells (%)	3	1.5
Cell Size (mm)	0.5	0.35
Poisson's Ratio	0.32	0.32

Table 5.5: Nominal Properties of Foam Core Materials [5.1]

*(*Perpendicular to the plane of the sheet i.e. parallel to the direction of foam rise; **Parallel to the plane of the sheet i.e. perpendicular to the direction of foam rise; $^{\spadesuit}$Using ASTM D 1621 Proc A; $^{\clubsuit}$Using ASTM D 1621 Proc B)*

Foam Material	Relative Density
H130/C70.130	0.0624
H80	0.0384

Table 5.6: Relative density values of foams determined from measured geometry and Equation 5.1

Specimen Designation	Material	Length (mm)	Width (mm)	Thickness (mm)	Immersion No. Off	95% RH No. Off
Laminate A (LA)	QEA1200	35	26	5 (5 plies)	4	4
Laminate B (LB)	QE1200	35	26	2 (2 plies)	4	4
Thick Foam (FT)	C70.130	50	50	23	6	3
Thin Foam (FN)	C70.130	50	50	8	6	3

Table 7.1: Summary of Moisture Uptake Specimens Exposed to Fresh Water at 40℃ and 95% RH at 40℃

Void Volume Fraction	Condition (a) M_∞ All voids filled	Condition (b) M_∞ Surface voids filled	Condition (c) M_∞ No voids filled
13.8%	15.6%	6.6%	1.8%
9.6%	11.3%	5.3%	1.9%

Table 7.2: Theoretical moisture saturation values (M_∞) for three conditions of ingress into voids and two extremes of void volume fraction.

Void Volume Fraction	Condition (a) M_∞ All voids filled	Condition (b) M_∞ Surface voids filled	Condition (c) M_∞ No voids filled
8.8%	10.5%	6.4%	1.7%
15.3%	16.8%	9.6%	1.5%

Table 7.3: Theoretical moisture saturation values (M_∞) for three conditions of ingress into voids and two extremes of void volume fraction.

Foam	Specimen No.	Immersion Temp. (°C)	Length of Exposure (days)	Laminate	Specimen No.	Immersion Temp. (°C)	Length of Exposure (days)
H130	0A	~	0	QE1200	0A	~	0
H130	0B	~	0	QE1200	0B	~	0
H130	0C	~	0	QE1200	0C	~	0
H130	4A	60	54	QE1200	4A	60	54
H130	4B	60	54	QE1200	4B	60	54
H130	4C	60	54	QE1200	4C	60	54
H130	1A	40	147	QE1200	1A	40	147
H130	1B	40	147	QE1200	1B	40	147
H130	1C	40	147	QE1200	1C	40	147
H130	5A	60	275	QE1200	2A	40	285
H130	5B	60	275	QE1200	2B	40	285
H130	3A	40	292	QE1200	5A	60	285
H130	3B	40	292	QE1200	5B	60	285
H130	3C	40	292	QEA1200	0A	~	0
H80	0A	~	0	QEA1200	0B	~	0
H80	0B	~	0	QEA1200	0C	~	0
H80	0C	~	0	QEA1200	4A	60	82
H80	5A	~	0	QEA1200	4B	60	82
H80	4A	60	12	QEA1200	4C	60	82
H80	4B	60	12	QEA1200	1A	40	285
H80	4C	60	12	QEA1200	1B	40	285
H80	1A	40	82	QEA1200	5A	60	285
H80	1B	40	82	QEA1200	5B	60	285
H80	1C	40	82				
H80	5B	60	275				
H80	5C	60	275				
H80	3A	40	292				
H80	3B	40	292				
H80	3C	40	292				

Table 8.1: Summary of DMTA Programme

Material	**Storage Modulus at 35°C (MPa)**	**Manufacturer Quoted Elastic Modulus (MPa)**	**Storage Modulus as % of Manufacturer Quoted**
QEA1200	3316	23150	14%
QE1200	3560	20707	17%
H130	81.4	140	58%
H80	47.7	80	59%

Table 8.2: Comparison of Room Temperature Storage Modulus Values with Manufacturer's Quoted Elastic Modulus Values (see Tables 5.2 and 5.5)

Material	Tan δ Peak Value (Standard Deviation)	Tan δ Peak Temp. T_g (°C) (Standard Deviation)
QEA1200	0.2884 (0.0069)	112.36 (0.71)
QE1200	0.4551 (0.0140)	87.57 (0.86)
H130	0.1547 (0.0002)	108.60 (0.50)
H80	0.1819 (0.0050)	100.96 (0.49)

Table 8.3: Magnitude and Temperature of the Tan δ Peaks in the Unaged Materials

Ageing Condition	Mean Storage Modulus (MPa) (Standard Deviation)	% Change from Unaged Condition
Dry (Unaged)	3316 (141)	0
82 days @ 60°C	2530 (208)	23.7% ↓
285 days @ 60°C	1687 (14)	49.1% ↓
285 days @ 40°C	1662 (547)	49.9% ↓

Table 8.4: Summary of Mean Storage Modulus Results for QEA1200 Material

Ageing Condition	Loss Modulus Peak Value (MPa) (Standard Deviation)	Loss Modulus Peak Temp. (°C) (Standard Deviation)	% Change in Peak Value	% Change in Temp.
Dry (Unaged)	321.8 (21.1)	101.6 (1.3)	0	0
82 days @ 60°C	266.7 (15.6)	93.2 (0.2)	17.1% ↓	8.3% ↓
285 days @ 60°C	169.8 (18.7)	96.9 (0.3)	47.2% ↓	4.6% ↓
285 days @ 40°C	162.5 (40.9)	93.8 (1.5)	49.5% ↓	7.6% ↓

Table 8.5 Summary of Mean Peak Loss Modulus Values and Temperatures for the QEA1200 Material

Ageing Condition	Tan δ Peak Value (MPa) (Standard Deviation)	Tan δ Peak Temp. (°C) (Standard Deviation)	% Change in Peak Value	% Change in Temperature
Dry (Unaged)	0.2884 (0.0069)	112.36 (0.71)	0	0
82 days @ 60°C	0.2933 (0.0078)	99.32 (0.41)	1.7% ↑	11.6% ↓
285 days @ 60°C	0.2414 (0.0102)	101.65 (0.45)	16.3% ↓	9.5% ↓
285 days @ 40°C	0.2629 (0.0044)	99.0 (1.20)	8.8% ↓	11.9% ↓

Table 8.6: Summary of Mean Peak Tan δ Values and Temperatures for the QEA1200 Material

Ageing Condition	Mean Storage Modulus (MPa) (Standard Deviation)	% Change from Unaged Condition
Dry (Unaged)	3560 (139)	0
54 days @ 60°C	2805 (393)	21.2% ↓
285 days @ 60°C	2277 (285)	36.1% ↓
147 days @ 40°C	2270 (416)	36.2% ↓
285 days @ 40°C	3319 (281)	6.78% ↓

Table 8.7: Summary of Mean Storage Modulus Results for QE1200 Material

Ageing Condition	Loss Modulus Peak Value (MPa) (Standard Deviation)	Loss Modulus Peak Temp. (°C) (Standard Deviation)	% Change in Peak Value	% Change in Temp.
Dry (Unaged)	400.4 (11.7)	80.5 (0.33)	0	0
54 days @ 60°C	276.8 (58.4)	86.8 (0.34)	30.9% ↓	7.8% ↑
285 days @ 60°C	242.4 (47.5)	88.1 (0.29)	39.5% ↓	9.4% ↑
147 days @ 40°C	225.5 (33.0)	82.7 (0.59)	43.7% ↓	2.7% ↑
285 days @ 40°C	357.4 (63.8)	83.3 (0.31)	10.7% ↓	3.5% ↑

Table 8.8 Summary of Mean Peak Loss Modulus Values and Temperatures for the QE1200 Material

Ageing Condition	Tan δ Peak Value (MPa) (Standard Deviation)	Tan δ Peak Temp. (°C) (Standard Deviation)	% Change in Peak Value	% Change in Temp.
Dry (Unaged)	0.4551 (0.014)	87.6 (0.86)	0	0
54 days @ 60°C	0.2927 (0.011)	92.9 (0.05)	35.6% ↓	6.0% ↑
285 days @ 60°C	0.3072 (0.0108)	93.4 (0.25)	32.5% ↓	6.6% ↑
147 days @ 40°C	0.3428 (0.015)	87.1 (0.75)	24.7% ↓	0.5% ↓
285 days @ 40°C	0.3524 (0.0156)	87.95 (0.55)	22.6% ↓	0.4% ↑

Table 8.9: Summary of Mean Peak Tan δ Values and Temperatures for the QE1200 Material

Ageing Condition	Mean Storage Modulus (MPa) (Standard Deviation)	% Change from Unaged Condition
Dry (Unaged)	81.4 (2.3)	0
54 days @ 60°C	84.4 (9.8)	3.7% ↑
147 days @ 40°C	75.0 (11.0)	7.9% ↓
292 days @ 40°C	73.7 (2.2)	9.5% ↓

Table 8.10: Summary of Mean Storage Modulus Results for H130 Foam Material

Ageing Condition	Loss Modulus Peak Value (MPa) (Standard Deviation)	Loss Modulus Peak Temp. (°C) (Standard Deviation)	% Change in Peak Value	% Change in Temp.
Dry (Unaged)	4.25 (0.13)	96.8 (0.29)	0	0
54 days @ 60°C	4.99 (0.60)	96.7 (0.54)	17.5% ↑	0.1% ↓
147 days @ 40°C	4.64 (0.67)	89.2 (0.99)	9.27% ↑	7.9% ↓
292 days @ 40°C	4.58 (0.19)	90.2 (0.11)	7.8% ↑	6.8% ↓

Table 8.11: Summary of Mean Peak Loss Modulus Values and Temperatures for the H130 Foam Material

Ageing Condition	Tan δ Peak Value (MPa) (Standard Deviation)	Tan δ Peak Temp. (°C) (Standard Deviation)	% Change in Peak Value	% Change in Temp.
Dry (Unaged)	0.1547 (0.0002)	108.6 (0.5)	0	0
54 days @ 60°C	0.2040 (0.0108)	107.5 (0.2)	31.9% ↑	1.0% ↓
275 days @ 60°C	0.2273 (0.0001)	113.6 (0.0)	46.9% ↑	4.6% ↑
147 days @ 40°C	0.2299 (0.0028)	107.6 (0.7)	48.6% ↑	0.92% ↓
292 days @ 40°C	0.2328 (0.0113)	109.1 (1.5)	50.5% ↑	0.46% ↑

Table 8.12: Summary of Mean Peak Tan δ Values and Temperatures for the H130 Foam Material

Ageing Condition	Mean Storage Modulus (MPa) (Standard Deviation)	% Change from Unaged Condition
Dry (Unaged)	47.72 (0.95)	0
12 days @ 60°C	42.99 (1.04)	9.9% ↓
82days @ 40°C	41.29 (2.28)	13.5% ↓
292 days @ 40°C	40.12 (4.08)	15.9% ↓

Table 8.13: Summary of Mean Storage Modulus Results for H80 Foam Material

Ageing Condition	Loss Modulus Peak Value (MPa) (Standard Deviation)	Loss Modulus Peak Temp. (°C) (Standard Deviation)	% Change in Peak Value	% Change in Temp.
Dry (Unaged)	3.017 (0.008)	89.6 (0.8)	0% ↓	0% ↑
12 days @ 60°C	2.994 (0.069)	92.5 (0.4)	0.76% ↓	3.2% ↑
82 days @ 40°C	2.931 (0.182)	90.0 (0.6)	2.85% ↓	0.31% ↑
292 days @ 40°C	2.930 (0.267)	90.6 (0.4)	2.88% ↓	1.1% ↑

Table 8.14: Summary of Mean Peak Loss Modulus Values and Temperatures for the H80 Foam Material

Ageing Condition	Tan δ Peak Value (MPa) (Standard Deviation)	Tan δ Peak Temp. (°C) (Standard Deviation)	% Change in Peak Value	% Change in Temp.
Dry (Unaged)	0.1819 (0.0050)	101.0 (0.5)	0	0
12days @ 60°C	0.2291 (0.0030)	104.2 (0.3)	25.9% ↑	3.2% ↑
275 days @ 60°C	0.2231 (0.0036)	107.1 (0.7)	22.6% ↑	6.0% ↑
82 days @ 40°C	0.2605 (0.0046)	103.9 (0.3)	43.2% ↑	2.9% ↑
292 days @ 40°C	0.2689 (0.0088)	106.7 (0.04)	47.8% ↑	5.7% ↑

Table 8.15: Summary of Mean Peak Tan δ Values and Temperatures for the H80 Foam Material

Specimen Number	No. of Plies in Overlaminate	Fillet Radius (mm)	Filled Gap Size (mm)
1	4	0	0
2	2	0	0
3	4	30	0
4	2	30	0
5	2	30	25
6	0	30	0

Table 9.1: Summary of Six Joint Geometries Tested

Specimen Number	Flange Core		Web Core		Overlaminate/Web		Fillet	
	$\Delta(\sigma_1+\sigma_2)$ (MPa)	Position (mm)	$\Delta(\sigma_1+\sigma_2)$ (MPa)	Position (mm)	$\Delta\sigma_{11}+\alpha\Delta\sigma_{22}$ (MPa)	Position (mm)	$\Delta(\sigma_1+\sigma_2)$ (MPa)	Position (mm)
1	-1.575	-27.3	-0.418	-24.15	-5.583	-30.45	-	-
	-1.741	27.3	-0.422	26.25	-15.3144	27.3	-	-
2	-1.222	-21.6	-0.402	-25.92	-7.156	-30.24	-	-
	-1.193	27.36	-0.381	27.36	-6.862	28.8	-	-
3	-1.369	-34.56	-0.607	-30.24	-20.742	-31.38	-12.905	-33.12
	-1.039	27.36	-0.527	21.6	-10.526	33.12	-9.967	38.88
4	-1.298	-27.36	-0.844	-25.92	-12.877	-30.24	-5.395	-33.12
	-1.148	18.72	-0.771	23.04	-16.956	27.36	-5.006	38.88
5	-1.343	-34.56	-0.365	-27.36	-7.761	-30.24	-11.694	-41.76
	-0.676	41.76	-0.323	28.8	-6.966	31.68	-8.464	50.4
6	-1.497	-25.92	-1.092	-25.92	-29.678	-27.36	-24.028	-28.8
	-1.195	36.0	-0.975	25.92	-26.515	27.36	-23.207	28.8

Table 9.2: Values and Positions of Maximum Stress Sums in the Six Tee Joint Geometries

Joint	Gap Size (mm)	Plies in Overlaminate	Fillet Radius (mm)	Experiment Deflection (mm)	FE Clamped Deflection (mm)	Difference %
2	0	2	0	-1.340	-1.259	6.04
3	0	4	30	-1.144	-1.125	1.66
4	0	2	30	-1.231	-1.173	4.71

Table 10.1: Validation of FE Model using Clamped Static Load Deflection Results

Joint No.	Flange Core		Web Core		Overlaminate/Web		Fillet		
	$\Delta(\sigma_1+\sigma_2)$ (MPa)	Position (mm)	$\Delta(\sigma_1+\sigma_2)$ (MPa)	Position (mm)	$\Delta\sigma_{11}+\alpha\Delta\sigma_2$ 2 (MPa)	Position (mm)	$\Delta(\sigma_1+\sigma_2)$ (MPa)	x mm	y mm
1	-0.626	±25	-0.342	±25	-35.885	±31	-	-	-
2	-0.706	±22.22	-0.383	±25	-34.476	±29	-	-	-
3	-0.517	±27	-0.409	±25	-16.800	±31	-5.136	±38	116
4	-0.569	±25	-0.464	±25	-17.602	±29	-5.86	±38	116
5	-0.513	±45	-0.088	±25	-9.950	±27	-7.77	±40	114
6	-0.628	±25	-0.418	±25	-15.007	±25	-10.753	±29	128

Table 10.2: Maximum Stress Values Determined from Finite Element Results (Simply Supported Case)

Joint No.	Flange Core		Web Core		Overlaminate/Web		Fillet	
	Mean Peak $\Delta(\sigma_1+\sigma_2)$ (MPa)	Mean Position (mm)	Mean Peak $\Delta(\sigma_1+\sigma_2)$ (MPa)	Mean Position (mm)	Mean Peak $\Delta\sigma_{11}+\alpha\Delta\sigma_{22}$ (MPa)	Mean Position (mm)	Mean Peak $\Delta(\sigma_1+\sigma_2)$ (MPa)	Mean Posn. (mm)
1	-1.658	±27.3	-0.420	±25.20	-11.704*	±28.88	-	-
2	-1.208	±24.5*	-0.392	±26.64	-7.009	±29.52	-	-
3	-1.204*	±30.96*	-0.567	±25.92*	-15.634*	±32.25	-11.436*	±36.00
4	-1.223	±23.04*	-0.808*	±24.48	-14.921*	±28.80	-5.301	±36.00
5	-1.010*	±38.16*	-0.344	±28.08	-7.364	±30.96	-10.079*	±46.08
6	-1.346*	±30.96*	-1.034	±25.92	-28.097	±27.36	-23.618	±28.8

Table 10.3: Mean Maximum Stress Values and Positions Determined from TSA Data in Table 7.2

Gap Size (mm)	Gap Filler	Maximum Stress (MPa)	Max. Stress Position (mm)	Minimum Stress (MPa)	Min. Stress Position (mm)
5	Epoxy Filler	-0.381	± 25	-0.227	0
10	Epoxy Filler	-0.287	± 25	-0.165	0
15	Epoxy Filler	-0.200	± 25	-0.117	0
20	Epoxy Filler	-0.132	± 25	-0.0868	0
25	Epoxy Filler	-0.088	± 25	-0.0766	0
5	Air	-0.460	± 25	-0.267	0
10	Air	-0.470	± 25	-0.280	0
15	Air	-0.484	± 25	-0.299	0
20	Air	-0.508	± 25	-0.321	0
25	Air	-0.565	± 25	-0.336	0

Table 10.4: Parametric Study - Comparison of Maximum and Minimum Stress Values within Web Core with different gap fillers and sizes

Gap Size (mm)	Gap Filler	Maximum Stress (MPa)	Max. Stress Position (mm)	Minimum Stress (MPa)	Min. Stress Position (mm)
5	Epoxy Filler	-0.655	±25	-0.573	0
		-0.644	±42		
10	Epoxy Filler	-0.665	±45	-0.540	0
15	Epoxy Filler	-0.693	±45	-0.485	0
20	Epoxy Filler	-0.714	±48	-0.447	0
25	Epoxy Filler	-0.725	±48	-0.428	0
5	Air	-0.829	±25	-0.400	0
10	Air	-0.834	±25	-0.405	0
15	Air	-0.844	±25	-0.412	0
20	Air	-0.859	±25	-0.423	0
25	Air	-0.879	±25	-0.437	0

Table 10.5: Parametric Study - Comparison of Maximum and Minimum Stress Values within Flange Core with different gap fillers and sizes

Joint (ageing duration)	Flange Nominal	Flange Peak	Web Nominal	Web Peak
Unloaded Joint (60 days)	54.50 ↑	15.43 ↑	26.1 ↑	28.4 ↓
Unloaded Joint (144 days)	10.55 ↑	46.52 ↑	28.8 ↑	26.0 ↓
Statically Loaded Joint (60 days)	41.08 ↑	26.45 ↑	17.6 ↑	24.3 ↓
Statically Loaded Joint (144 days)	29.96 ↑	36.48 ↑	28.9 ↑	13.7 ↓
Cyclically Loaded Joint (60 days)	20.41 ↑	18.13 ↑	10.5 ↓	39.4 ↓
Cyclically Loaded Joint (144 days)	29.09 ↑	37.61 ↑	0.2 ↓	36.5 ↓

Table 11.1: Percentage Changes in Normalised Results with Respect to the Unaged Case (↑ denotes increase, ↓ denotes decrease)

Joint	Between Start of Exposure and Test 1 (60 days)	Between Test 1 and Test 2 (84 days)
Statically Loaded	67.7% ↓	45.6% ↓
Cyclically Loaded	66.2% ↓	51.1% ↓

Table 11.2: Measured Stiffness Reduction in the two Loaded Joints due to Stress Relaxation or Creep effects

	Original (Unaged) Values			Reduction	Aged Values		
Material	E_x (GPa)	E_y (GPa)	G_{xy} (MPa)	%	E_x (GPa)	E_y (GPa)	G_{xy} (MPa)
QE1200	20707	5800	7450	36.15	13221.4	3703.3	4756.8
QEA1200	23150	5800	8203	49.5	11690.75	3703.3	4142.5
XE900	14400	5800	4500	36.15	9194.4	3703.3	2873.3
H130	140	~	52	9.5	126.7	~	47.06
H80	80	~	31	15.9	67.28	~	26.07
Epoxy Fillet	3300	~	3500	36.15	2107.05	~	2234.8
Wood Insert	1120	~	120	0	1120	~	120

Table 11.3: Material Properties Modified for the Effects of Ageing

Model Geometry	Flange Nominal	Flange Peak	Web Nominal	Web Peak
Joint 3 (30 mm fillet radius, 4-ply O/L)	3.23 ↑	5.5 ↑	3.98 ↑	3.20 ↑
Joint 4 (30 mm fillet radius, 2-ply O/L)	2.79 ↑	5.06 ↑	4.25 ↑	2.25 ↑

Table 11.4: Percentage Changes in Normalised Results with Respect to the Unaged Case (↑ denotes increase)

FIGURES

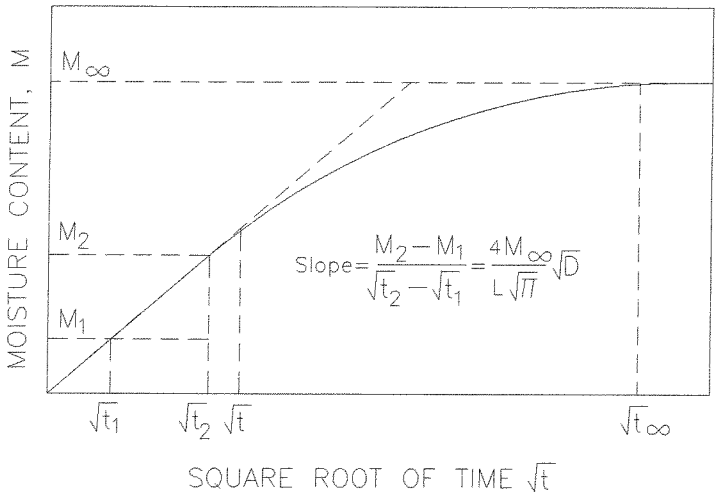

Figure 2.1: Characteristic Fickian Diffusion Curve [2.4]

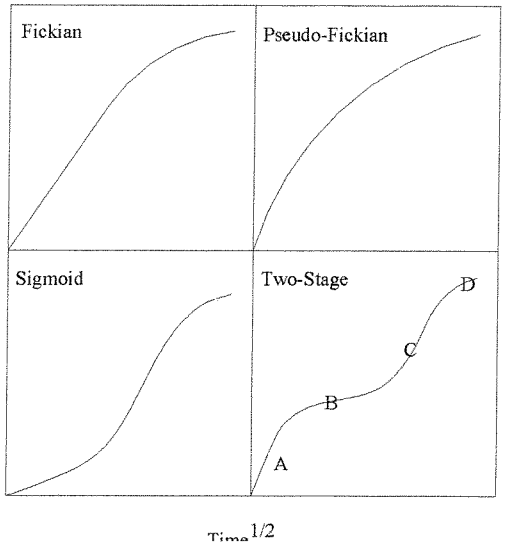

Figure 2.2: Absorption Behaviour [2.20]

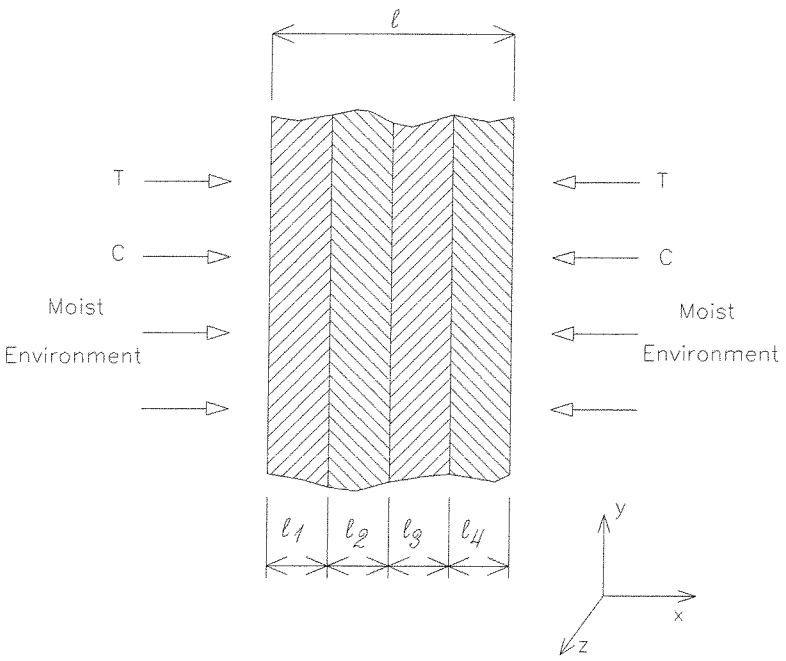

Figure 2.3: An Illustration of the Problem (Springer [2.4]): Moisture Absorption in a Laminated Plate

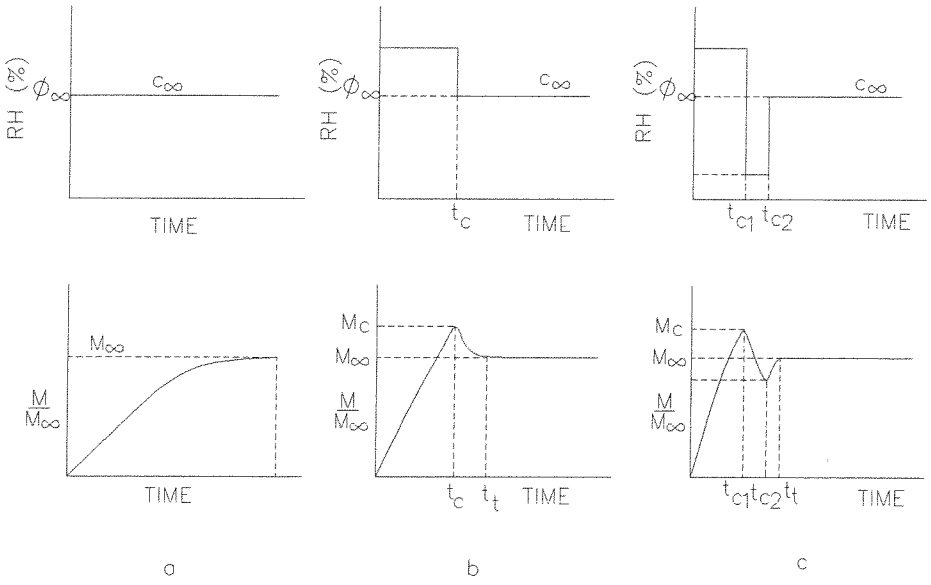

Figure 2.4: Accelerated Conditioning Methods: (a) Single Stage, (b) Two Stage, (c) Three Stage

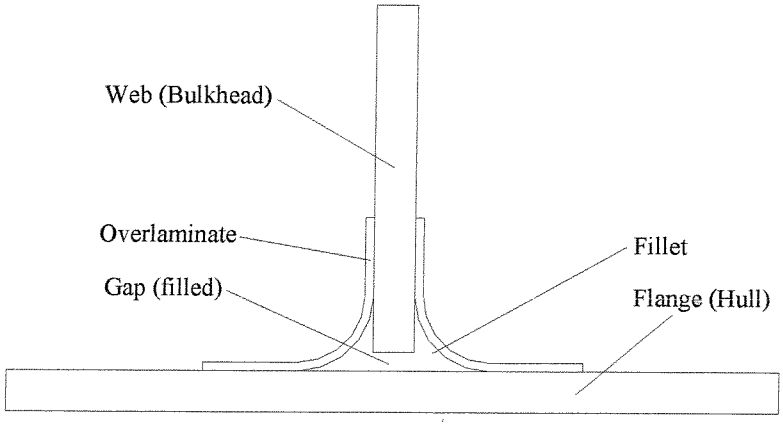

Figure 3.1: Typical Single Skin Tee Joint Construction

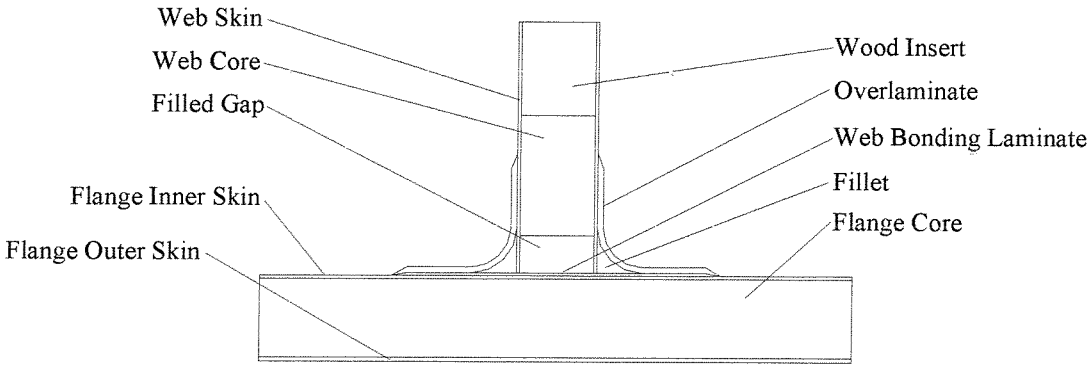

Figure 3.2: Sandwich Construction Tee Joint Schematic

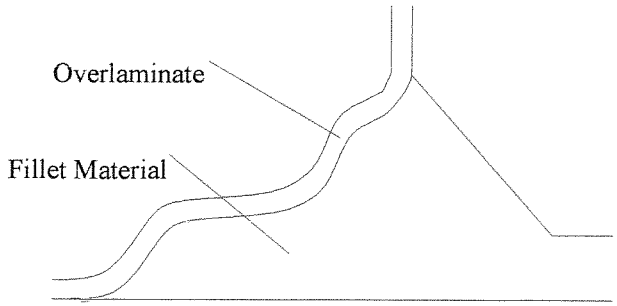

Figure 3.3: Improved Fillet Geometry [3.20]

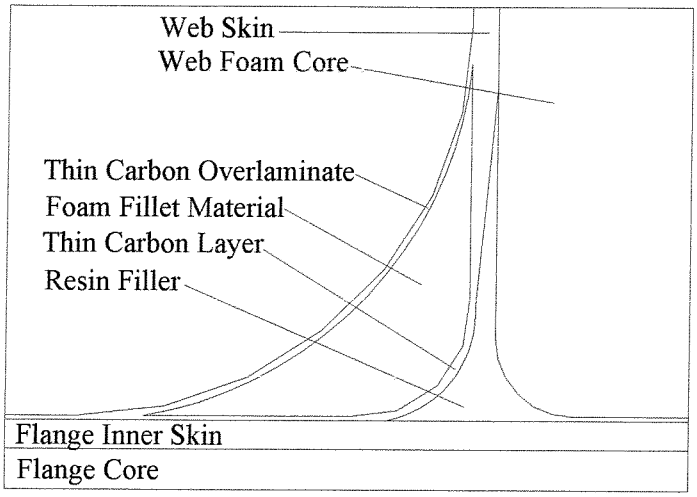

Figure 3.4: Improved joint with continuation of load path from web skin around the fillet [3.20]

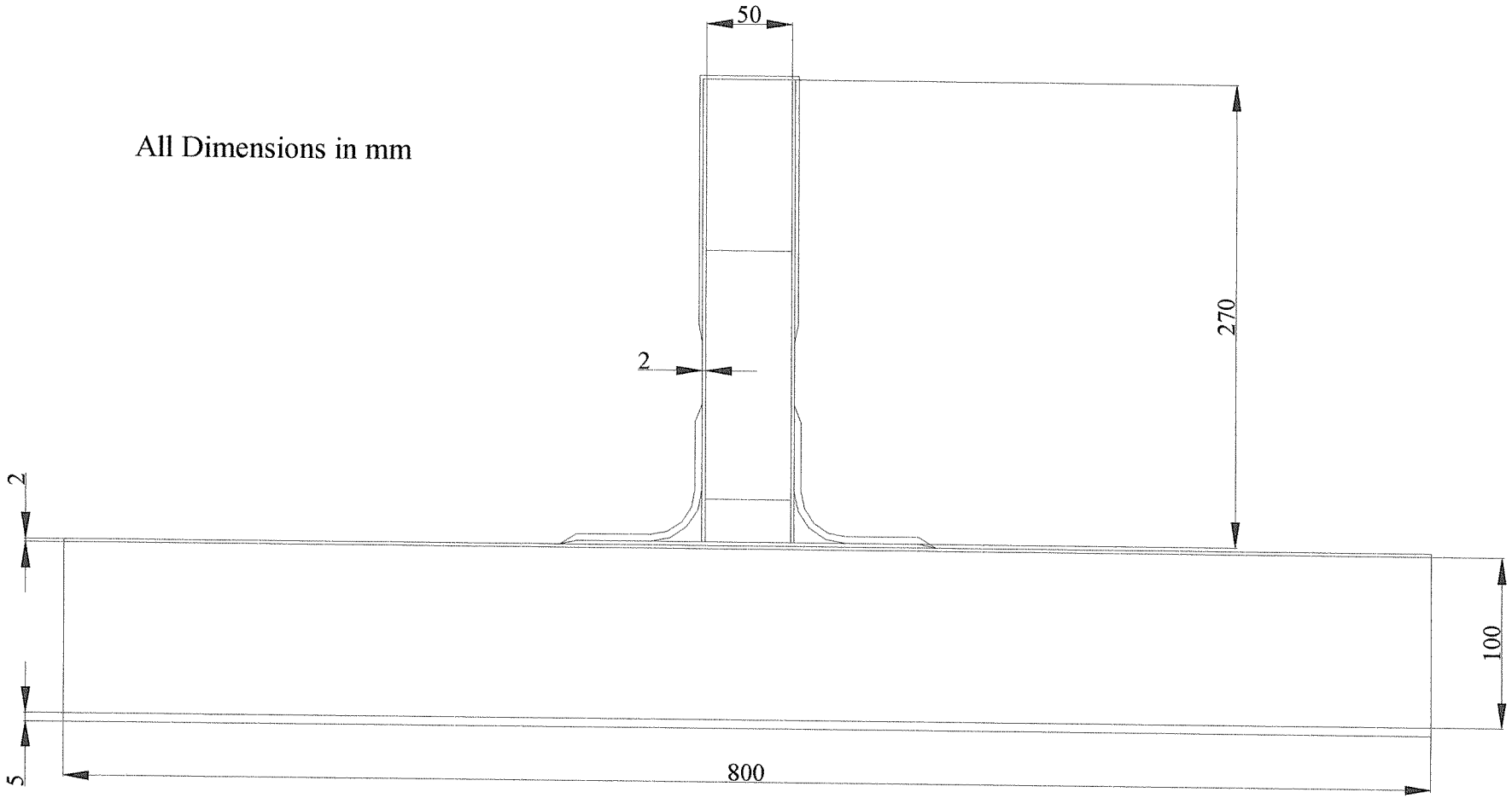

Figure 5.1: Tee Joint Test Piece Dimensions

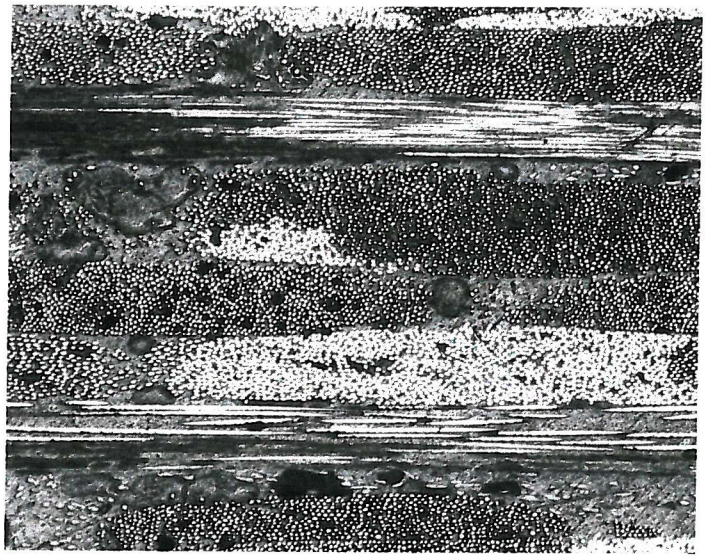

Figure 5.2: QEA1200 Batch 1 Laminate Material showing a representative cross-section with voids (× 40)

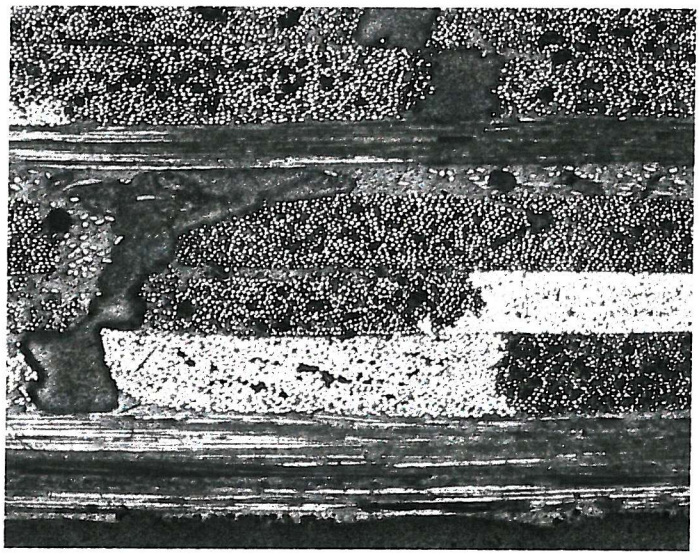

Figure 5.3: QEA1200 Batch 1 Laminate Material showing large localised voids between plies (× 40)

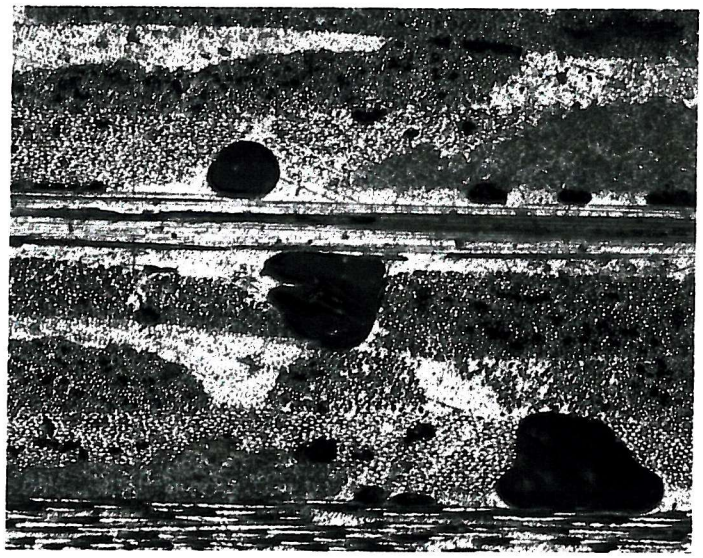

Figure 5.4: QEA1200 Batch 2 Laminate Material showing a representative cross-section with large voids (× 40).

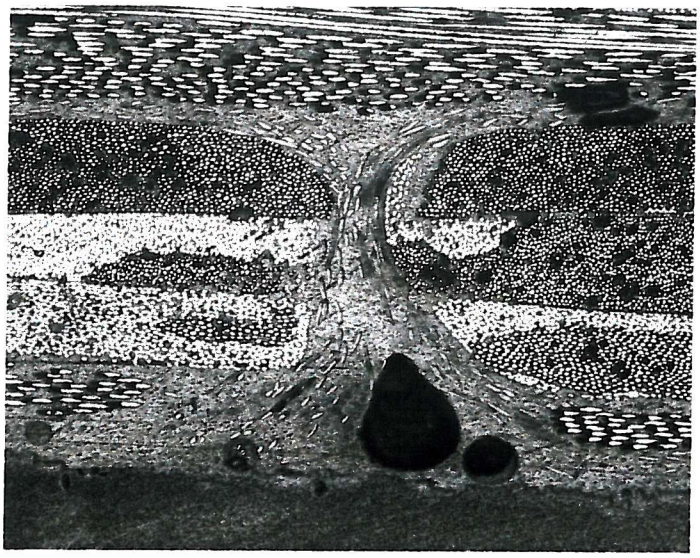

Figure 5.5: QEA1200 Batch 2 Laminate Material exhibiting a resin rich layer and defect at the surface (× 40).

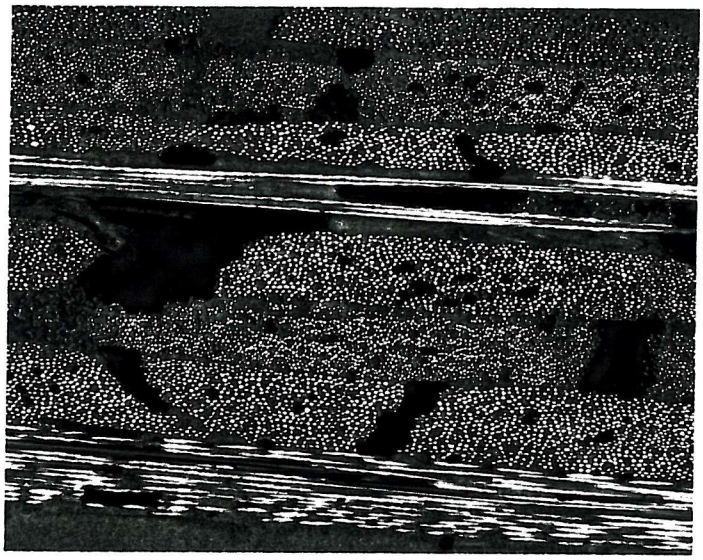

Figure 5.6: QE1200 Batch 1 Material showing large void areas between laminae (× 40)

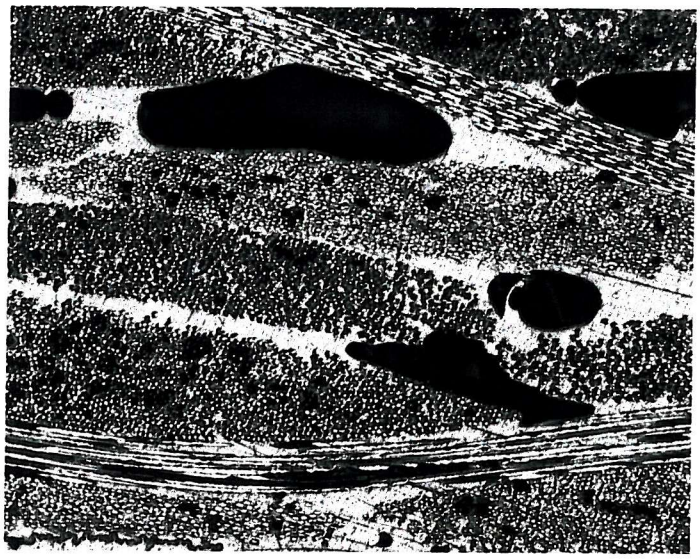

Figure 5.7: Q E1200 Batch 2 Material showing large voids and resin rich areas (× 40).

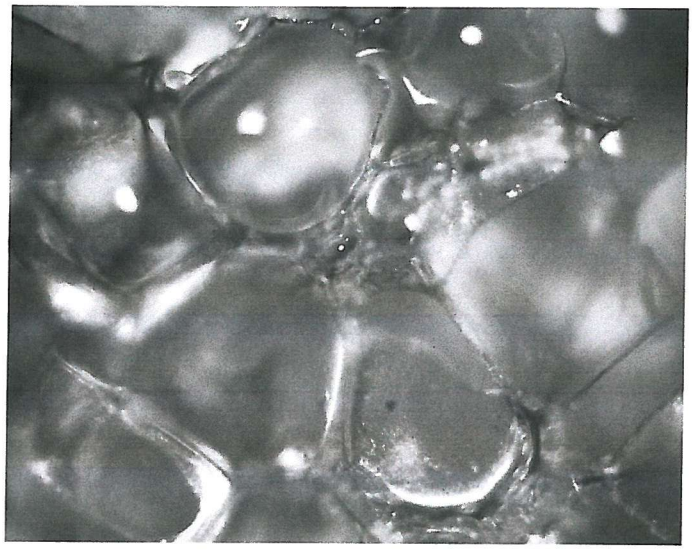

Figure 5.8: Micrograph showing foam cell structure (C70.130) (×80)

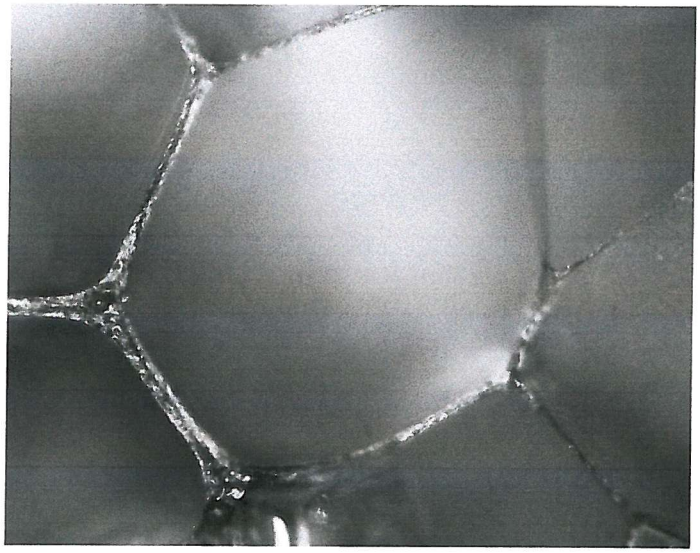

Figure 5.9: Micrograph of single cell for geometry determination using image analysis (C70.130) (×160)

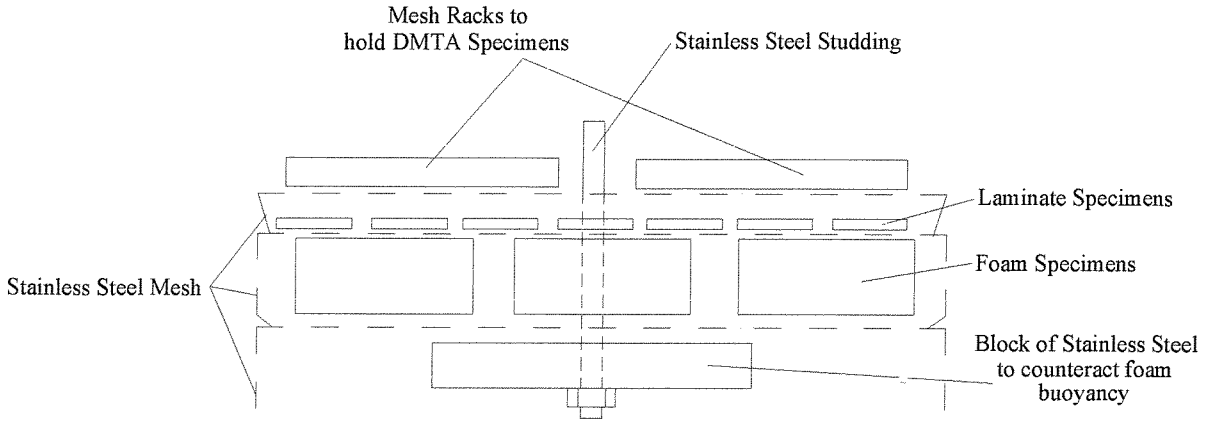

Figure 6.1: Schematic of Typical Rack Arrangement in Bath

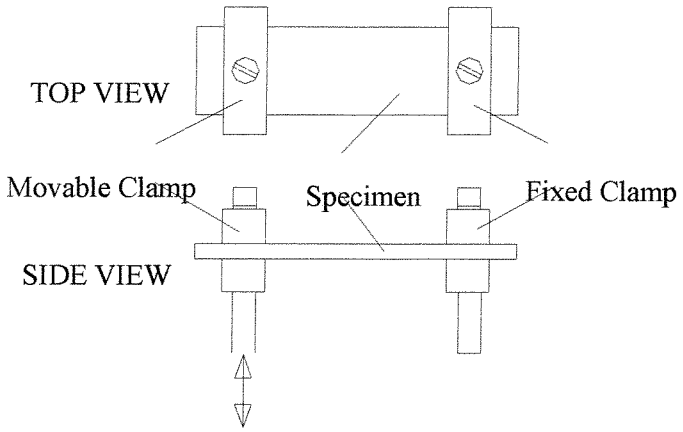

Figure 6.2: DMTA Single Cantilever Clamp Arrangement

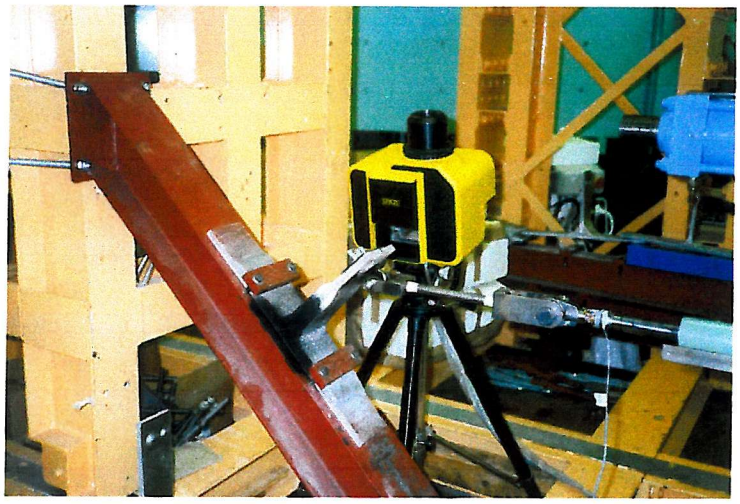

Figure 6.3: SPATE Equipment Scanning Single Skin Tee Joint Under 45° Pull-off Load in FORTReSS

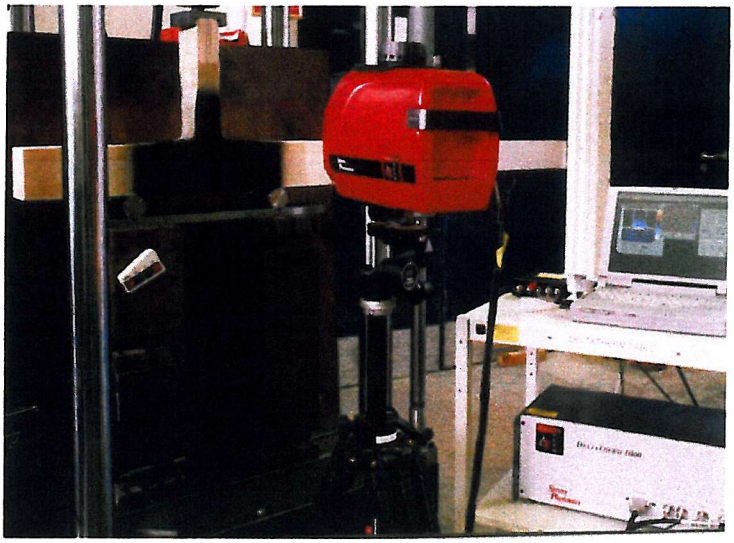

Figure 6.4: DeltaTherm 1000 Scanning Sandwich Tee Joint Loaded in Compression (Note black paint on specimen and signal plot on computer)

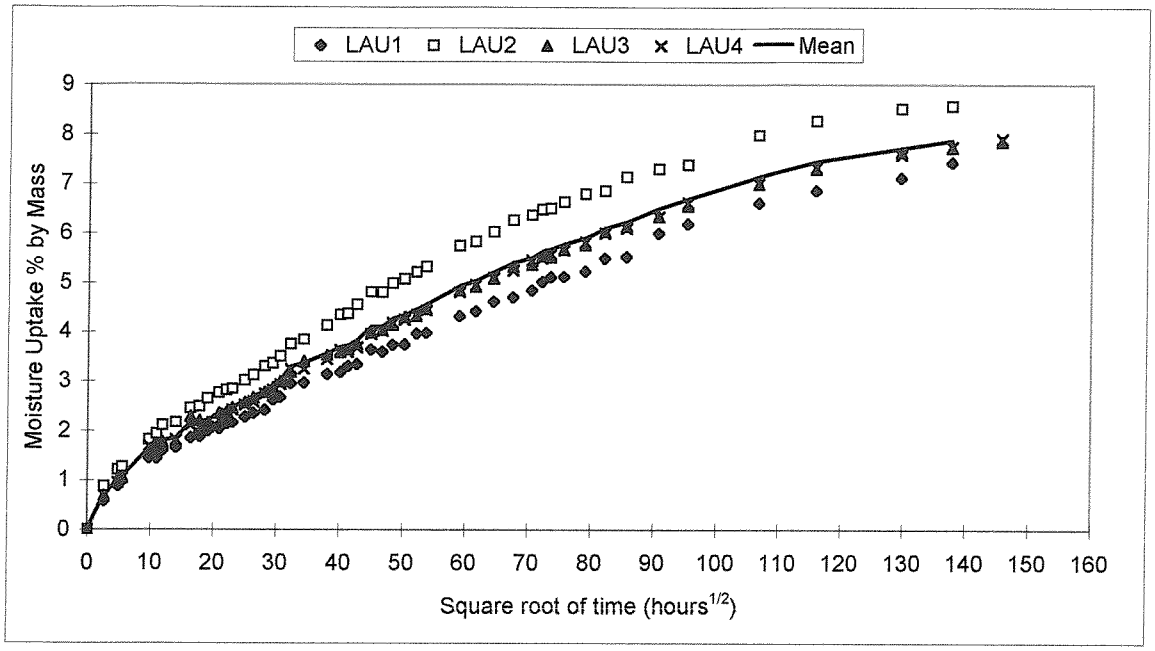

Figure 7.1: Moisture uptake in QEA1200 specimens immersed in fresh water at 40°C

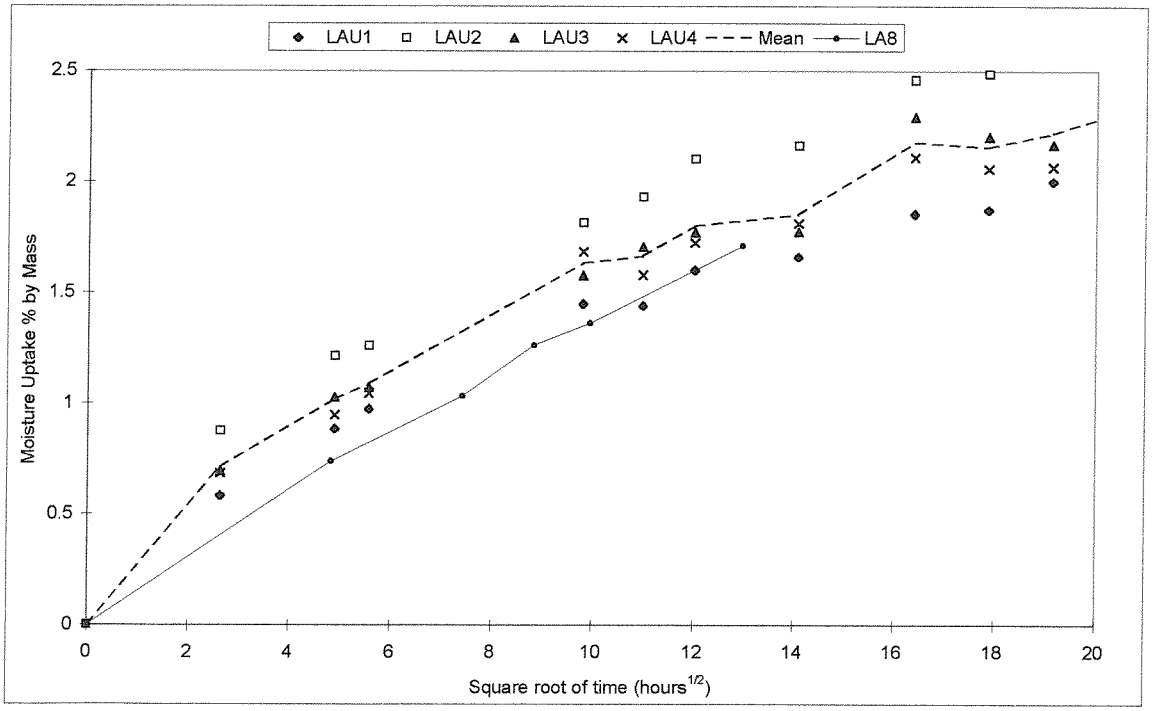

Figure 7.2: QEA1200 Initial uptake including specimen LA8, which has its cut edges sealed

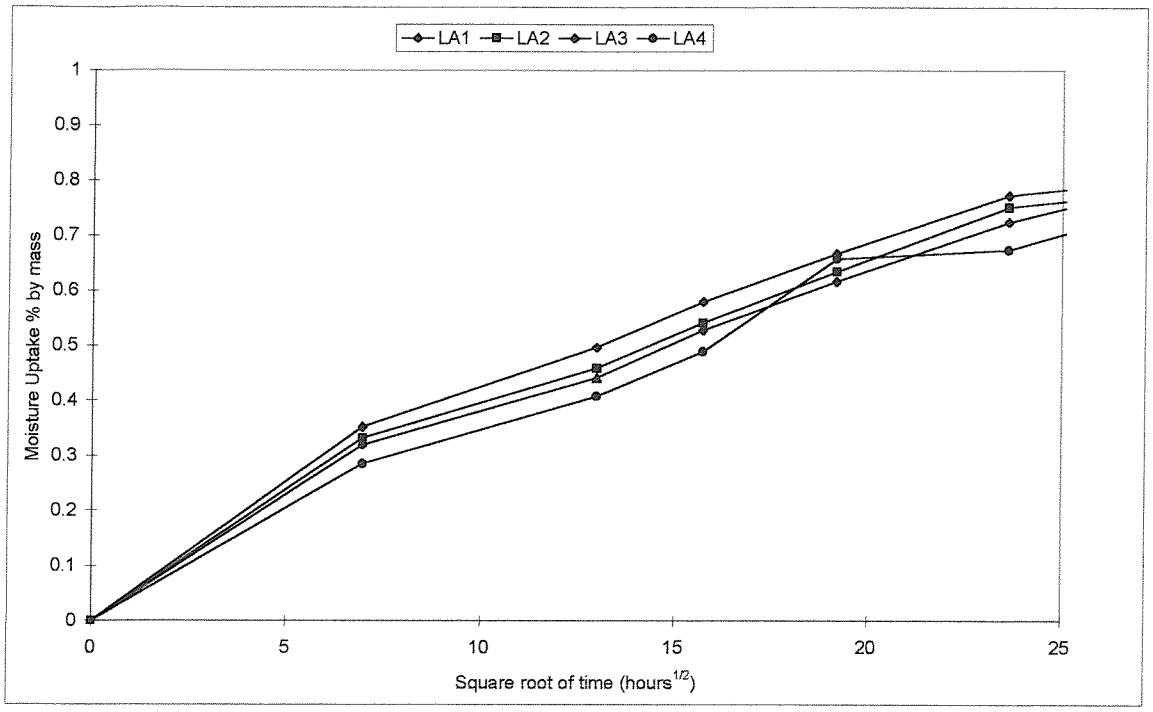

Figure 7.3: Moisture uptake in QEA1200 specimens exposed to 95% RH at 40°C

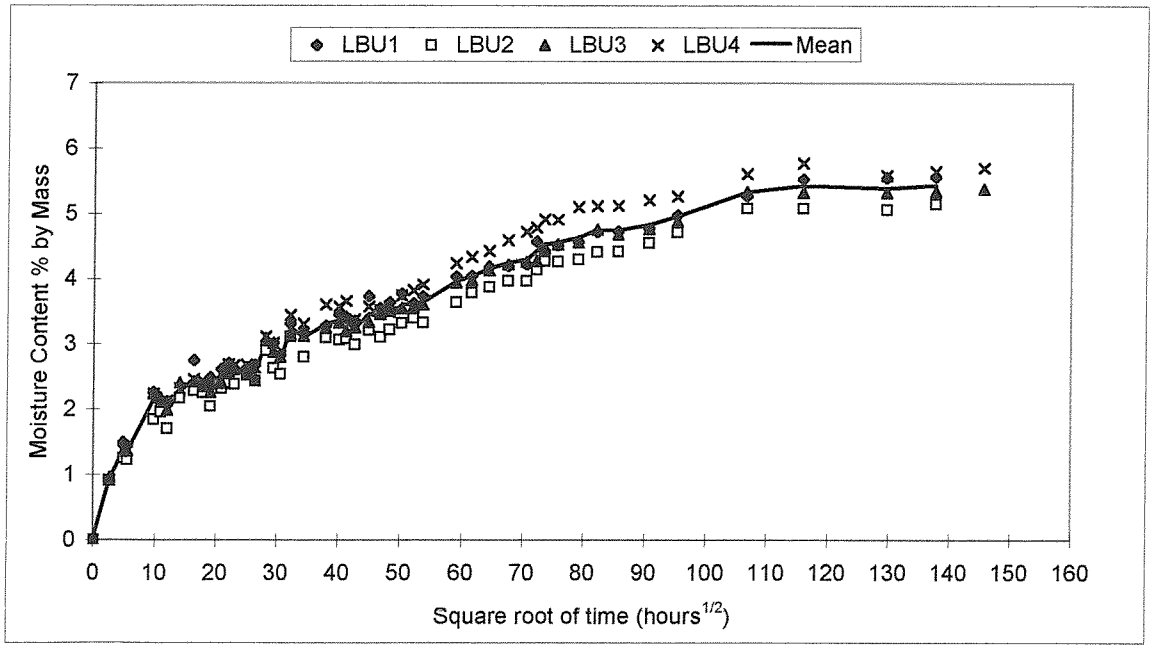

Figure 7.4: Moisture uptake in QE1200 specimens immersed in fresh water at 40°C

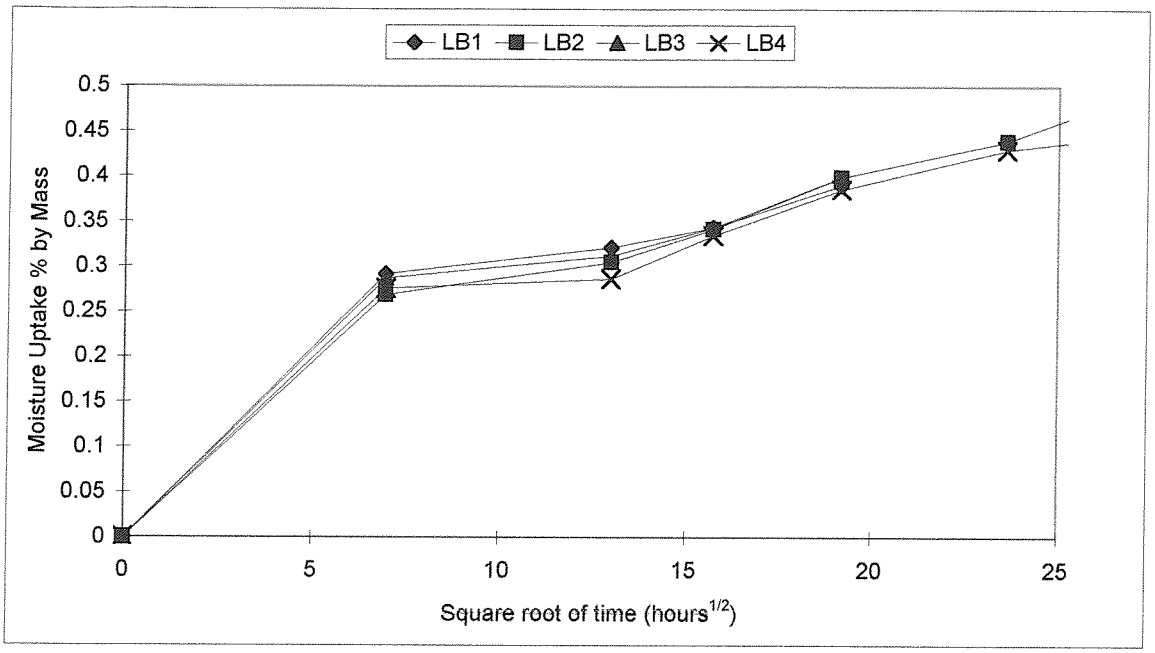

Figure 7.5: Moisture uptake in QE1200 specimens exposed to 95% RH at 40°C

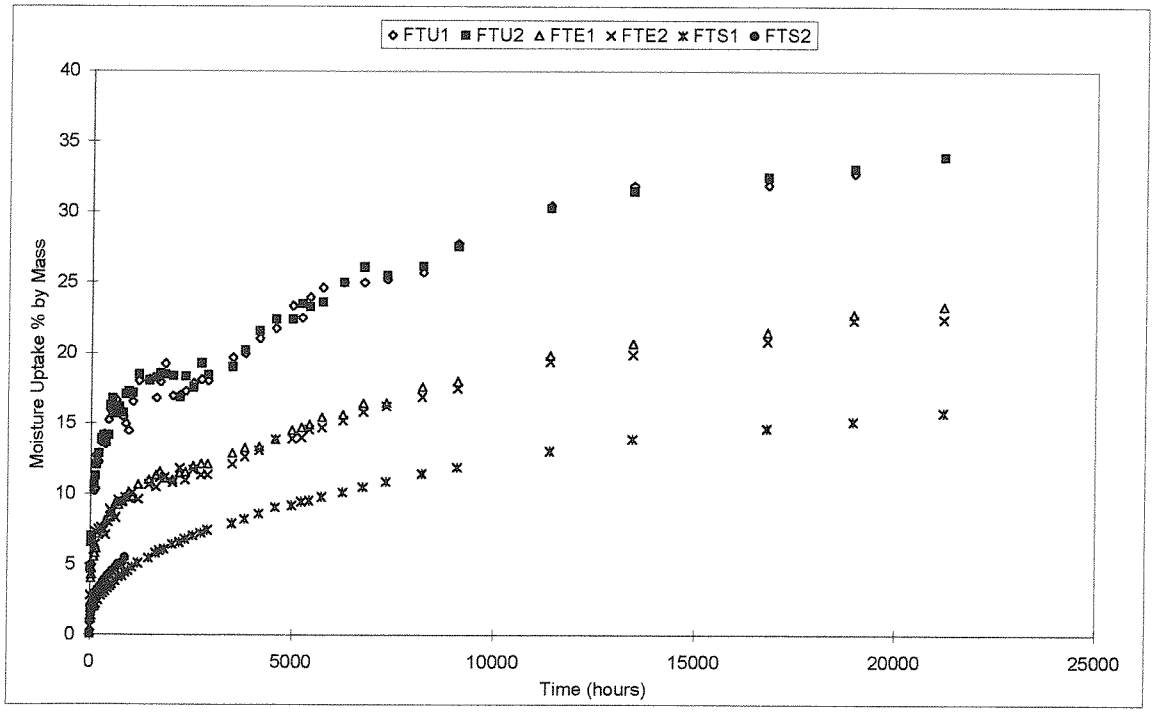

Figure 7.6: Moisture uptake in thick foam specimens immersed in fresh water at 40°C vs. time

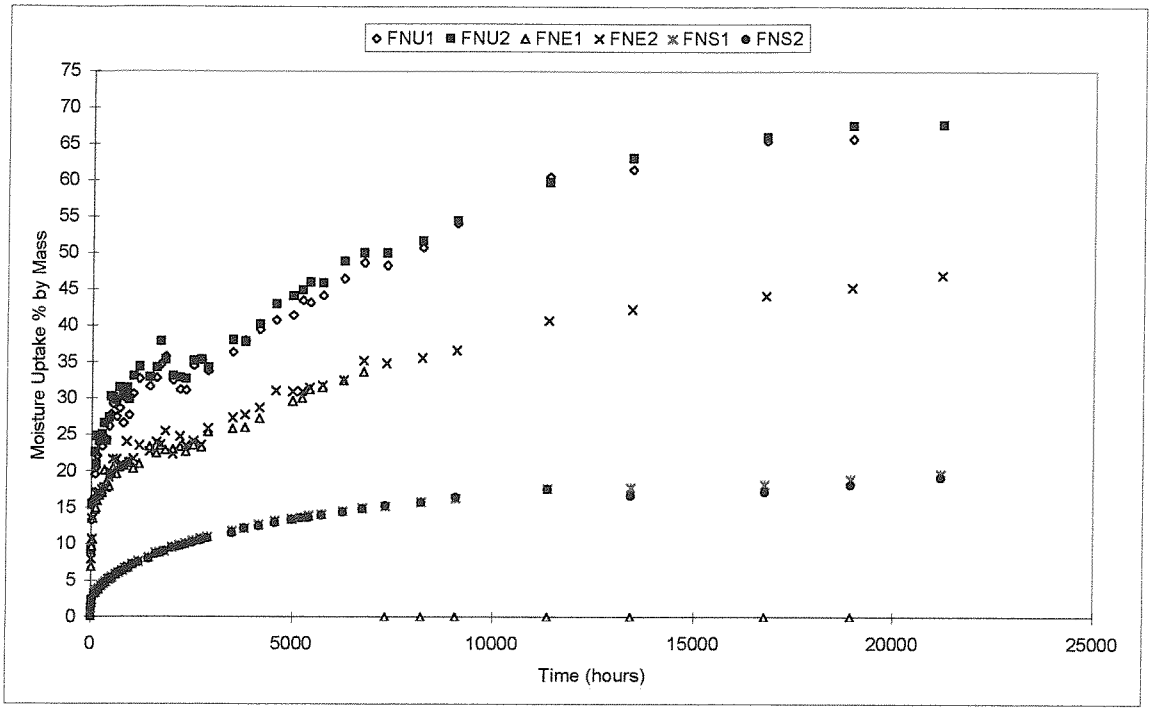

Figure 7.7: Moisture uptake in thin foam specimens immersed in fresh water at 40°C vs. time

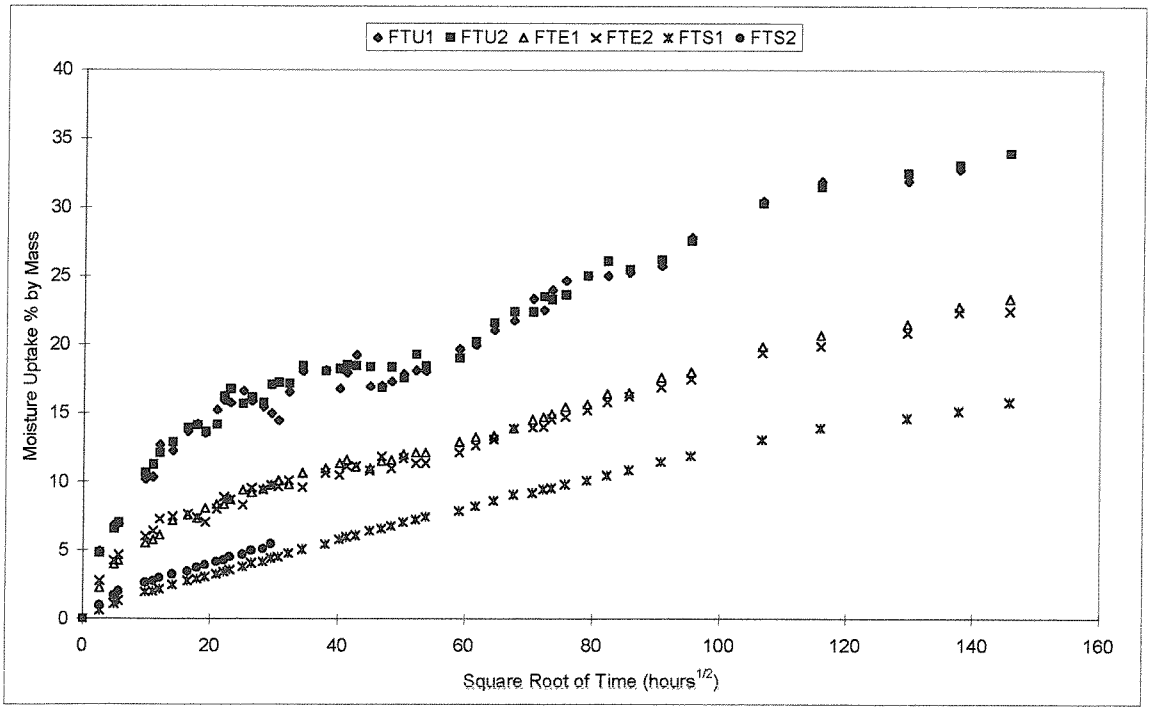

Figure 7.8: Moisture uptake in thick foam specimens immersed in fresh water at 40°C vs. square root of time

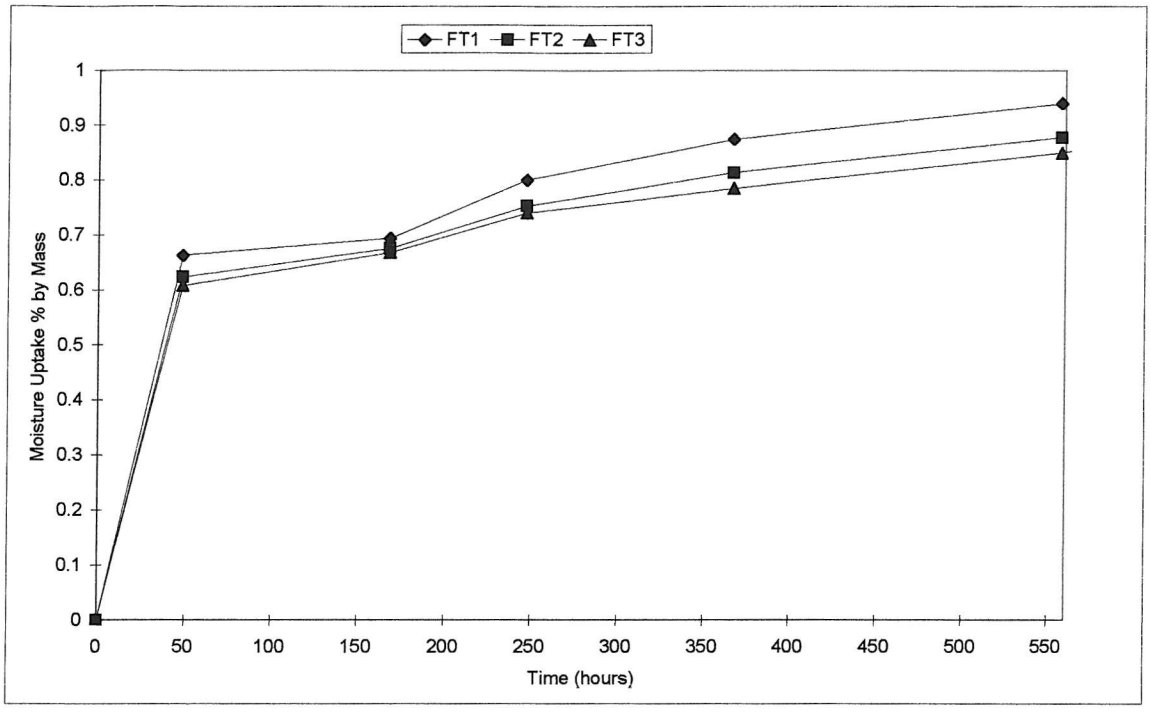

Figure 7.9: Moisture uptake in thick foam specimens exposed to 95% RH at 40°C

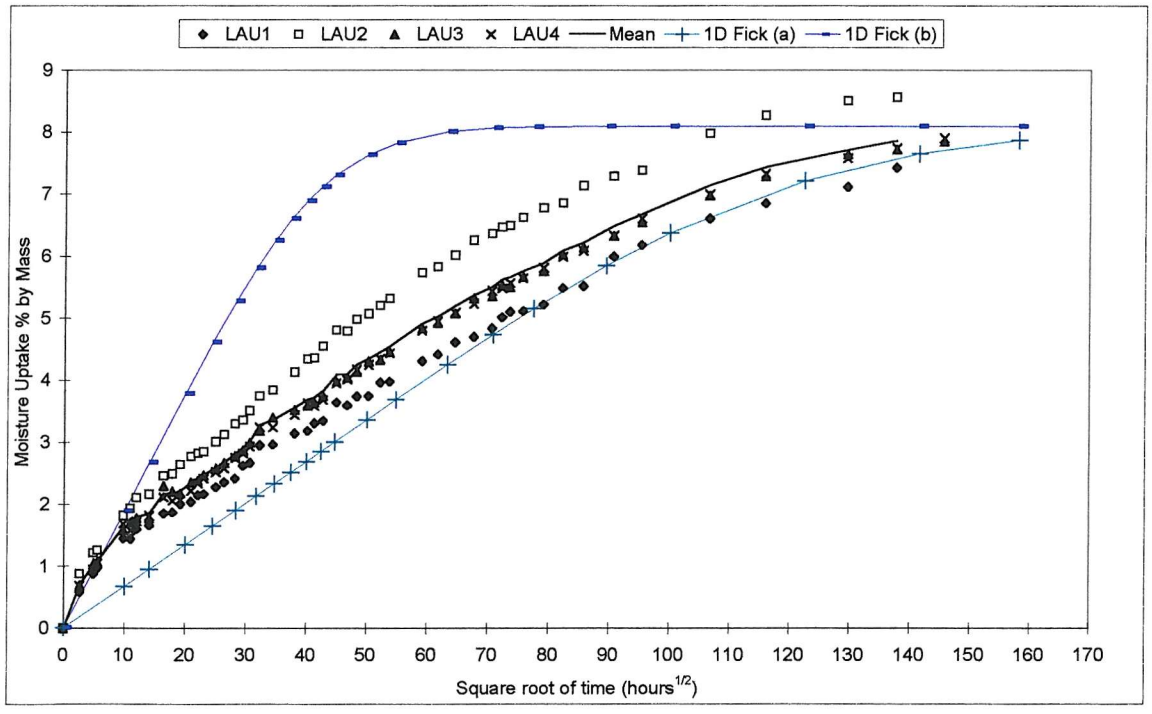

Figure 7.10: QEA1200 moisture uptake results with upper and lower bounds of the one-dimensional form of the Fickian model

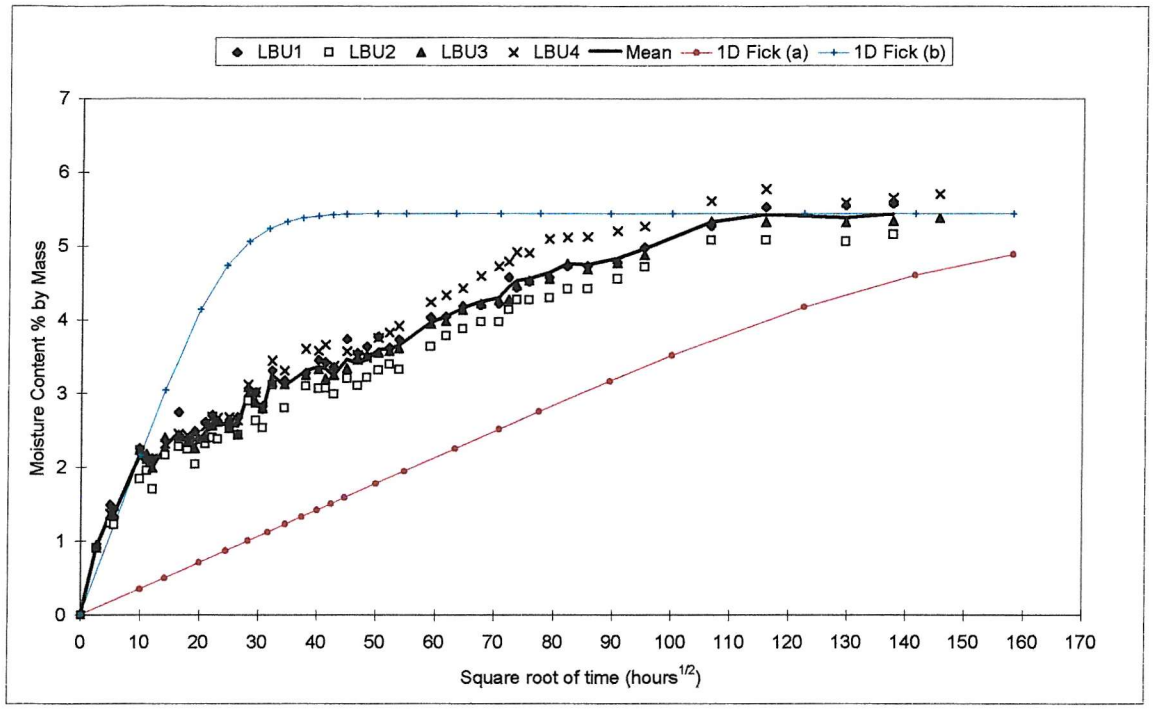

Figure 7.11: QE1200 moisture uptake results with upper and lower bounds of one-dimensional Fickian model

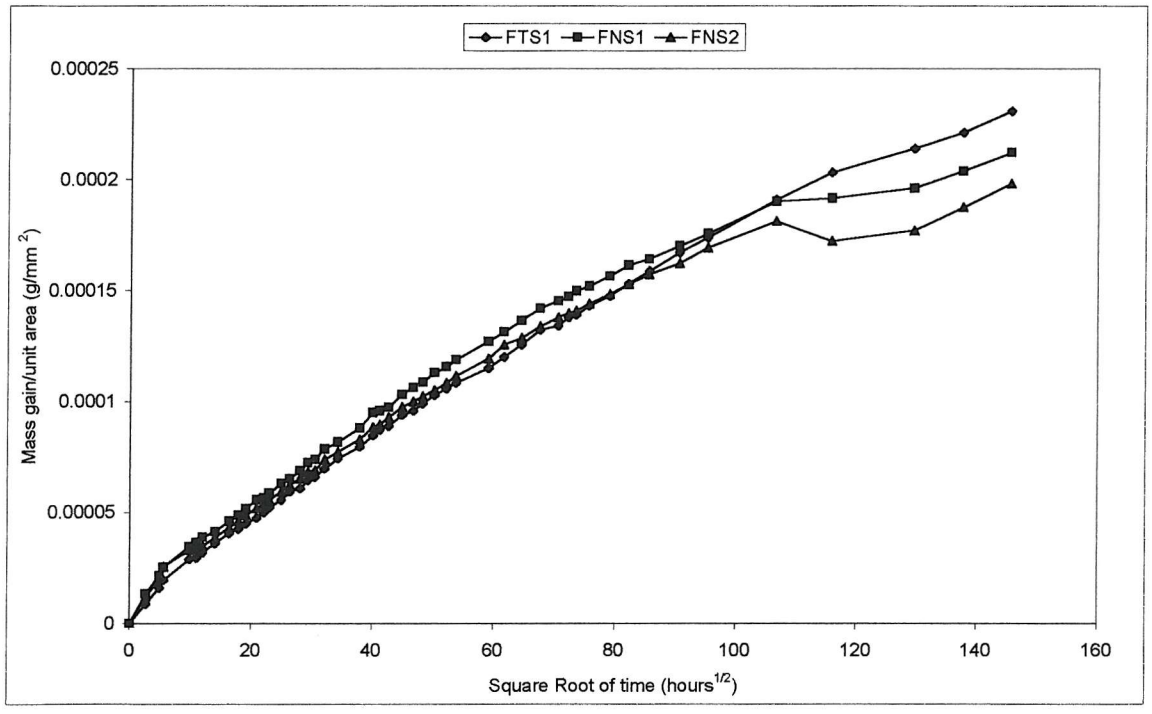

Figure 7.12: Sealed foam absolute mass gain/unit area

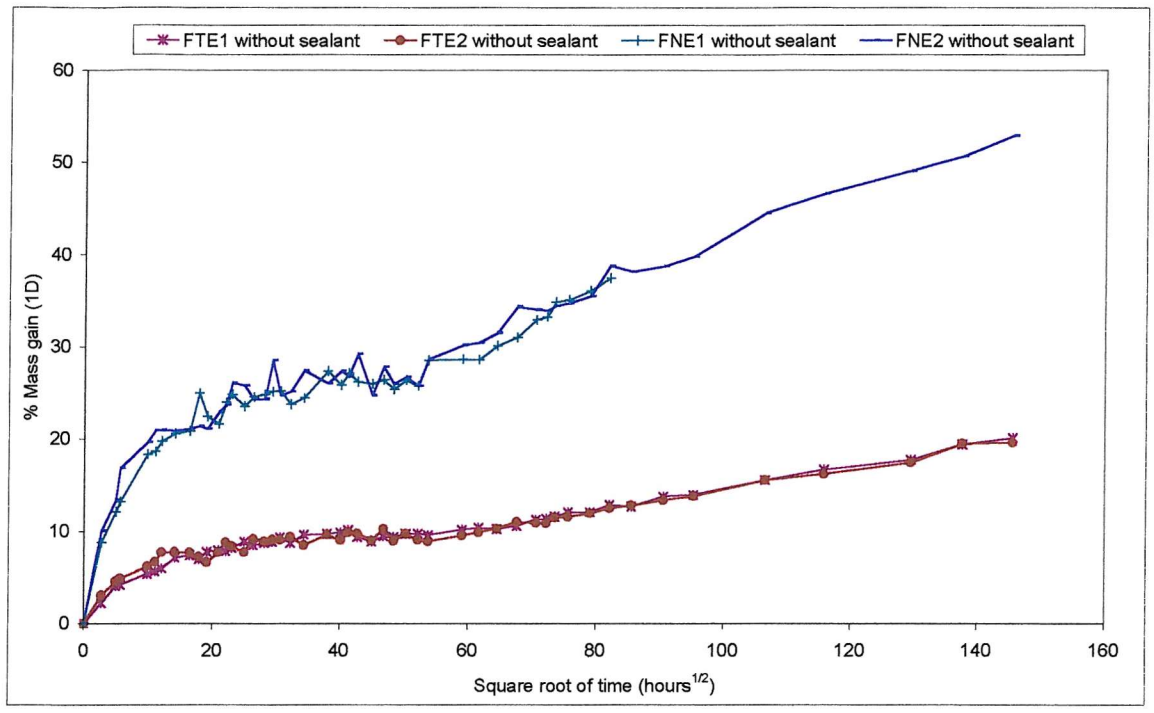

Figure 7.13: Edge-sealed foam % mass gain, without sealant mass and mass of moisture taken up by sealant (i.e. one-dimensional moisture uptake condition, but including moisture uptake into open cells on two faces)

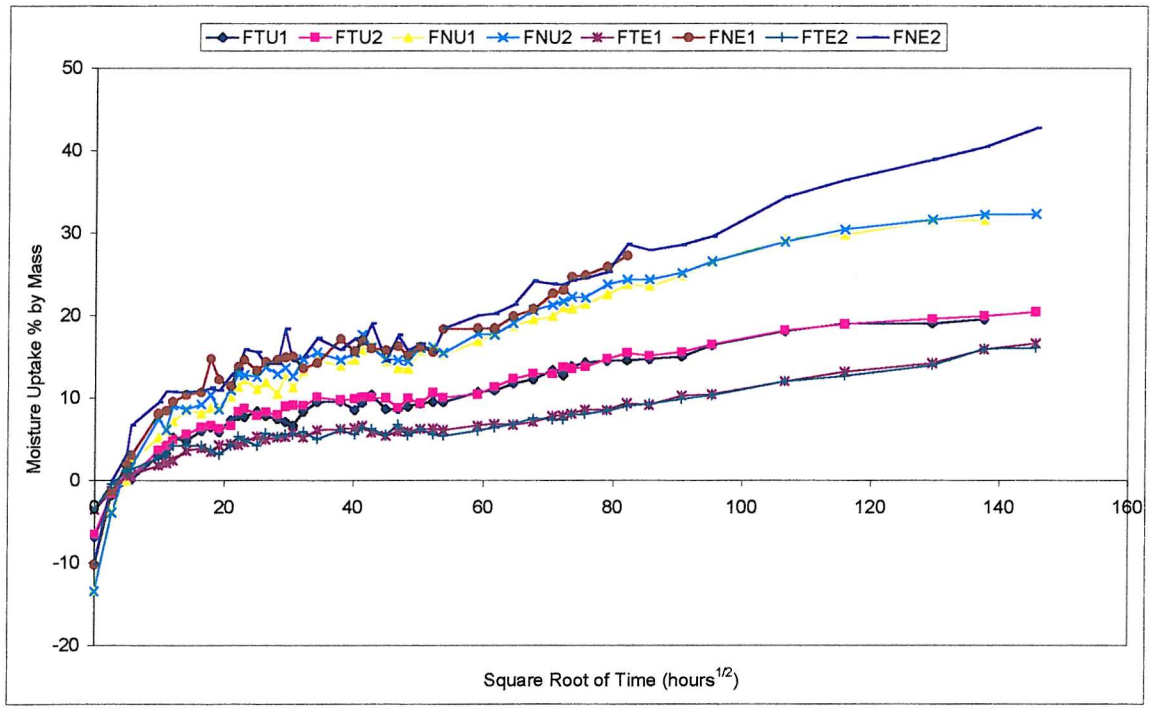

Figure 7.14: Thick (FT) and thin (FN) foam moisture uptake including three-dimensional case with moisture in open cells on cut surfaces removed (U1, U2) and one-dimensional case with moisture in sealant and open cells removed and excluding mass of dry sealant (E1, E2), i.e. the true one-dimensional condition

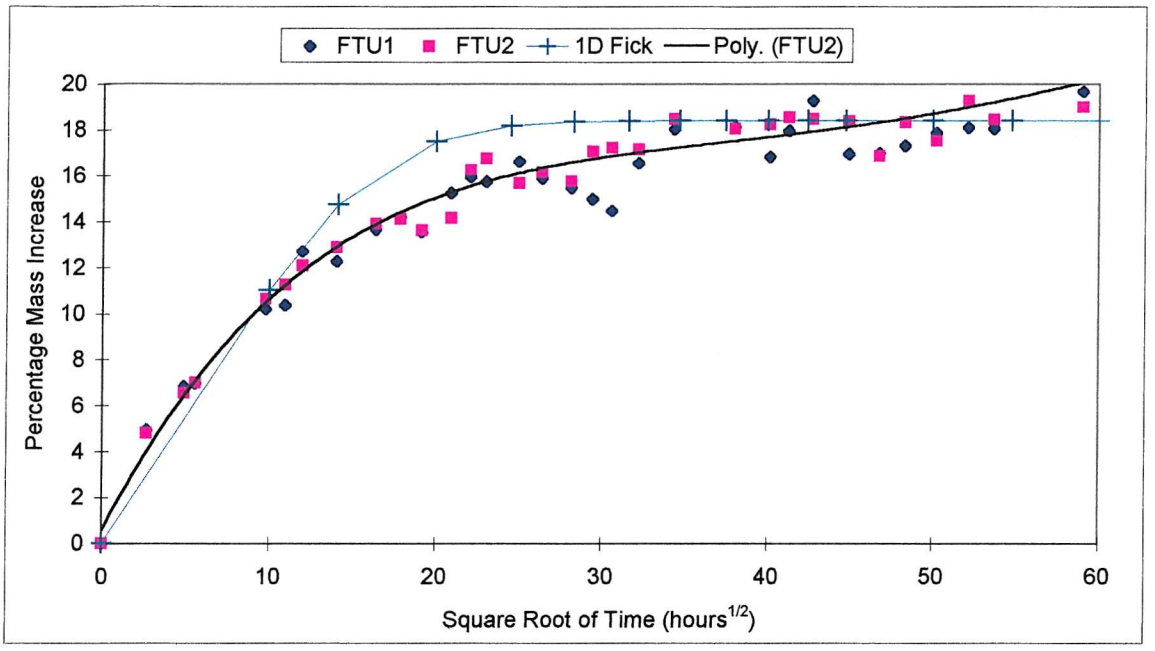

Figure 7.15: One-dimensional Fickian model for initial part of thick foam 3D uptake curve

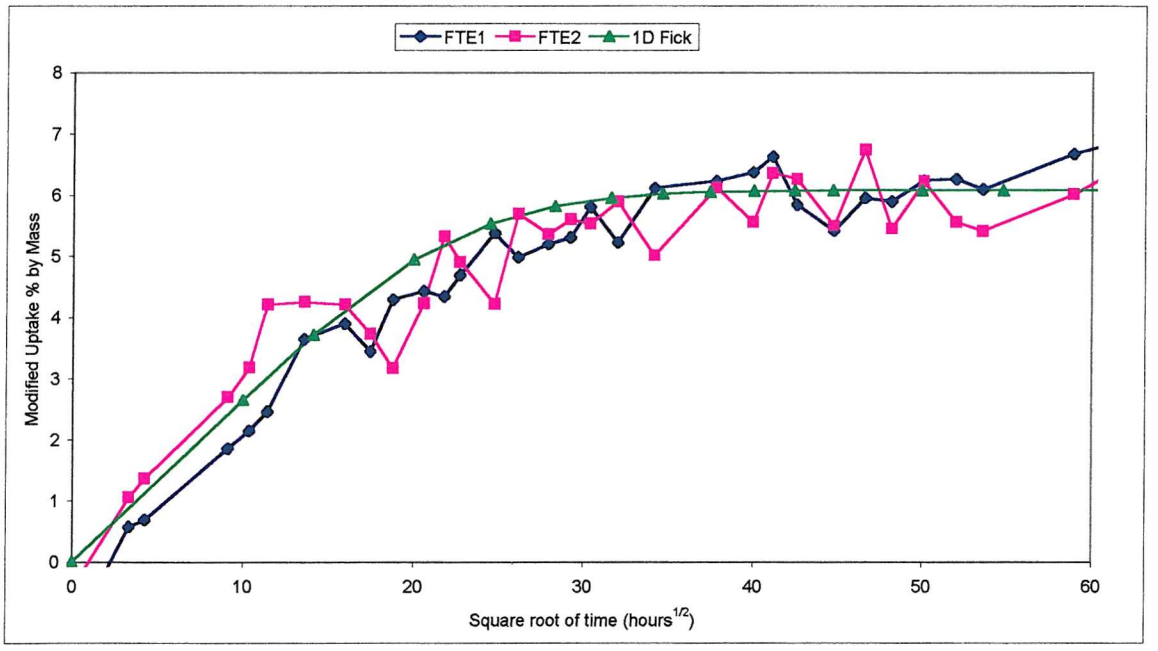

Figure 7.16: Thick foam approximation to one-dimensional uptake with fit of one-dimensional Fickian model

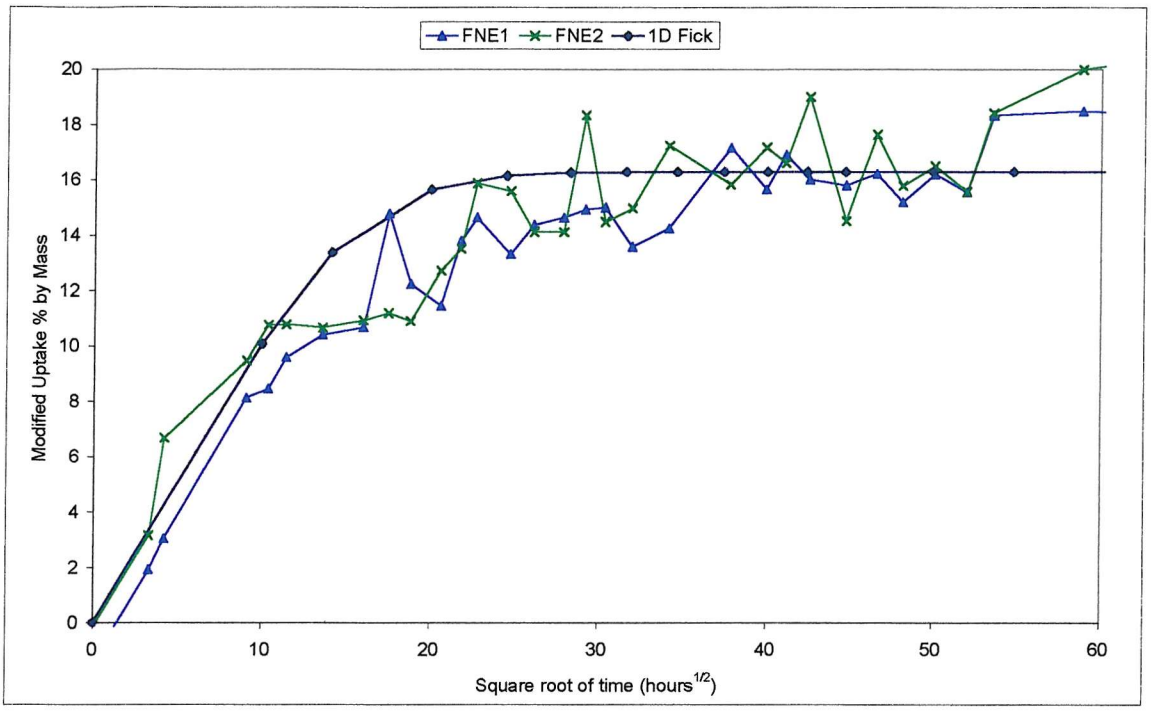

Figure 7.17: Thin foam approximation to one-dimensional uptake with fit of one-dimensional Fickian model

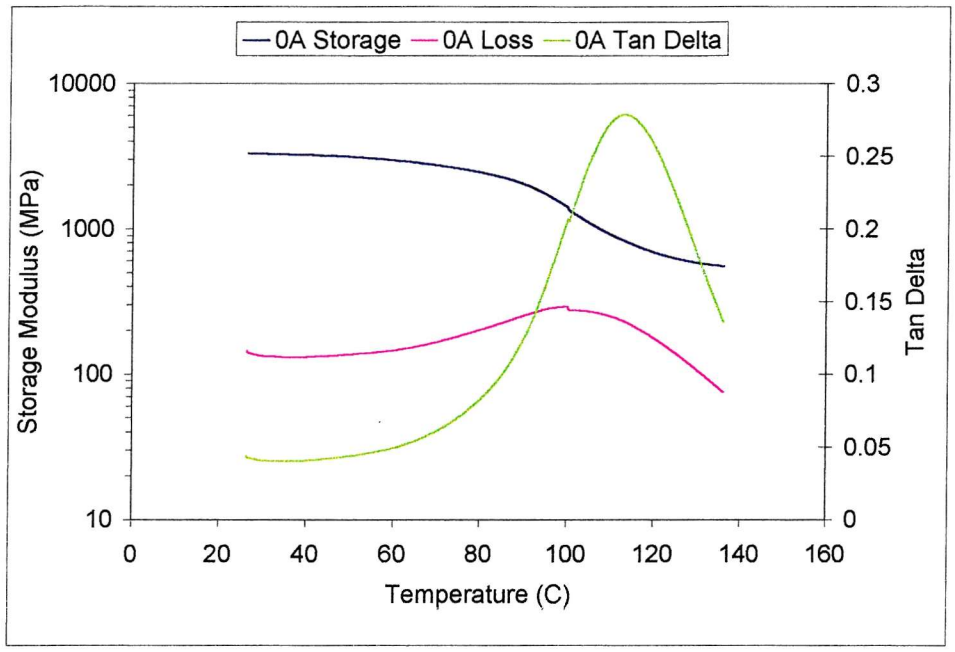

Figure 8.1: QEA1200 – Example of Unaged Results from Specimen 0A

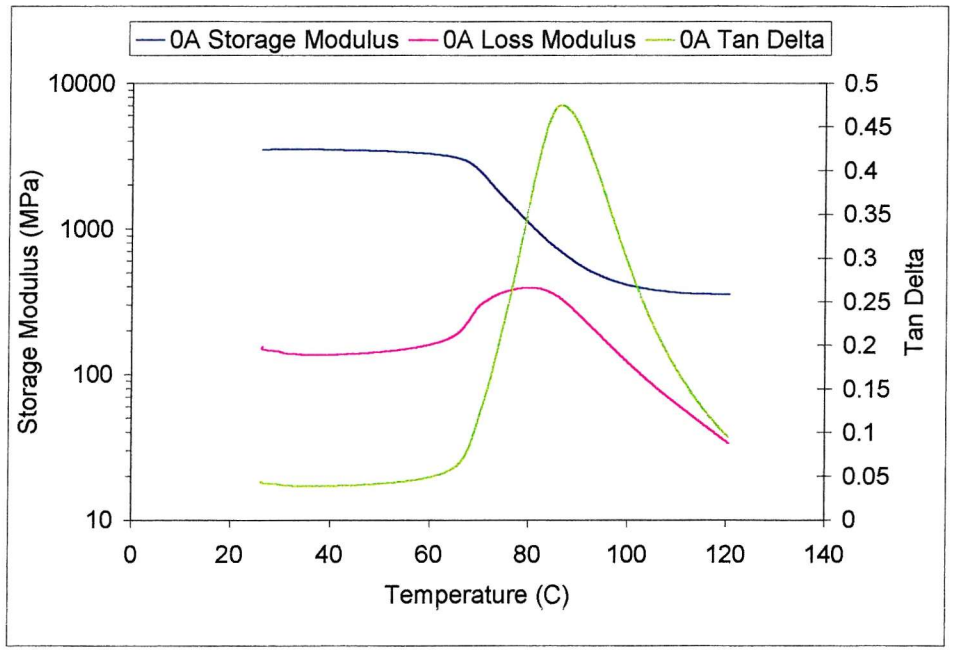

Figure 8.2: QE1200 – Example of Unaged Results from Specimen 0A

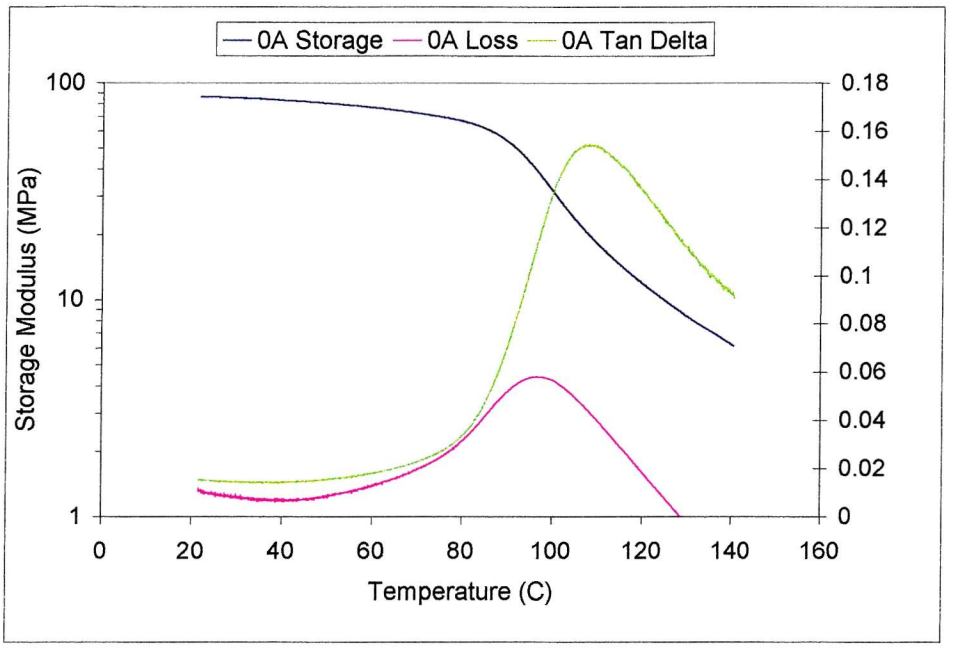

Figure 8.3: H130 – Example of Unaged Results from Specimen 0A

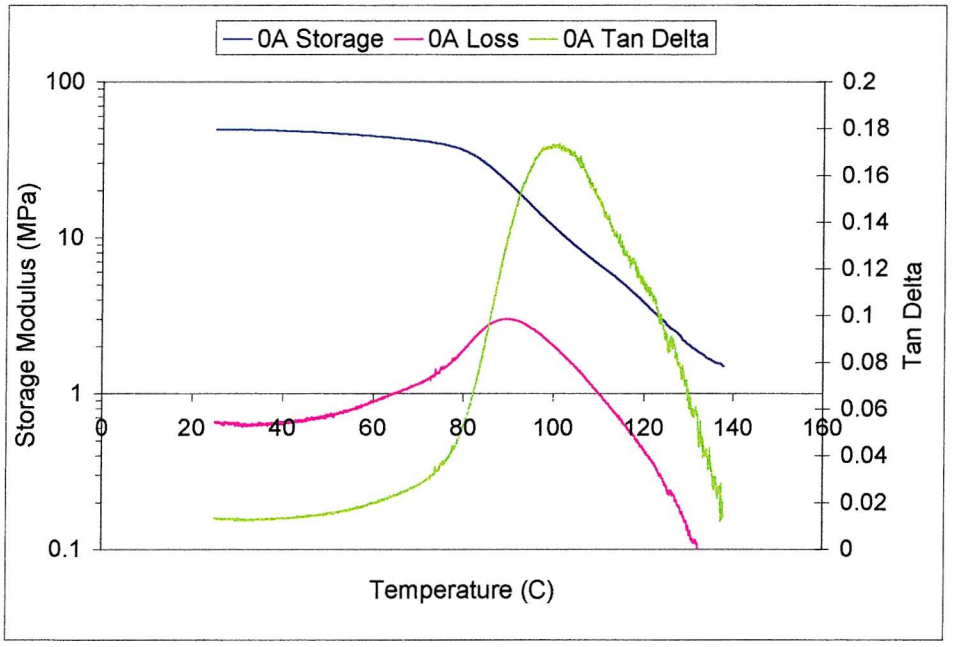

Figure 8.4: H80 – Example of Unaged Results from Specimen 0A

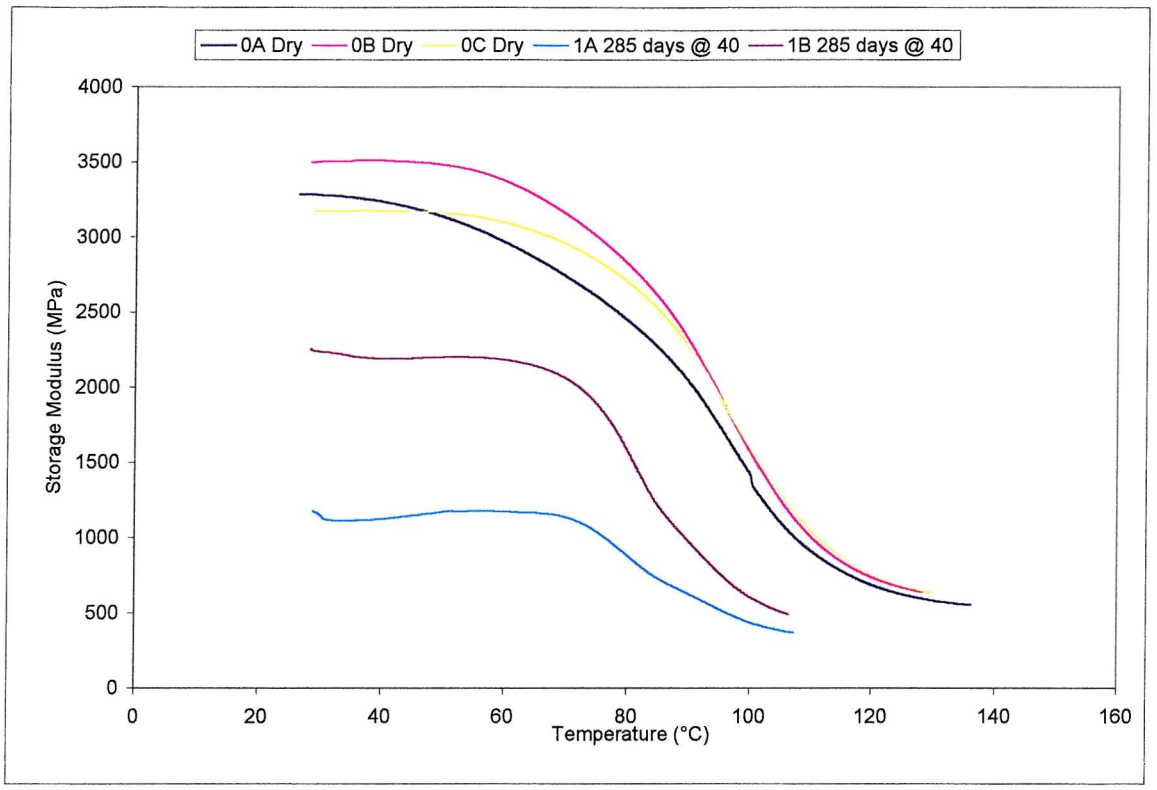

Figure 8.5 (a): Storage Modulus Results of QEA1200 Material Unaged and Aged at 40℃

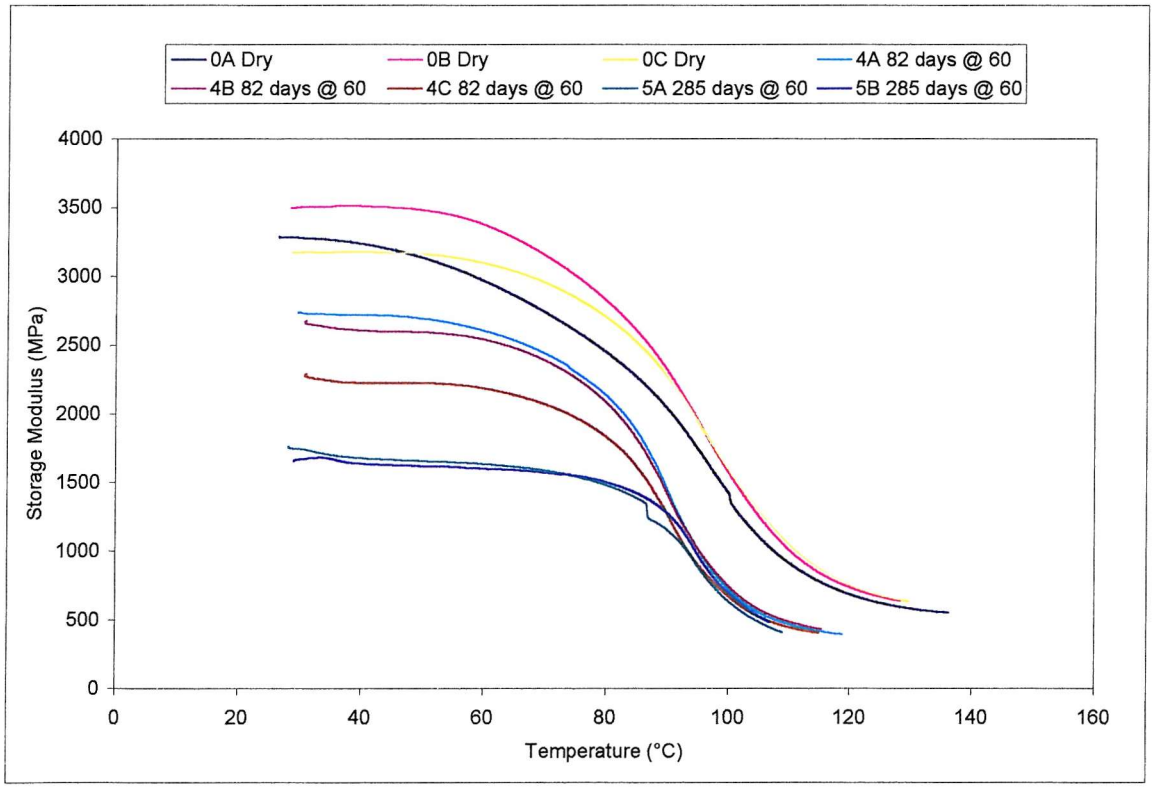

Figure 8.5 (b): Storage Modulus Results of QEA1200 Material Unaged and Aged at 60℃

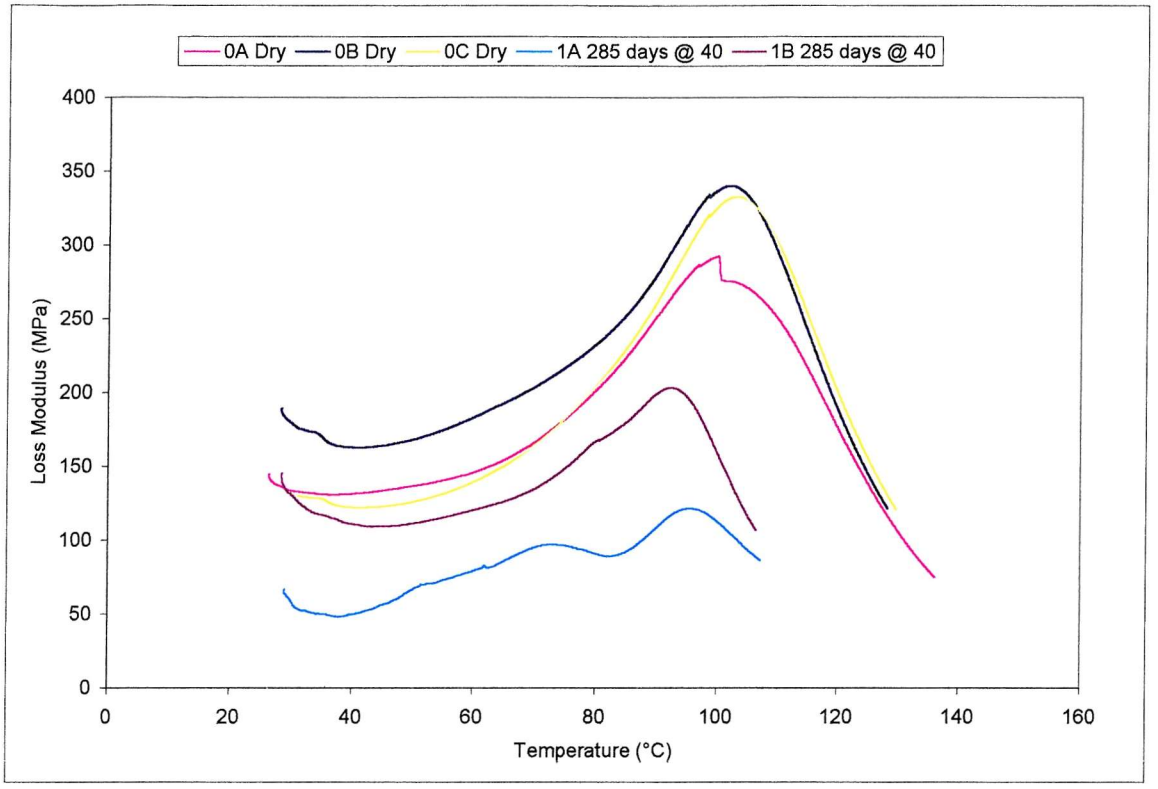

Figure 8.6 (a): Loss Modulus Results of QEA1200 Material Unaged and Aged at 40 ℃

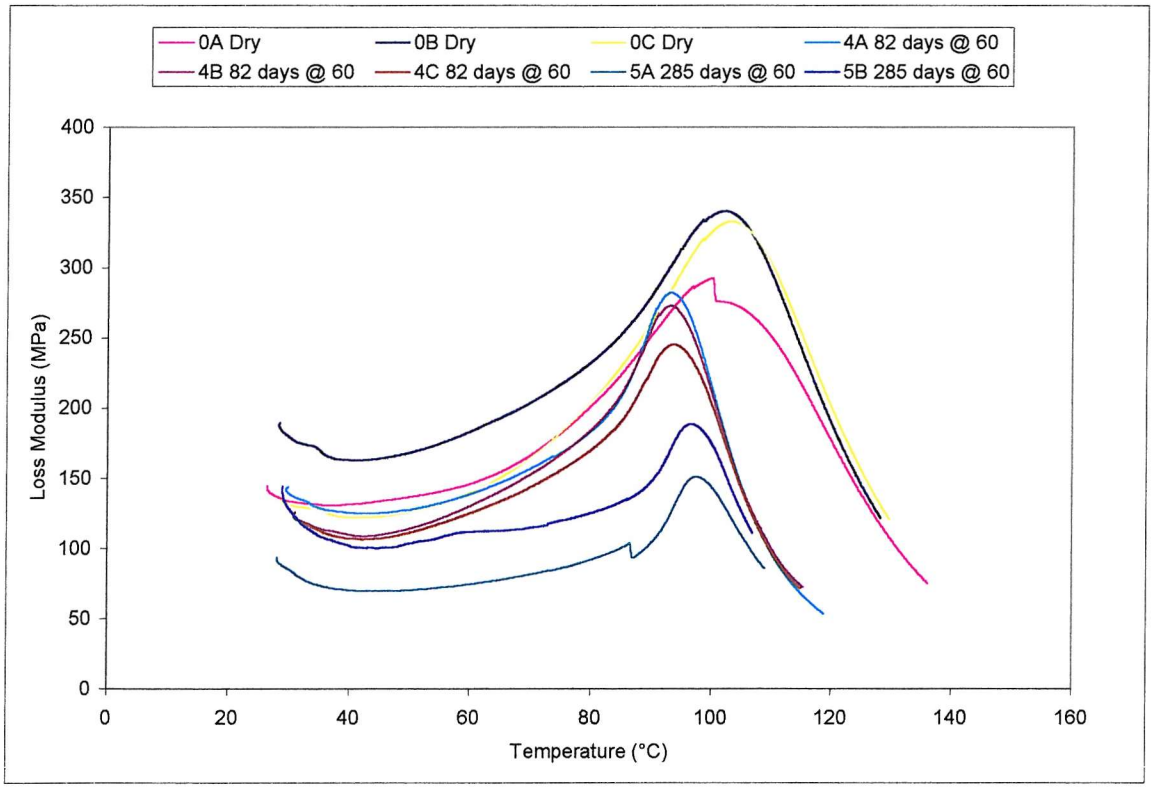

Figure 8.6 (b): Loss Modulus Results of QEA1200 Material Unaged and Aged at 60 ℃

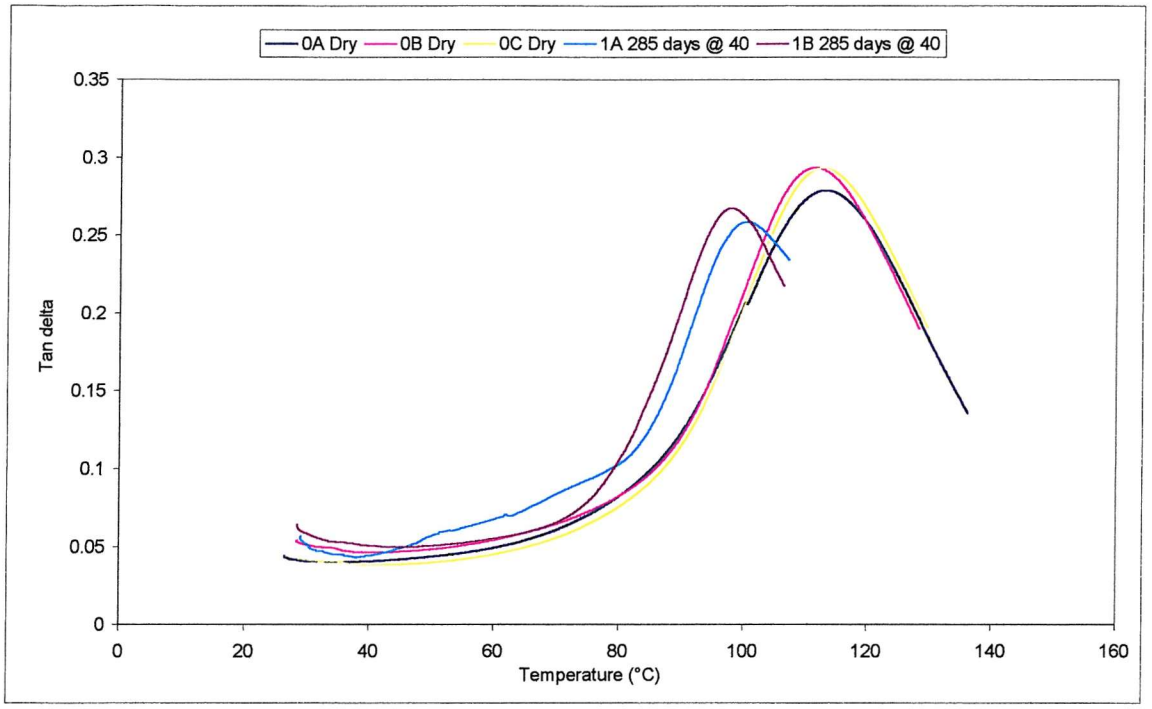

Figure 8.7 (a): Tan δ Results of QEA1200 Material Unaged and Aged at 40 ℃

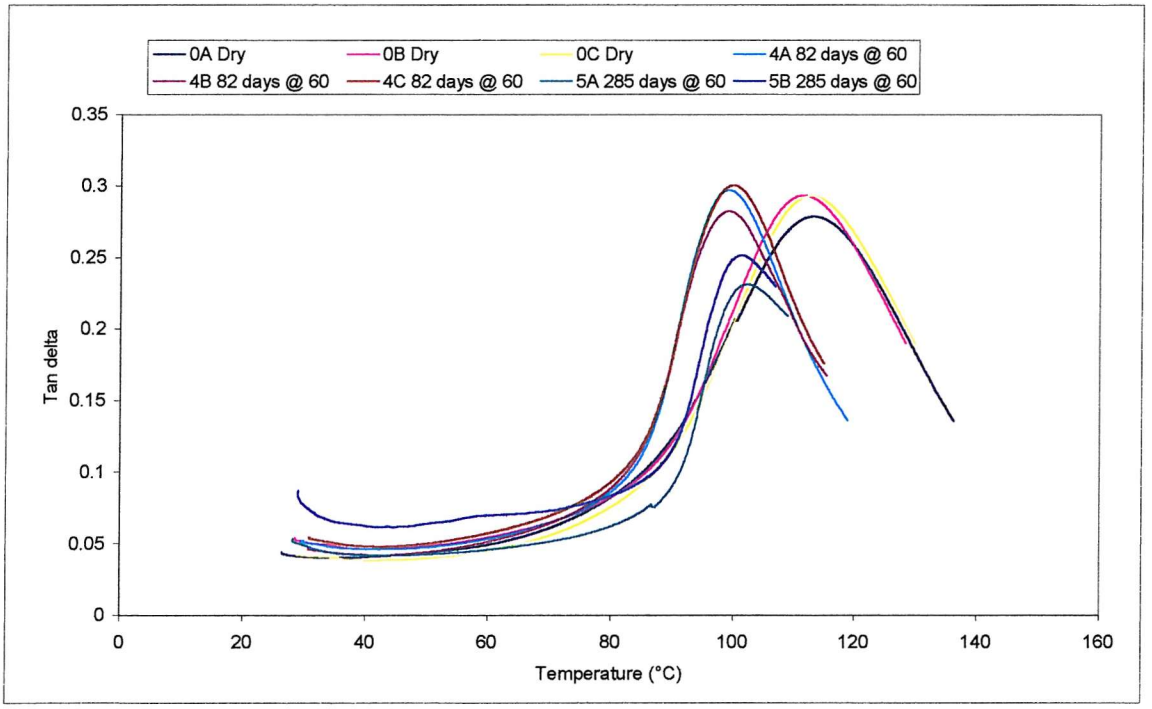

Figure 8.7 (b): Tan δ Results of QEA1200 Material Unaged and Aged at 60 ℃

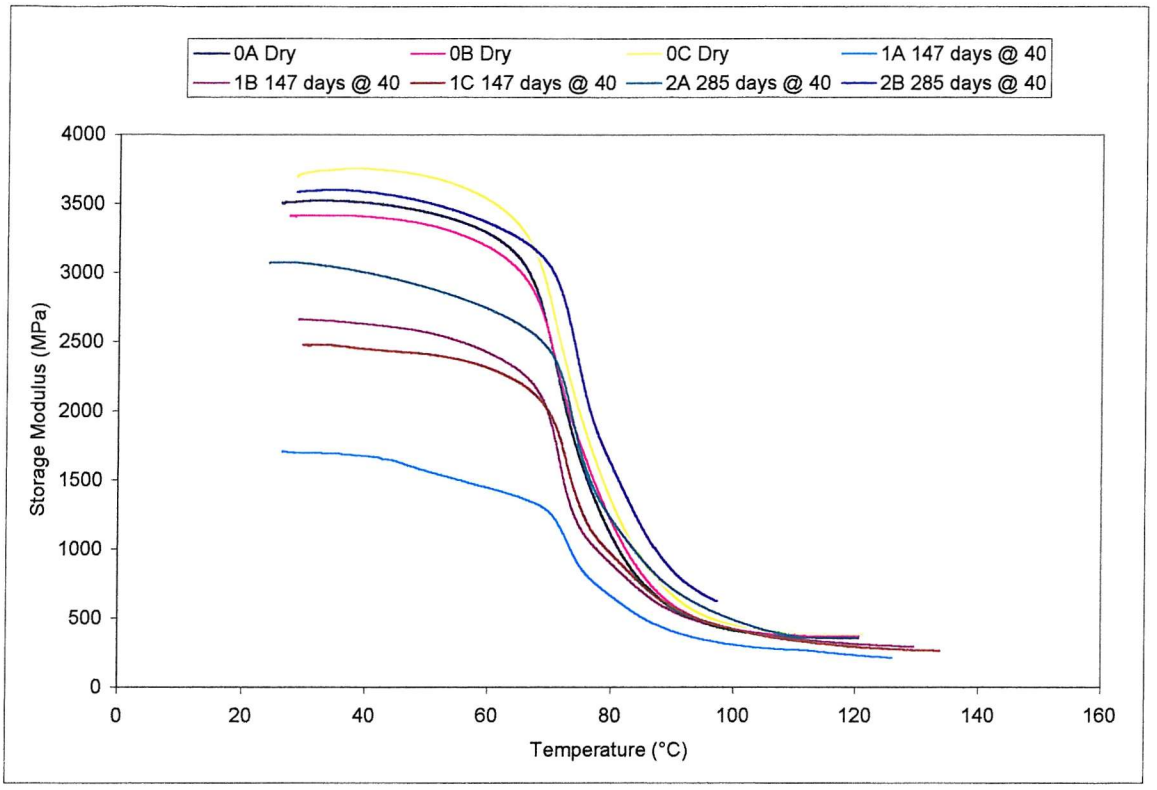

Figure 8.8 (a): Storage Modulus Results of QE1200 Material Unaged and Aged at 40 ℃

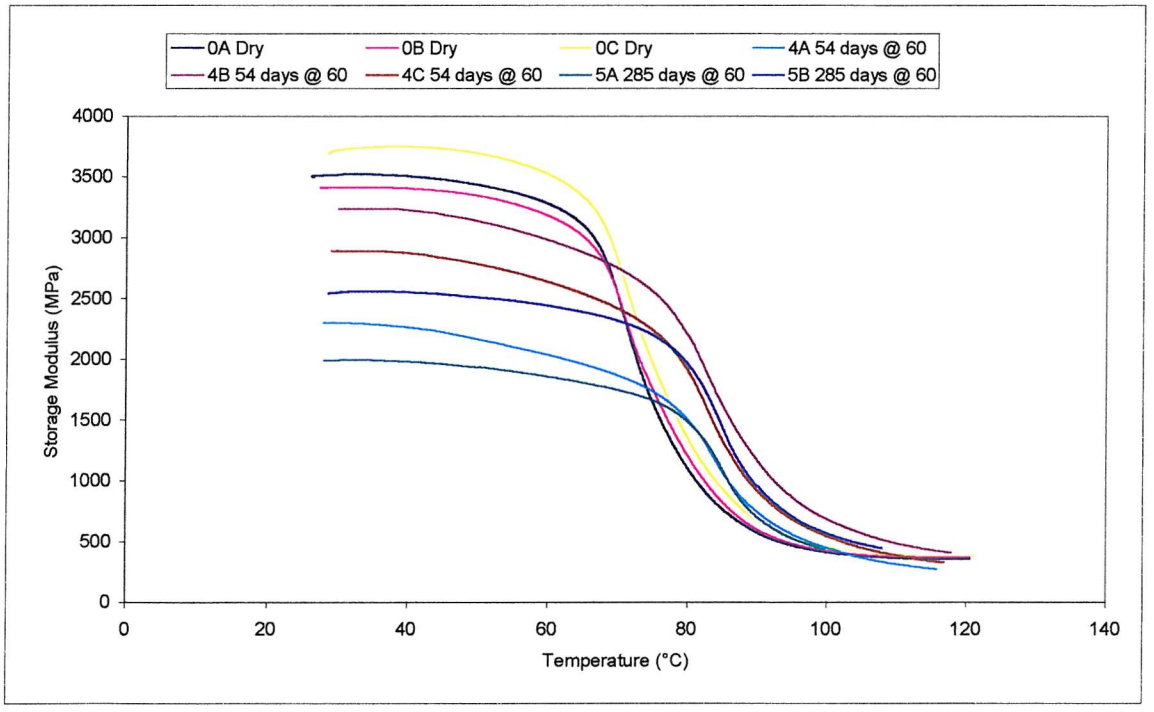

Figure 8.8 (b): Storage Modulus Results of QE1200 Material Unaged and Aged at 60 ℃

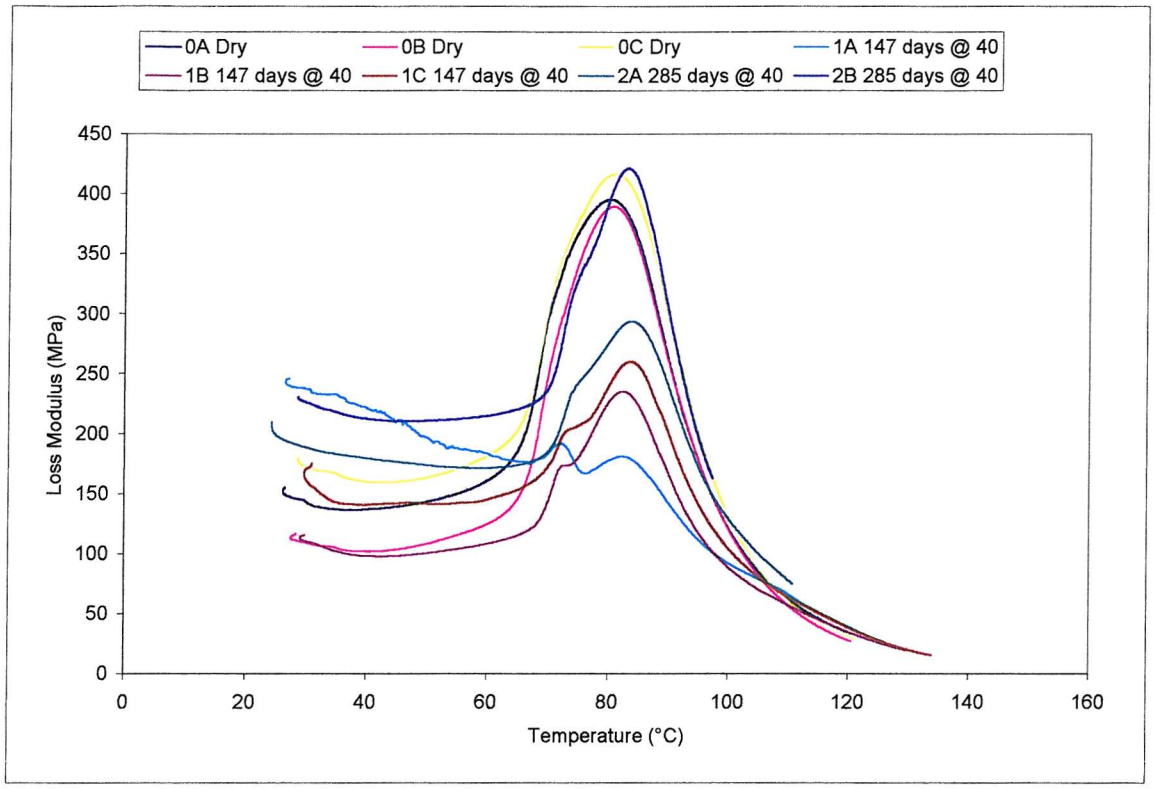

Figure 8.9 (a): Loss Modulus Results of QE1200 Material Unaged and Aged at 40 ℃

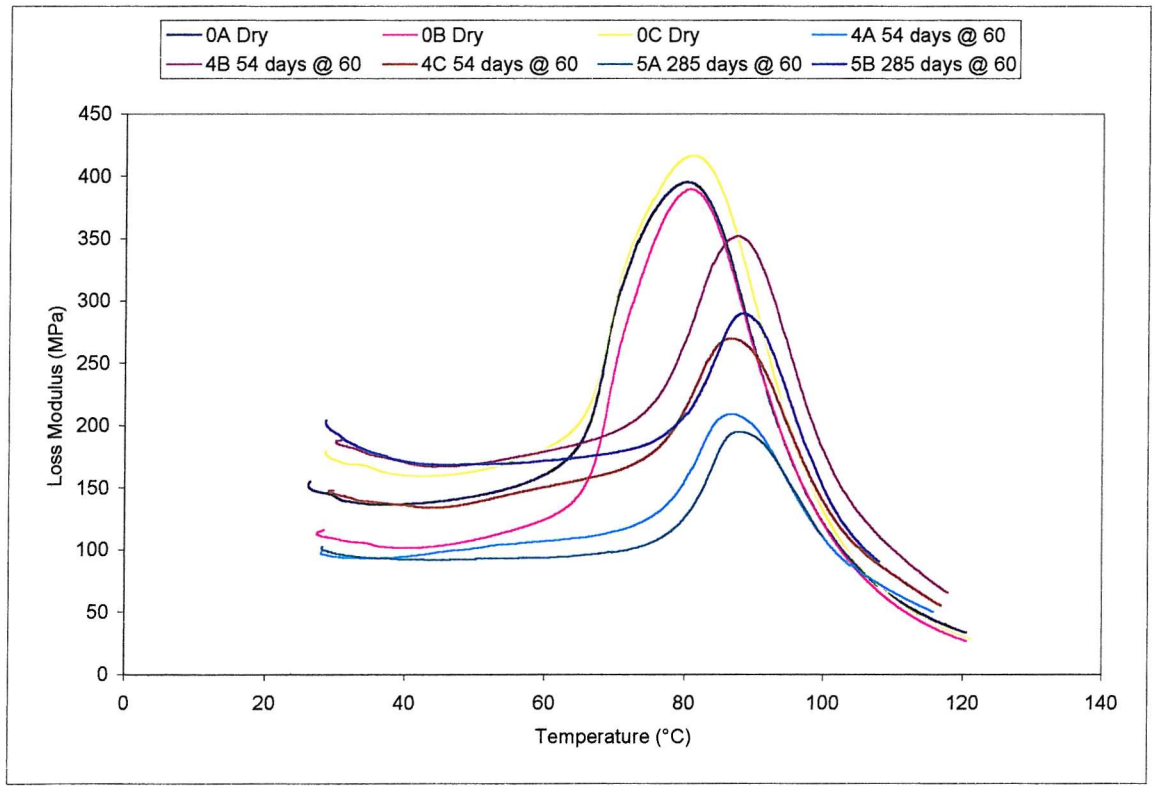

Figure 8.9 (b): Loss Modulus Results of QE1200 Material Unaged and Aged at 60 ℃

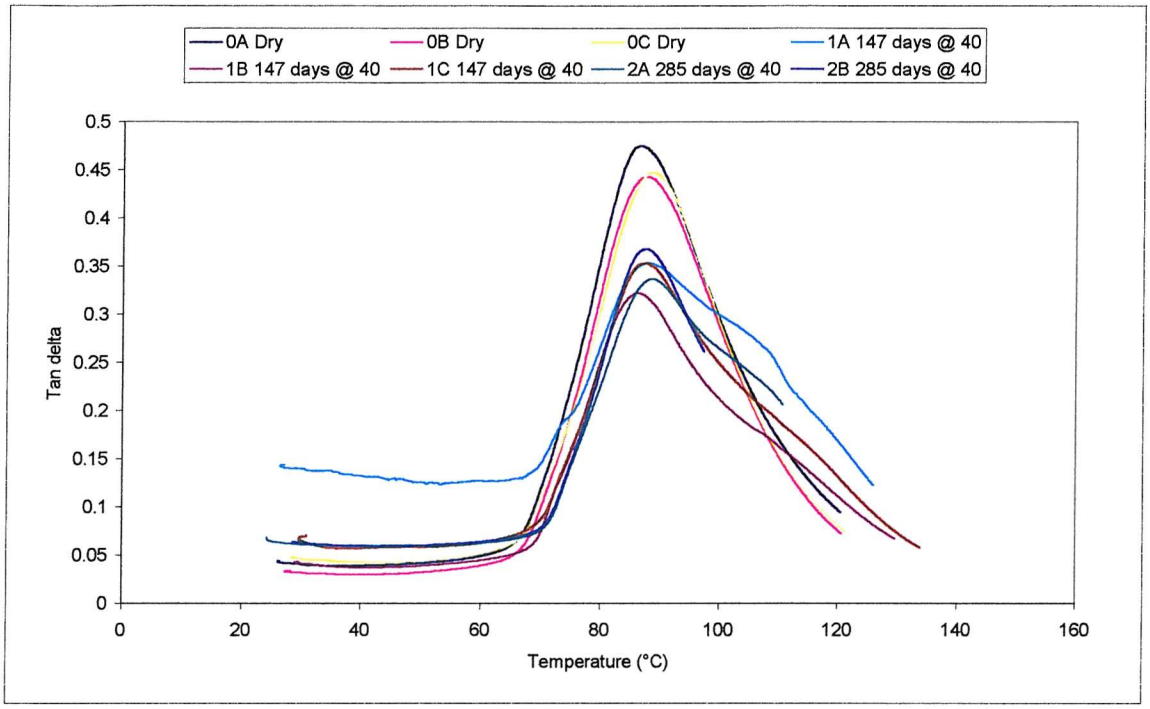

Figure 8.10 (a): Tan δ Results of QE1200 Material Unaged and Aged at 40℃

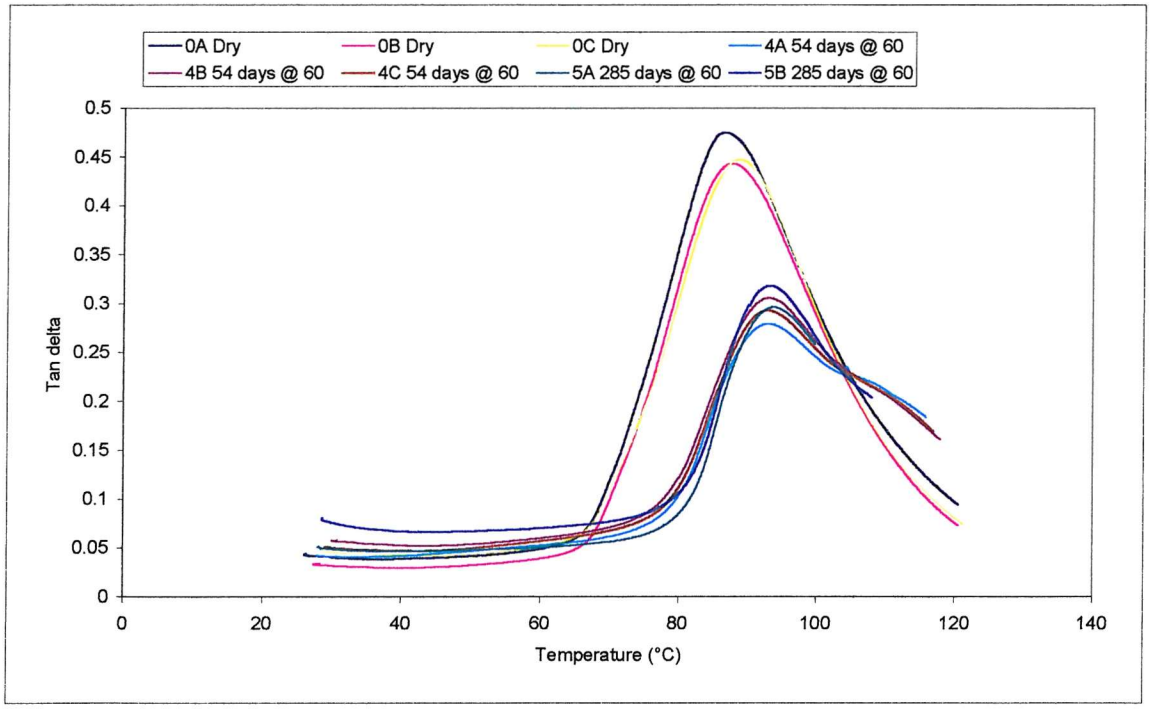

Figure 8.10 (b): Tan δ Results of QE1200 Material Unaged and Aged at 60℃

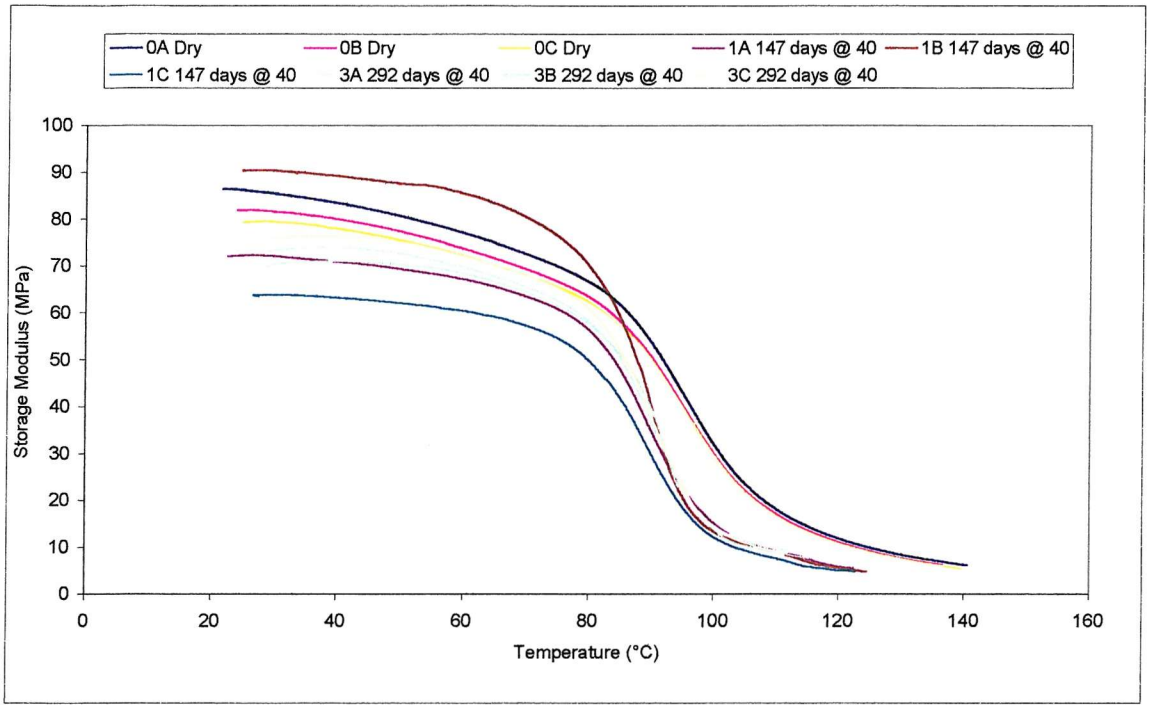

Figure 8.11 (a): Storage Modulus Results of H130 Material Unaged and Aged at 40 ℃

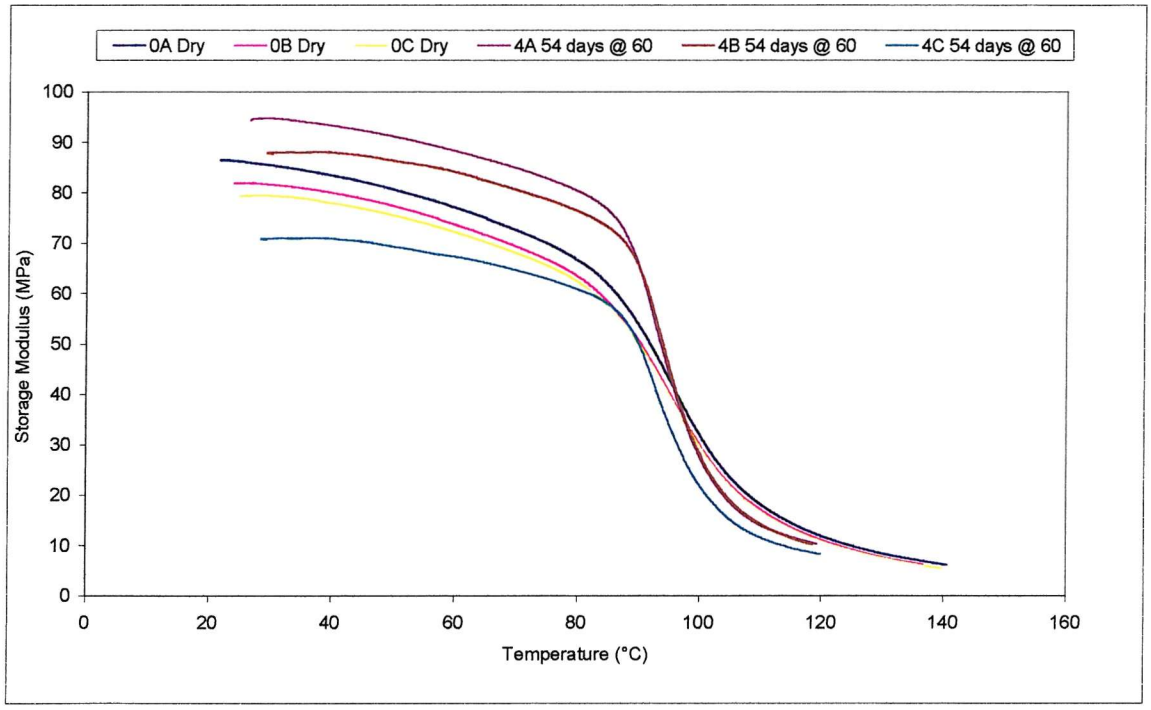

Figure 8.11 (b): Storage Modulus Results of H130 Material Unaged and Aged at 60 ℃

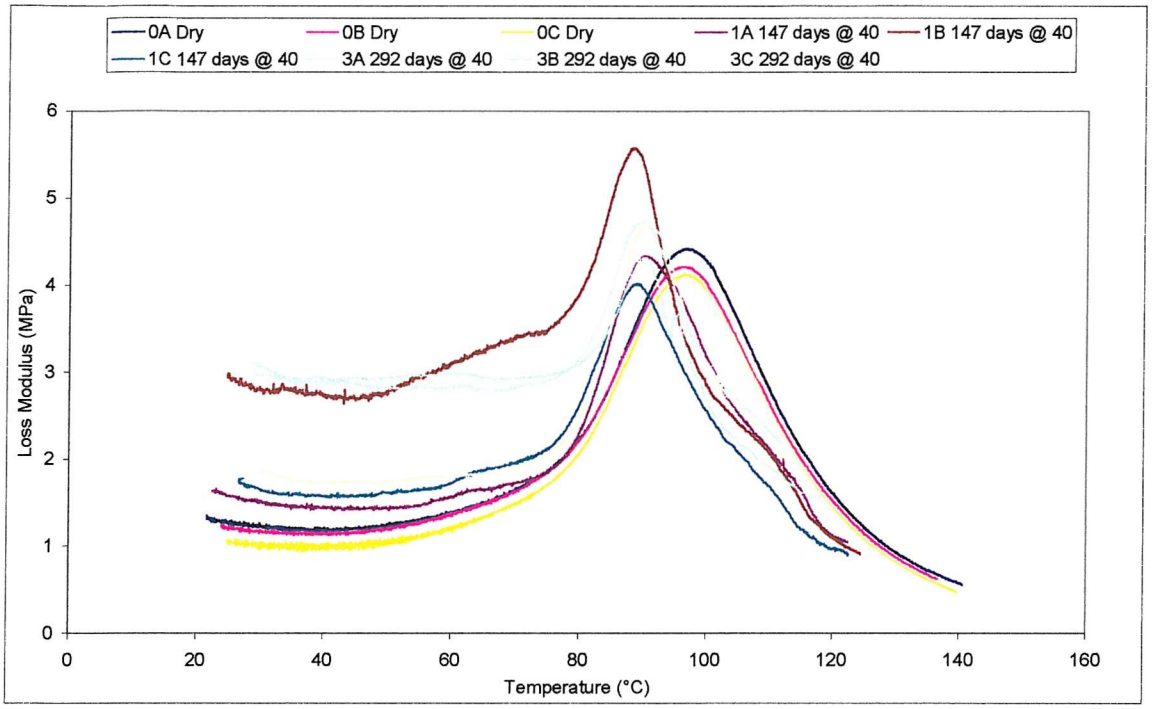

Figure 8.12 (a): Loss Modulus Results of H130 Material Unaged and Aged at 40 ℃

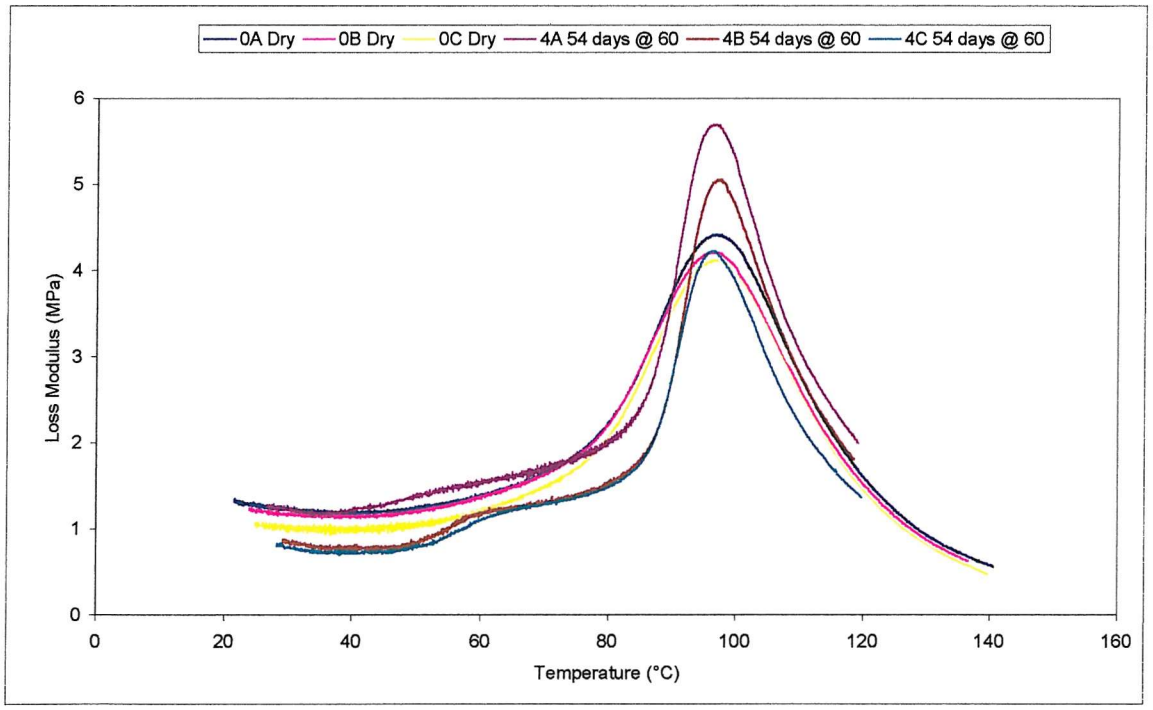

Figure 8.12 (b): Loss Modulus Results of H130 Material Unaged and Aged at 60 ℃

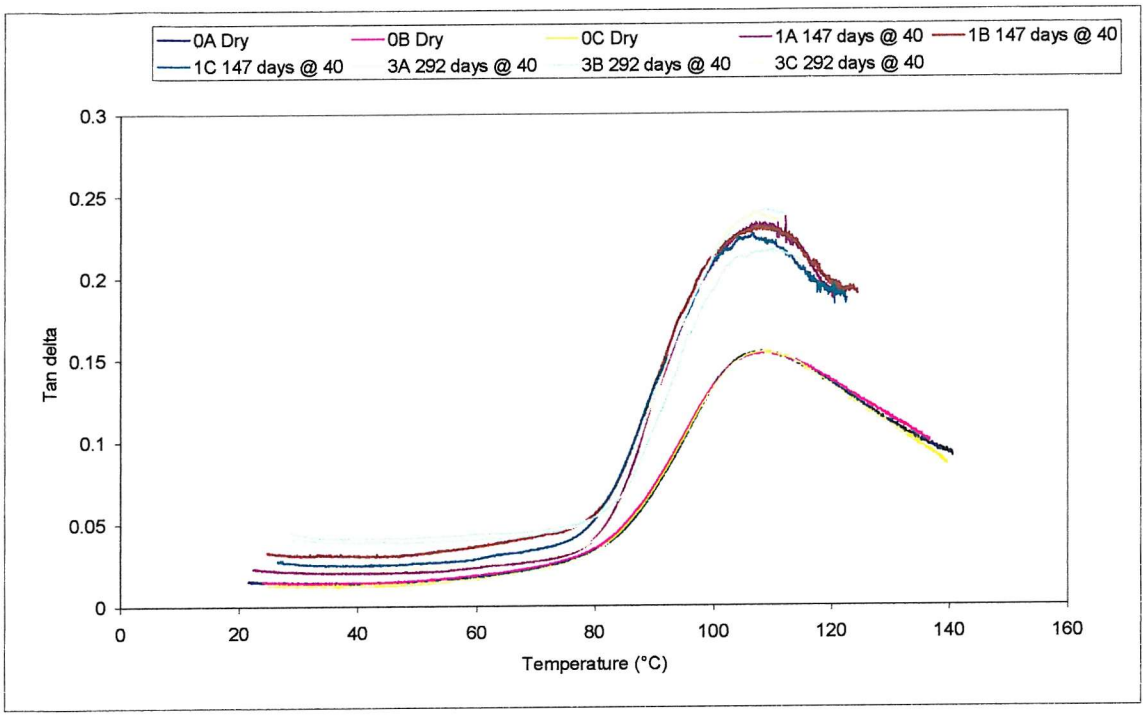

Figure 8.13 (a): Tan δ Results of H130 Material Unaged and Aged at 40℃

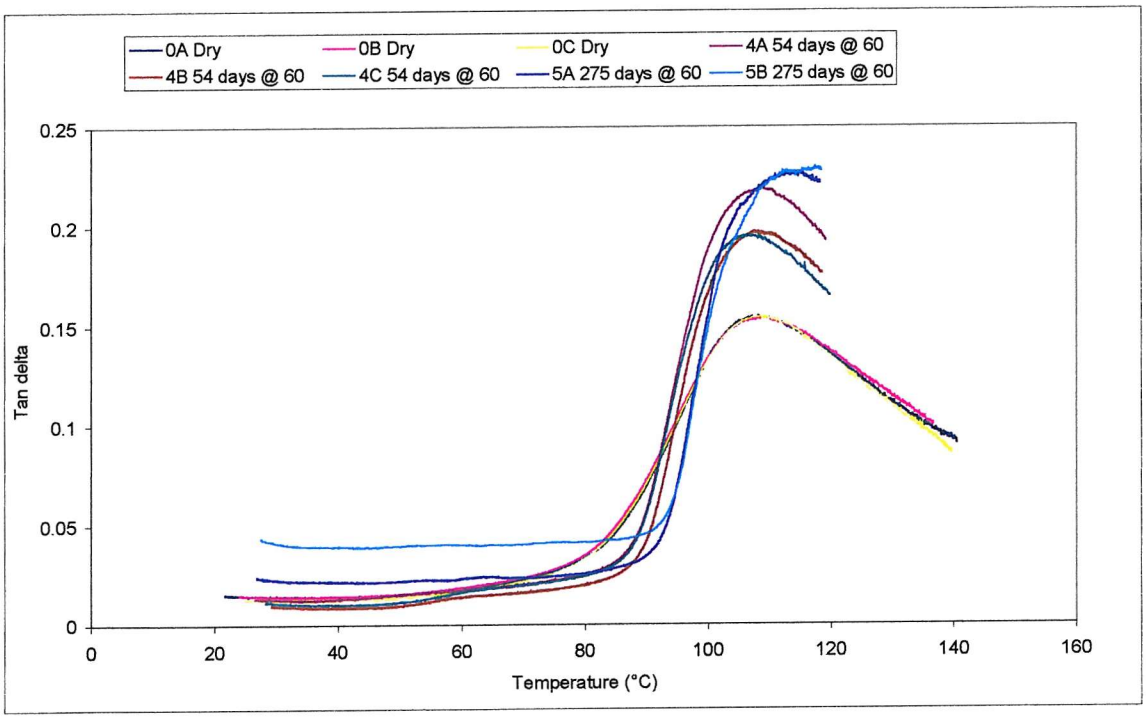

Figure 8.13 (b): Tan δ Results of H130 Material Unaged and Aged at 60℃

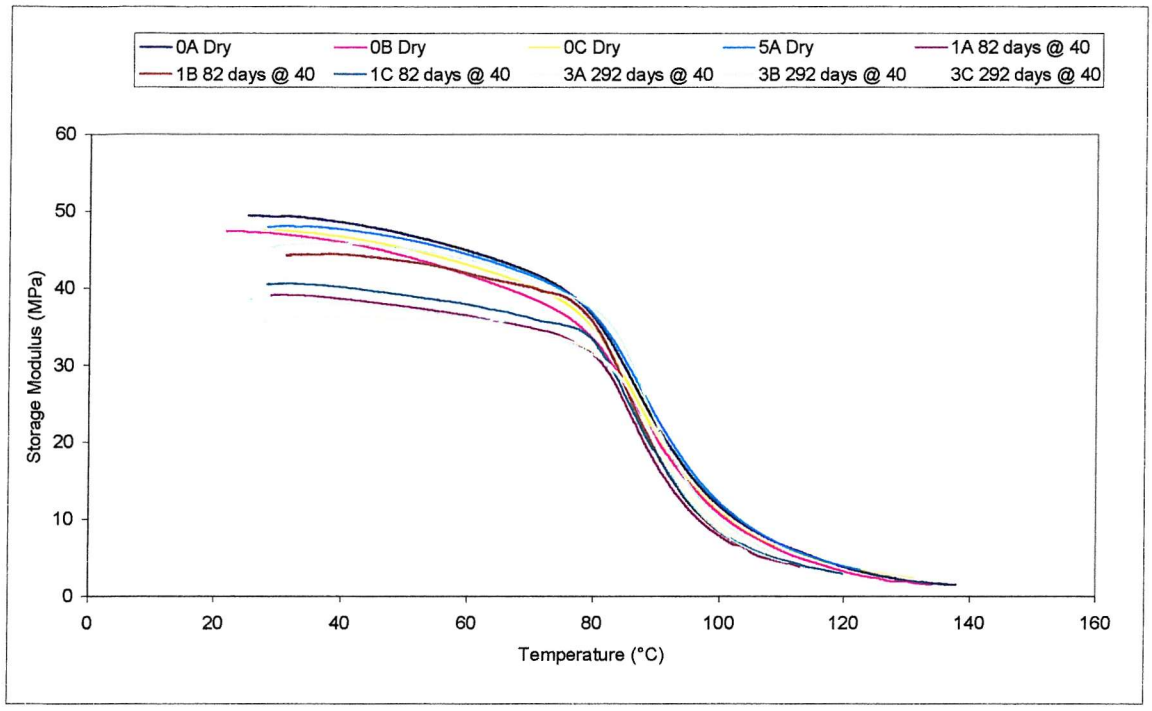

Figure 8.14 (a): Storage Modulus Results of H80 Material Unaged and Aged at 40 ℃

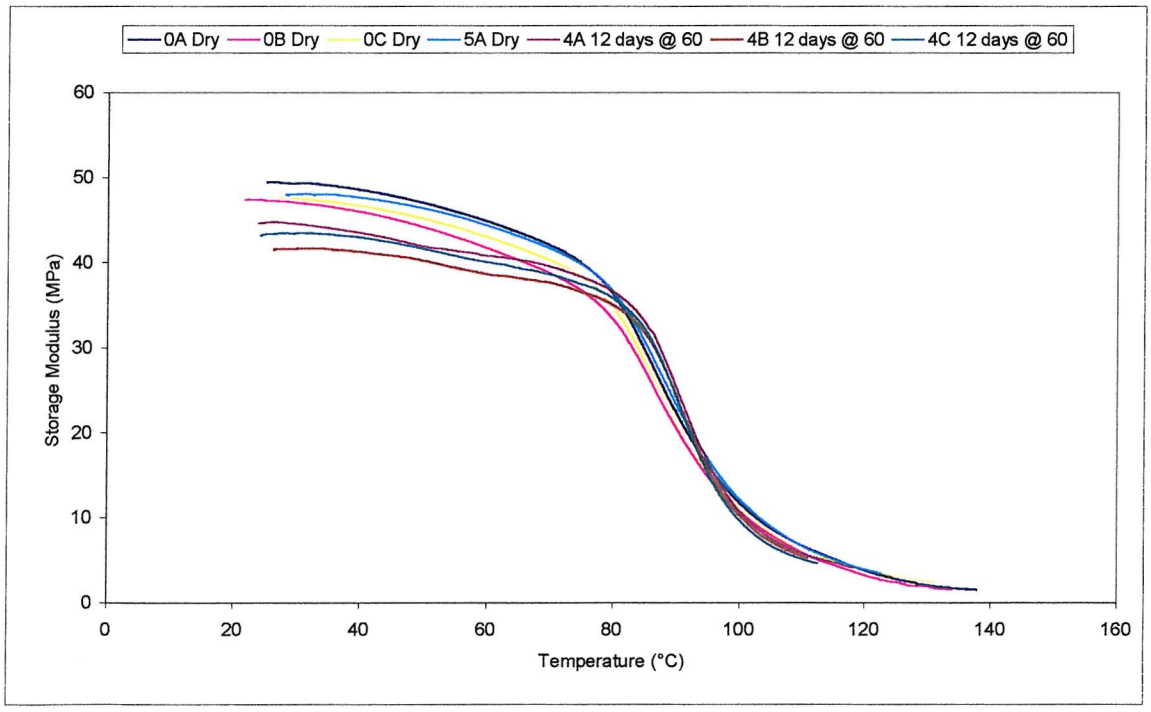

Figure 8.14 (b): Storage Modulus Results of H80 Material Unaged and Aged at 60 ℃

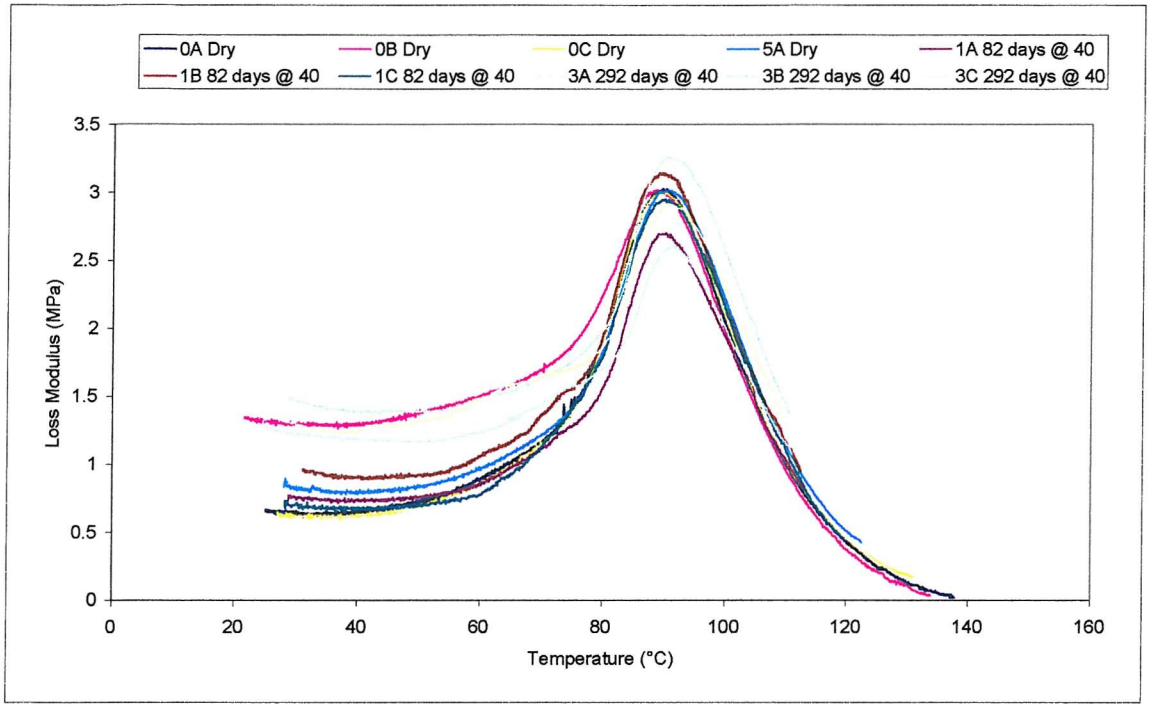

Figure 8.15 (a): Loss Modulus Results of H80 Material Unaged and Aged at 40℃

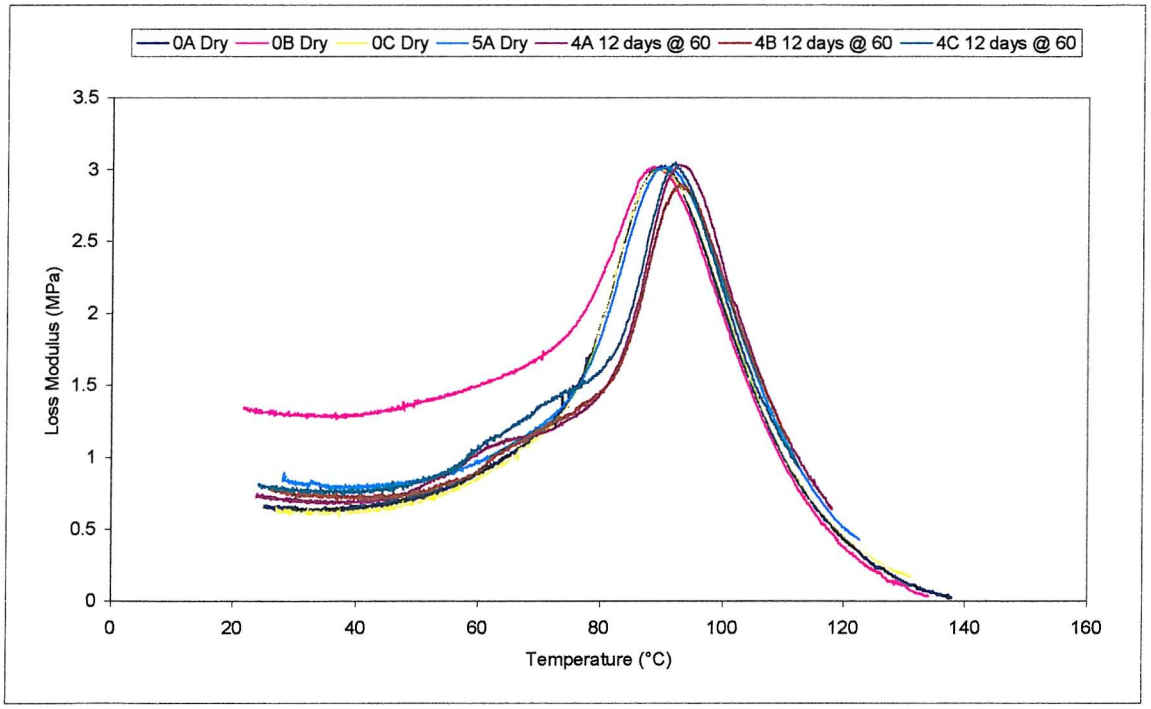

Figure 8.15 (b): Loss Modulus Results of H80 Material Unaged and Aged at 60℃

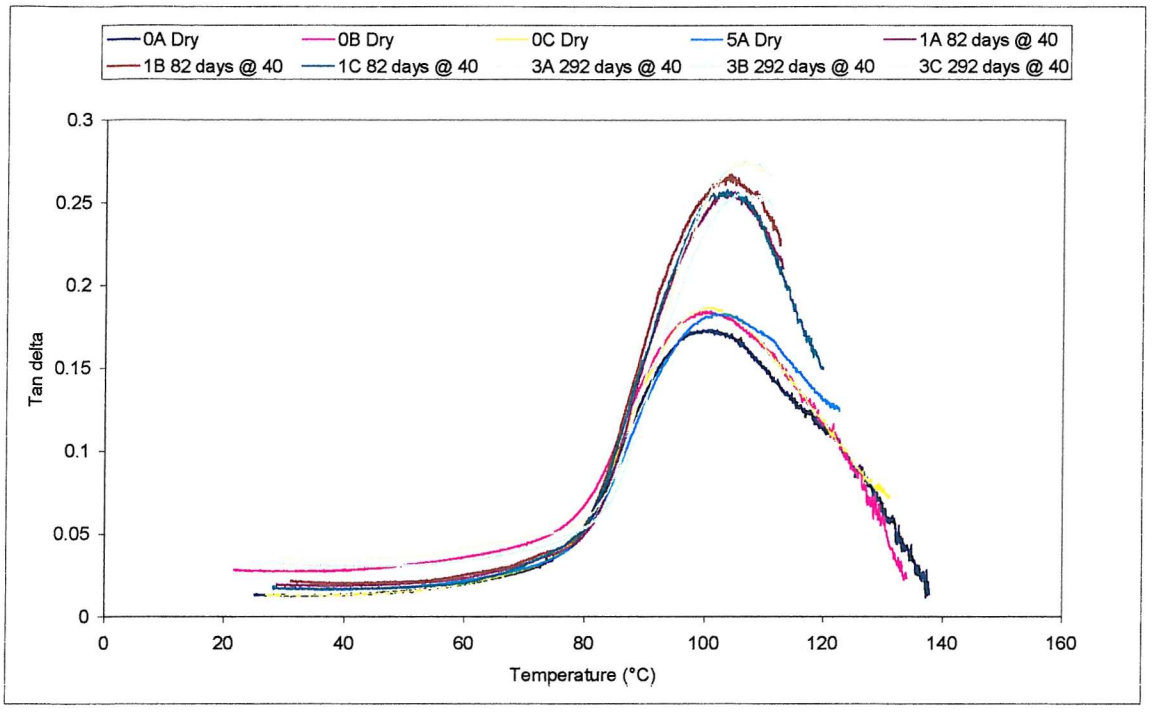

Figure 8.16 (a): Tan δ Results of H80 Material Unaged and Aged at 40 ℃

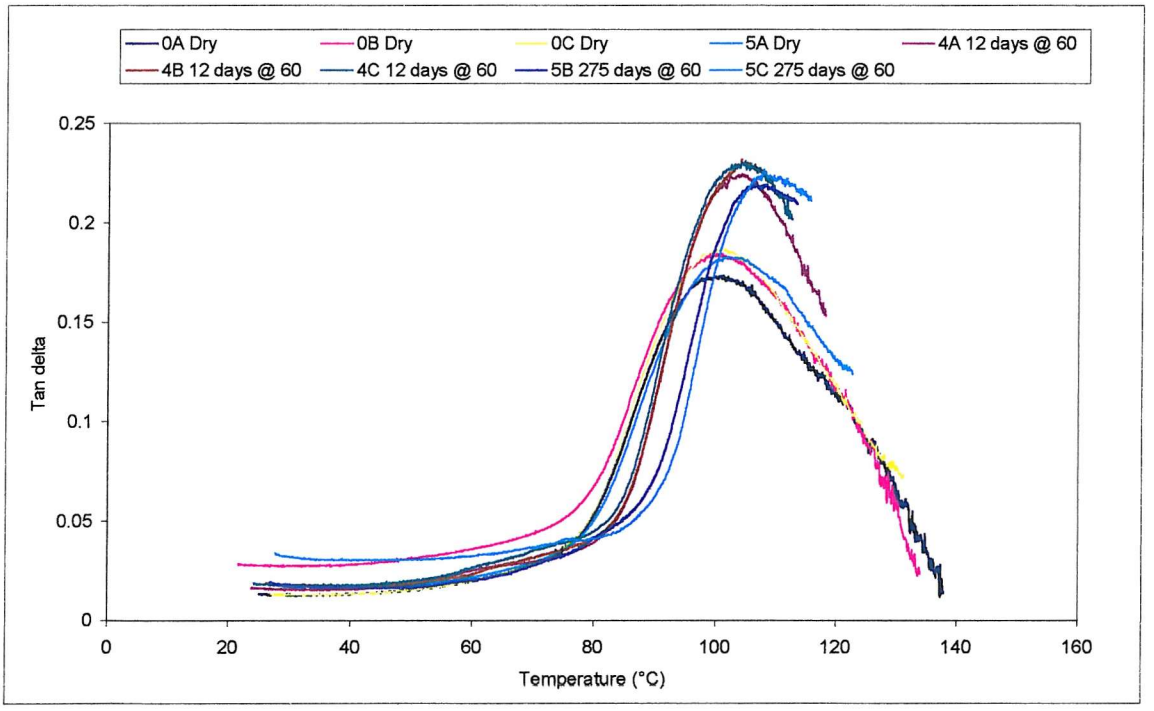

Figure 8.16 (b): Tan δ Results of H80 Material Unaged and Aged at 60 ℃

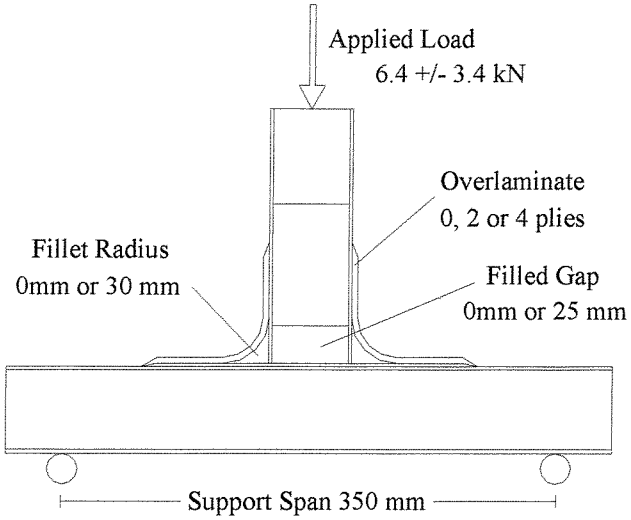

Figure 9.1: Schematic of Tee Joint Compression Load Set-up showing the Tested Geometry Parameters

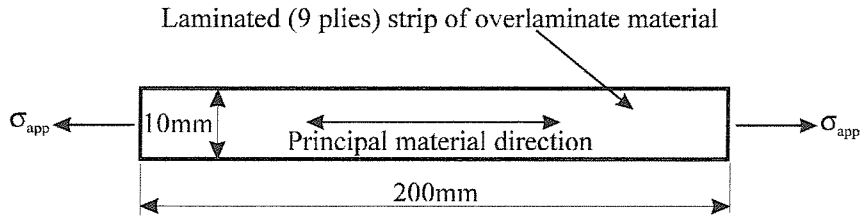

Figure 9.2: Schematic of Test Specimen Showing Mode of Loading for Laminate Material Calibration

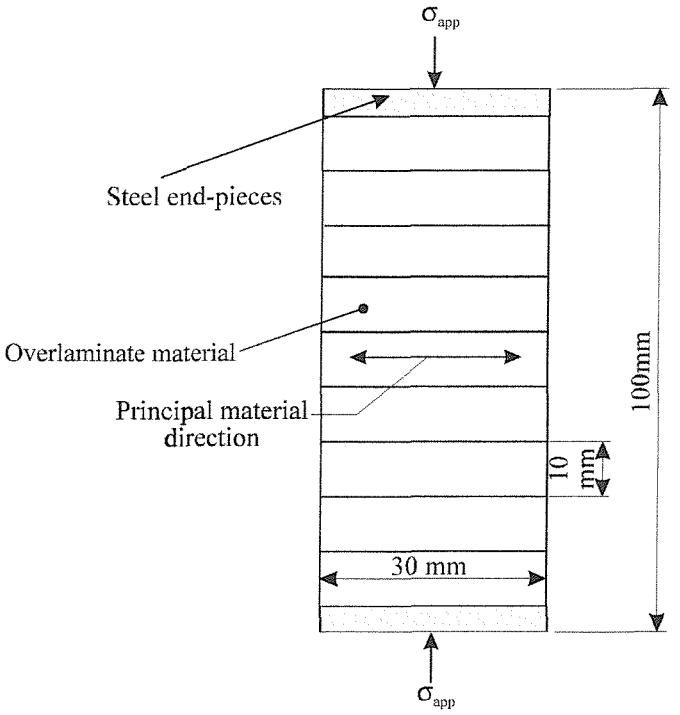

Figure 9.3: Schematic of Laminate 'Tower Block' Specimen for Determination of α^*

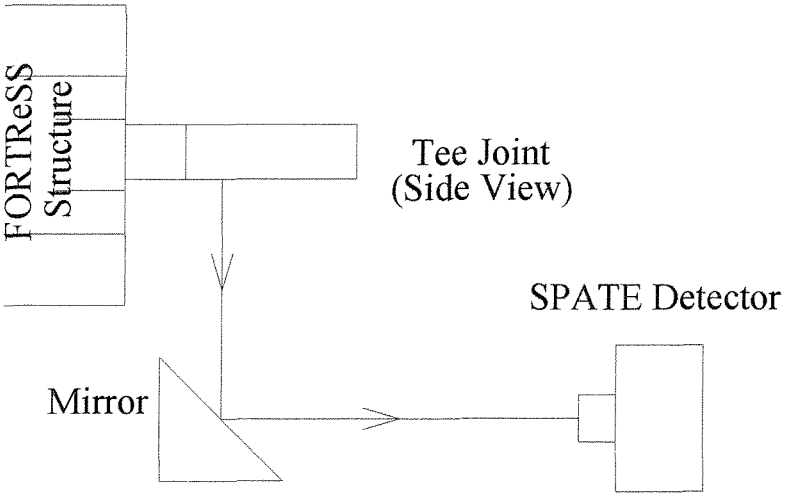

Figure 9.4: Experimental Arrangement

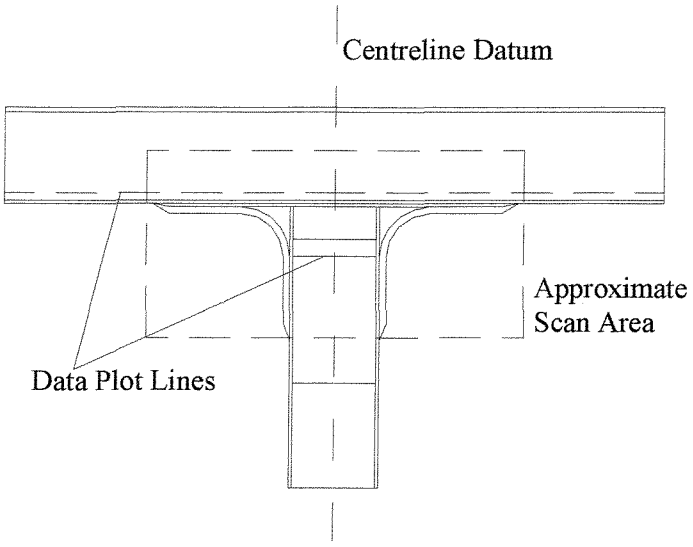

Figure 9.5: Schematic of Joint Showing Scan Area, Plot Lines

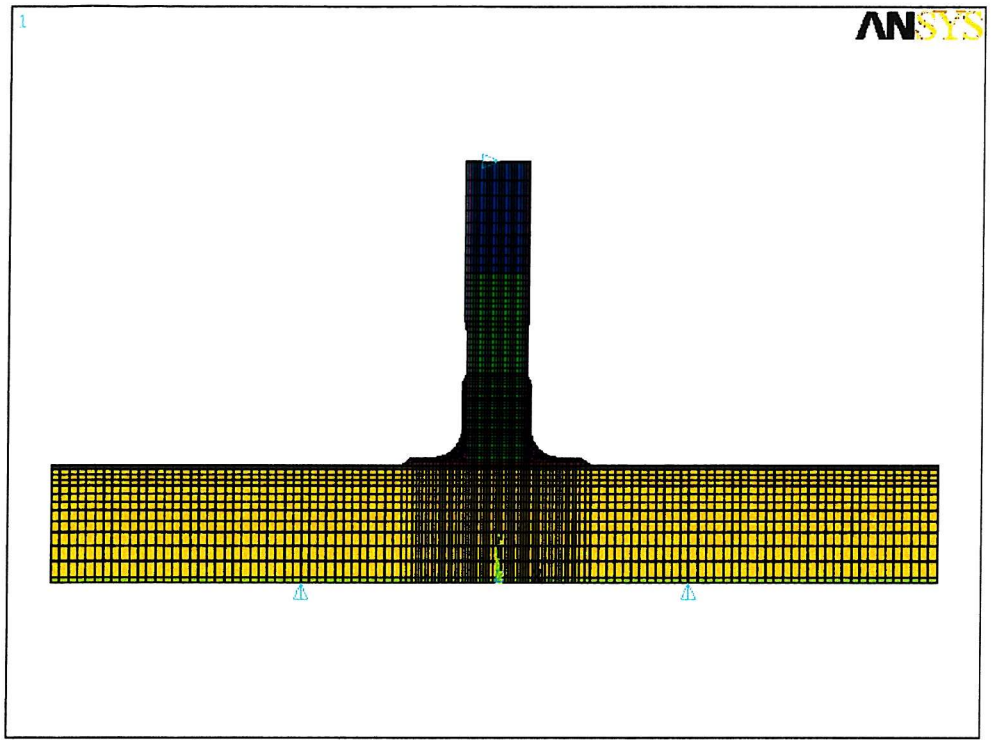

Figure 10.1: Finite Element Mesh of Complete Joint (Colours denote different materials)

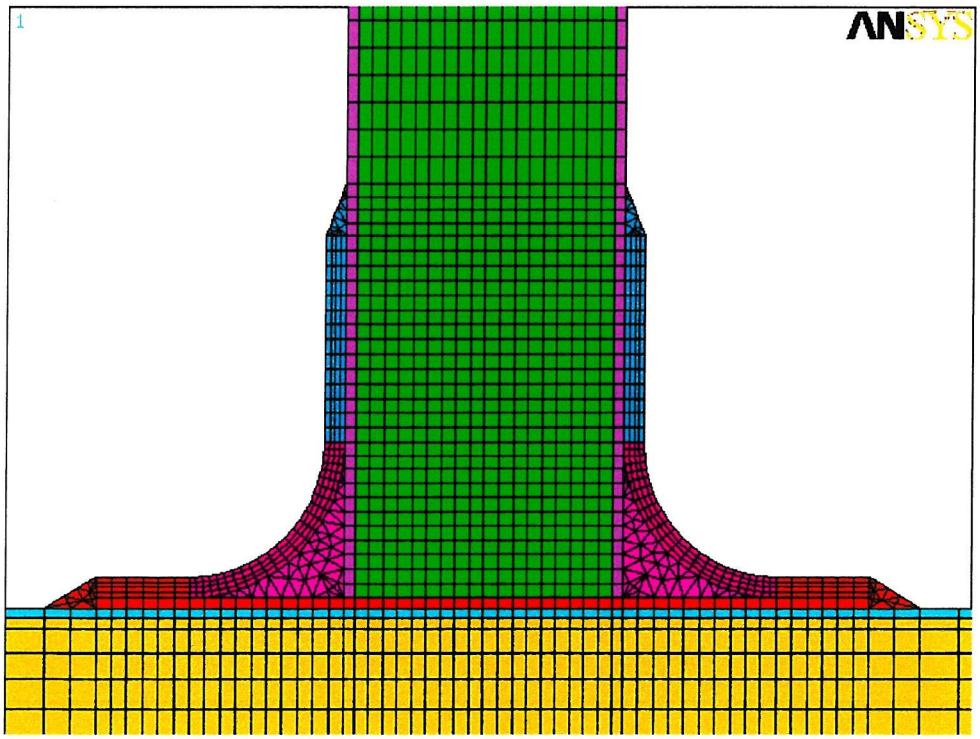

Figure 10.2: Detail of FE Mesh in Area of Interest on Joint

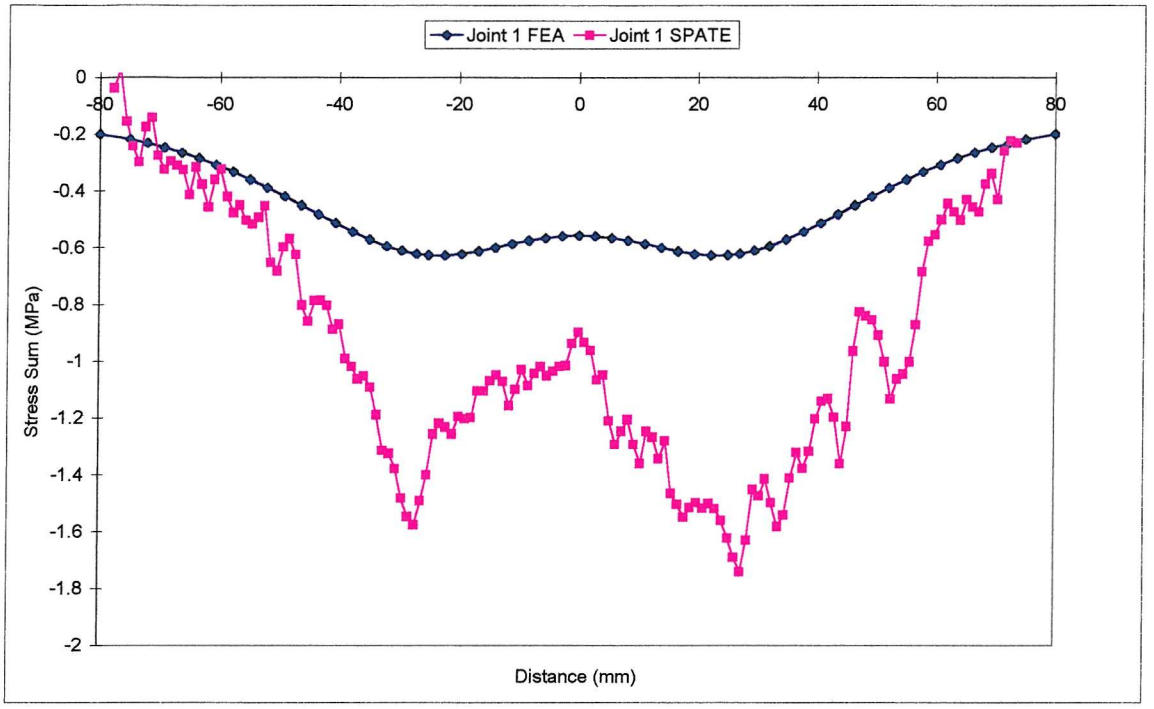

Figure 10.3(a): TSA and FEA Stress Distributions through Flange Core of Joint 1

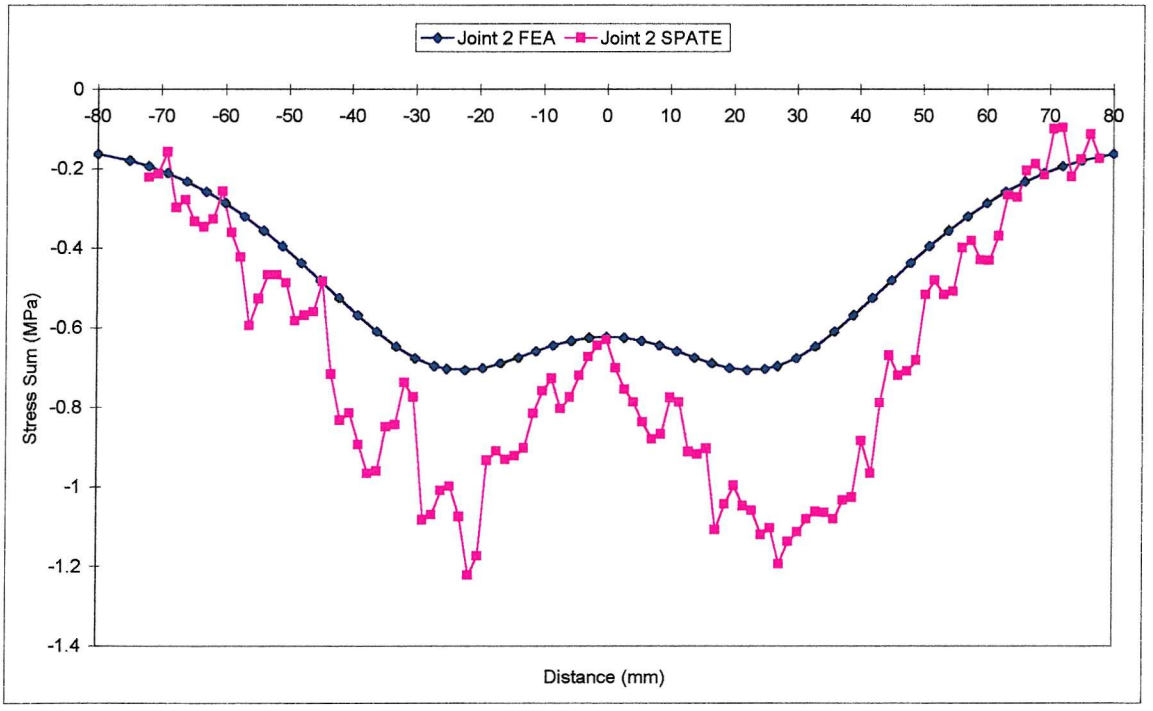

Figure 10.3(b): TSA and FEA Stress Distributions through Flange Core of Joint 2

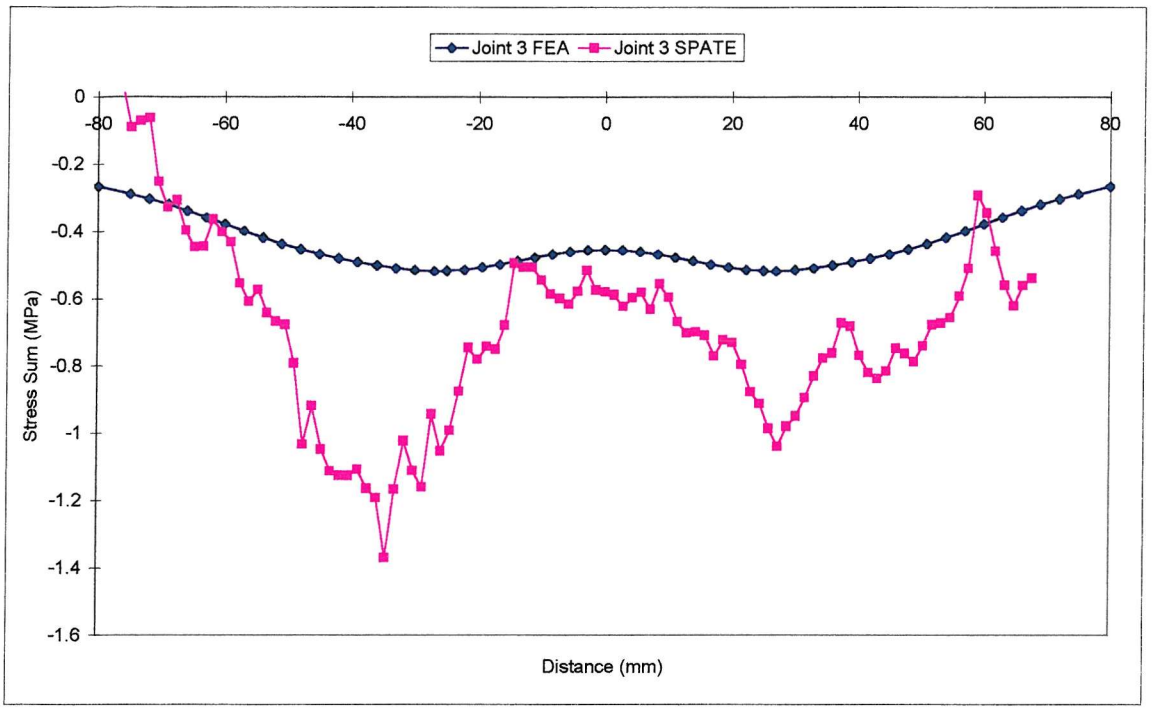

Figure 10.3(c): TSA and FEA Stress Distributions through Flange Core of Joint 3

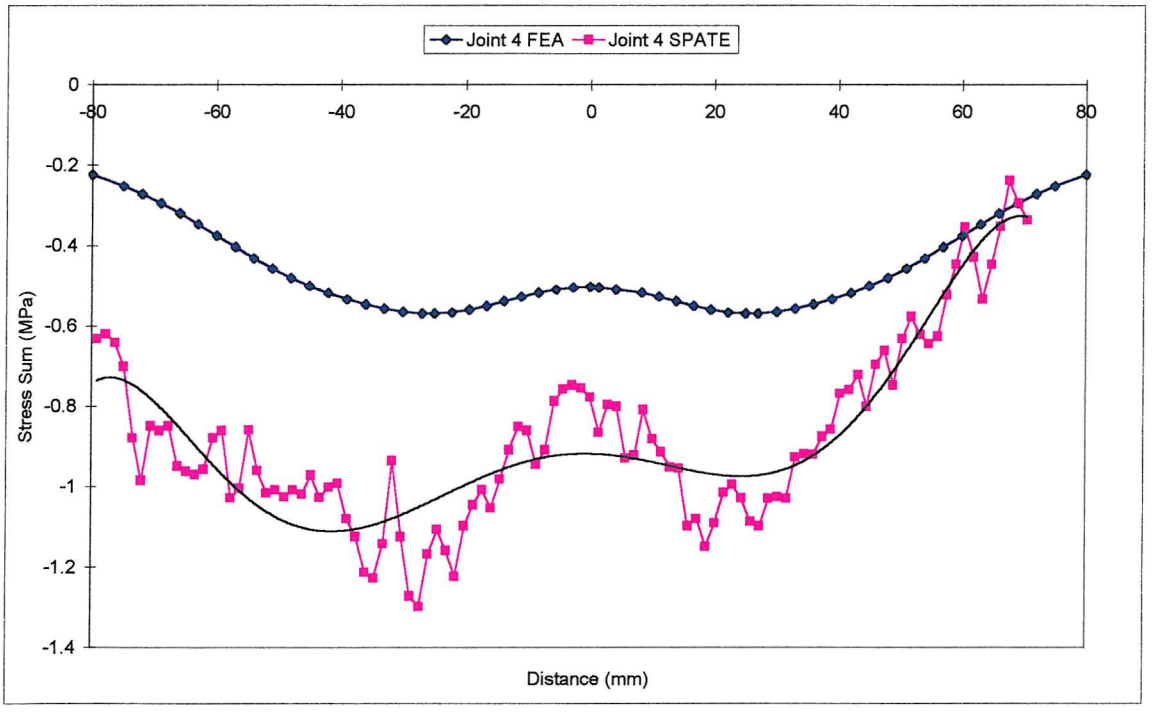

Figure 10.3(d): TSA and FEA Stress Distributions through Flange Core of Joint 4

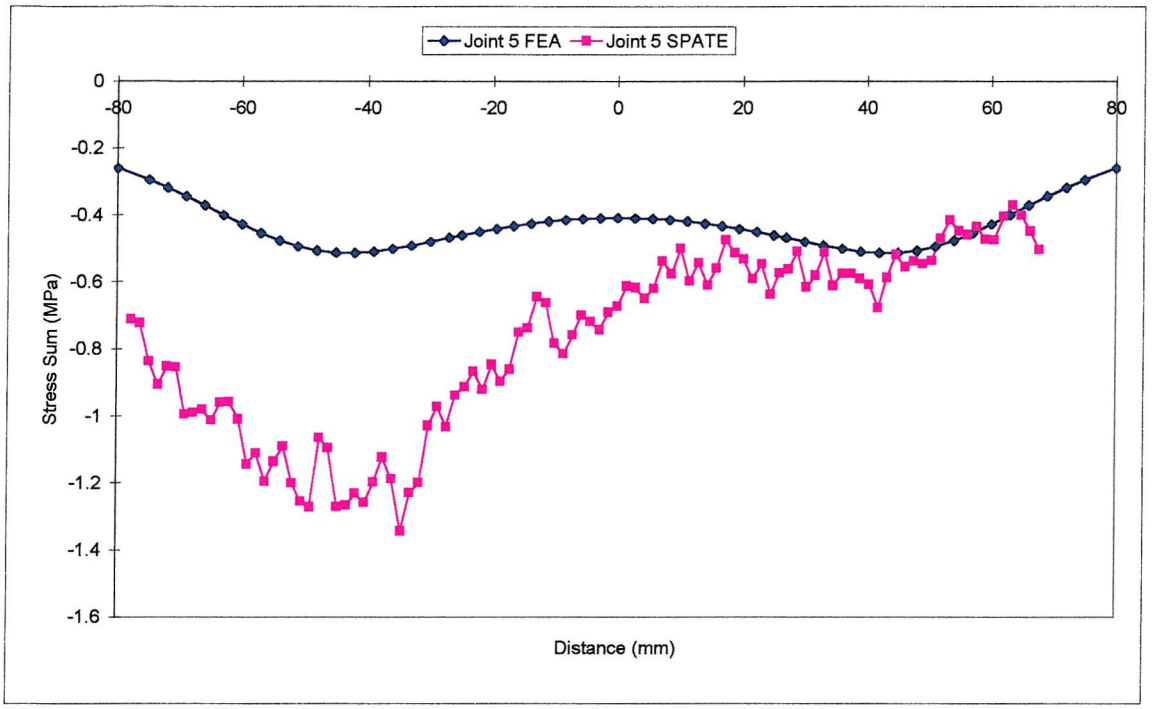

Figure 10.3(e): TSA and FEA Stress Distributions through Flange Core of Joint 5

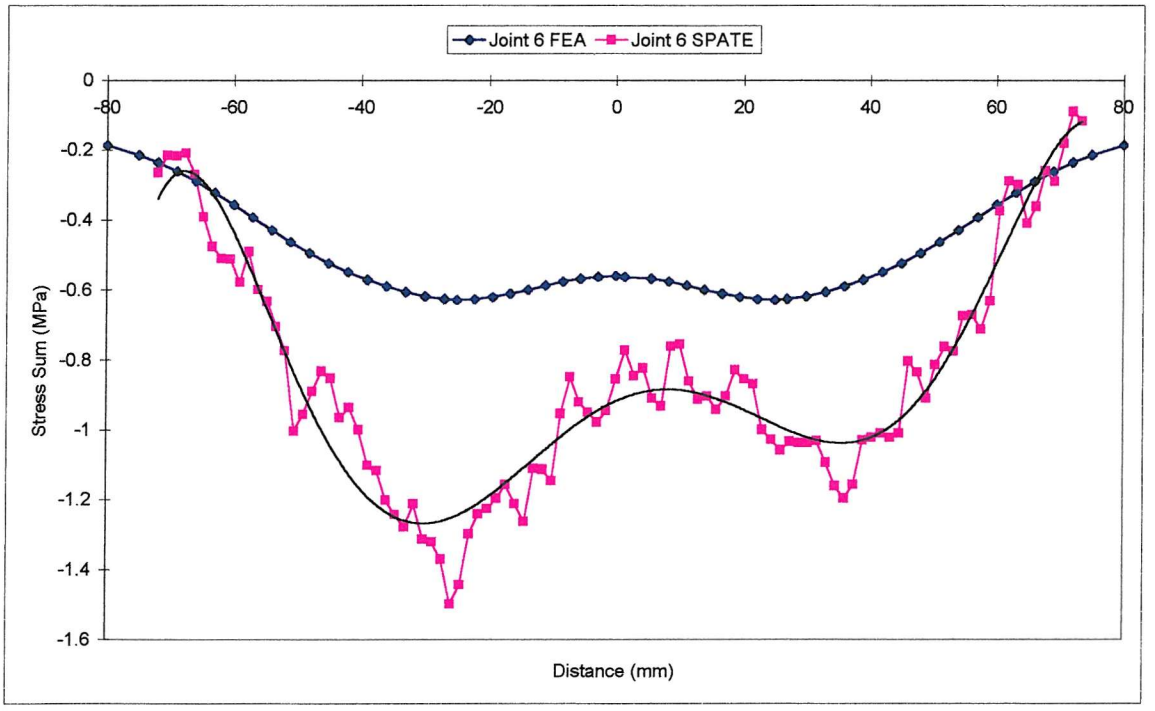

Figure 10.3(f): TSA and FEA Stress Distributions through Flange Core of Joint 6

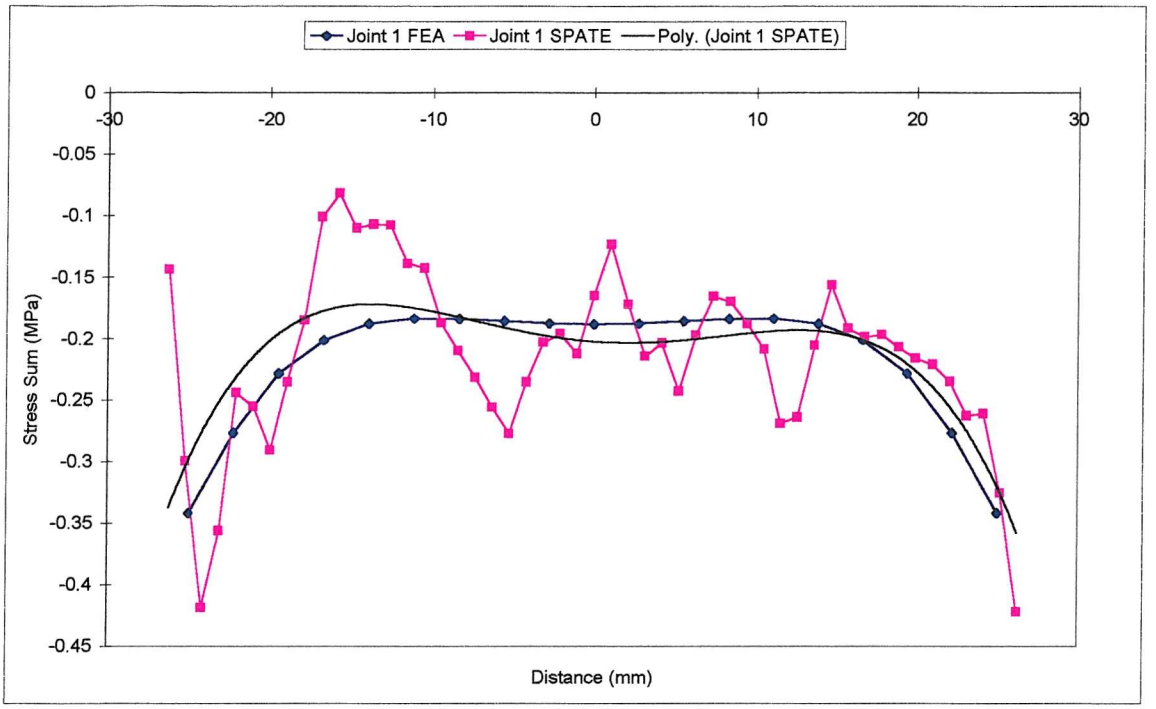

Figure 10.4(a): TSA and FEA Stress Distributions through Web Core of Joint 1

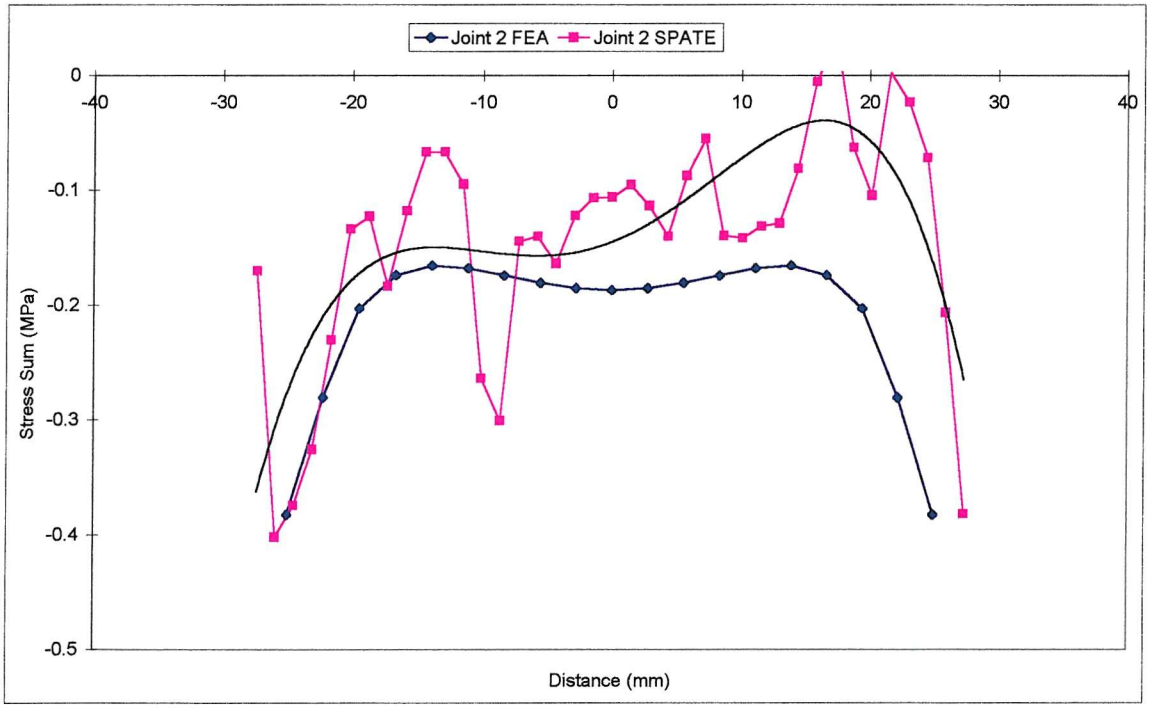

Figure 10.4(b): TSA and FEA Stress Distributions through Web Core of Joint 2

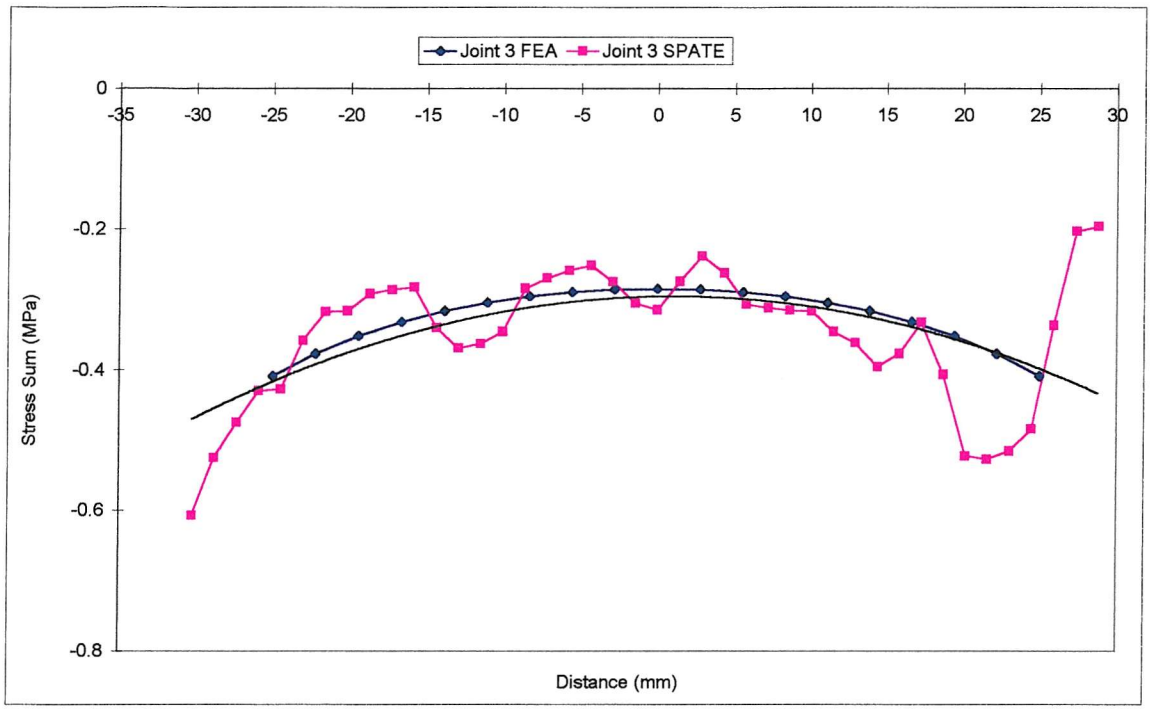

Figure 10.4(c): TSA and FEA Stress Distributions through Web Core of Joint 3

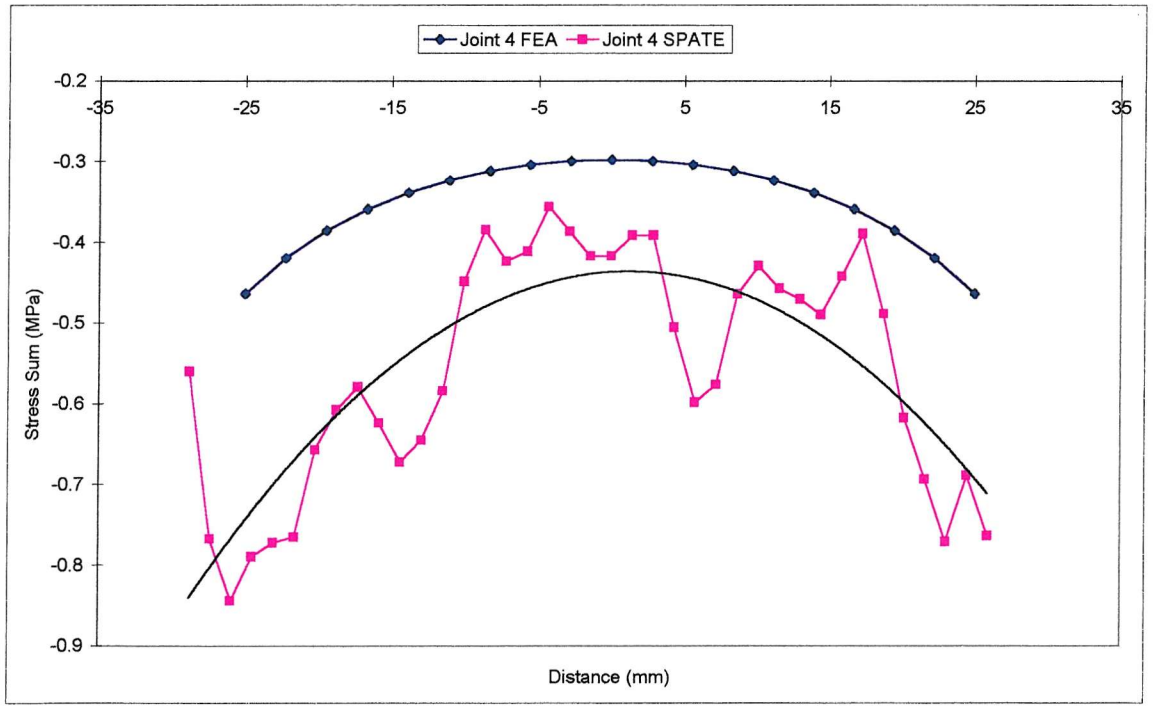

Figure 10.4(d): TSA and FEA Stress Distributions through Web Core of Joint 4

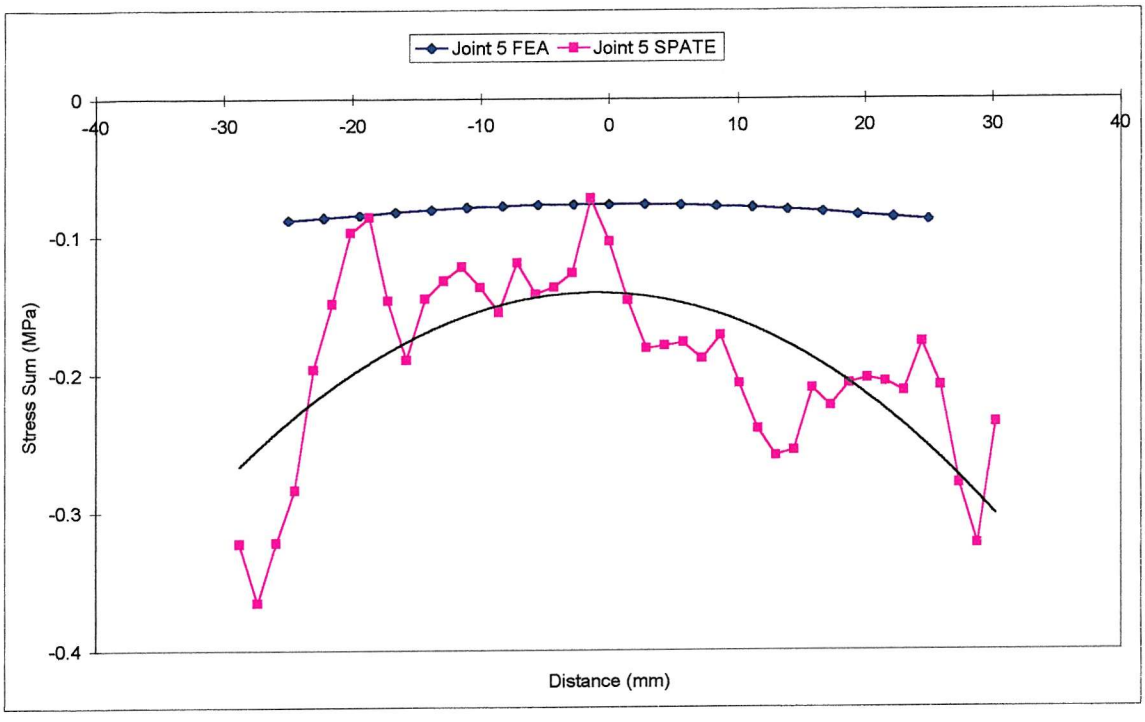

Figure 10.4(e): TSA and FEA Stress Distributions through Web Core of Joint 5

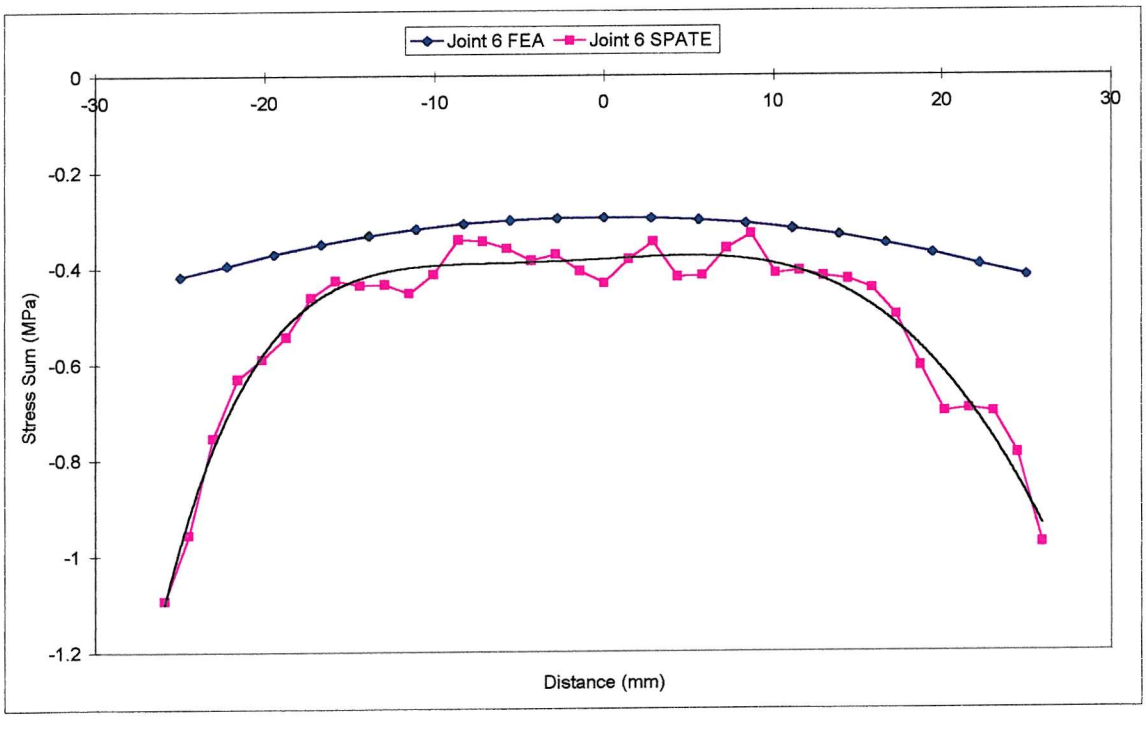

Figure 10.4(f): TSA and FEA Stress Distributions through Web Core of Joint 6

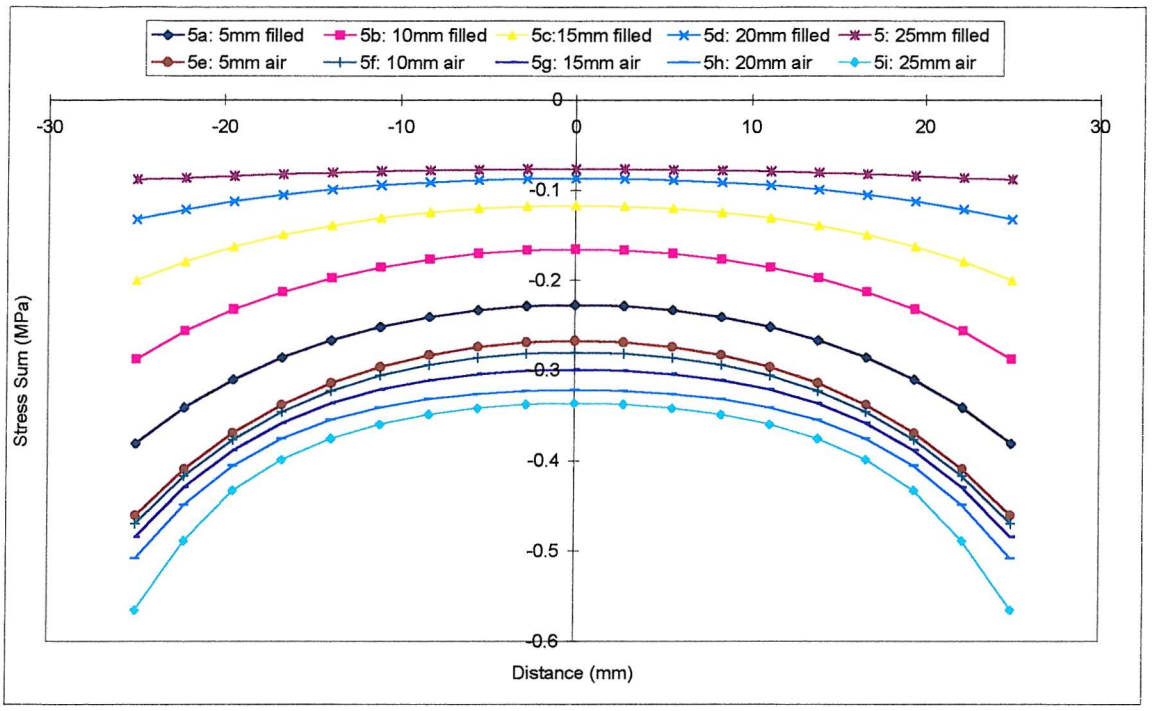

Figure 10.5: Parametric Study – Comparison of Stresses Through Web Core with Different Gap Sizes and Fillers

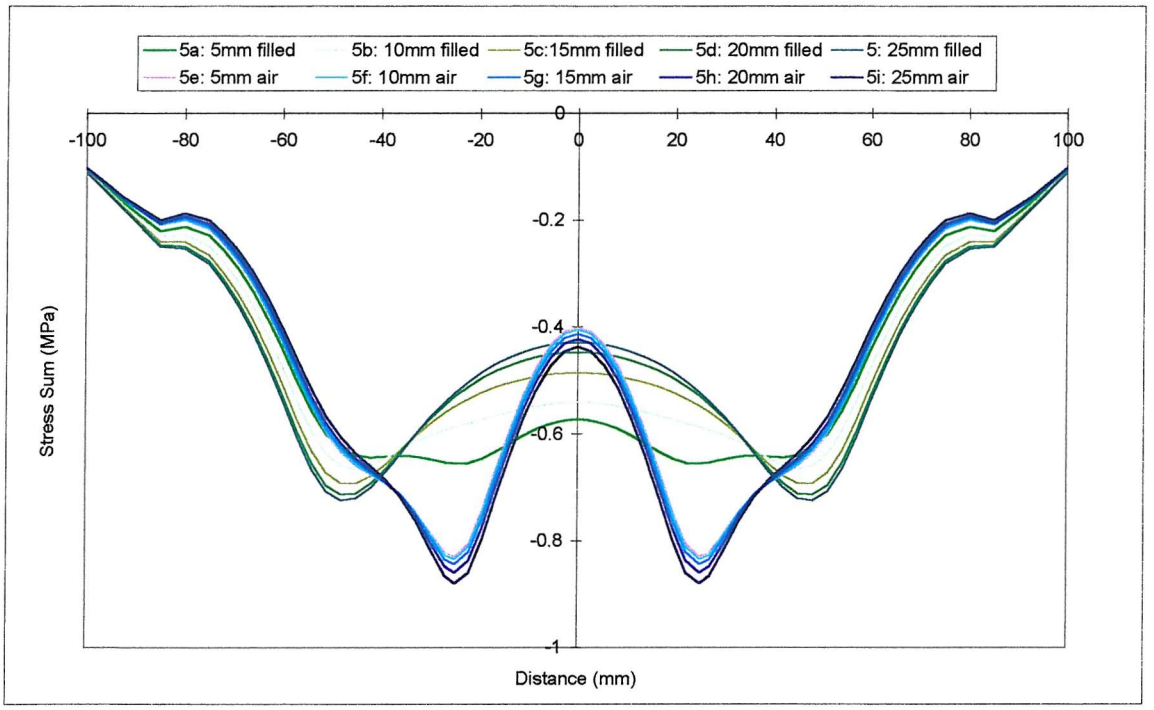

Figure 10.6: Parametric Study – Comparison of Stresses Through Flange Core with Different Gap Sizes and Fillers

Figure 11.1: Arrangement of Joints within Chamber (from front: statically loaded, cyclically loaded, unloaded)

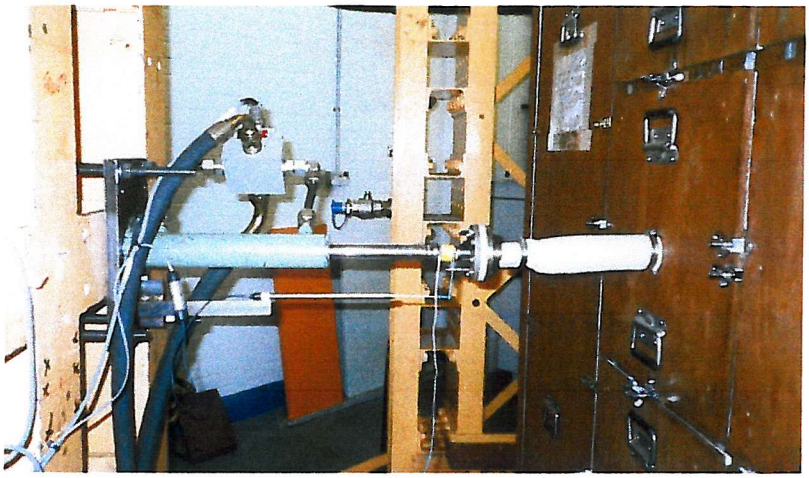

Figure 11.2: Hydraulic ram extension entering chamber through sleeve (on the right); ram reacts against FORTReSS (on left).

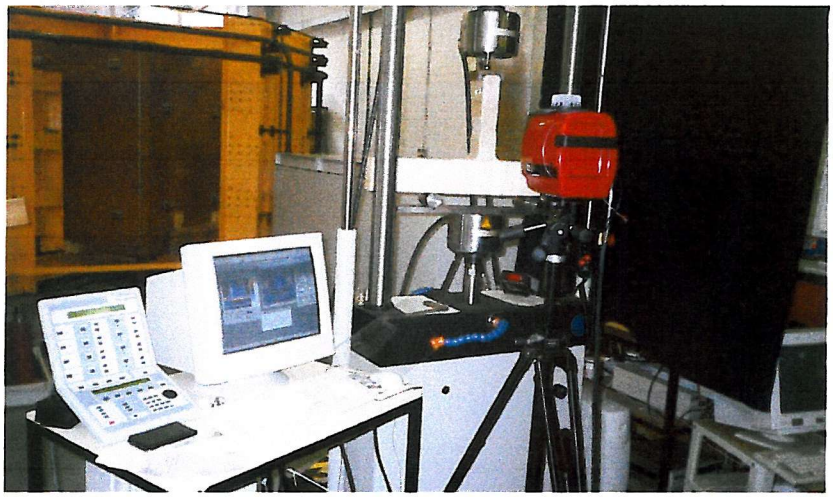

Figure 11.3: DeltaTherm test set-up for aged joint work (note chamber within the yellow steelwork of FORTReSS in the background)

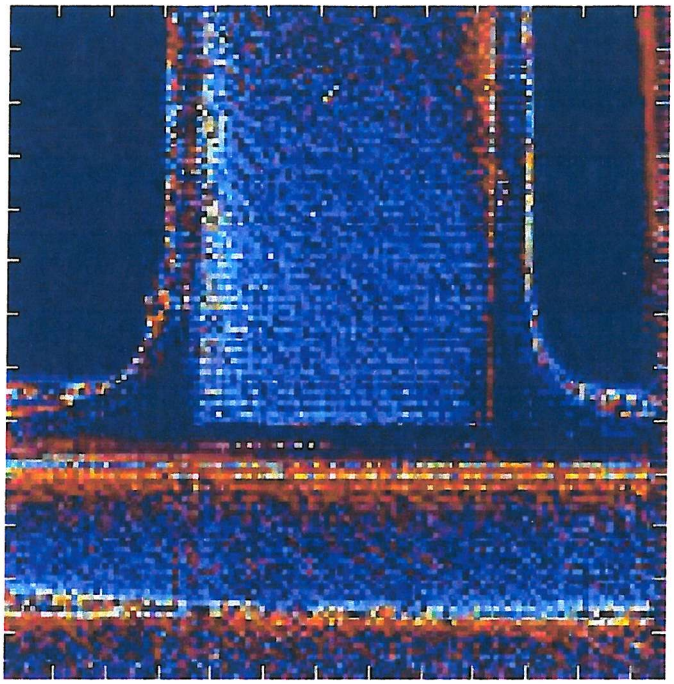

Figure 11.4: DeltaTherm image from a joint directly after being removed from the chamber, showing excessive noise

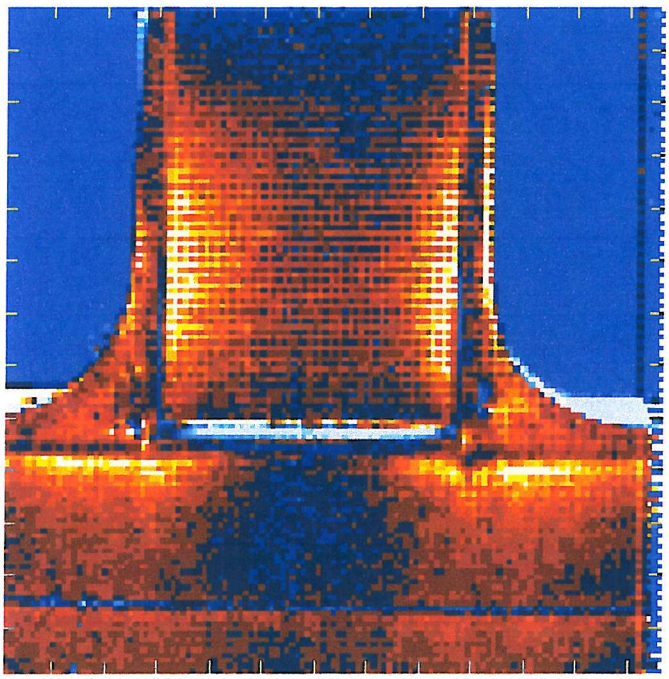

Figure 11.5: DeltaTherm image from a joint allowed to stand for 2 hours after being removed from the chamber, showing greatly reduced noise

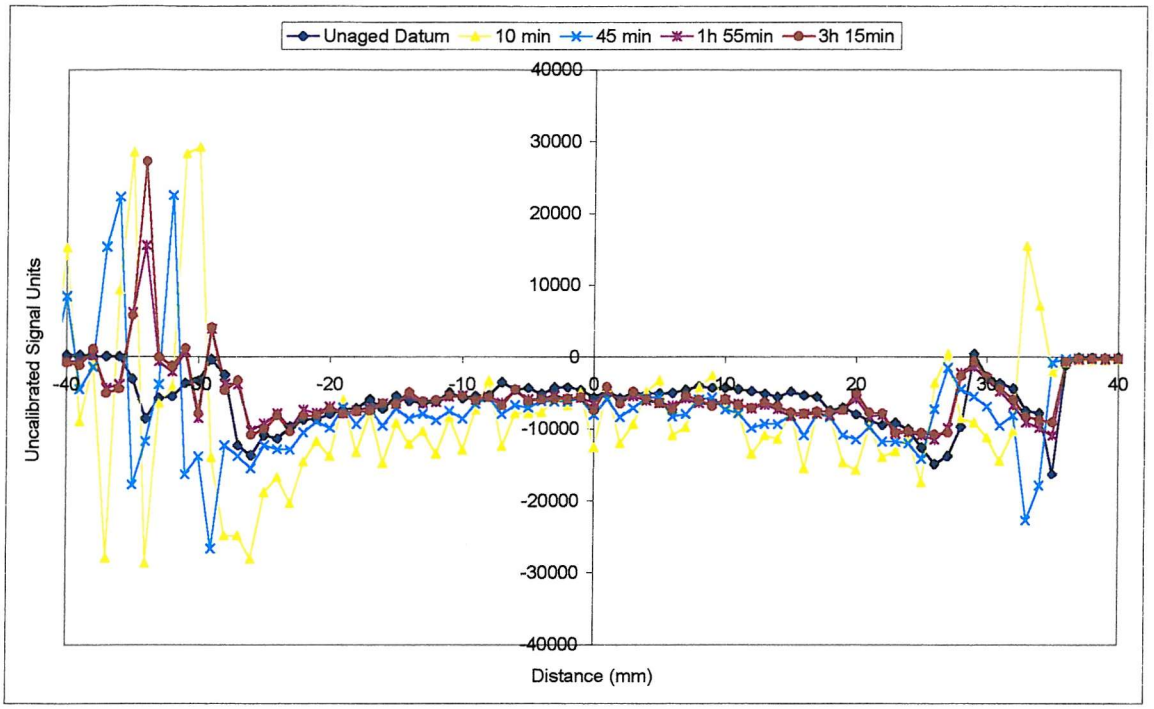

Figure 11.6(a): Unloaded Joint Web results after 60 days exposure
(times in legend refer to time readings were taken after removal from the chamber)

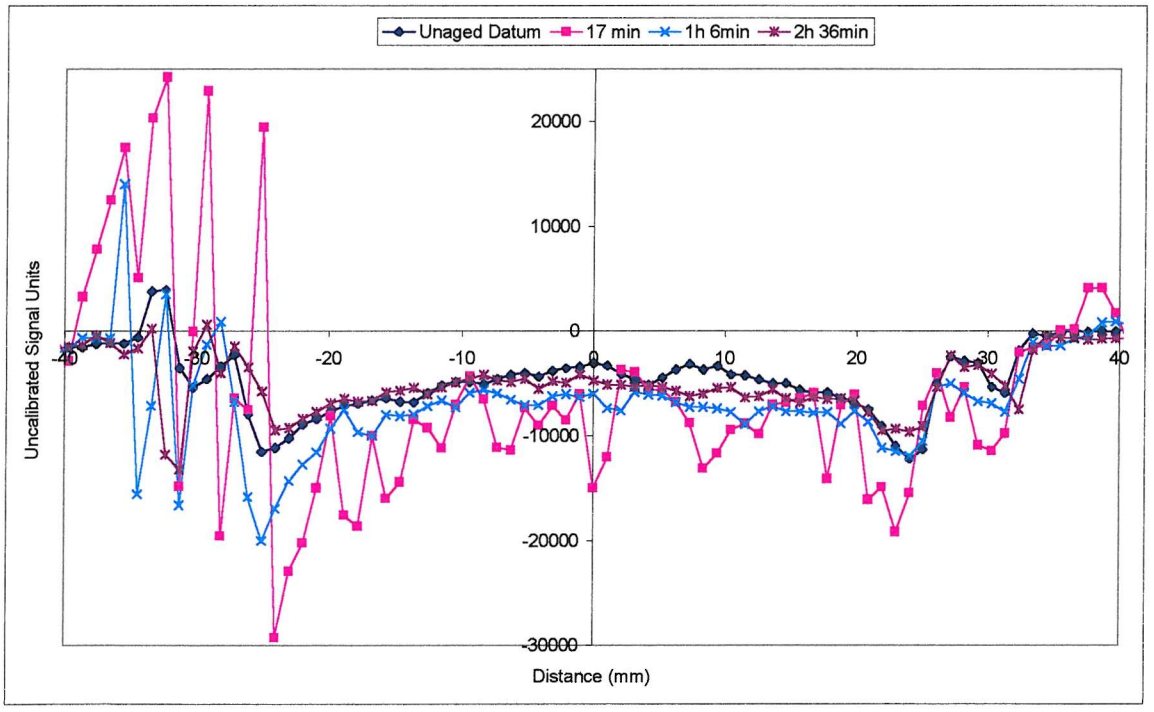

Figure 11.6(b): Unloaded Joint Web results after 144 days exposure
(times in legend refer to time readings were taken after removal from the chamber)

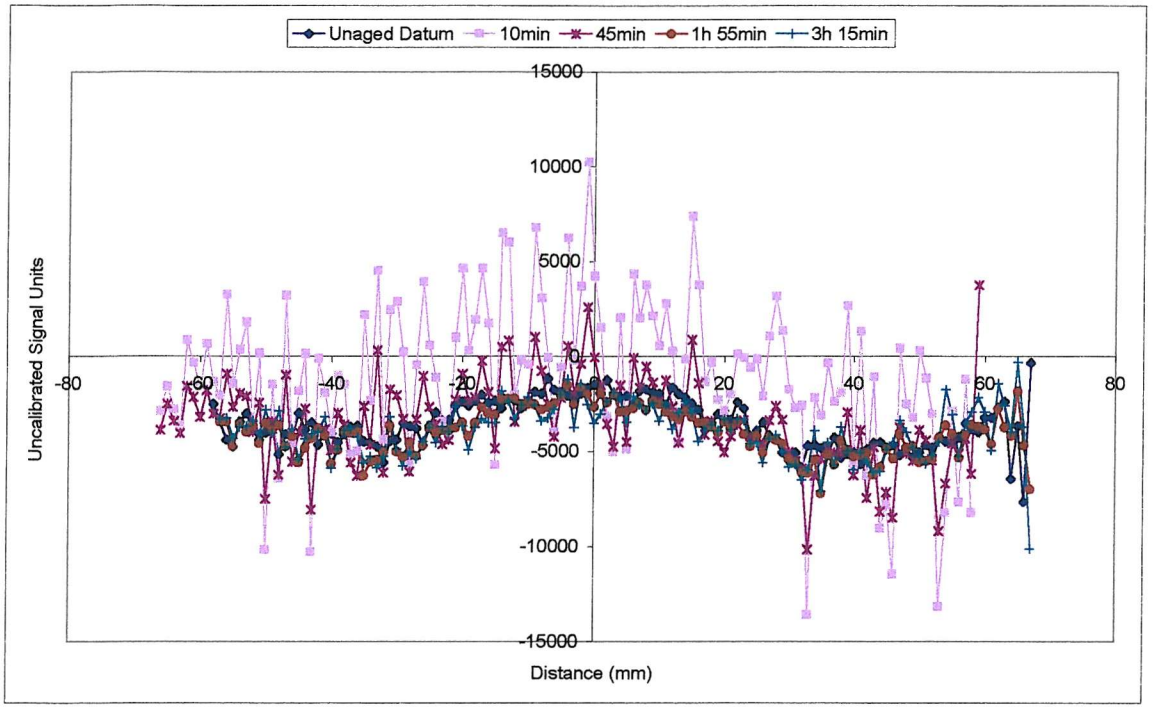

Figure 11.6(c): Unloaded Joint Flange results after 60 days exposure
(times in legend refer to time readings were taken after removal from the chamber)

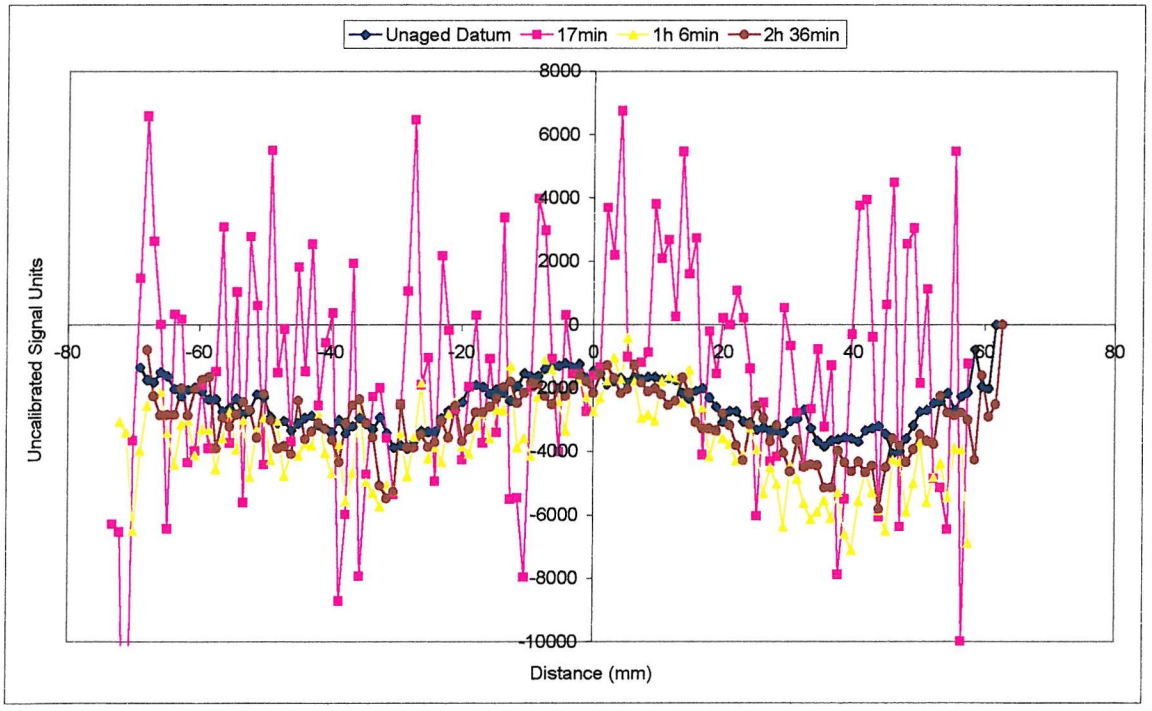

Figure 11.6(d): Unloaded Joint Flange results after 144 days exposure
(times in legend refer to time readings were taken after removal from the chamber)

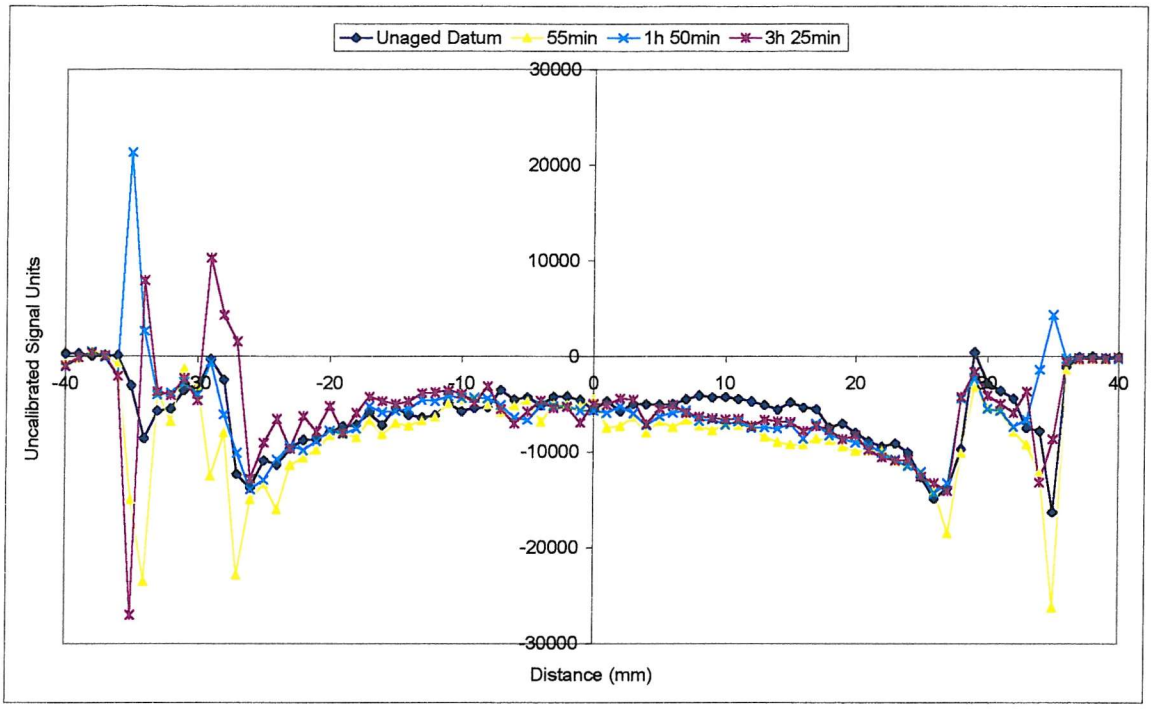

Figure 11.7(a): Statically Loaded Joint Web results after 60 days exposure (times in legend refer to time readings were taken after removal from the chamber)

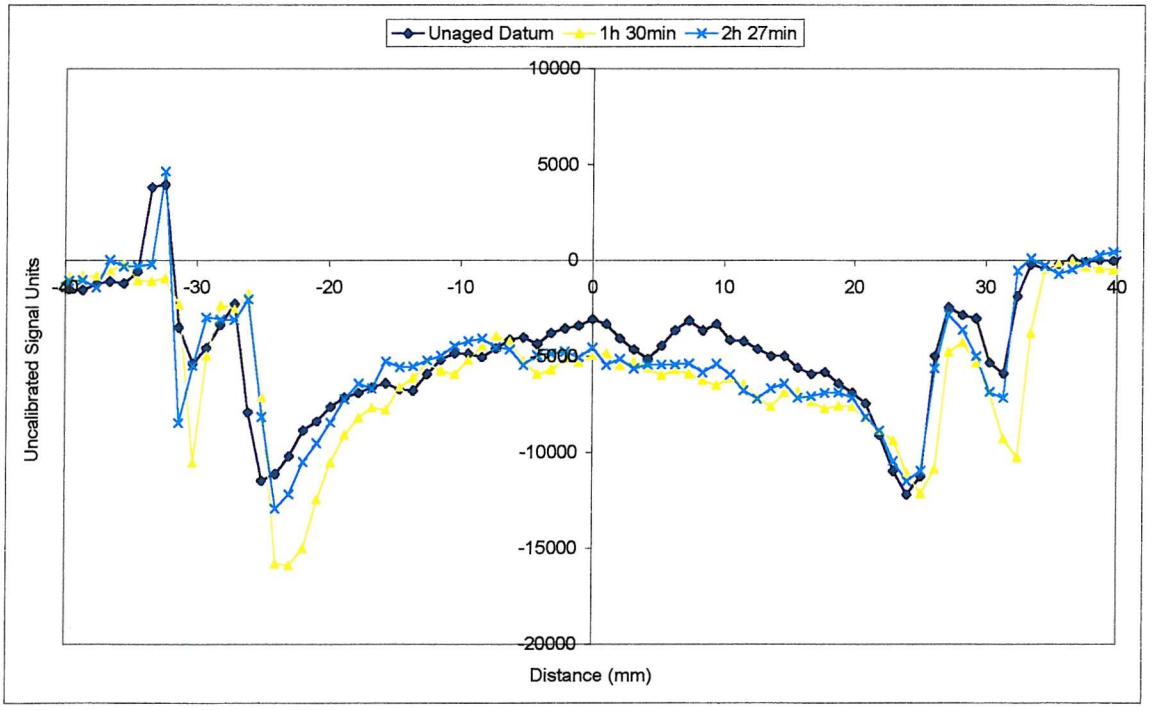

Figure 11.7(b): Statically Loaded Joint Web results after 144 days exposure (times in legend refer to time readings were taken after removal from the chamber)

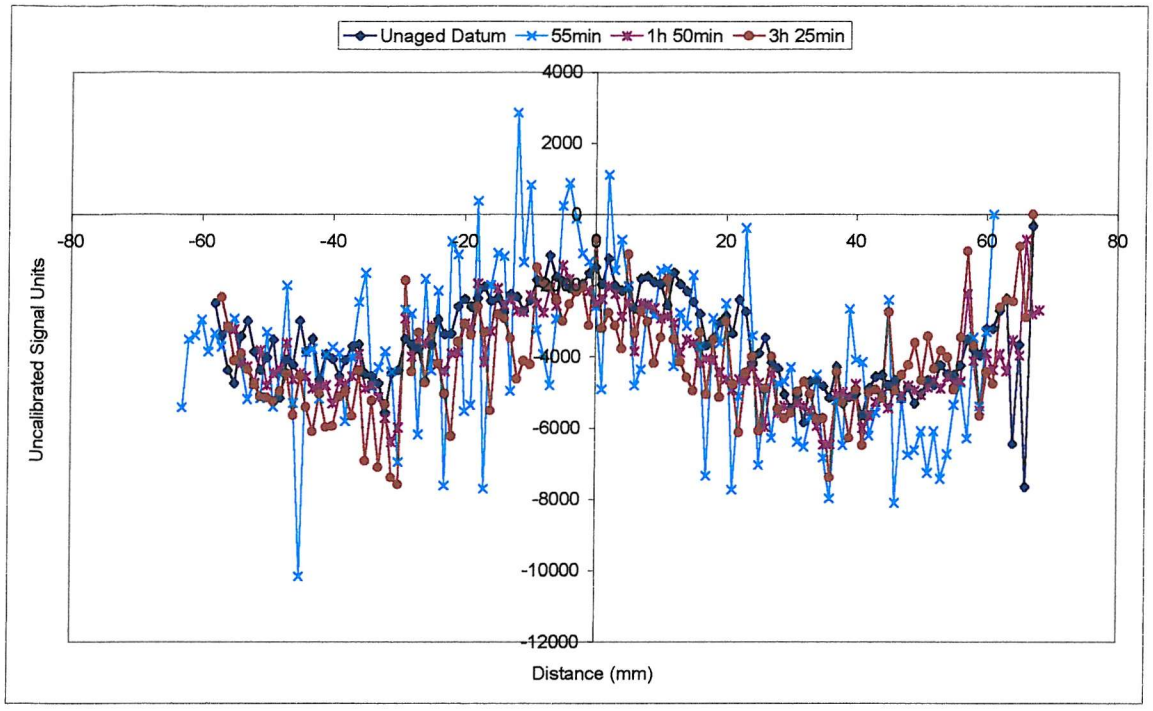

Figure 11.7(c): Statically Loaded Joint Flange results after 60 days exposure (times in legend refer to time readings were taken after removal from the chamber)

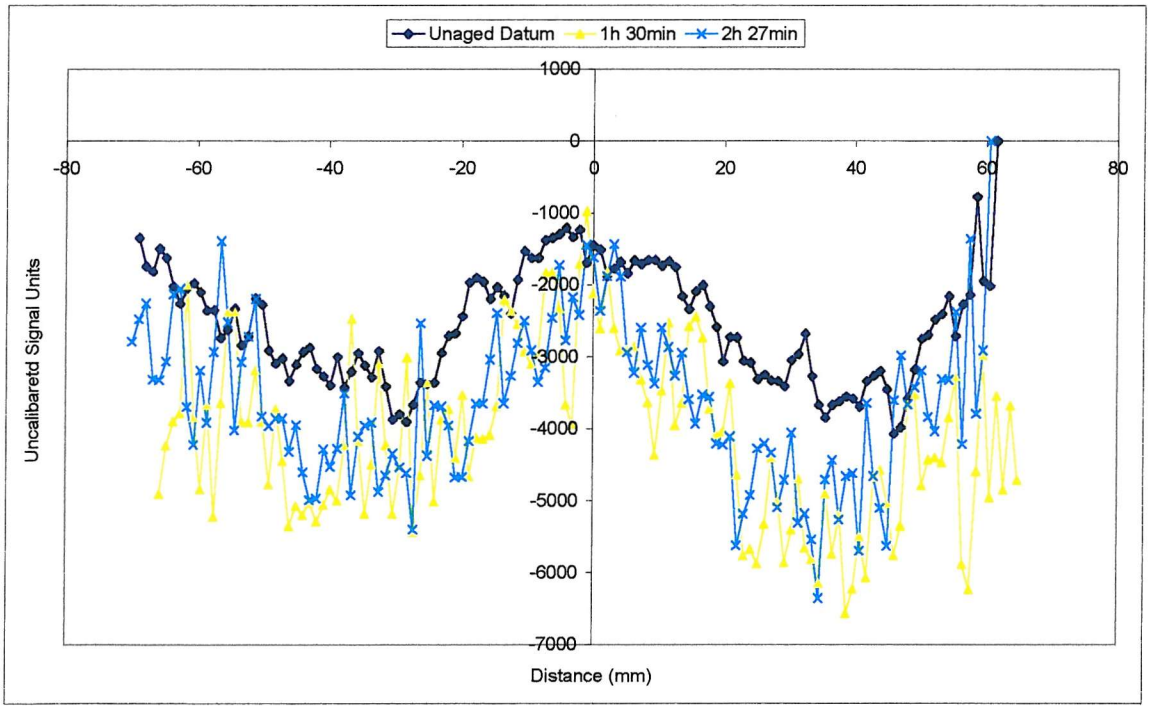

Figure 11.7(d): Statically Loaded Joint Flange results after 144 days exposure (times in legend refer to time readings were taken after removal from the chamber)

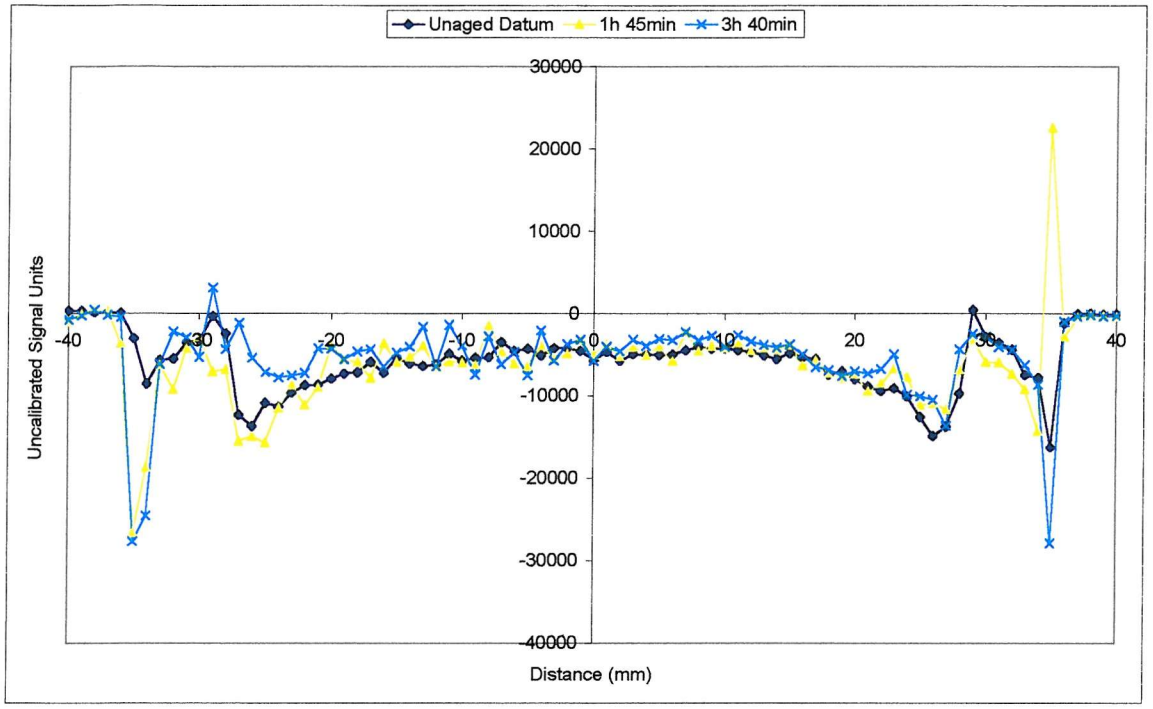

Figure 11.8(a): Cyclically Loaded Joint Web results after 60 days exposure
(times in legend refer to time readings were taken after removal from the chamber)

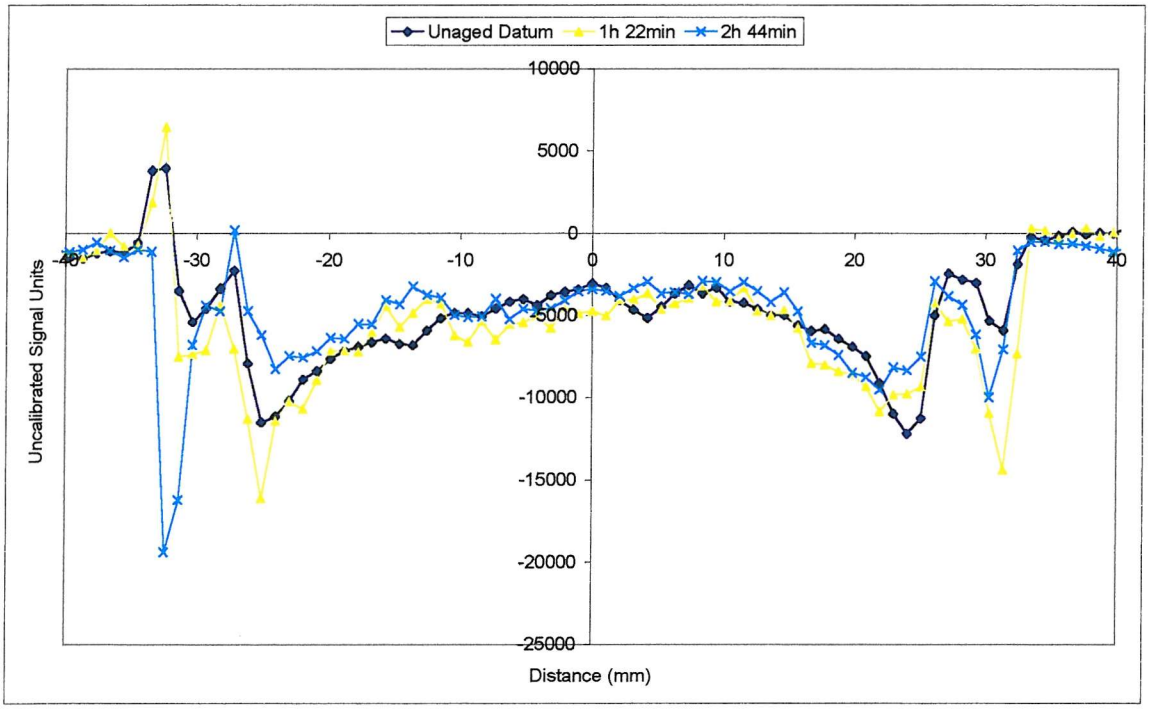

Figure 11.8(b): Cyclically Loaded Joint Web results after 144 days exposure
(times in legend refer to time readings were taken after removal from the chamber)

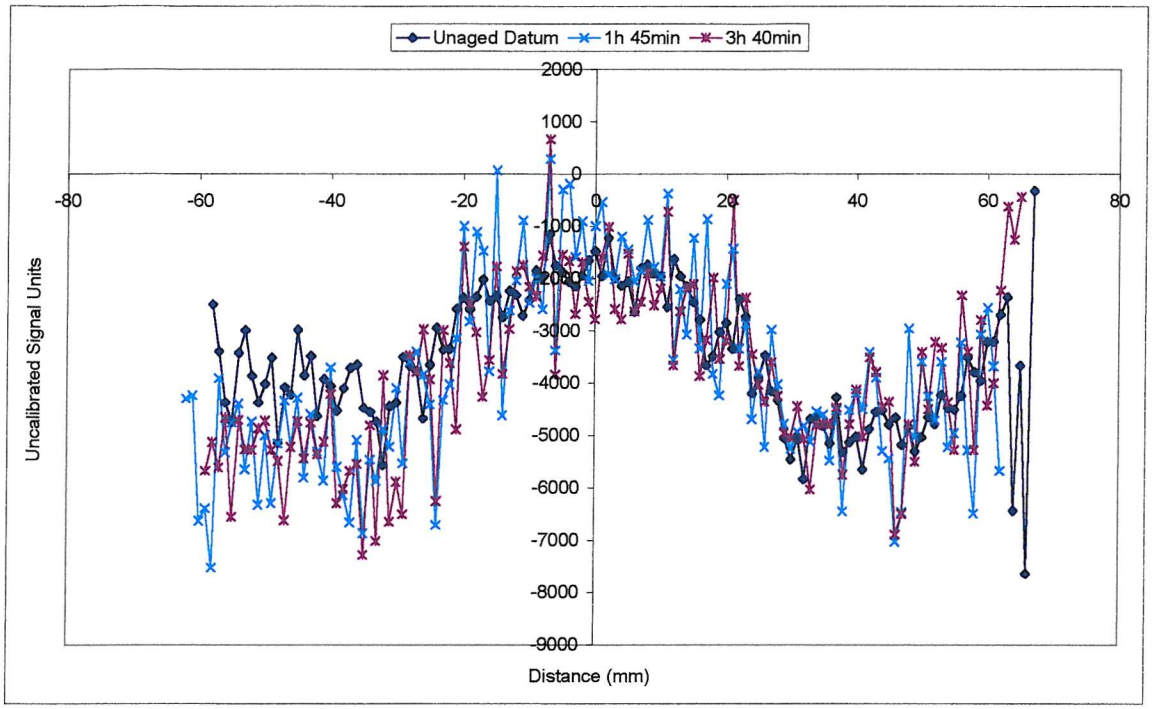

Figure 11.8(c): Cyclically Loaded Joint Flange results after 60 days exposure (times in legend refer to time readings were taken after removal from the chamber)

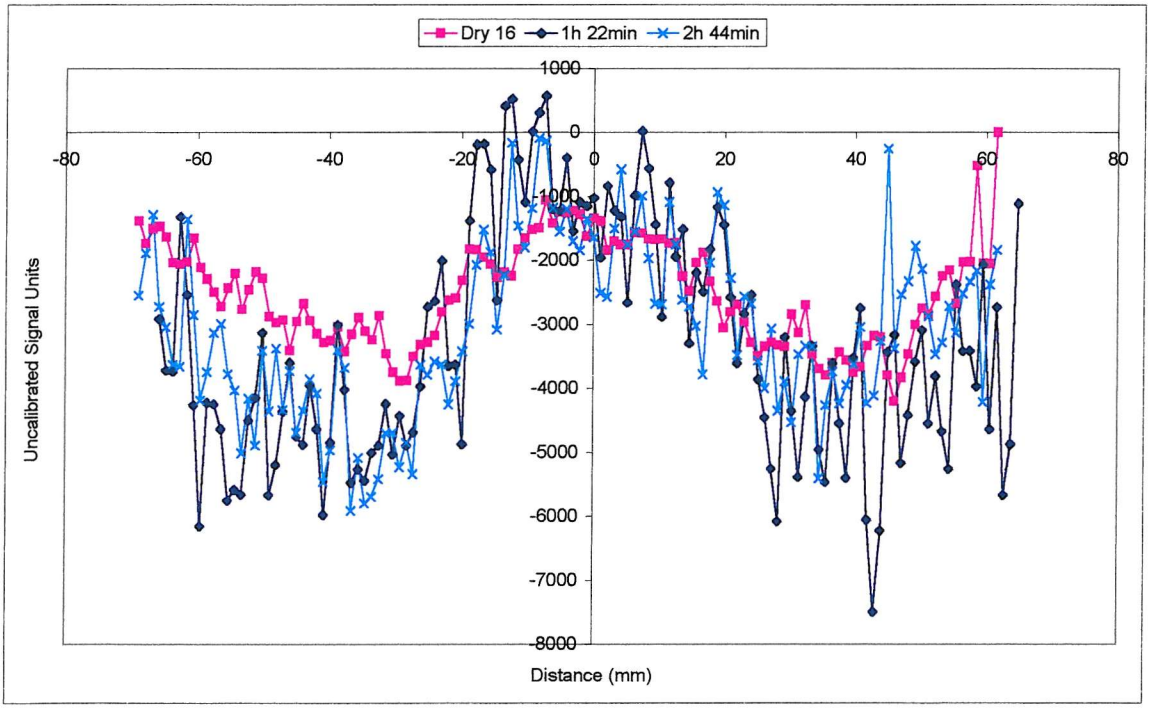

Figure 11.8(d): Cyclically Loaded Joint Flange results after 144 days exposure (times in legend refer to time readings were taken after removal from the chamber)

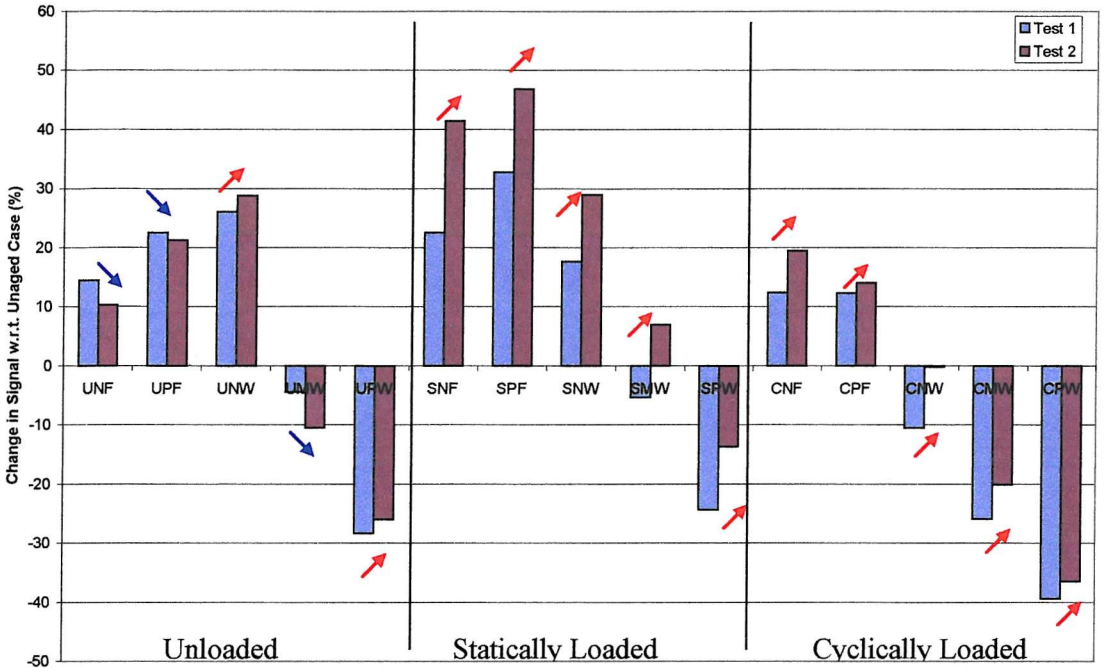

Figure 11.9: Bar chart showing trends in normalised results, where Test 1 (blue) was taken after 60 days exposure and Test 2 (maroon) was taken after 144 days exposure. (U = unloaded, S = statically loaded, C = cyclically loaded; N = nominal stress area, M = moderate stress area, P = peak stress area; F = flange, W = web)

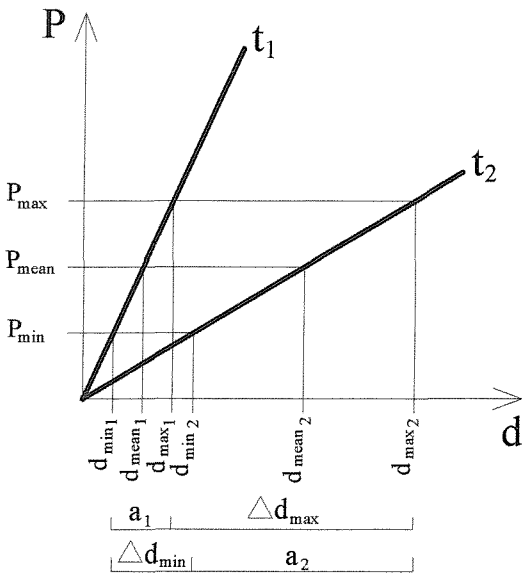

Figure 11.10: Schematic load (P) – deflection (d) curves for the linear elastic region where duration of hygrothermal exposure t_1 is less than t_2 and the subscripts max, min and mean refer to the maximum, minimum and mean load or deflection in the applied cyclic mode of loading.